A System Identification and Control Engineering Approach for Optimizing mHealth Behavioral Interventions Based on Social Cognitive Theory

by

César Antonio Martín Moreno

A Dissertation Presented in Partial Fulfillment
of the Requirements for the Degree
Doctor of Philosophy

Approved July 2016 by the
Graduate Supervisory Committee:

Daniel E. Rivera, Chair
Eric B. Hekler
Matthew M. Peet
Konstantinos S. Tsakalis

ARIZONA STATE UNIVERSITY

August 2016

ABSTRACT

Behavioral health problems such as physical inactivity are among the main causes of mortality around the world. Mobile and wireless health (mHealth) interventions offer the opportunity for applying control engineering concepts in behavioral change settings. Social Cognitive Theory (SCT) is among the most influential theories of health behavior and has been used as the conceptual basis of many behavioral interventions. This dissertation examines adaptive behavioral interventions for physical inactivity problems based on SCT using system identification and control engineering principles. First, a dynamical model of SCT using fluid analogies is developed. The model is used throughout the dissertation to evaluate system identification approaches and to develop control strategies based on Hybrid Model Predictive Control (HMPC). An initial system identification informative experiment is designed to obtain basic insights about the system. Based on the informative experimental results, a second optimized experiment is developed as the solution of a formal constrained optimization problem. The concept of Identification Test Monitoring (ITM) is developed for determining experimental duration and adjustments to the input signals in real time. ITM relies on deterministic signals, such as multisines, and uncertainty regions resulting from frequency domain transfer function estimation that is performed during experimental execution. ITM is motivated by practical considerations in behavioral interventions; however, a generalized approach is presented for broad-based multivariable application settings such as process control. Stopping criteria for the experimental test utilizing ITM are developed using both open-loop and robust control considerations.

A closed-loop intensively adaptive intervention for physical activity is proposed relying on a controller formulation based on HMPC. The discrete and logical features of HMPC naturally address the categorical nature of the intervention components that

include behavioral goals and reward points. The intervention incorporates online controller reconfiguration to manage the transition between the behavioral initiation and maintenance training stages. Simulation results are presented to illustrate the performance of the system using a model for a hypothetical participant under realistic conditions that include uncertainty. The contributions of this dissertation can ultimately impact novel applications of cyberphysical system in medical applications.

To my wife Rady and my daughters Isabella, Cristina and Bianca for all their love, support and patience during our years in Tempe.

To my parents Ivonne and César who have been my role-model for hard work, persistence and dedication, and for transmitting me their visionary thoughts.

To my sisters Ivonne and Olguita for always being there with support and motivation for all the family.

ACKNOWLEDGMENTS

First and foremost, I would like to express my deepest gratitude to my advisor Dr. Daniel E. Rivera for all his support, guidance, and understanding during these years. His knowledge, dedication, patience, and approach to research have been fundamental for the successful completion of this work. In particular I would like to thank him for his dedication in reviewing my publications, and for teaching me how research activities can be performed in effective and productive ways.

I would like to thank my committee members, Dr. Konstantinos Tsakalis, and Dr. Matthew Peet for their support and comments on the content of this work, which have been invaluable. My special thanks to Dr. Eric Hekler, who also serves in my committee, for all his support, and for sharing with me his enthusiasm and passion toward searching solutions for important behavioral health related problems. Dr. Hekler proved to be a generous person, always willing to share his knowledge to achieve greater scientific goals. I am also very grateful to Drs. William Riley, Matthew Buman, and Marc Adams for sharing their knowledge, experience and views that were fundamental for the construction of dynamical models that represent human behavior.

Additionally, I would like to extend my sincere gratitude to Drs. Konstantinos Tsakalis, Hans Mittelmann, Daniel Rivera, Armando Rodriguez, Jennie Si, Walter Higgins, and Ying-Cheng Lai for providing me with a solid foundation in the graduate courses at ASU.

I wish to express gratitude to past and current members of the Control System Engineering Lab (CSEL): Sunil Deshpande, Yuwen Dong, Kevin Timms, Penghong Guo, Mohammad Freigoun, Gustavo Seixas, and Alicia Magann for all their support, encouragement, and for the good times we had in the laboratory. It was important to combine research activities with conversations about important things in life, and occasional jovial moments.

I am privileged for having such a wonderful and supportive family. My wife Rady, and my daughters Isabella, Cristina and Bianca were responsible for make me feeling always at home, regardless of the distance to our country. My parents Ivonne and César are my inspiration and motivation that made possible achieving this important life goal. My sisters, parents in law, brother in law, and sisters in law have been very supportive, always sending us good vibes that helped to obtain the strength to keep going on with our plans.

This work would not have been possible without organizations which supported my education, research, and development. My Ph.D. studies have been partially supported by Escuela Superior Politécnica del Litoral (ESPOL) and Secretaria de Educación Superior, Ciencia, Tecnolgía e Innovación (SENESCYT) from Ecuador. Support for this work has been provided by the National Science Foundation (NSF) through grant IIS-1449751. Additional support has been received from the Piper Health Solutions Consortium at Arizona State University. The opinions expressed in this document are the author's own and do not necessarily reflect the views of NSF or the Virginia G. Piper Charitable Trust.

TABLE OF CONTENTS

CHAPTER Page

CHAPTER Page

CHAPTER Page

CHAPTER Page

LIST OF TABLES

LIST OF FIGURES

Figure Page

Figure Page

Figure Page

Figure Page

Figure Page

Chapter 1

INTRODUCTION

1.1 Motivation

Control system engineering principles have been applied in a diverse series of fields. These go beyond mechanical, chemical, civil and electrical engineering, to include the social and natural sciences in important problems involving economic, environmental and biological systems, among others. One key advantage of a control system representation of systems is its ability to support the design of a model-based controller that can manipulate the system response to accomplish a desired goal.

Health is a major concern in society; therefore significant research efforts have focused on this problem. Many infectious diseases are under control in developed countries, creating the need to address behavioral health problems. For example, three behavioral risk factors - tobacco use, poor diet, and inactivity - contribute to four major chronic diseases: heart disease, type 2 diabetes, lung disease, and cancer. Together, these behaviors account for more than 50% of preventable deaths (Hekler *et al.*, 2013b). Given these facts, the following questions are considered: Are dynamical systems capable of describing human behavior? Is system identification a viable approach for experimentally developing models from human participants in behavioral interventions? Can controllers, designed on the basis of control engineering principles, be useful for behavioral interventions?

Some significant efforts have been made to integrate control systems principles into behavioral health. In the work Rivera *et al.* (2007) a procedure to design a general adaptive behavioral intervention based on control principles is proposed. In

other work, a dynamical systems model for the Theory of Planned Behavior (TPB) (Navarro-Barrientos *et al.*, 2011), an influential behavioral theory, and its applications for improvements on gestational weight gain interventions (Dong, 2014; Dong *et al.*, 2013, 2014) have been presented. Other contributions in this area have focused on control systems principles for understanding and optimizing interventions for smoking cessation (Timms *et al.*, 2014d,c,b), and fibromyalgia pain treatment (Deshpande *et al.*, 2012, 2014b,a).

Many control systems and engineering techniques have been applied to address behavioral problems. The use of fluid analogies (Rivera *et al.*, 2007) has allowed the interpretation of behavioral concepts to physical systems that can be mathematically modeled (Navarro-Barrientos *et al.*, 2011; Dong, 2014); furthermore, system identification techniques have been applied to find and validate mathematical estimations of behavioral systems, with and without previous knowledge of the model structure (Deshpande, 2014; Timms *et al.*, 2014c). To deliver adaptive interventions, control design strategies have also been applied: Hybrid Model Predictive Controllers (HMPC), relying on multiple degree of freedom parameterizations (Nandola and Rivera, 2013), have been used to facilitate the formulation and implementation of controllers applied to behavioral problems (Deshpande *et al.*, 2014a,b; Dong *et al.*, 2013, 2014).

E-health is defined as an emerging field in the intersection of medical informatics with public health and business, referring to health services and information delivered through the internet and related technologies (Eysenbach, 2001). mHealth (Hekler *et al.*, 2013b) incorporates mobile and wireless interventions. These emerging fields are supported by advances in computing informatics and technology that have allowed the application of engineering principles to areas, like behavioral sciences, that traditionally were not considered because they involved infrequent and/or self-reported measurements.

The behavioral sciences have traditionally utilized three broad methods of scientific inquiry to identify efficacious behavior change strategies including highly-controlled laboratory-based experiments, epidemiologic correlational studies, and randomized controlled trials (Hekler *et al.*, 2013b). mHealth technologies have opened new avenues for gathering a much wider realm of data (e.g., wearable sensors, mobile-phone based sensing, and digital footprints from internet tools like social media) and for intervening upon behavior in context via mobile technologies like smartphones and other wearable technologies (Hekler *et al.*, 2013b). These new data streams and intervention mechanisms have challenged traditional behavioral theories in their ability to provide insights about Intensively Adaptive Interventions (IAI; Riley *et al.* (2015b)). Since behavioral health makes use of theories to guide the research to prevent or treat diseases, promote health, and/or enhance well-being (Collins, 2012), new methods are needed that can take advantage of these new data streams to support more effective theories, and subsequently lead to optimized behavioral interventions (Spruijt-Metz *et al.*, 2015).

1.2 Modeling Behavioral Theories

A prevalent concept for describing behavior change is Social Cognitive Theory (SCT; Bandura (1986)); it has been used as the basis for many health behavior interventions (Lopez *et al.*, 2011; Villanti *et al.*, 2010) and has served as the theoretical basis for most eHealth diet and physical activity interventions (Norman *et al.*, 2007). SCT has a long history rooted in learning theory and the role of respondent and operant conditioning in shaping behavior. The seminal work of Bandura and Walters (1963) on social learning theory expanded learning theory by incorporating observational or vicarious learning. Social learning theory, however, did not include the self-beliefs or perceptions of the individual that could influence behavior, leading to

the introduction of self-efficacy (Bandura, 1977). SCT grew from Self-Efficacy Theory as cognitive, self-regulatory, and self-reflective processes became central to Bandura's thinking (Bandura, 1986).

Health behavior theories such as SCT are conceptual models of the hypothesized influences on behavior and their interrelations, and the assumed linear relations within these models are amenable to various statistical modeling techniques such as Structural Equation Modeling (SEM) developed by Bollen (1989). For example, Anderson-Bill *et al.* (2011) conducted a large, cross-sectional SEM study of a web-based weight management intervention and showed that perceived social support and self-regulatory skills were associated with physical activity and nutrition behavior. Many of the recent SEM studies have been based on a conceptual schematic of SCT published by Bandura (2004). This schematic, shown in Fig. 1.1, depicts self-efficacy directly influencing behavior and also indirectly influencing behavior via its effects on outcome expectancies, goals, and sociocultural factors such as facilitators and impediments. This schematic, however, is a simplified and incomplete conceptual model of SCT when compared to the narrative descriptions of SCT elucidated over decades. For example, SCT specifies a number of factors such as social persuasion and observational learning that influence self-efficacy but the schematic in Fig. 1.1 shows no influences on self-efficacy. SCT postulates that outcome expectancy is influenced by many more factors besides self-efficacy, most prominently the direct and observational experiences of outcomes over time. These additional influences on outcome expectancy are not represented in the schematic, hence a more complete and comprehensive conceptual schematic of SCT is needed to guide statistical and informative dynamical modeling approaches.

Behavior has long been considered amenable to a control systems approach. Hanneman (1988), Powers (1973), and Carver and Scheier (1998) have argued that dynam-

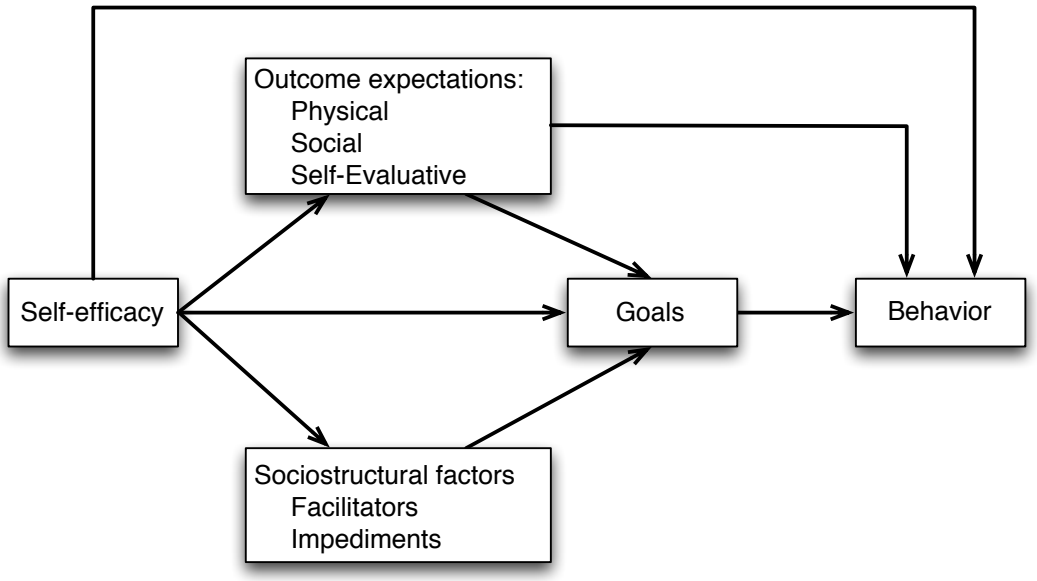

Figure 1.1: Conceptual Schematic of the Social Cognitive Theory (SCT), as Presented in Bandura (2004).

ical regulatory systems are critical to understanding behavior; in that sense significant efforts have been previously made on modeling behavioral theories using control engineering principles. For almost two decades the Theory of Planned Behavior (TPB) (Ajzen and Madden, 1986) has been used to describe the relationship between constructs such as behavior, intentions, attitudes, norms and perceived control. Many behavioral settings have been explained through the TPB framework (Godin *et al.*, 1993; Norman *et al.*, 2000). In the work of Navarro-Barrientos *et al.* (2011) a mathematical representation of TPB was developed relying on a path analysis from Structural Equation Modeling (SEM) that ultimately led to the derivation of a dynamic fluid analogy that parallels the problem of inventory management in supply chains (Schwartz *et al.*, 2006).

A fluid analogy for TPB is shown in Fig. 1.2, where each η_i represents the level of each inventory, coefficients γ_{ij} and β_{ij} are the inflow and outflow resistances re-

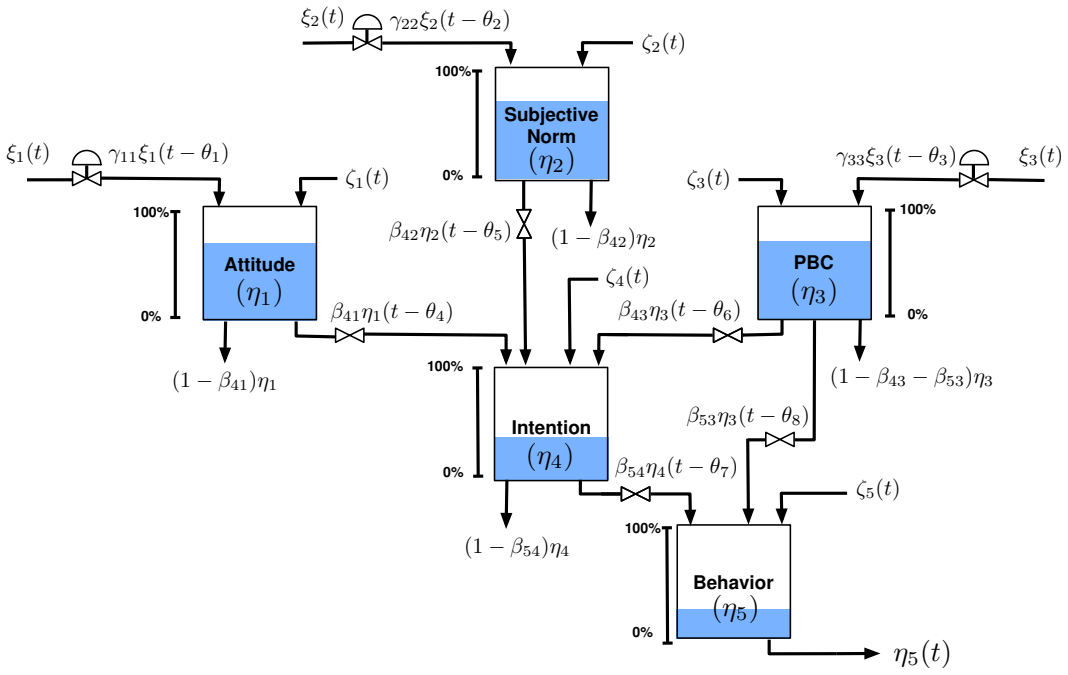

Figure 1.2: Fluid Analogy for the Theory of Planned Behavior (TPB) Presented by Navarro-Barrientos *et al.* (2011). PBC Stands for Perceived Behavioral Control.

spectively, each ζ_i is an external disturbance and coefficients θ_i represent time delays. From the fluid analogy a dynamical system description can be derived by applying the principle of conservation of mass to each inventory in such a way that accumulation corresponds to the net difference between the mass inflows and outflows:

$$\text{Accumulation} = \text{Inflow} - \text{Outflow} \tag{1.1}$$

The TPB dynamical model together with an energy balance physiological model have been applied for behavioral weight change interventions (Navarro-Barrientos *et al.*, 2011) and specifically to address gestational weight gain problems (Dong *et al.*, 2012, 2013).

1.3 Designing System Identification Experiments for Low Physical Activity Behavioral Problems

Nearly 50 % of all deaths can be attributed to behavior, particularly physical inactivity, poor diet, and smoking (Mokdad *et al.*, 2004). These behaviors influence many chronic diseases (e.g., cancer, cardiovascular disease) and rising healthcare costs (Schroeder, 2007). Current behavioral interventions are not completely successful addressing this problem (Conn *et al.*, 2011). Improving interventions will require a transdisciplinary perspective that synergistically integrates and enhances theories and methods from fields including behavioral science, Human Computer Interaction (HCI), and control systems engineering. Like a three-legged stool (Hekler, E.B., Personal comments) as is depicted in Fig. 1.3, an Intensively Adaptive Intervention (IAI; Riley *et al.* (2015b)) can only be supported when the following are integrated into a robust data-supported dynamic theoretical model:

- Lessons from behavioral science about behavior and intervention strategies.
- Insights from HCI on strategies for building usable systems that can fit into a persons daily life for long-term usage
- Methods from control systems engineering for providing a methodology for adapting the intervention to the specific and changing needs of each individual.

The focus is on finding numerical values of the parameters from the SCT dynamical model applied over an open-loop IAI for promoting physical activity, specifically walking/running, among inactive adults aged 21 years or older. In this dissertation walking/running is chosen because:

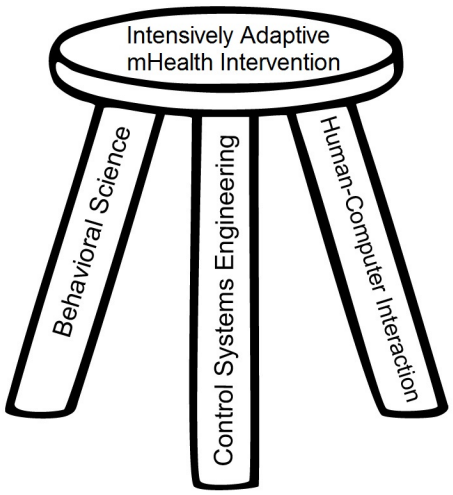

Figure 1.3: Three Legged Stool Analogy for Intensively Adaptive Interventions (IAI; Riley *et al.* (2015b)).

- the availability of current wearable technologies (e.g., Jawbone UPa wrist-worn accelerometry-based activity monitor with valid measurements of steps) that can passively track the behavior and fit into a persons life,
- walking and running are important types of physical activity that impact several health conditions, such as cancer, cardiovascular disease, and diabetes, and
- support is available from behavioral scientists with extensive experience designing and evaluating interventions for steps based on behavioral theory, particularly SCT (King *et al.*, 2013; McMahon *et al.*, 2014).

While the focus is on physical activity, the findings and methods should be applicable across a range of health risk behaviors, thus improving the overall impact of this research. While there are many possible interventions that could be incorporated into a dynamical behavioral model, a logical starting point is to target goal-setting and positive reinforcement, as illustrated in Fig. 1.4.

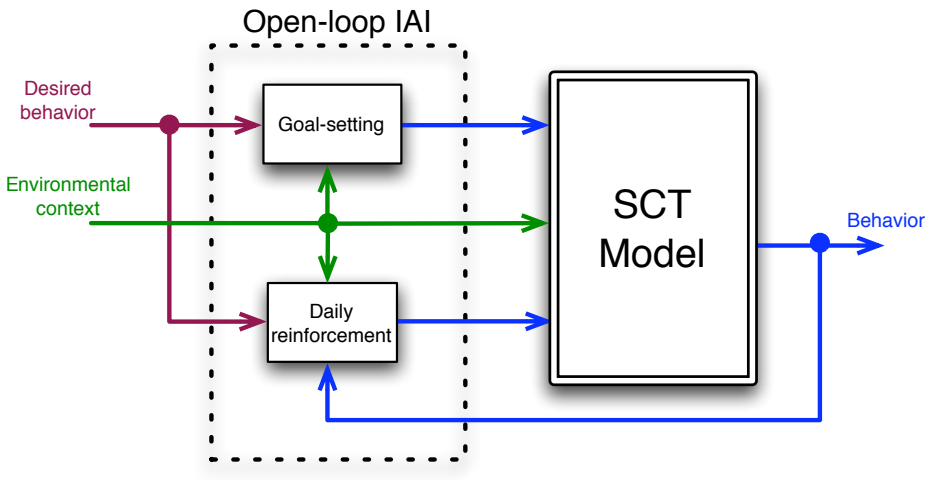

Figure 1.4: Conceptual Representation of the Open-Loop IAI Components Acting on the SCT Model.

Goal-setting is a pivotal behavioral strategy that is utilized in many research- and non-research-based behavioral interventions. Based on the central role of goal-setting, a pivot first decision a IAI would likely need to make is to determine what an appropriate goal should be. To examine this, the recommended daily step goal will be randomized each day pulling from a reasonable range for each person (i.e., baseline median of steps to double the baseline median of steps). Based on previous work (Hekler *et al.*, 2012), a simple intervention that provides only adaptive step goals and positive reinforcement can improve the behavioral performance of a patient.

The second intervention component deals with the amount of points to give after achieving a step goal. This concept is built on earlier work (King *et al.*, 2013; Adams *et al.*, 2013) and general research on token economies (e.g., the mechanism whereby tokens/points are traded in for rewards such as gift cards) as the reinforcement mechanism. Points will be utilized as a reinforcer that could be delivered contingent upon reaching the daily step goal that can then be traded in for self-chosen rewards (e.g.,

gift cards, donations, or social contracts). Much previous research suggests the importance of using a continuous-reinforcement schedule (i.e., contingently providing a reinforcer [points] when a behavioral goal is met) when initiating a behavior (Ferster, 1970).

Input signals content must be judiciously designed to be sufficiently informative such that model with good prediction properties can be obtained, and at the same time considering physical and economic constraints that are particular for a human physical activity situation.

1.4 Closed-loop Intensively Adaptive Intervention

Once a validated model representing *behavior* and the other SCT constructs within the low physical activity behavioral situation is obtained, the logical next step is to design an optimized closed-loop Intensively Adaptive Intervention (IAI) using control engineering principles. The intervention must rely on the same two components: Goal-setting and daily reinforcement. The proposed intervention is illustrated in Fig. 1.5 where feedback is incorporated such that the input values are now defined in dependence of the amount of error between the desired and actual behavior.

The presence of the feedback loop from behavior (i.e., actual steps per day) allows the system to take corrective actions on the inputs to achieve the setpoint tracking goal. If values of SCT model parameters are known, a model predictive control (MPC; Camacho and Bordons (2004)) strategy can be employed, such that outputs can be anticipated with some level of accuracy, and the system can take corrective actions over the inputs promptly. The procedure should also be designed with appropriate levels of rejection to disturbances that may affect the system, whether these are measured or not. The MPC formulation has proven its effectiveness and versatility especially in multivariable control problems with constraints on inputs and/or

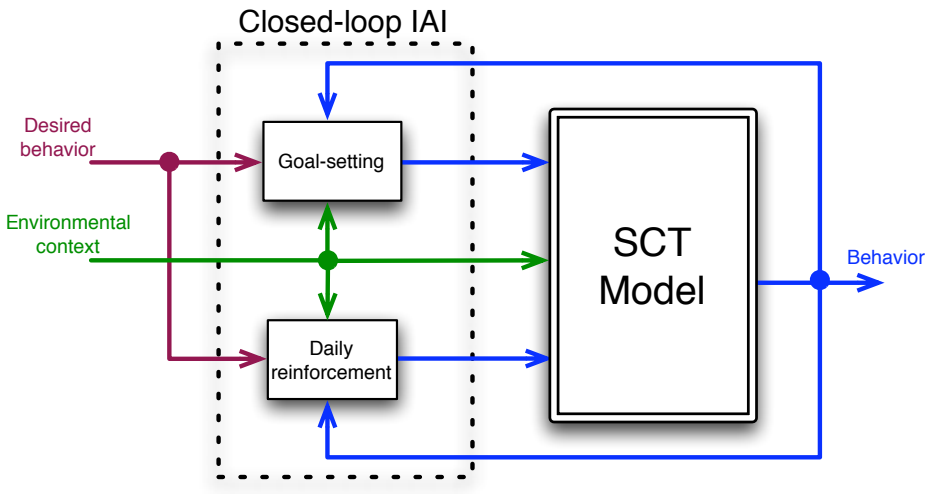

Figure 1.5: Conceptual Diagram of the Closed-Loop IAI Over the SCT Model.

outputs. Behavioral problems deal with discrete intervention dosages to human participants and may include logical considerations. The proposed strategy should be able to consider the simultaneous use of continuous and discrete values in the model states, and/or control inputs; hence a Hybrid Model Predictive Controller (HMPC; Nandola and Rivera (2013)) structure is applied. HPMC is a strategy that has proven its versatility over behavioral problems (Deshpande, 2014; Deshpande *et al.*, 2014b; Dong *et al.*, 2013, 2014).

Finally, one important consideration in the design of the closed-loop intervention is the capability of the system to recognize when individuals have steadily achieved the required level of physical activity, and hence they can move to a long term maintenance phase. The existence of this phase is grounded on the improved capabilities of individuals to maintain their achieved levels of physical activity for longer periods, with fewer reinforcement actions (i.e., rewards).

1.5 Research Goals

This section summarizes the main research goals of this dissertation. At the highest level, the goal is to design an effective long term adaptive behavioral intervention for a low physical activity problem, grounded in a well-recognized behavioral theory and considering the physical, economic and operational constraints that intervening on human behavior requires. The specific research goals are developed on the basis of problems described in previous sections: 1) obtaining a dynamical model for behavior relying on SCT, 2) designing appropriate system identification experiments utilizing open-loop interventions, and 3) designing closed-loop interventions relying on predictive control ideas.

1.5.1 Obtaining a Dynamical Model of SCT

The goal here is to develop a dynamic computational model of SCT based on theoretical descriptions and prior statistical modeling findings with the intent of providing a more complete structural model for statistical modeling approaches, and a dynamic computational model that can take advantage of the intensive longitudinal data becoming available to generate quantitative predictions, testable experiments, and optimized interventions.

1.5.1.1 Basic SCT Model

In contrast to TPB, which has a well-defined graphical representation of the theoretical constructs and their interdependencies (Ajzen and Madden, 1986), the schematic representation of SCT (Bandura, 2004) is a simplified schematic of a more complete theory described primarily in narrative form. Therefore, a more comprehensive conceptual model of SCT is proposed, and this conceptual representation is

extended to a computational model of SCT that represents SCT constructs as state variables and their relations among them as state transitions via differential equations. The SCT conceptual model will be translated to differential equations through the construction of a fluid analogy and a further application of the principle of conservation of mass to each inventory as was described before. The proposed fluid analogy of the SCT is illustrated in Fig. 1.6. It was developed in conjunction with behavioral scientists from our research team (Riley *et al.*, 2015a), and it will be further described in details in Chapter 2.

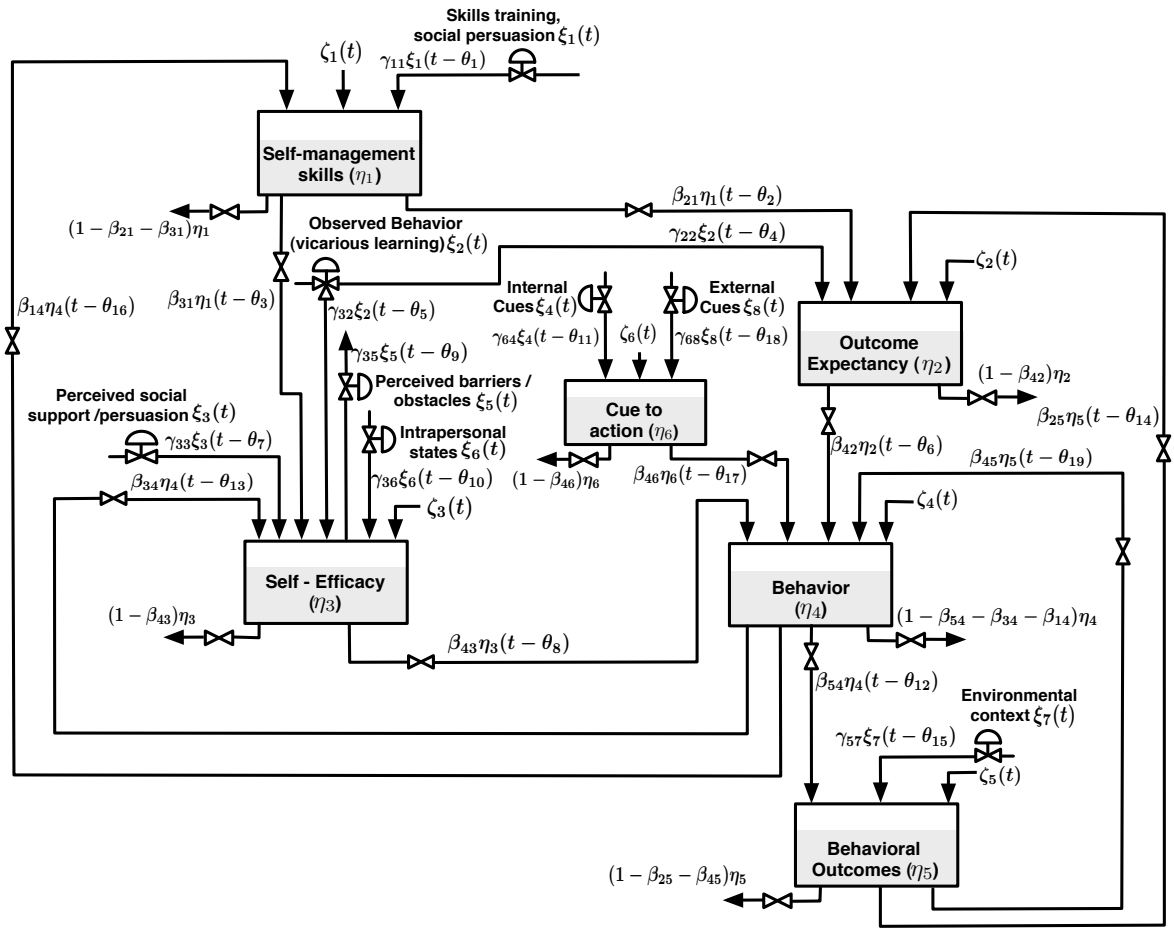

Figure 1.6: Proposed Fluid Analogy for Social Cognitive Theory.

1.5.1.2 Improvements to the SCT Model

There are other well-known phenomena that can be observed in behavioral situations and are not described by SCT, such as habituation (Thompson and Spencer, 1966). This is an important feature of behavioral response resulting from continuous stimulus. These features may be incorporated to the model as additional constructs (i.e., inventories), relationships, or nonlinear actions. These additions to the SCT model should be carefully studied and the decision to incorporate them must be made based on the impact on the specific behavioral problem that is trying to be addressed, and the increased complexity that may result from this addition.

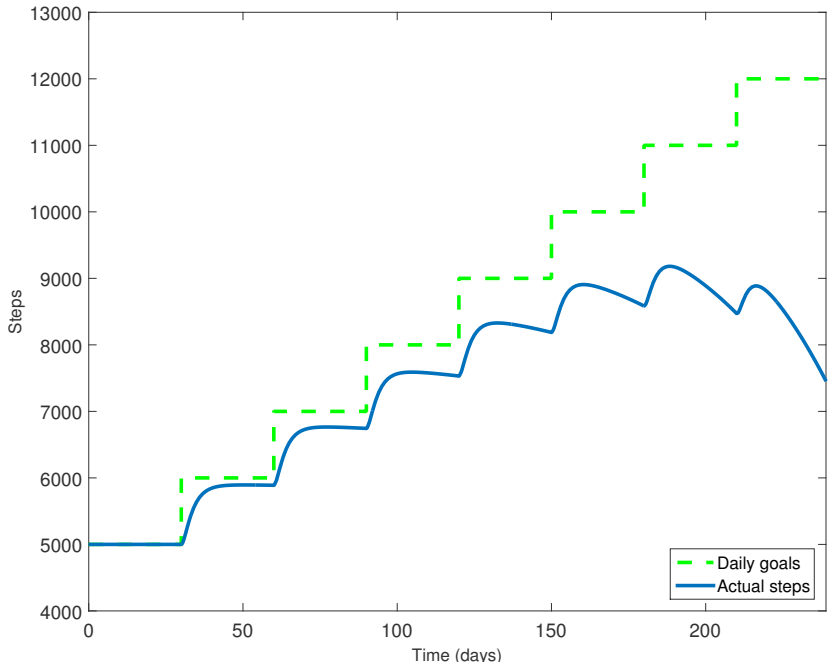

Figure 1.7: Hypothetical Representation of the Inverted U for a Physical Activity Behavioral Problem Showing Step-Goals and Actual Steps.

The persistent application of a given action (e.g., incremented step-goals) may lead to a negative response. An example for a hypothetical physical activity problem

is illustrated in Fig. 1.7 where daily step goals and actual steps are presented. This type of response takes an "inverted U" form (Grant and Schwartz, 2011) and it turns into a feature called the ideal step-goal range that is explained next. If individuals receive step-goals that are incrementing over time, there might be a moment when instead of incrementing their physical activity they tend to reduce it. This effect is caused by a reduction on their perceived capability to perform the behavior caused by a goal that they consider too ambitious to reach. Based on this effect each individual should possess an ideal step-goal range where the goals are ambitious but doable.

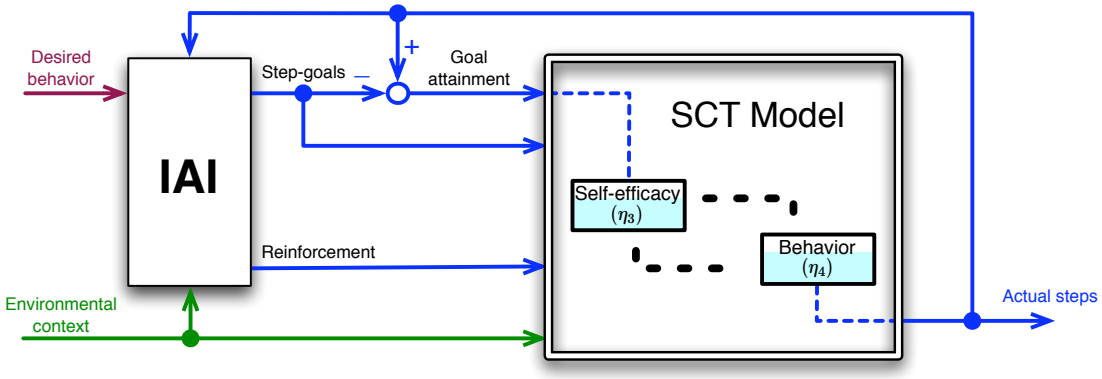

Figure 1.8: Proposed Improvement to the SCT Model to Incorporate the Ideal Step-Goal Range Feature Over the Intensively Adaptive Intervention (IAI).

One alternative to incorporate this feature to the SCT model is to introduce the *self-efficacy* inventory with a signal that represents how much confidence individuals may earn or lose, if they achieve or not the set goal for a given day. This signal is called *goal attainment*, and is represented by the difference between the actual steps and the set goal for a specific day as is depicted in Fig. 1.8. If individuals meet or surpass the set goal on a given day, the *self-efficacy* level is incremented and future behavior is reinforced; on the other hand, if the goal is not achieved *self-efficacy* receives a negative effect, and the ability to reach more steps in the future is affected.

More details are presented in Section 2.7.2.

For validation purposes a subsection of the model will be contrasted to data from a real physical activity intervention through the use of semi-physical identification methods. Results will give an insight about the capability of the model to represent behavioral situations.

1.5.2 Designing System Identification Experiments

Once the structure of the SCT dynamic model has been specified, the next step is to design system identification experiments that are sufficiently informative to allow the estimation of numerical values for the model parameters. Initially little information is available about the dynamic nature of the system; hence the proposed approach starts with the formulation of an informative experiment utilizing some of the typical choices of input signals for system identification (e.g., Random, PRBS, multisine, etc.). Results from the informative experiment serve as a basis for a final experiment to find the model parameters. This experiment is formulated as an optimization problem.

1.5.2.1 Design of an Informative Experiment

The primary goal of the informative experiment is to glean insights about the dynamic properties of the system through the estimation of model parameters (i.e., gains, time constants). The experiment will be designed *a priori* based on previous work focused on modeling the individual and collective impact of intervention components on physical activity in a peer-led counseling intervention (Hekler *et al.*, 2013a). This approach is important because standard population-level clinical trials, while useful for providing insights on the efficacy of an intervention package, are not suitable for understanding the individual dynamic response to intervention components,

particularly over time at an idiographic (i.e., single-subject) level.

The intervention components (i.e., inputs) at any sampling instant k are represented by $u(k)$ and they have to be implemented under strict clinical constraints such as high/low limits on the intervention component levels

$$u_{min} \leq u(k) \leq u_{max}, \quad \forall k, \tag{1.2}$$

bounded rates of change

$$|u(k) - u(k-1)| \leq b, \quad \forall k, \tag{1.3}$$

and how often the mechanism can change via a switching time (T_{sw}) constraint

$$\sum_{j=1}^{T_{sw}-1} \big(u(k) - u(k+j)\big) = 0, \quad \forall k = 1 + n \cdot T_{sw}, \quad n = 0, 1, 2, \ldots \tag{1.4}$$

The central idea is to introduce variability in data that can help capture the inherent dynamical relationships. As this is an idiographic study design, each individual will receive a different experimental design based on control systems methods of pseudo randomization to support orthogonal (i.e., statistically independent) delivery of intervention components. The first intervention component goal-setting, will be generated among a series of goals from an initial baseline behavior (e.g., 5000 daily steps) and the target value of 10000 steps. For the second intervention component, the focus will be on varying the amount of reinforcement points (i.e., the number of points provided per day) available to glean insights about the appropriate amount of points to provide for any given behavioral response.

1.5.2.2 Design of an Optimized Experiment

The primary goal of the optimized experiment is to delineate a judiciously-selected protocol for allowing intervention features to be systematically activated and deacti-

vated and reactivated taking into account an improved understanding of the behavior change process brought about by the informative experiment.

The proposed design is posed as an open-loop optimal control problem. It is assumed that an *a priori* input-output model is known from insights from the SCT model and informative experiment. For the purpose of illustration, it is assumed that the interest is in modeling the dynamical relationship G between points given for a pre-specified behavioral threshold (e.g., 10,000 steps per day) using the SCT framework. In the proposed approach an input (daily reinforcement) sequence over time is designed such that it reinforces behavior to reach a desired output y_{des} (behavioral threshold) which can vary over time. This is achieved by assigning points so that the participant reaches the desired behavioral trajectory as closely as possible. Mathematically, this can be written as:

$$\min_{u \in \mathbf{U}} \|G \cdot u - y_{des}\| \tag{1.5}$$

where $\mathbf{U}$ is defined by the set of linear inequalities (amplitude and move restriction on input) and equalities (switching time constraint) and the objective function considers the 2-norm of the error. The resulting optimization problem is, in general, a convex mixed-integer quadratic program that can be efficiently solved, for most problems in practice, using commercial solvers such as Gurobi and CPLEX.

One of the challenges of the design procedure is how to incorporate logical conditions into the optimization routine to consider the deliverance of reward points based on the attainment to the behavioral threshold. Fig. 1.9 illustrates the process through what is called the "If/Then" block. At the beginning of the day an specific amount of available points is offered to the patient such that at the end of the day the actual behavior (i.e., performed steps) is compared to the set goal. If the goal was achieved then the announced available points are granted to the individual, and they become

the granted reinforcement points.

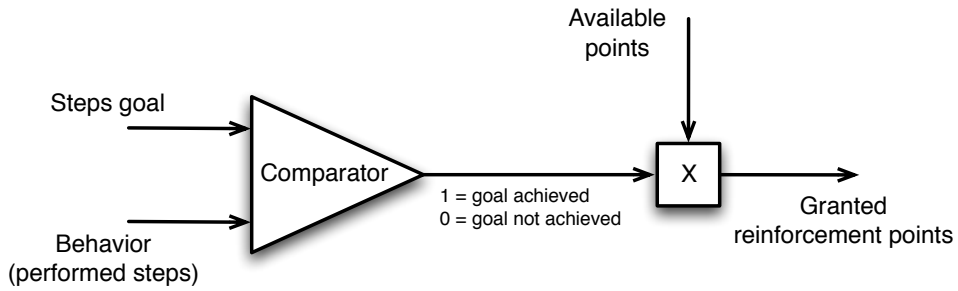

Figure 1.9: Conceptual Representation of the "If/Then" Block That Defines the Deliverance of Reward Points in Dependence of the Goal Attainment.

The "If/Then" block must be incorporated within the optimization procedure that search for values of the intervention components. This will be done by defining logic constraints through a big-M formulation (Williams, 2013) that uses the following elements to represent such type of conditions:

- Auxiliary binary variables to represent each logic condition.
- Maximum and minimum bounds for each involved continuous variable.
- Relational operators ($\leq$ and $\geq$) to represent worst case conditions using the maximum and minimum bounds.

Another goal of the optimized experiment is to obtain input signals with less variability according to patient-friendly definitions (Deshpande *et al.*, 2012). This is done inherently by the optimization procedure and via the move size constraint described in (1.3). The performance in terms of this feature will be measured and contrasted to results from the informative experiment.

1.5.2.3 Redesign of the Informative Experiment Using an Identification Test Monitoring Approach

During the formulation of the informative experiment, the time length was considered fixed and was defined based on previous physical activity interventions. However "patient-friendliness" concepts motivate the search for the shortest necessary duration of the experiment. This is a very important consideration in behavioral settings where interventions can last months and resources can be consumed quickly. To address this problem, the proposed approach uses *identification test monitoring*, a concept presented by Rivera *et al.* (2003), with the purpose of finding the shortest possible experimental data set with sufficient information for an adequate identification, in terms of specific pre-defined conditions of the problem, and assuming that noise is the main source of uncertainty in the estimation procedure.

The identification test monitoring procedure relies on the computation of statistical uncertainties associated with nonparametric frequency domain estimation procedures. For a SISO system the additive uncertainty ℓ_a between a real plant G and its estimate $\hat{G}$ for each frequency ω can be defined as:

$$\ell_a(\omega) = |G(\omega) - \hat{G}(\omega)|, \quad \forall\omega \tag{1.6}$$

Additive uncertainties can be statistically characterized to a specified probability as is illustrated in Fig. 1.10 where confidence regions are drawn as circles of radius ℓ_a over each frequency estimate.

Deterministic and periodic input signals can be used to compute statistical uncertainties in more accurate settings. Multisine signals meet the specified features and their spectrum can be constructed by the designer in such a way the frequency grid of interest can be directly specified. Another advantage of multisine signals is that they allow the construction of orthogonal in-frequency signals, a feature that is very

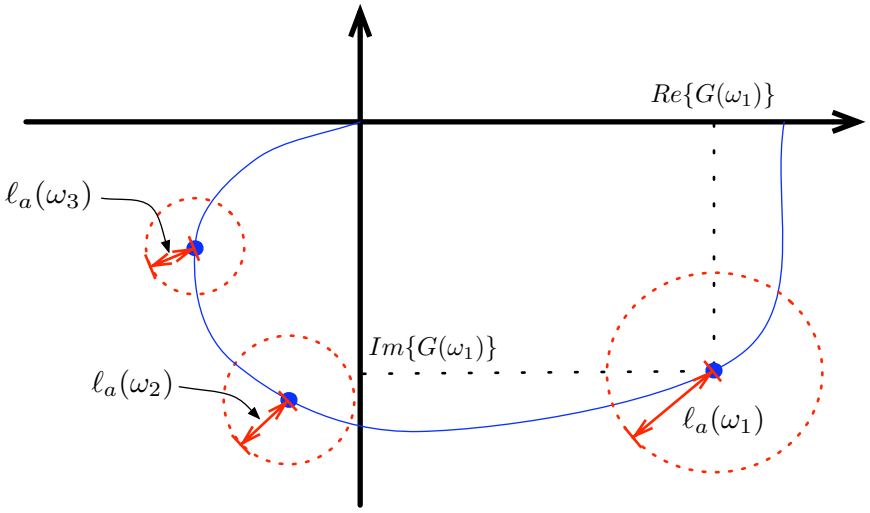

Figure 1.10: Representation of Statistical Confidence Regions for a Given Probability at Each Frequency Point, Based on Additive Uncertainties for Transfer Function Estimates $\hat{G}$ and Presented Over a Nyquist Plot.

important for the MIMO formulation. A basic specification of a multisine signal $u(k)$ at any sampling instant k is:

$$u(k) = \lambda \sum_{j=1}^{n_s} \sqrt{2\alpha_j} \cos(\omega_j k T + \phi_j) \qquad (1.7)$$
$$\omega_j = \tfrac{2\pi j}{N_s T}, \quad k = 1, \ldots, N_s$$

where N_s is the signal period, $n_s \leq N_s/2$ is the number of sinusoids (i.e., number of frequencies in the grid), T is the sampling time, α_j is a factor used to specify the relative power of the jth harmonic, ω_j is frequency, λ is a scaling factor, and ϕ_j is the harmonic phase. In this dissertation, two different approaches for transfer function and uncertainty computations are presented:

Uncertainty Computations Based on the Empirical Transfer Function Estimation (ETFE) Method

Based on this representation for a SISO plant, and using the Empirical Transfer Function Estimation (ETFE) method (Ljung, 1999) to estimate the plant model, Bayard (1993) computed the following additive uncertainty with a statistical confidence of $(1-\rho)\times 100\%$:

$$\ell_a^2(\omega) = \frac{2\hat{\sigma}^2|\overline{W}(\omega)|^2}{\alpha_j m N_s} F_{1-\rho}(2, mN_s - 2n_s) \tag{1.8}$$

where m is the number of cycles that the original multisine signal has been repeated, $F_{1-\rho}(\nu_1,\nu_2)$ denotes the $(1-\rho)\times 100$ percentiles for a Fisher distribution with ν_1 over ν_2 degrees of freedom, $\overline{W}(q)$ is a known stable transfer function representing the effect of output noise disturbance in the system, and $\hat{\sigma}^2$ is the output noise variance estimator.

The computation of statistical uncertainties will be adjusted to consider a Multiple Input Multiple Output (MIMO) plant, such as the one defined for the SCT model. It also includes the definition of multisine signals that are orthogonal in-frequency using a "zippered" power spectra design (Rivera *et al.*, 2009) to allow the representation of independent transfer functions for each input-output direction of the MIMO plant. This method requires that data is considered at steady state; hence no changes on the input signal content (e.g., amplitude or frequency content) are allowed.

Uncertainty Computations Based on the Local Polynomial Method (LPM)

The Local Polynomial Method (LPM) for periodic signals (Pintelon *et al.*, 2011) is utilized to incorporate some additional features that will help to present its application in a more general setting. The included features are

- Increments on input signal amplitudes at each decision cycle with the purpose of increase persistence of excitation while maintaining the system under operating conditions.

- Frequency content adjustments on the signal period at each decision cycle. This must be done by using harmonically related frequency grids such that the uncertainty computation can be aggregated from one cycle to the other.

- The use of LPM enables the incorporation of the two previous features, since it considers the transient terms for transfer function and uncertainty computation; hence sampled data can be used without the necessity of waiting for steady state conditions.

Relying on the LPM estimates, a $100 \times (1-\rho)\%$ circular confidence region (Pintelon and Schoukens, 2012) can be constructed as

$$\ell_a(\omega) = \sqrt{-\ln \rho}\ \hat{\sigma}_{\hat{G}}(\omega) \tag{1.9}$$

where $\hat{\sigma}^2_{\hat{G}}(\omega)$ is the sample variance of the estimated transfer function at a given frequency ω.

According to the identification test monitoring premise, uncertainties are computed at every cycle of the multisine input signal(s), and their value will influence in the decision to halt or continue the experiment. Stopping criteria will be defined and computed considering the following facts:

- Consideration of uncertainties in one individual transfer function element, as well as a more general multivariable uncertainty bound that can be computed considering maximum singular values at each frequency.

- The initial approach for computation of open-loop stopping criteria relies on the percentage change on uncertainties from one iteration to the other; subsequently, a control-related stopping criterion can also be defined relying on robust performance ideas.

To evaluate the use of robust performance ideas for the monitoring procedure, the following assumptions are made: The bound $\bar{\ell}_a$ is interpreted as a scalar weight on a normalized additive perturbation $\Delta_a(s)$, where the total perturbation is $L_A(s)$

$$L_A(s) = \bar{\ell}_a \cdot \Delta_a(s), \quad \bar{\sigma}(\Delta_a(\omega)) \leq 1 \quad \forall\omega \tag{1.10}$$

and the symbol $\bar{\sigma}(\cdot)$ stands for the maximum singular value of a matrix. The block diagram representation of the additive uncertainty of an estimated plant $\tilde{P}$ within a closed loop system is shown in Fig. 1.11, where C is a feedback controller, d' is a disturbance input and w_P is a performance scalar weight. Under these conditions and

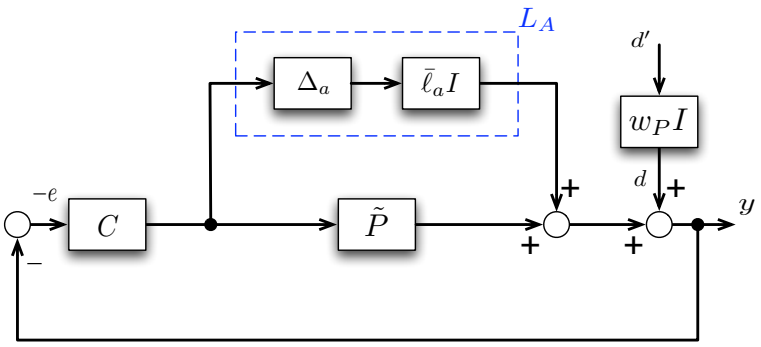

Figure 1.11: Block Diagram of a Closed-Loop System Subject to Additive Uncertainty $L_A = \bar{\ell}_a \cdot \Delta_a$.

considering a H_∞ performance objective, the robust stability and robust performance conditions (Morari and Zafiriou, 1989) are satisfied if:

$$\bar{\sigma}(w_P\tilde{E}) + \bar{\sigma}(\bar{\ell}_a\tilde{P}^{-1}\tilde{H}) \leq 1, \quad \forall\omega \tag{1.11}$$

where $\tilde{P}$ is the nominal plant represented by the estimated frequency response; $\tilde{E}$ and $\tilde{H}$ are the sensitivity and complementary sensitivity respectively, calculated as:

$$\tilde{E} = (I + \tilde{P}C)^{-1} \tag{1.12}$$

$$\tilde{H} = \tilde{P}C(I + \tilde{P}C)^{-1} \tag{1.13}$$

The stopping criterion must state that the experiment can be halted if the condition presented in (1.11) is satisfied for a pre-defined number of contiguous cycles. Complete details are presented in Chapter 3.

1.5.3 Designing Closed-loop Interventions Relying on Hybrid Predictive Model Control Ideas

The goal is to design a closed-loop Intensively Adaptive Intervention (IAI) utilizing control engineering principles, and specifically Hybrid Model Predictive Control (HMPC) ideas to deal with the discrete natural condition of signals in behavioral settings. The proposed approach is presented in Fig. 1.5 where the basic intervention components are

- A *goal-setting* (u_8) component focused on establishing the appropriate goal for each individual (e.g., 10,000 steps).
- A *daily reinforcement* action (u_9, u_{10}), that represents a measure of the daily available reward points that are under the knowledge of the participant, that are eventually delivered to the individuals based on their behavioral achievements. Points must have an equivalent to tangible rewards (e.g., gift cards).

In general, model predictive control is a strategy that effectively uses knowledge of the dynamical model to predict the performance of the system over a finite time horizon, and hence finding the best set of inputs via an optimization problem such that the control goals (e.g., setpoint tracking, disturbance rejection) are accomplished. The system states and outputs are computed over a prediction horizon p, while the optimal inputs are found for a move horizon m; however the inputs are applied only

at the actual time. This is a receding horizon control strategy and is illustrated in Fig. 1.12 for manipulations of step goals (u_8) only. It is assumed that the measured disturbance component (d) can be forecasted for the prediction horizon.

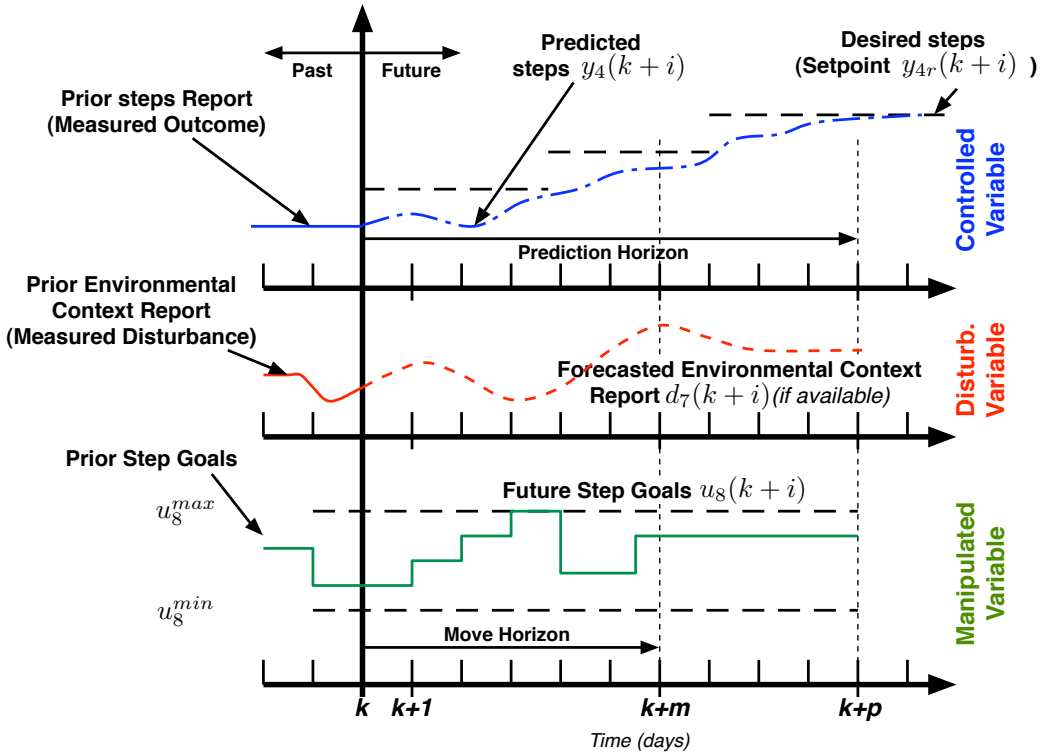

Figure 1.12: Conceptual Representation of the Receding Horizon Control Strategy to the Physical Activity Behavioral Problem With Control Moves Computed Only for Step Goals (u_8), and Considering Steps (y_4) as the Output and Environmental Context ($d_7 = \xi_7$) as a Measured Disturbance.

The HMPC formulation considers the simultaneous description of continuous and discrete states and inputs. This is achieved via a mixed logical and dynamical (MLD) structure (Bemporad and Morari, 1999). The system is represented by

$$x(k+1) = Ax(k) + B_1u(k) + B_2\delta(k) + B_3z(k) + B_dd(k) \tag{1.14}$$

$$y(k+1) = Cx(k+1) + d'(k+1) + v(k+1) \tag{1.15}$$

$$E_2\delta(k) + E_3 z(k) \leq E_5 + E_4 y(k) + E_1 u(k) - E_d d(k) \tag{1.16}$$

where $u(k), x(k), y(k), d(k), d'(k)$ are vectors representing the control inputs, states, outputs, measured and unmeasured disturbances respectively, $\delta(k)$ and $z(k)$ are auxiliary variables for the MLD formulation. The remaining variables are described in Chapter 5. The optimization problem consist of finding the sequence of control actions $u(k)$,.., $u(k+m-1)$, $\delta(k)$,.., $\delta(k+p-1)$, and $z(k)$,.., $z(k+p-1)$ that solves

$$\begin{aligned}\min_{\{[u(k+i)]_{i=0}^{m-1},[\delta(k+i)]_{i=0}^{p-1},[z(k+i)]_{i=0}^{p-1}\}} & \sum_{i=1}^{p} \|y(k+i) - y_r\|_{Q_y}^2 + \sum_{i=0}^{m-1} \|\Delta u(k+i)\|_{Q_{\Delta u}}^2 \\ + \sum_{i=0}^{m-1} \|u(k+i) - u_r\|_{Q_u}^2 & + \sum_{i=0}^{p-1} \|\delta(k+i) - \delta_r\|_{Q_\delta}^2 + \sum_{i=0}^{p-1} \|z(k+i) - z_r\|_{Q_z}^2\end{aligned} \tag{1.17}$$

subject to (1.16) and

$$y_{min} \leq y(k+i) \leq y_{max}, \quad 1 \leq i \leq p \tag{1.18}$$

$$u_{min} \leq u(k+i) \leq u_{max}, \quad 0 \leq i \leq m-1 \tag{1.19}$$

$$\Delta u_{min} \leq \Delta u(k+i) \leq \Delta u_{max}, \quad 0 \leq i \leq m-1 \tag{1.20}$$

where y_r, u_r, δ_r, and z_r are the referential (i.e., desired) values for each respective signal.

One objective of the closed-loop IAI is to ensure that individuals maintain their levels of physical activity even after the initial, and more aggressive, part of the intervention has been completed. The idea is to keep monitoring the performance of participants to detect when they have reached the required levels of behavior for a predefined time interval. If that is the case, the system can be moved to a second maintenance phase where reward points can be partially or completely removed such that individuals continue following step goals based on their achieved self-efficacy levels. This can be implemented over the HMPC approach by reconfiguring the

weight matrices (Q_u) for the required inputs, in the optimization problem presented in (1.17). A detailed formulation of the problem is presented in Chapter 5.

1.6 Contributions of the Dissertation

This dissertation presents a framework for the design of effective intensively adaptive interventions based on control systems principles for low physical activity behavioral problems. The development definition of identification test monitoring is consequently described. Different research activities have been developed in several stages, covering important aspects of design procedures.

The contributions of this work in terms of modeling behavioral theories can be summarized as follows:

- Development of a novel dynamical systems model for Social Cognitive Theory (SCT), relying on fluid analogies to represent the relations among different constructs as are described in narrative form by the theory. The modeling study includes the definition of operational and stability conditions.

- Enhancement of the model by incorporating habituation, a nonlinear phenomenon. This is performed via a parameter varying technique using a gain scheduling approach.

- Application of semiphysical system identification routines to find values for parameters according to the SCT model, for a given noise set of input-output data.

- Incorporation of model improvements motivated by the physical activity problem. In particular, understanding the ideal step-goal range of individuals, achieved by linking the effect of *goal attainment* to *self-efficacy*.

The contributions of this dissertation in terms of designing system identification experiments in an open-loop intensively adaptive behavioral intervention are

- Development of an open-loop system identification experiment using random yet bounded input signals.

- Development of a novel MIMO identification test monitoring procedure to find the shortest possible experiment with sufficient information for identification purposes. This approach relies on the computation of frequency domain transfer function estimates, yielding to the definition of additive uncertainty bounds that are used in the formalization of stopping criteria that enable the decision to halt or continue the experiment.

- Development of an enhanced identification test monitoring procedure incorporating transient responses in the computation of transfer functions and uncertainties, such that additional input signal modifications can be considered. These additional modifications over the input signals are: amplitude modifications, and changes on the harmonic frequency content.

- Formulation of more general stopping criteria for MIMO identification test monitoring. These criteria rely on the application of robust control ideas over a closed-loop representation.

- Development of a novel optimized system identification experiment utilizing initial results from the informative experiment. This experiment is formulated as an optimization problem where the objective is to track a desired output behavior profile, relying on the informative model, and under operational and economic constraints.

In terms of designing a long term closed-loop Intensively Adaptive Intervention (IAI) for the physical activity behavioral problem, the contributions of this dissertation are

- Development of an intervention algorithm relying on Hybrid Model Predictive Control (HMPC) framework that is able to personalize the discrete level of interventions components, reaching the objectives of setpoint tracking, and disturbance rejection.

- Extension of the mixed logical dynamical (MLD) structure to allow the formulation of structures that are specific to the behavioral problem. This was used to represent the effect of the If/Then block that allows the deliverance of reward points when the set goal has been achieved.

- Development of a reconfiguration strategy of HMPC parameters to allow the introduction of the maintenance stage, where rewards might be reduced based on the incremented capacity of individuals to reach the set goal. This is done by reconfiguring the weight matrices used in the objective function for optimization.

1.7 Dissertation Outline

Following this introduction, the dissertation continues with Chapter 2 that presents the detailed formulation of the dynamical systems model for SCT. The chapter shows how the fluid analogy is developed, including the definition of a system of differential equations that represents the model. Model enhancements are also presented, incorporating two important behavioral features: habituation and ideal range for step-goals. The semiphysical identification procedure is presented and the model is validated via simulation of representative cases and reconciliation to a data set from

an actual physical activity intervention.

In Chapter 3 the general multivariable identification test monitoring procedure is presented. A frequency domain approach for computing transfer functions and uncertainties is developed. Two different alternatives are proposed: the first relies on Empirical Transfer Function Estimates (ETFE) utilizing sampled data measured at steady state. The second approach uses the Local Polynomial Method (LPM), which includes the effects of transient responses, such that additional modifications in the inputs are allowed. A general stopping criterion is also developed relying on robust control ideas. Finally a simulation study is presented using as a reference, a process control plant model.

Chapter 4 describes how open-loop behavioral intensively adaptive interventions are developed for system identification purposes. The design of the informative and optimized experiments is detailed. For the informative experiment two different approaches are presented: the first one using random generated input signals under operational constraints; the second one uses multisine input signals with frequency content specifically designed to excite frequencies of interest. The two different identification test monitoring approaches are applied (i.e., utilizing ETFE or LPM), and a complete simulation study representing a hypothetical low physical activity problem is presented.

Chapter 5 presents the design of closed-loop intensively adaptive behavioral interventions with the purpose to reach and sustain the required amount of physical activity. The design procedure relies on Hybrid Model Predictive Control (HMPC) ideas that allow the simultaneous use of discrete and continues values for inputs and states. The chapter describes how the HMPC algorithm is adapted and improved to represent the discrete nature of the behavioral intervention components and some of the logical blocks of the model. Some of the HMPC parameters are reconfigured

during experimental execution to allow the initiation of a maintenance stage where behavior is sustained mainly by the improved capacity of individuals earned in the early stages of the intervention. During this phase, rewards can be partially removed.

Finally the dissertation concludes in Chapter 6 with a summary and conclusions of the major contributions of this work. The chapter includes directions and suggestions for future work.

1.8 Publications

The material presented in this dissertation has been taken primarily from a series of published and submitted papers with the following detail: The material for Chapter 2 has been taken from:

1. C. A. Martín, D. E. Rivera, W.T. Riley, E. B. Hekler, M. P. Buman, M. A. Adams and A. C. King. A dynamical systems model of Social Cognitive Theory. In *Proceedings of the 2014 American Control Conference (ACC)*, pages 2407-2412, July 2014. (Martín *et al.*, 2014).

2. W.T. Riley, C. A. Martín, D. E. Rivera, E. B. Hekler, M. A. Adams, M. P. Buman, M. Pavel and A. C. King. Development of a dynamical systems model of Social Cognitive Theory. In *Translational Behavioral Medicine: Practice, Policy and Research*, pages 1 - 13, November 2015, doi = 10.1007/s13142-015-0356-6. (Riley *et al.*, 2015a).

Contents from this chapter have been partially adapted into the following papers:

3. W.T. Riley, C. A. Martín, and D. E. Rivera. The importance of behavior theory in control system modeling of physical activity sensor data. In *Proceedings of the 2014 36th Annual International Conference of the IEEE Engineering in*

Medicine and Biology Society, pages 6880 - 6883, August 2014. (Riley *et al.*, 2014).

4. K. P. Timms, C. A. Martín, D. E. Rivera, W.T. Riley, and E. B. Hekler. Leveraging intensive longitudinal data to better understand health behaviors. In *Proceedings of the 2014 36th Annual International Conference of the IEEE Engineering in Medicine and Biology Society*, pages 6888 - 6891, August 2014. (Timms *et al.*, 2014a).

5. E. B. Hekler, P. Klasnja, W. T. Riley, M. P. Buman, J. Huberty, D. E. Rivera, and C. A. Martín. Agile science: creating useful products for behavior change in the real world. In *Translational Behavioral Medicine*, volume 6, issue 2, pages 317 - 328, 2016. (Hekler *et al.*, 2016).

The material from Chapter 3 has been adapted from:

6. C. A. Martín, D. E. Rivera, and E.B. Hekler. An identification test monitoring procedure for MIMO systems based on statistical uncertainty estimation. In *Proceedings of the* 54^{th} *Conference on Decision and Control (CDC) 2015*, pages 2719 - 2724, December 2015. (Martín *et al.*, 2015c).

7. C. A. Martín, D. E. Rivera, and E.B. Hekler. An enhanced identification test monitoring procedure for MIMO systems relying on uncertainty estimates. Submitted to *the* 55^{th} *Conference on Decision and Control (CDC) 2016*. (Martín *et al.*, 2016b).

Contents of Chapter 4 have been adapted from:

8. C. A. Martín, S. Deshpande, E.B. Hekler, and D. E. Rivera. A system identification approach for improving behavioral interventions based on Social Cognitive

Theory. In *Proceedings of the 2015 American Control Conference*, pages 5878 - 5883, July 2015. (Martín *et al.*, 2015a).

9. C. A. Martín, D. E. Rivera, and E.B. Hekler. Design of informative identification experiments for behavioral interventions. In *Proceedings of the 17th IFAC Symposium on System Identification, SYSID 2015*, pages 1325 - 1330, October 2015. (Martín *et al.*, 2015b).

Finally, the material presented in Chapter 5 is described in:

10. C. A. Martín, D. E. Rivera, and E.B. Hekler. A decision framework for an adaptive behavioral intervention for physical activity using hybrid model predictive control. In *Proceedings of the 2016 American Control Conference*, pages 3576 - 3581, July 2016. (Martín *et al.*, 2016a).

The following publications are submitted or under preparation:

1. C. A. Martín, D. E. Rivera, W.T. Riley, E. B. Hekler, M. P. Buman, M. A. Adams, and A. Magann. Development of a dynamical model of Social Cognitive Theory for adaptive behavioral interventions. To be submitted to *IEEE Transactions on Control Systems Technology*.

2. D. E. Rivera, C. A. Martín, K. P. Timms, S. Deshpande, N.N. Nandola, and E.B. Hekler. Control systems engineering for optimizing behavioral mHealth interventions. In S. Murphy, J. Rehg, and S. Kumar (Eds.) *Mobile health: sensors, analytic methods, and applications*, 2016.

3. C. A. Martín, D. E. Rivera, and E.B. Hekler. A control engineering approach for optimizing physical activity behavioral interventions. Submitted to *IEEE Ecuador Technical Chapters Meeting (ETCM)*, 2016.

4. E.B. Hekler, D.E. Rivera, C.A. Martin, P. Klasnja, W.T. Riley, M.P. Buman, M. Adams, S. Phatak, E. Korinek, and M. Freigoun. Control-System Driven Intensively Adaptive Interventions: A Detailed Account on how Control Systems Engineering Can be Used to Advance Behavioral Science Theory and Practice.

5. E. Korinek, S. Phatak, D.E. Rivera, C.A. Martin, M. Freigoun, and E.B. Hekler. EAdaptive Step Goals: A longitudinal growth model of daily steps for a smartphone-based walking intervention.

6. S. Phatak, E. Korinek, D.E. Rivera, C.A. Martin, M. Freigoun, and E.B. Hekler. A System Identification Validation Study of a Dynamical Model Version of Social Cognitive Theory.

The following are additional journal publications that are anticipated from this dissertation:

1. C. A. Martín, D. E. Rivera, and E.B. Hekler. A MIMO approach for the formulation of identification test monitoring experiments relying in robust performance ideas.

2. C. A. Martín, D. E. Rivera, and E.B. Hekler. Designing informative and optimized system identification experiments for open-loop physical activity behavioral interventions.

3. C. A. Martín, D. E. Rivera, and E.B. Hekler. Decision policies for closed-loop physical activity behavioral interventions relying on a HMPC formulation.

Chapter 2

MODELING BEHAVIORAL INTERVENTIONS USING SOCIAL COGNITIVE THEORY

2.1 Overview

Behavioral theories play a central role in the creation of behavior change strategies and thus their choice within a specific problem is important. Social Cognitive Theory (SCT) has been used as the basis for many behavioral interventions (Lopez *et al.*, 2011); it provides a conceptual framework of the theorized influences on behavior and their interdependences that is amenable to various modeling techniques. Robust computational modeling approaches can provide a flexible and rigorous test to confirm, revise, or refute SCT and other theories (Nilsen and Pavel, 2013). Further computational models can aid in better specifying contextually relevant and instantaneous interrelationships measured continuously via mobile and wireless technologies. In a recent review of mobile health interventions, SCT or one of its variants served as the basis for all smoking cessation interventions that reported a theoretical basis and was the predominant theoretical basis for weight management interventions reviewed (Riley *et al.*, 2011).

While not specified in SCT, external stimuli are shown to affect behavior according to the principles of behavioral response habituation (Thompson and Spencer, 1966), including: decreased responses following repeated application of stimuli, recovery of responses when stimuli are withheld, and reduction of responses with increased stimulation frequency. To then illustrate that the effectiveness of an increasing positive stimulus in humans is often nonmonotonic, an "inverted U" phenomenon (Grant and

Schwartz, 2011) has been incorporated into the linear SCT model. For the case of low physical activity, this feature is expressed as an ideal range of step goals dependent on the current level of training and predisposition to walk of individuals.

In this chapter, a dynamical systems model for SCT is proposed based on its constructs and interrelationships (Bandura, 1986). Simulations of the model using physical activity of individuals over time as a referential behavior are performed. The model features a nonlinear structure that addresses habituation, and some linear modifications to represent the ideal range of step goals. Through a semi-physical identification procedure, a subsection of the model is reconciled to actual data from MILES, a lifestyle intervention involving mobile technology. A model like the one proposed in this paper can ultimately serve as the controller model in an intensively adaptive intervention using MPC (Riley *et al.*, 2015b; Nandola and Rivera, 2013).

The chapter is organized as follows: Section 2.2 presents a brief description of SCT and its core elements. Section 2.3 describes the development of the fluid analogy based on the interconnections between the constructs and components of SCT. Section 2.4 presents how the model was constructed including mathematical details, assumptions and how habituation is represented. Section 2.5 discusses simulation results for a hypothetical case study. Section 2.6 contrasts experimental data obtained from a physical activity intervention against simulations using the model. Section 2.7 presents model improvements that can be applied specifically to a physical activity intervention.

2.2 Social Cognitive Theory

Social Cognitive Theory (SCT) has its basis in early learning theory, which does not account for behaviors learned by means other than prior experience. This led to the seminal work of Bandura (Bandura and Walters, 1963) on Social Learning Theory

(SLT), which incorporated the principles of observational or vicarious learning. SLT, however, failed to incorporate the self-belief and perceptions of the individual, leading to the introduction of the concept of *self-efficacy* (Bandura, 1977).

SCT describes a human agency model in which individuals proactively self-reflect, self-regulate, and self-organize (Bandura, 1989). Core to this perspective is the concept of reciprocal determinism or triadic reciprocity depicted in Fig. 2.1 in which personal influences (cognitions, affect, biology) and environment interact and mutually shape one another. Both of these factors interact and influence behavior, and that behavior, in turn, reciprocally shapes personal and environmental factors.

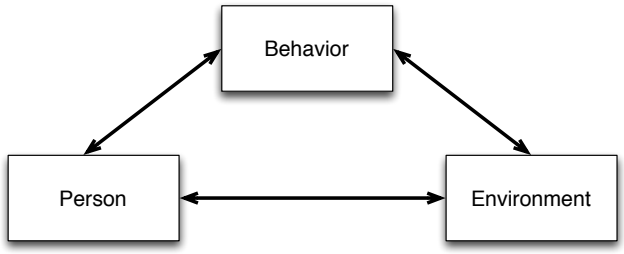

Figure 2.1: Triadic Reciprocal Determinism of Social Cognitive Theory.

In essence, SCT estimates the ability of an individual to engage in a determined behavior based on internal and external parameters and their interrelationships. Some of these are self-perceived and others can be externally measured.

The following SCT components are generated as a consequence of the variation of external or internal stimuli, considered outputs from an engineering point of view. These components are:

- *Self-efficacy*, the perceived capability to do what is required to perform a given behavior. It plays a core role as a personal factor that influences behavior. It is influenced by behavior and the environment.

- *Outcome expectancies*, the perceived likelihood that performing a given behavior

will result in certain outcomes. It is also a central component of the personal factors that influence behavior and are influenced by environment and behavior.

- *Behavioral outcomes*, the outcomes obtained as a result of engagement in the behavior of interest. These are directly related to outcome expectancies and the future behavior.

- *Self-management skills*, the set of skills involving a class of complex behaviors such as self-monitoring, goal setting, self-reinforcement, stimulus control, and related methods by which an individual increases the potential success for a given behavior. These contribute directly to *self-efficacy*.

- *Behavior*, the actual behavior studied, which can correspond to a particular metric of physical activity (e.g., number of daily steps taken, minutes spent in daily moderate-to-vigorous physical activity) or to involvement with an addictive substance (e.g., the number of cigarettes or alcoholic drinks consumed in a given day).

According to the theory, there are variables that act as stimuli to promote or discourage behavior and the previous components. These are considered inputs, and can be external or internal to the individual. They are:

- *Skills training*. These activities help to increase (or decrease) the self-management skills of the individual. An example for physical activity is learning to use a pedometer.

- *Observed behavior (vicarious learning)*. This influences not only *self-efficacy* for engaging in the behavior, but also outcome expectancies as the individual observes results of others performing the behavior.

- *Perceived social support and verbal persuasion.* These can help to increase *self-efficacy.* An example is the availability of others to engage in physical activity with the individual or to verbally support increased physical activity of the individual.

- *Perceived barriers and obstacles.* These are external conditions that affect behavior. For example, physical activity can be reduced because of insufficient time, bad weather, and limited access to exercise facilities or safe walking paths.

- *Intrapersonal states.* These consist of an array of physical, mental, and emotional states of the individual, such as happiness and sadness, that either increase or decrease *self-efficacy* at any given time.

- *Environmental context.* This influences directly the resultant *behavioral outcomes.*

- *Internal and external cues.* These directly influence behavior. In SCT, *self-efficacy* and outcome expectancies are often conceptualized as predispositions for engaging in any given behavior that is then triggered by a *cue to action.* In a more granular model, *cue to action* is likely to be treated as discrete and episodic inputs.

2.3 Developing a Fluid Analogy for SCT

The proposed fluid analogy of Social Cognitive Theory (SCT) is presented in Fig. 2.2. It depicts how the various components of SCT relate with one another over time, particularly to understand behavior. The use of a fluid analogy allows the organization of behavioral ideas into a structured framework that can be used to find a mathematical model. Main constructs are treated as inventories; other components

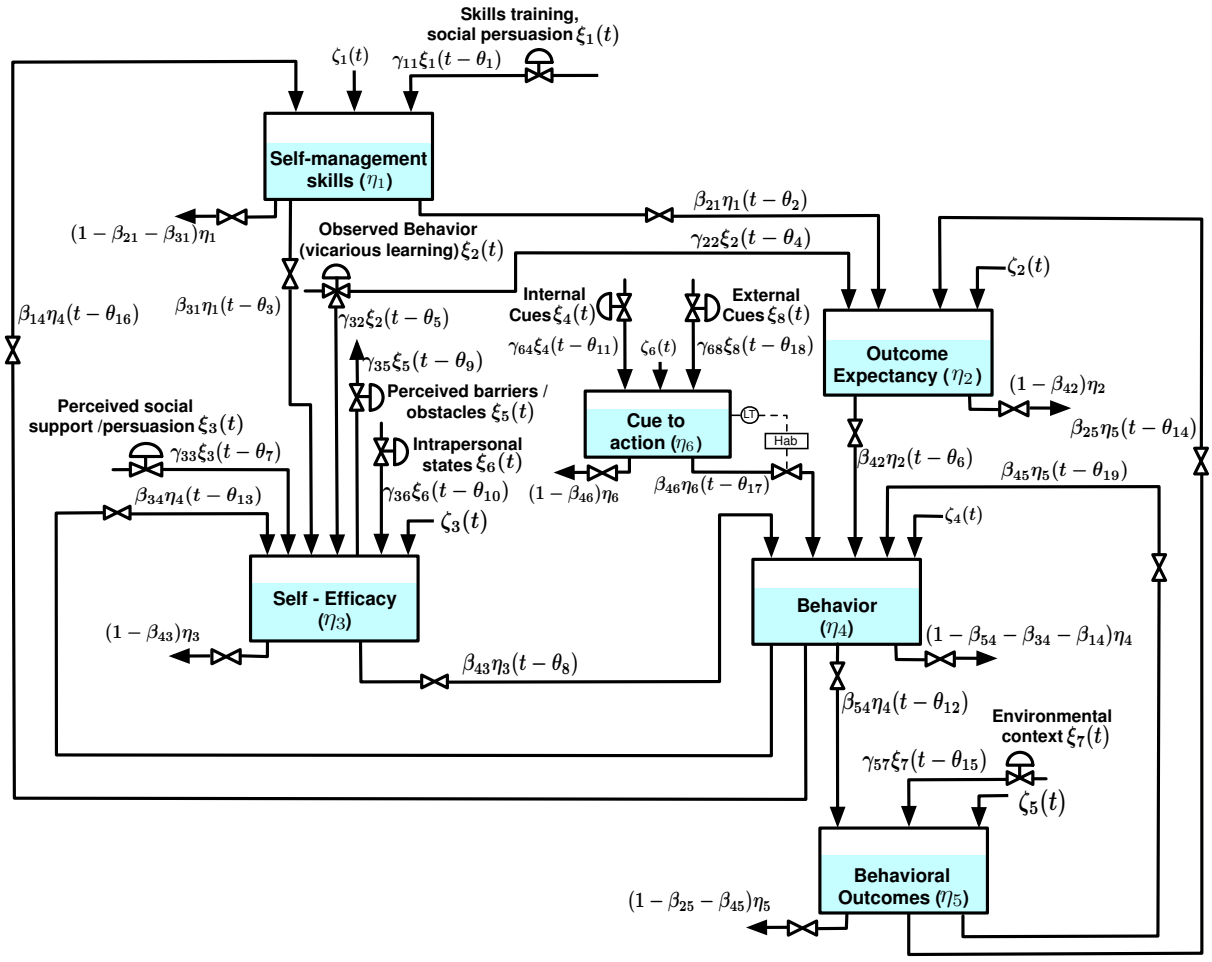

Figure 2.2: Fluid Analogy for Social Cognitive Theory, Augmented With Habituation.

and properties are depicted as inflows and/or outflows.

In the schematic, *behavior* (η_4) is represented as a fluid inventory that changes in frequency and/or duration over time based on various putative SCT factors. This model was developed based on a daily time frame (i.e., aggregate frequency and/or duration of behavior within any given day). Similar models with more or less granular time frames could be adapted from this daily time frame depending on the behavior of interest (e.g., smoking or cancer screening behaviors) and time frame of interest.

Self-efficacy (SE) (η_3) is a core construct of SCT and is represented as an inventory of varying levels that differs not only between individuals and specific behaviors,

but also fluctuates within an individual over time. SE functions as both an independent variable influencing the likelihood of engaging in the associated behavior, and a dependent variable influenced by a number of factors that increase or decrease the inventory at any given time. The following are the SCT factors that are theorized to increase or decrease the SE inventory:

1. *Perceived barriers and obstacles* (ξ_5) to engaging in any given behavior deplete *self-efficacy* (SE).

2. *Perceived social support and verbal persuasion* from others increases SE (ξ_3).

3. *Observed behavior* (vicarious learning) (ξ_2) of others successfully performing the behavior increases SE.

4. *Intra-personal states* of the individual (ξ_6) either add to or deplete the level of SE.

5. Prior experience engaging in the behavior (β_{34}) is a gain parameter representing the critical learning feedback loop that adds or depletes SE to subsequently engage in the behavior. This is a feedback loop in which successfully engaging in the behavior increases SE to engage in the behavior, which subsequently increases the likelihood of engaging in the behavior.

6. *Self-management or self-regulatory skills* (η_1) influence both SE and *outcome expectancies*. Inputs into the *self-management* inventory include formal skills training, observational learning, and verbal persuasion (ξ_1).

The inventory outcome expectancies (η_2) is another important construct in SCT that contributes to the likelihood of any given behavior. These behaviors are inherently followed by positive and/or negative consequences, some proximal and some

distal, or lack of consequences. For example, engaging in physical activity could result, short term, in feeling fatigued or invigorated. Social reinforcement may ensue from engaging in physical activity. Over the longer-term, physical activity may lead to improved health, or conversely in injury. These *behavioral outcomes* (η_5) produce a feedback loop to outcome expectancies (β_{25}). Experiencing and/or expecting positive outcomes from engaging in the behavior will lead to an increased likelihood of subsequently engaging in the behavior. As previously noted, these *behavioral outcomes* are greatly influenced by the *environmental context* in which the behavior occurs (ξ_7).

The second input into outcome expectancies is observational learning or modeling (ξ_2). Observing the consequences of the behavior experienced by others adds or depletes the *outcome expectancy* inventory for that behavior. The third component that influences outcome expectancies is self-regulatory or *self-management skills* (β_{21}).

Finally, *cue to action* (η_6) directly influences behavior and is treated as an inventory that represents the various cues to action that occur during the day. These cues can be external (e.g., friend asks to take a walk) or internal (e.g., getting tired or stiff from sitting). They can occur naturally (e.g., good weather) or artificially (e.g., alarm reminder on phone to go for a walk) in the environment. To complete the fluid analogy model, disturbances (ζ) are added. Disturbances are any exogenous factors that influence the inventories and can be viewed as unexplained variance.

Path diagrams are part of Structured Equation Modeling (SEM; Bollen (1989)). They are used to depict the associations among a set of variables that later can be represented in the form of linear equations. In this case, a reverse process is developed. The path diagram for Social Cognitive Theory shown in Fig. 2.3, is obtained from the connections established in the proposed fluid analogy.

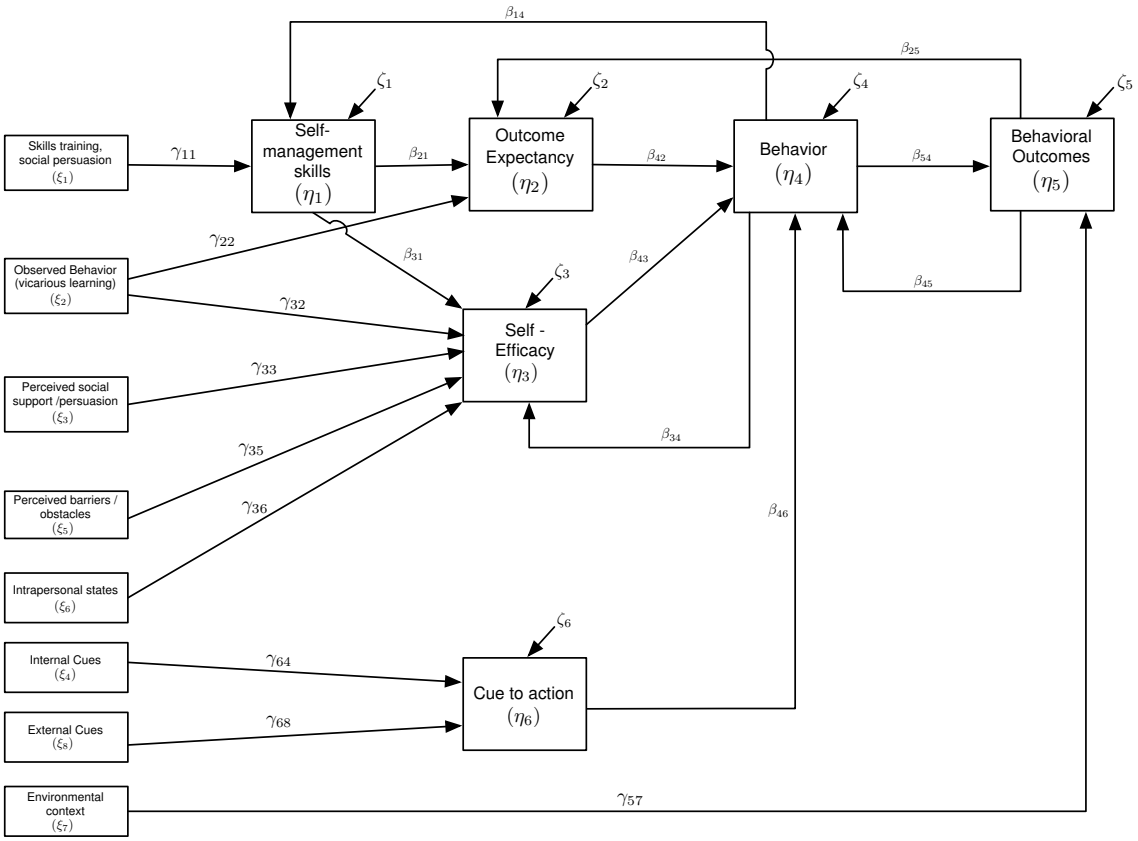

Figure 2.3: Path Diagram for Social Cognitive Theory Derived From the Fluid Analogy.

2.4 Dynamical Model Description

To obtain a mathematical model from the proposed fluid analogy, it is necessary to describe how the inventories and their respective inflows and outflows fit within the mathematical perspective of dynamical systems. This procedure was previously described by Navarro Barrientos, Rivera and Collins in a dynamic model for the Theory of Planned Behavior (Navarro-Barrientos *et al.*, 2011).

Six inventories are considered in the diagram, and their levels are represented by the variables η_1,..,η_6. Eight exogenous inputs are shown and represented by ξ_1,..,ξ_8. From each inventory there are a number of inflow resistances represented by the

coefficients γ_{11},..,γ_{68} and outflow resistances represented by β_{21},..,β_{54}. One approach to conceptualize these resistances is to consider those as the fraction of each inventory or input that leaves the previous instance and then feeds the next inventory.

There are other parameters that represent the physical characteristics of each inventory and flow; these have an important effect on the dynamic behavior of the system. First time constants τ_1,..,τ_6 represent the capacity and allow for exponential decay (or growth) of the inventory. Time delays (θ_1,..,θ_{19}) for each flow signal are also used. Finally unmeasured disturbances (which may reflect unmodeled dynamics) are considered as ζ_1,..,ζ_6.

2.4.1 Differential Equation Representation

After the application of the fluid analogy the behavioral variables are treated as physical entities. The principle of mass conservation is used: the sum of the inflows minus the outflows gives an accumulation term denoted by the time constant τ times the rate of change in the level of the inventory. The sum of all outflows must add up to the value of the respective inventory. For that reason, at each inventory output, an outflow of $(1 - \beta_{jk} - ... - \beta_{lm})\eta_i(t)$ is included in the model, where the β's are the respective outflow coefficients.

To demonstrate how the equations are derived, a subsection of the fluid analogy including only the first inventory (*Self-management Skills* (η_1)) with its inflows and outflows is presented in Fig. 2.4.

The principle of mass conservation applied to η_1 is

$$\begin{aligned}\tau_1 \frac{d\eta_1}{dt} =& \gamma_{11}\xi_1(t-\theta_1) + \beta_{14}\eta_4(t-\theta_{16}) + \zeta_1(t) - \beta_{31}\eta_1(t) - \beta_{21}\eta_1(t) \\ & - (1 - \beta_{21} - \beta_{31})\eta_1(t)\end{aligned} \tag{2.1}$$

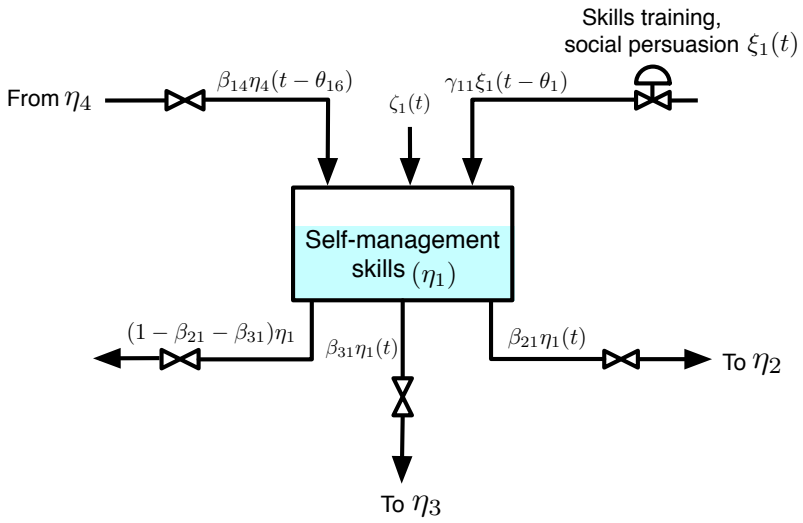

Figure 2.4: *Self-Management Skills* Inventory (η_1) Showing All its Inflows and Outflows

which following simplifications yields

$$\tau_1 \frac{d\eta_1}{dt} = \gamma_{11}\xi_1(t-\theta_1) + \beta_{14}\eta_4(t-\theta_{16}) - \eta_1(t) + \zeta_1(t) \tag{2.2}$$

Applying the same procedure for all the inventories, the following system of differential equations is obtained:

$$\tau_2 \frac{d\eta_2}{dt} = \gamma_{22}\xi_2(t-\theta_4) + \beta_{21}\eta_1(t-\theta_2) + \beta_{25}\eta_5(t-\theta_{14}) - \eta_2(t) + \zeta_2(t) \tag{2.3}$$

$$\begin{aligned}\tau_3 \frac{d\eta_3}{dt} =& \gamma_{32}\xi_2(t-\theta_5) + \gamma_{33}\xi_3(t-\theta_7) - \gamma_{35}\xi_5(t-\theta_9) + \gamma_{36}\xi_6(t-\theta_{10}) \\ &+ \beta_{31}\eta_1(t-\theta_3) + \beta_{34}\eta_4(t-\theta_{13}) - \eta_3(t) + \zeta_3(t)\end{aligned} \tag{2.4}$$

$$\begin{aligned}\tau_4 \frac{d\eta_4}{dt} =& \beta_{42}\eta_2(t-\theta_6) + \beta_{43}\eta_3(t-\theta_8) + \beta_{46}\eta_6(t-\theta_{17}) + \beta_{45}\eta_5(t-\theta_{19}) \\ &- \eta_4(t) + \zeta_4(t)\end{aligned} \tag{2.5}$$

$$\tau_5 \frac{d\eta_5}{dt} = \gamma_{57}\xi_7(t-\theta_{15}) + \beta_{54}\eta_4(t-\theta_{12}) - \eta_5(t) + \zeta_5(t) \tag{2.6}$$

$$\tau_6 \frac{d\eta_6}{dt} = \gamma_{64}\xi_4(t-\theta_{11}) + \gamma_{68}\xi_8(t-\theta_{18}) - \eta_6(t) + \zeta_6(t) \tag{2.7}$$

The model per (2.2)–(2.7) consists of a system of first-order differential equations,

but to describe a more elaborate transient response (such as overdamped, critically damped or underdamped responses), a second order system could be used (Navarro-Barrientos *et al.*, 2011). If second order dynamics are present, these can be conceptualized as being part of an inventory system that is subject to self-regulation. This will be illustrated with an example considering only one inventory as a reference: to represent *cue to action* (η_6) as a system with one zero and two poles and assuming for simplicity that the input ξ_4 (*internal cue*) is equal to zero, the equation (2.7) can be rewritten as

$$\tau_6^2 \frac{d^2\eta_6}{dt^2} + 2\zeta\tau_6 \frac{d\eta_6}{dt} = \gamma_{68}\left(\xi_8(t-\theta_{18}) + \tau_a \frac{d\xi_8(t-\theta_{18})}{dt}\right) - \eta_6(t) + \zeta_6(t) \tag{2.8}$$

that, after neglecting delays and perturbations, yields to the transfer function:

$$\frac{\eta_6(s)}{\xi_8(s)} = \frac{\gamma_{68}(\tau_a s + 1)}{\tau_6^2 s^2 + 2\zeta\tau_6 s + 1} \tag{2.9}$$

To depict this second order system within the fluid analogy, a self-regulatory controller for each inventory should be included. To illustrate this process, in Fig. 2.5 the inventory *cue to action* (η_6) is shown with its inflows and outflows, excluding ξ_4.

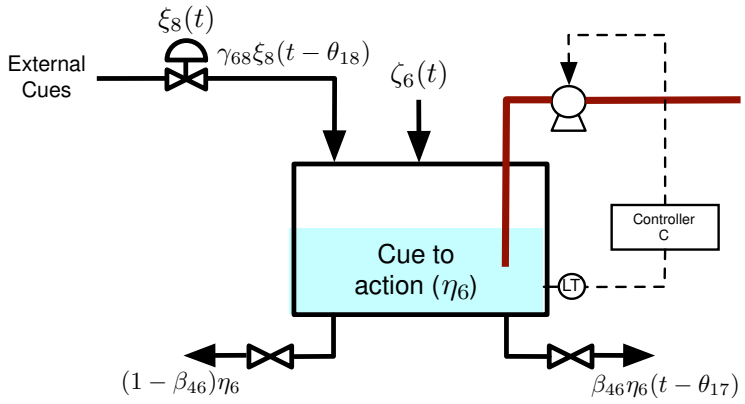

Figure 2.5: Inventory *Cue to Action* (η_6) With the Addition of a Feedback Controller to Represent a Second Order System.

To obtain a more general representation, in concordance with control systems

literature, the following variables are substituted:

$$d = \xi_8; \quad y = \eta_6; \quad \tau = \tau_6; \quad K = \gamma_{68}$$

yielding the following transfer function:

$$\frac{y(s)}{d(s)} = \frac{K(\tau_a s + 1)}{\tau^2 s^2 + 2\zeta\tau s + 1} \tag{2.10}$$

Fig. 2.6 represents a block diagram for a general second order inventory system with the proposed variables, where τ_p is the first order time constant for the tank.

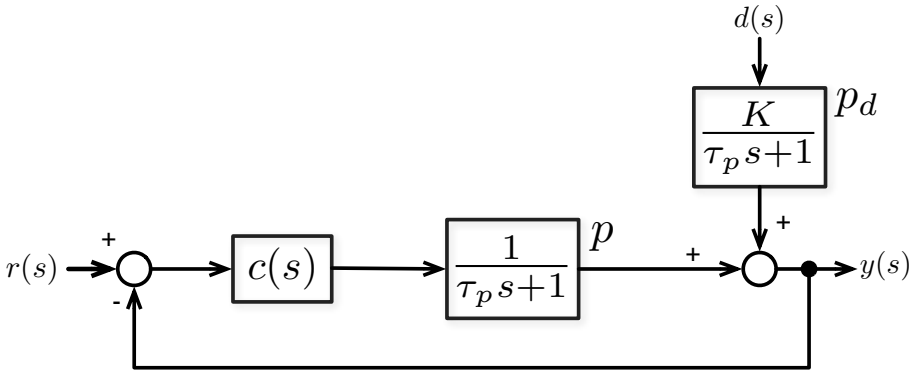

Figure 2.6: Block Diagram for a Second Order Inventory System.

The controller $c(s)$ must be selected such that the transfer function from $d(s)$ to $y(s)$ matches the required second order system. To obtain a mathematical representation of the controller, a reverse engineering procedure is performed using the Internal Model Controller (IMC) design method (Morari and Zafiriou, 1989), applied to the following first order plant model:

$$\tilde{p} = \frac{1}{\tau_p s + 1} \tag{2.11}$$

From here the initial q-parametrized controller, and the obtained filter are

$$\tilde{q} = \tau_p s + 1, \quad f = \frac{\lambda s}{(\lambda_1 s + 1)(\lambda_2 s + 1)} \tag{2.12}$$

resulting in

$$q = \frac{\lambda s(\tau_p s + 1)}{(\lambda_1 s + 1)(\lambda_2 s + 1)} \tag{2.13}$$

The required transfer function can be represented in terms of the IMC controller as

$$\frac{y}{d} = (1 - \tilde{p}q)p_d = \Big(1 - \frac{\lambda s}{(\lambda_1 s + 1)(\lambda_2 s + 1)}\Big)\frac{K}{\tau_p s + 1} \tag{2.14}$$

After some mathematical simplifications the result from (2.14) is compared to (2.10), from where the following relations are obtained:

$$\lambda_1 \lambda_2 = \tau^2 = \tau_p \tau_a \tag{2.15}$$

$$\lambda_1 + \lambda_2 = 2\zeta\tau \tag{2.16}$$

$$\lambda = \tau_p + \tau_a - 2\zeta\tau \tag{2.17}$$

and the values for the filter coefficients (λ_i) can be derived. To avoid a neglected controller the following condition must be satisfied:

$$\lambda_1 + \lambda_2 \neq \tau_p + \tau_a \tag{2.18}$$

Using these representations, the transfer function $c(s)$ can be represented in a classical feedback controller form as

$$c(s) = \frac{(2\zeta\tau - \tau_a - \tau_p)s}{\tau_a s + 1} \tag{2.19}$$

The presence of a feedback controller creates a connection to another behavioral theory, self-regulation (Carver and Scheier, 1998).

2.4.2 Model Considerations

The following model assumptions are considered to enforce the mass conservation principle and for simulation purposes:

- The time unit is in days.
- The β coefficients must satisfy the following constraints to enforce that the sum of outflows must add up to the value of the respective inventory:

$$\beta_{21} + \beta_{31} \leq 1, \quad \beta_{42} \leq 1, \quad \beta_{43} \leq 1$$

$$\beta_{54} + \beta_{34} + \beta_{14} \leq 1, \quad \beta_{25} + \beta_{45} \leq 1, \quad \beta_{46} \leq 1$$

- The initial levels of the inventories are determined by solving the system of equations at steady state, obtaining the following results:

$$\bar{\eta}_1 = \gamma_{11}\bar{\xi}_1 + \beta_{14}\bar{\eta}_4$$

$$\bar{\eta}_2 = A + (\beta_{21}\beta_{14} + \beta_{25}\beta_{54})\bar{\eta}_4$$

$$\bar{\eta}_3 = B + (\beta_{31}\beta_{14} + \beta_{34})\bar{\eta}_4$$

$$\bar{\eta}_4 = \frac{\beta_{46}\bar{\eta}_6 + \beta_{42}A + \beta_{43}B + \beta_{45}\gamma_{57}\bar{\xi}_7}{1 - \beta_{42}(\beta_{21}\beta_{14} + \beta_{25}\beta_{54}) - \beta_{43}(\beta_{31}\beta_{14} + \beta_{34}) - \beta_{45}\beta_{54}}$$

$$\bar{\eta}_5 = \gamma_{57}\bar{\xi}_7 + \beta_{54}\bar{\eta}_4$$

$$\bar{\eta}_6 = \gamma_{64}\bar{\xi}_4 + \gamma_{68}\bar{\xi}_8$$

where

$$A = \gamma_{22}\bar{\xi}_2 + \beta_{21}\gamma_{11}\bar{\xi}_1 + \beta_{25}\gamma_{57}\bar{\xi}_7$$

$$B = \gamma_{32}\bar{\xi}_2 + \gamma_{33}\bar{\xi}_3 - \gamma_{35}\bar{\xi}_5 + \gamma_{36}\bar{\xi}_6 + \beta_{31}\gamma_{11}\bar{\xi}_1$$

- All inventories are restricted to have values within 0 and 100 %.
- Uncertainties are represented as zero mean stochastic signals.
- The exogenous signals: *intrapersonal states* (ξ_6) and *environmental context* (ξ_7) are considered as auto-correlated noise since they may occur in a nearly random way.

All time delays are considered to be zero; this is for simplicity and clarity of results.

2.4.3 *Stability Analysis*

Using the state space representation of the system based on the SCT model, the state matrix is

$$\mathbf{A} = \begin{pmatrix} -\frac{1}{\tau_1} & 0 & 0 & \frac{\beta_{14}}{\tau_1} & 0 & 0 \\ \frac{\beta_{21}}{\tau_2} & -\frac{1}{\tau_2} & 0 & 0 & \frac{\beta_{25}}{\tau_2} & 0 \\ \frac{\beta_{31}}{\tau_3} & 0 & -\frac{1}{\tau_3} & \frac{\beta_{34}}{\tau_3} & 0 & 0 \\ 0 & \frac{\beta_{42}}{\tau_4} & \frac{\beta_{43}}{\tau_4} & -\frac{1}{\tau_4} & \frac{\beta_{45}}{\tau_4} & \frac{\beta_{46}}{\tau_4} \\ 0 & 0 & 0 & \frac{\beta_{54}}{\tau_5} & -\frac{1}{\tau_5} & 0 \\ 0 & 0 & 0 & 0 & 0 & -\frac{1}{\tau_6} \end{pmatrix} \tag{2.20}$$

The system is stable if all the eigenvalues of $\mathbf{A}$ have negative real parts. To verify this condition the characteristic equation of the matrix $\mathbf{A}$ is computed as

$$D(s) = |s\mathbf{I} - \mathbf{A}| = a_5 s^5 + a_4 s^4 + a_3 s^3 + a_2 s^2 + a_1 s + a_0 \tag{2.21}$$

with:

$$a_5 = \tau_1\tau_2\tau_3\tau_4\tau_5 \tag{2.22}$$

$$a_4 = \tau_1\tau_2\tau_3\tau_4 + \tau_1\tau_2\tau_3\tau_5 + \tau_1\tau_2\tau_4\tau_5 + \tau_1\tau_3\tau_4\tau_5 + \tau_2\tau_3\tau_4\tau_5 \tag{2.23}$$

$$\begin{aligned} a_3 =& \tau_1\tau_2\tau_5(1 - \beta_{34}\beta_{43}) + \tau_1\tau_2\tau_3(1 - \beta_{45}\beta_{54}) + \tau_1\tau_2\tau_4 + \tau_1\tau_3\tau_4 + \tau_1\tau_3\tau_5 \\ &+ \tau_2\tau_3\tau_4 + \tau_1\tau_4\tau_5 + \tau_2\tau_3\tau_5 + \tau_2\tau_4\tau_5 + \tau_3\tau_4\tau_5 \end{aligned} \tag{2.24}$$

$$\begin{aligned} a_2 =& \tau_1\tau_5(1 - \beta_{34}\beta_{43}) + \tau_1\tau_2(1 - \beta_{34}\beta_{43} - \beta_{45}\beta_{54}) \\ &+ \tau_2\tau_5(1 - \beta_{34}\beta_{43} - \beta_{14}\beta_{31}\beta_{43}) + \tau_1\tau_3(1 - \beta_{45}\beta_{54} - \beta_{25}\beta_{42}\beta_{54}) \\ &+ \tau_2\tau_3(1 - \beta_{45}\beta_{54}) + \tau_3\tau_5(1 - \beta_{14}\beta_{21}\beta_{42}) + \tau_1\tau_4 \\ &+ \tau_2\tau_4 + \tau_3\tau_4 + \tau_4\tau_5 \end{aligned} \tag{2.25}$$

$$
\begin{aligned}
a_1 =& \tau_1(1 - \beta_{34}\beta_{43} - \beta_{45}\beta_{54} - \beta_{25}\beta_{42}\beta_{54}) \\
&+ \tau_2(1 - \beta_{34}\beta_{43} - \beta_{45}\beta_{54} - \beta_{14}\beta_{31}\beta_{43}) \\
&+ \tau_3(1 - \beta_{45}\beta_{54} - \beta_{14}\beta_{21}\beta_{42} - \beta_{25}\beta_{42}\beta_{54}) + \tau_4 \\
&+ \tau_5(1 - \beta_{34}\beta_{43} - \beta_{14}\beta_{21}\beta_{42} - \beta_{14}\beta_{31}\beta_{43})
\end{aligned} \tag{2.26}
$$

$$
a_0 = 1 - \beta_{34}\beta_{43} - \beta_{45}\beta_{54} - \beta_{14}\beta_{21}\beta_{42} - \beta_{14}\beta_{31}\beta_{43} - \beta_{25}\beta_{42}\beta_{54} \tag{2.27}
$$

The stability condition is satisfied if all of the coefficients of $D(s)$ are positive, therefore the set of conditions for stability is

$$
a_i > 0, \quad i = 0, \cdots, 5 \tag{2.28}
$$

Considering that all time constants τ_j are positive, the only possibility for any term a_i to be negative is if one or more of its internal factors $1 - (\beta_i\beta_j) - \cdots - (\beta_k\beta_l\beta_m)$ are negative. To prevent this for any specific internal factor, the following condition must be met:

$$
(\beta_i\beta_j) + \cdots + (\beta_k\beta_l\beta_m) < 1 \tag{2.29}
$$

One general way to meet this requirement is to consider that each gain β is less than one, therefore to have a stable system it is sufficient that all of the following conditions are met simultaneously:

$$
\beta_{21} < 1, \beta_{31} < 1, \beta_{42} < 1, \beta_{43} < 1, \beta_{54} < 1, \beta_{34} < 1, \beta_{14} < 1, \beta_{25} < 1, \beta_{45} < 1 \tag{2.30}
$$

2.4.4 Nonlinear Dynamics of Habituation Within the SCT Model

It was noted previously that human behavior is a complex process. Even when is described by elaborate theories such as SCT, it can change its direction based on particular scenarios; one of these is habituation. Habituation is a behavioral phenomenon that is triggered by repeated stimulation. It results in decreased responses

despite increased stimulus. It does not involve sensory adaptation, sensory fatigue, or motor fatigue (Rankin *et al.*, 2009); the decrease usually follows a negative exponential curve. Marsland (Marsland, 2009) proposed different methods for modeling some of the basic characteristics of habituation using the perspective of learning systems, with first order derivatives to depict exponential decays.

The start of the habituation process defines an inflection point where behavior stops following the previously defined response and begins an exponential decrement, disrupting the linear nature of the model. Many nonlinear modeling strategies have been defined to depict similar situations. Since the objective is to model SCT and habituation in the same structure, each one with its own exponential model, a parameter-varying strategy is proposed. For modeling purposes the focus will be only on the following common characteristics of habituation (Rankin *et al.*, 2009):

- Repeated application of the stimulus results in a progressive decrease in the response.
- If the stimulus is withheld, the response recovers at least partially over the observation time.
- More frequent stimulation results in a more rapid and/or more pronounced response decrement.

Additional features representing other habituation characteristics can be incorporated to the model. The complexity of this process depends on the behavioral situation of interest and the characteristics of the involved input/output signals.

In the linear model if a stimulus (e.g., *internal cue* ξ_4) is continually or repeatedly applied, the response (*behavior* η_4) will grow until it reaches its maximum value, and remains there. The inventory *cue to action* (η_6) can be considered an accumulation

of different cues such that its level is dependent on the magnitude and frequency of the received stimuli. This value is used to modify the parameter β_{46} that represents the effect of the inventory *cue to action* (η_6) over *behavior* (η_4).

An example of a gain schedule for physical activity is shown in Fig. 2.7, where a reduced value of β_{46} for higher values of (η_6) represents the reduction on the increased rate of behavior due to the effect of the repeated cues. If *cue to action* (η_6) is greater than 95 %, then β_{46} is fixed to zero; there will be no further increases in behavior, and it will decrease to its original value, as habituation suggests. The gain schedule, shown in Table 2.1 and depicted in Fig. 2.7, is suitable for a physical activity example, but since habituation occurs in different ways (depending on the particular behavioral situation and the types of cues), a proper gain schedule should be developed individually for each particular case.

Table 2.1: Lookup Table for β_{46}

Cue to action (η_6)	β_{46}
0 to 90%	0.44
91 to 95%	0.4
96 to 100%	0

2.5 Illustrative Simulations

The simulations were designed to represent the amount of physical activity performed by an individual during a period of 20 days. The model parameters were chosen to show the capability of the model to reply well known behavioral facts that are stated in SCT. Some scenarios are depicted, showing the dynamic response of

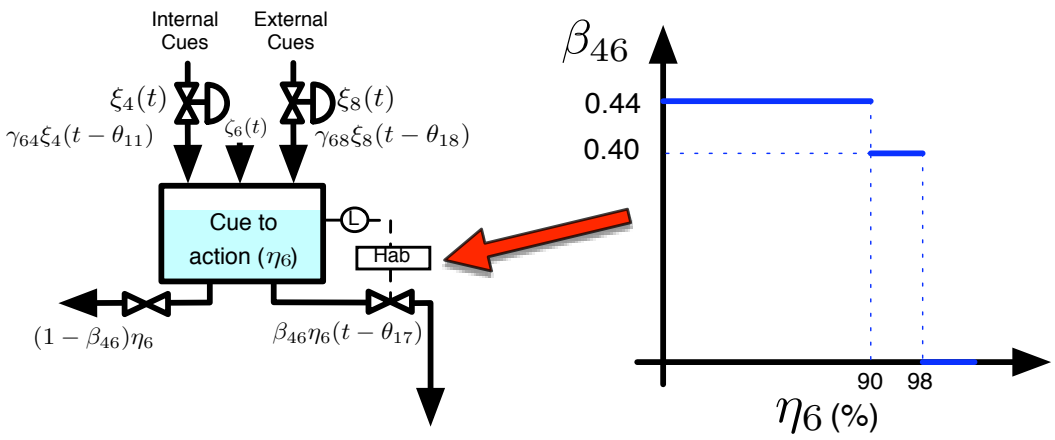

Figure 2.7: Gain Schedule Illustration for β_{46}

the system, to different variations on its inputs. All scenarios consider the following parameter values:

- $\tau_1 = 1, \tau_2 = 1, \tau_3 = 1, \tau_4 = 2, \tau_5 = 1, \tau_6 = 3$
- $\gamma_{11} = 3, \gamma_{22} = 1, \gamma_{32} = 2, \gamma_{33} = 1, \gamma_{35} = 1, \gamma_{36} = 1, \gamma_{57} = 2, \gamma_{64} = 15, \gamma_{68} = 15$
- $\beta_{21} = 0.3, \beta_{31} = 0.5, \beta_{42} = 0.3, \beta_{43} = 0.8, \beta_{45} = 0.1, \beta_{54} = 0.3, \beta_{34} = 0.2,$ $\beta_{25} = 0.3, \beta_{14} = 0.23, \beta_{46} = 0.44$

The first scenario is depicted in Fig. 2.8 and illustrates the effect of *cue to action* in the system under conditions of low *self-efficacy*. To produce low *self-efficacy*, *observed behavior* and *perceived social support* are held at constant low levels ($\xi_2 = 3, \xi_3 = 3$). The input *perceived barriers* is kept at a high value ($\xi_5 = 10$). Within this context, an external cue begins on day 2 ($\xi_8 = 5$), subsides on day 6-7, recurs on day 8 and then disappears on day 12. In the physical activity situation these cues could represent calls from friends asking the individual to go on a walk. The result of the applied signals on the inventories is a small, dampened increase on behavior that subsides when the *cue to action* is subsequently depleted. Because of the low *self-efficacy*, the

engagement on the behavior is minimal.

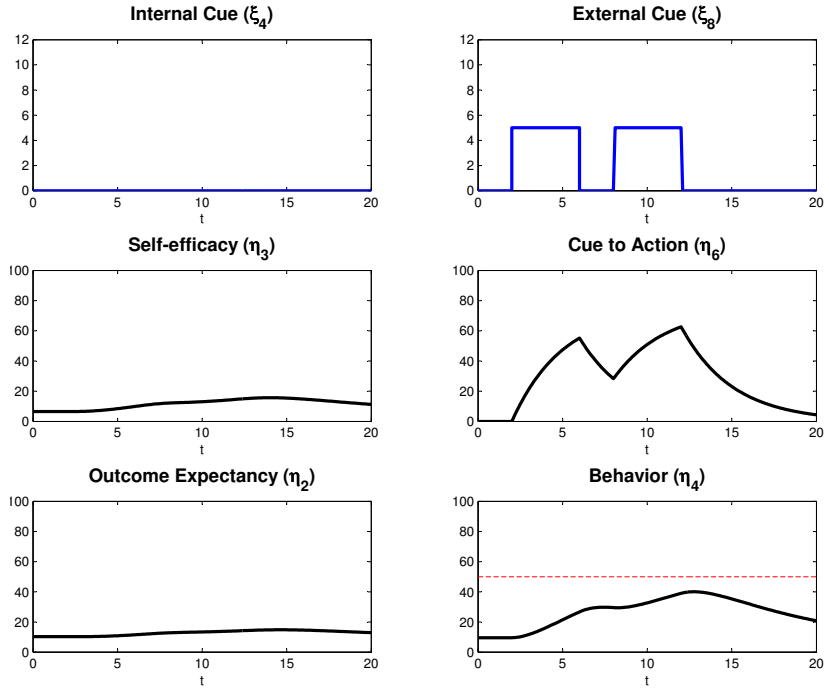

Figure 2.8: Scenario 1: Failure on the Initiation of Physical Activity Behavior Under Low *Self-Efficacy* and in the Presence of External Cues.

The second scenario, shown in Fig. 2.9, illustrates an initiation of the behavior and a further maintenance. The *external cue to action* (ξ_8) has similar values as the previous scenario, but within the context of high *self-efficacy*. *Observed behavior* and *perceived social support* are kept at high levels ($\xi_2 = 10, \xi_3 = 10$) and *perceived barriers* is decreased to a low level ($\xi_5 = 2$). The result is a considerable increase on the behavior inventory, and as a consequence some internal cues are now present (example: after a few days walking daily at the same time and one day resting, the individual experiences the internal necessity to walk). The behavior is sustained with fewer cues, but with an increased *self-efficacy* as a result of the feedback loop between SE and behavior.

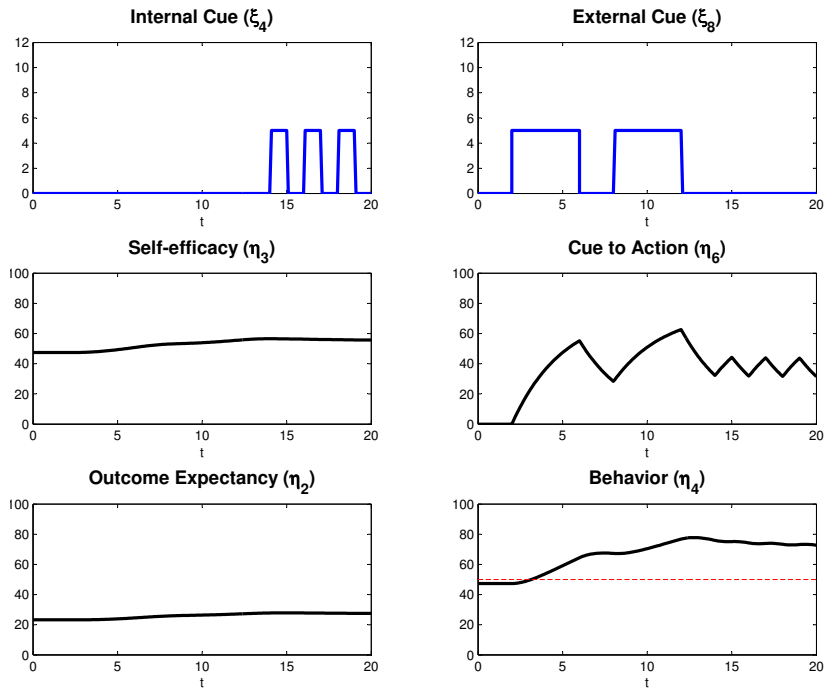

Figure 2.9: Scenario 2: Success of Initiation and Maintenance of Physical Activity Behavior Under High *Self-Efficacy* and in the Presence of External Cues and Additional Internal Cues.

Scenarios 1 and 2 represent well-known facts from the theory that are useful from the perspective of behavioral scientists, to illustrate the performance of the model in representing SCT. In the third scenario another way to represent the maintenance on the magnitude of the behavior is presented. Input conditions are the same as scenario 2 with the high *self-efficacy* initial condition, but now the recycle loop conformed by the inventories *behavior* (η_4), *behavioral outcomes* (η_5) and *outcome expectancy* (η_2) can be modeled with a more integrative effect so that it is capable of sustaining the magnitude of η_4. This is done with $\tau_4 = 15$ and $\beta_{46} = 0.9$, and results are shown in Fig. 2.10.

The fourth scenario, showed in Fig. 2.11, illustrates the effect of habituation. The only input shown is the *external cue* ($\xi_8 = 7$); the other inputs have the same values

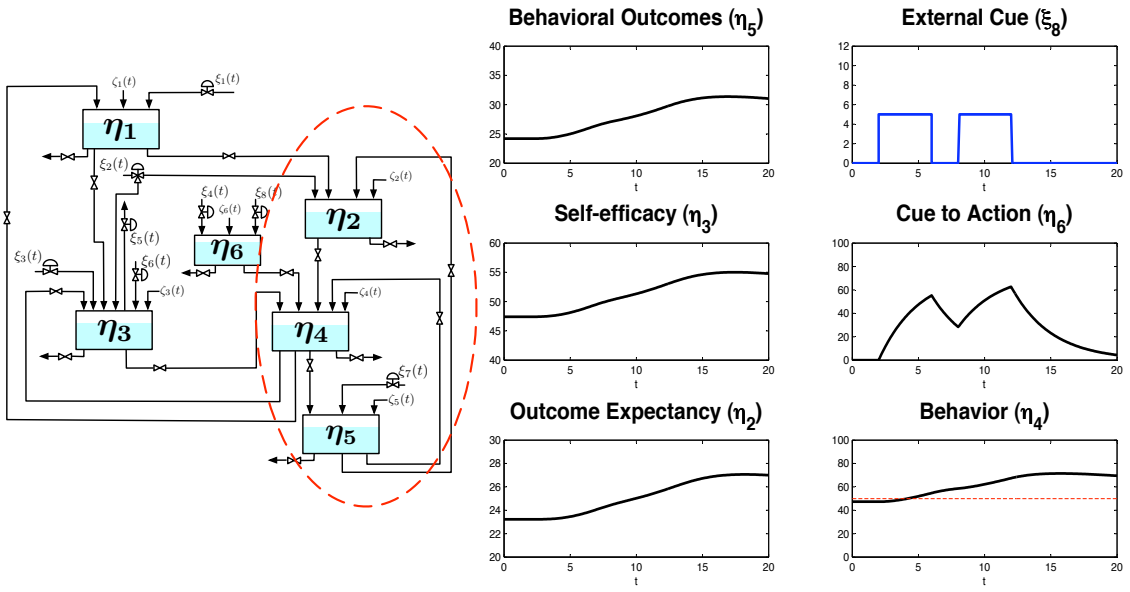

Figure 2.10: Scenario 3: Maintenance of Physical Activity Behavior Under High *Self-Efficacy* and a Model Depicting a Higher Degree of Integration.

defined in scenario 2. To allow the fast engagement in behavior, outputs *cue to action* (η_6) and *behavior* (η_4) are shown. *Behavior* (η_4) is depicted for both a linear case with no habituation and the proposed model (nonlinear) with the habituation gain schedule. An *external cue* (ξ_8) is applied from day 1 to day 14 (a friend calling the individual every day). Initially the individual responds with a sustained increase on the behavior, but after 7 days it starts to reduce the rate of increase (β_{46} reduced from 0.44 to 0.4). Later, a decrease begins in behavior that ultimately results in a complete reduction of the activity (β_{46} reduced to 0) and returns to the original value before the initial cue. At day 14, the repeated stimulus (ξ_8) is removed. Here it can be observed how the behavior resumed its increasing trend, as habituation theory suggests (Rankin *et al.*, 2009), but ultimately returns to the initial value.

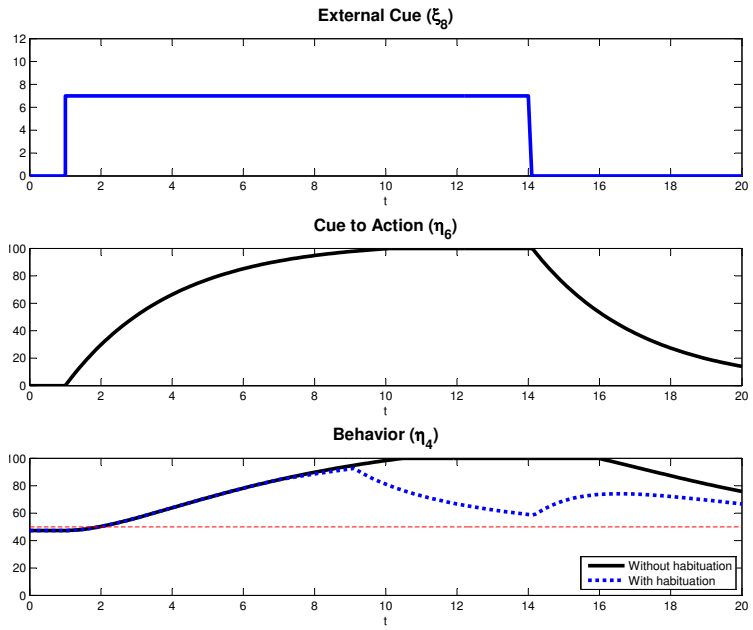

Figure 2.11: Scenario 4: Behavior Under a Persistent External Cue That Causes Habituation and Later Recovery After the Stimulus is Removed. High *Self-Efficacy* Conditions are Considered. Two Plots for Behavior are Shown: One Following a Linear Response (With no Habituation Considered), the Other Using the Proposed Model With a Nonlinear Block.

The final scenario, shown in Fig. 2.12, differs from the previous one only in the increased value of the *external cue* ($\xi_8 = 10$), that can be interpreted as a more frequent stimulation (e.g., a friend making more frequent calls per day). The result is an earlier engagement in the habituation process, as the principles of habituation suggest (Rankin *et al.*, 2009).

2.6 Semi-Physical Identification Using mHEALTH Intervention Data

In this section, measured data from a physical activity intervention is used to obtain model parameters from the proposed structure using semi-physical identification

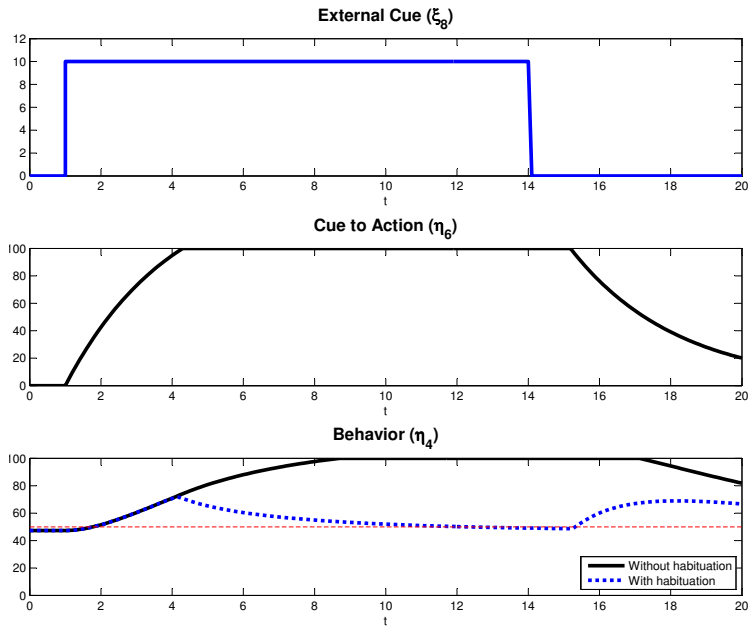

Figure 2.12: Scenario 5: Behavior Under a Higher External Cue (More Frequent Stimulus) That Causes Habituation and a Later Recovery Once the Stimulus Is Removed. Conditions of High *Self-Efficacy* are Considered.

techniques (Lindskog and Ljung, 1995). The data is taken from a study called Mobile Interventions for Lifestyle Exercise and Eating at Stanford (MILES) (King *et al.*, 2013), focused on behavioral interventions for physical activity in aging adults using mobile phones. The data is from a subset of the full sample; specifically, 68 adults ages 45 years and older agreed to participate in the experiment with the support of a smartphone for eight weeks. To measure behavioral variables, some well-validated questionnaires (King *et al.*, 2013) were used and the responses were obtained via a smartphone. Physical activity (behavior) was measured by an incorporated accelerometer, with the information also collected by the phone.

The MILES study included multiple between-person experimental conditions (i.e., different smartphone app interventions focused on promoting behavior change using

different motivational frames such as social, affective, or rational) and several variables measured on a daily basis. For comparison purposes, a smaller subset of participants with complete data was used, including interactions with the smartphone app features for the rational app (King *et al.*, 2013).

The selected variables and their respective match with the SCT model are

- Time spent (in seconds) on reading tips: *skills training* (ξ_1)
- Number of reminders sent to set a new goal: *external cues* (ξ_8)
- Self-reported physical activity *self-efficacy* (scale 1-11): *self-efficacy* (η_3)
- Average number of counts per minute: *behavior* (η_4).

The "counts" variable from the smartphone measures movement by the accelerometer, and is an indirect indication of the physical activity performed by the person who is carrying the phone. Fig. 2.13 illustrates the averaged data from six participants, including only the specified signals. Daily data and weekly averages are included.

In this data based study, the purpose is to explain the effects of two inputs over two outputs in the context of the model. However, there are other signals that were still present in the experiment and in the model but were not available as measurable data. Some of these signals like *environmental context* and *intrapersonal states* could be responsible for much of the variability in the outputs. To account for variability, weekly averaged data is used instead of daily data. This consideration may be interpreted as a smoothing filtering action applied to the original data. The model parameters are estimated using the sub-system illustrated in Fig. 2.14, by a grey-box system identification procedure (Lindskog and Ljung, 1995; Bohlin, 2006). This allows the search of parameters to keep the defined model structure.

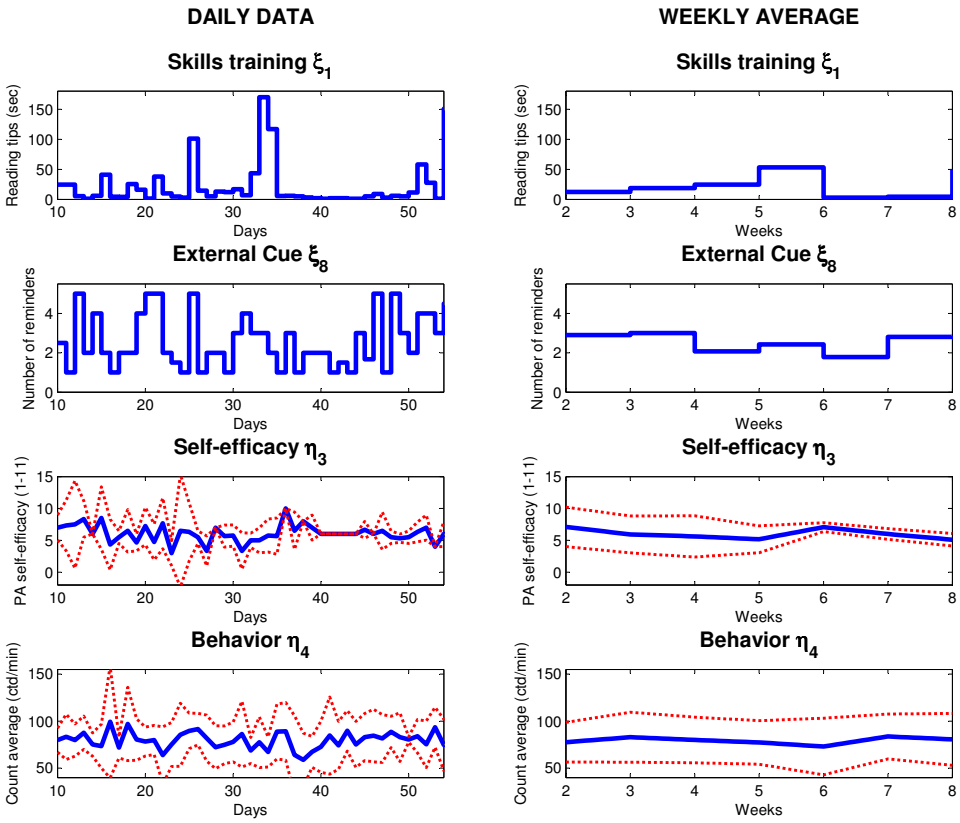

Figure 2.13: MILES Data Averaged for a Subset of Six Participants With the Required Signals for Raw Daily Sampling and Weekly Average Including 95 % Confidence Intervals.

Grey-box parameter estimation relies on two sources of information to estimate the required parameters: prior knowledge of the system (i.e., the SCT dynamical model) and experimental data. The state space representation of the system has the structure

$$\begin{aligned} \dot{\boldsymbol{x}}_{\boldsymbol{p}}(t) &= \mathbf{A}(\boldsymbol{\theta}_{\boldsymbol{p}})\boldsymbol{x}_{\boldsymbol{p}}(t) + \mathbf{B}(\boldsymbol{\theta}_{\boldsymbol{p}})\boldsymbol{u}_{\boldsymbol{p}}(t) + \boldsymbol{K}\boldsymbol{e}(t) \\ \boldsymbol{y}_{\boldsymbol{p}}(t) &= \mathbf{C}\boldsymbol{x}_{\boldsymbol{p}}(t) + \boldsymbol{v}(t) \end{aligned} \tag{2.31}$$

where:

- $\boldsymbol{x}_{\boldsymbol{p}} = [\eta_1 \dots \eta_6]$ denotes a vector of $n = 6$ state variables,
- $\boldsymbol{u}_{\boldsymbol{p}} = [\xi_1 \quad \xi_8]$ denotes a vector of $m = 2$ input variables,

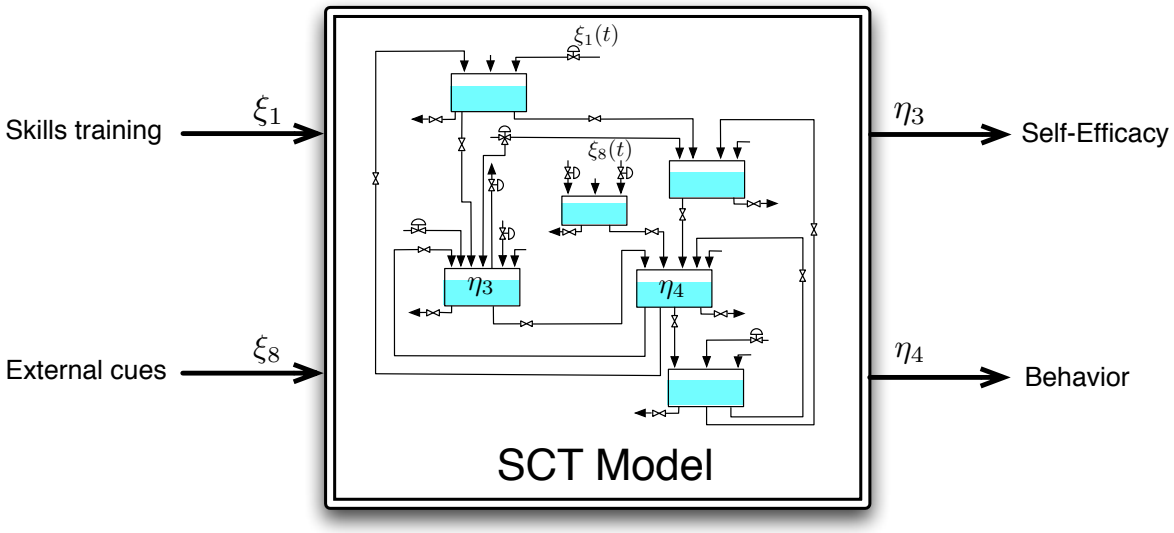

Figure 2.14: SCT Model Subsystem Used for Semiphysical Identification With the MILES Data.

- $\boldsymbol{y_p} = [\eta_3 \quad \eta_4]$ denotes a vector of $p = 2$ output variables,
- $\mathbf{A} \in \mathbb{R}^{n\times n}, \mathbf{B} \in \mathbb{R}^{n\times m}, \mathbf{C} \in \mathbb{R}^{p\times n}$ are the state matrices,
- $\boldsymbol{\theta_p} \in \mathbb{R}^{np}$ denotes a vector of $np = 18$ unknown model parameters,
- $\boldsymbol{e}(t)$ and $\boldsymbol{v}(t)$ are uncertainties associated to each one of the states and outputs.

Based on the SCT structure the unknown model parameters are

$$\begin{aligned}\boldsymbol{\theta_p} = [&\tau_1 \quad \tau_2 \quad \tau_3 \quad \tau_4 \quad \tau_5 \quad \tau_6 \quad \beta_{14} \quad \beta_{21} \quad \beta_{25} \quad \beta_{31} \\ &\beta_{34} \quad \beta_{42} \quad \beta_{43} \quad \beta_{46} \quad \beta_{54} \quad \beta_{45} \quad \gamma_{11} \quad \gamma_{68}]^\top\end{aligned} \tag{2.32}$$

and the state matrices are

$$\mathbf{A}(\boldsymbol{\theta_p}) = \begin{pmatrix} -\frac{1}{\tau_1} & 0 & 0 & \frac{\beta_{14}}{\tau_1} & 0 & 0 \\ \frac{\beta_{21}}{\tau_2} & -\frac{1}{\tau_2} & 0 & 0 & \frac{\beta_{25}}{\tau_2} & 0 \\ \frac{\beta_{31}}{\tau_3} & 0 & -\frac{1}{\tau_3} & \frac{\beta_{34}}{\tau_3} & 0 & 0 \\ 0 & \frac{\beta_{42}}{\tau_4} & \frac{\beta_{43}}{\tau_4} & -\frac{1}{\tau_4} & \frac{\beta_{45}}{\tau_4} & \frac{\beta_{46}}{\tau_4} \\ 0 & 0 & 0 & \frac{\beta_{54}}{\tau_5} & -\frac{1}{\tau_5} & 0 \\ 0 & 0 & 0 & 0 & 0 & -\frac{1}{\tau_6} \end{pmatrix} \tag{2.33}$$

$$\mathbf{B}(\boldsymbol{\theta_p}) = \begin{pmatrix} \frac{\gamma_{11}}{\tau_1} & 0 \\ 0 & 0 \\ 0 & 0 \\ 0 & 0 \\ 0 & 0 \\ 0 & \frac{\gamma_{68}}{\tau_6} \end{pmatrix} \tag{2.34}$$

$$\mathbf{C} = \begin{pmatrix} 0 & 0 & 1 & 0 & 0 & 0 \\ 0 & 0 & 0 & 1 & 0 & 0 \end{pmatrix} \tag{2.35}$$

To estimate $\boldsymbol{\theta}$, the well-known prediction-error identification methods (PEM) (Ljung, 1999) are used. The one-step ahead prediction error of the system is

$$\boldsymbol{\varepsilon}(t, \boldsymbol{\theta_p}) = \boldsymbol{y_p}(t) - \hat{\boldsymbol{y}}_{\boldsymbol{p}}(t|t-1, \boldsymbol{\theta_p}) \tag{2.36}$$

where $\hat{\boldsymbol{y}}_{\boldsymbol{p}}(t|t-1, \boldsymbol{\theta_p})$ is the predicted output based on estimated models.

Computations are executed in MATLAB using the commands *idgrey* and *greyest* from the System Identification Toolbox based on PEM methods. The estimated values of the model parameters are

- $\tau_1 = 0.66, \tau_2 = 2.25, \tau_3 = 0.55, \tau_4 = 3, \tau_5 = 0.94, \tau_6 = 0.64$

- $\gamma_{11} = 1.32, \gamma_{22} = 1, \gamma_{32} = 1, \gamma_{33} = 1, \gamma_{35} = 1, \gamma_{36} = 1, \gamma_{57} = 1, \gamma_{64} = 1,$ $\gamma_{68} = 0.88$

- $\beta_{21} = 0.9, \beta_{31} = 0.05, \beta_{42} = 0.9, \beta_{43} = 0.5, \beta_{54} = 0.67, \beta_{34} = 0.18,$ $\beta_{25} = 0.5, \beta_{14} = 0.65, \beta_{46} = 0.01, \beta_{45} = 0.1$

The results are shown in Fig. 2.15, including the MILES data and simulations based on the model, with the specified parameters.

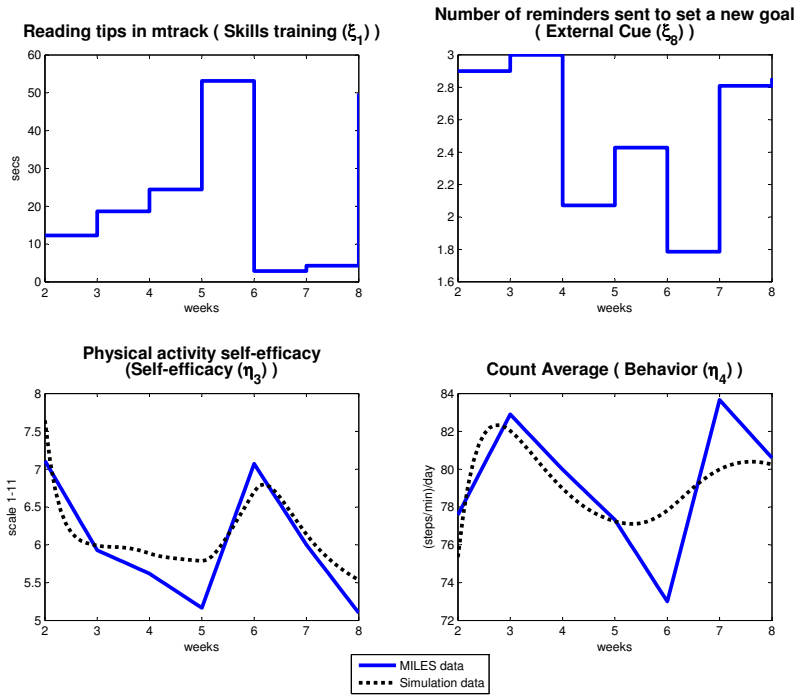

Figure 2.15: Data From MILES Study (Solid Line) Contrasted Against Simulation Results From the Model (Dotted Line) Considering the Same Input Values for Both Scenarios.

A similar pattern between the responses from the model and the MILES data can be observed. The percentage of fit between the two signals is calculated using the

formula

$$\%fit = 100\left(1 - \frac{\|\boldsymbol{y_p} - \hat{\boldsymbol{y}}_{\boldsymbol{p}}\|}{\|\boldsymbol{y_p} - \text{mean}(\boldsymbol{y_p})\|}\right) \tag{2.37}$$

where $\|.\|$ stands for two-norm, that for a vector $\boldsymbol{r}$ is equal to $\|\boldsymbol{r}\| = \sqrt{\boldsymbol{r}^T\boldsymbol{r}}$. The computed fits are

$$\begin{aligned} \textit{Self-efficacy}(\eta_3) &= 49.54\% \\ \textit{Behavior}(\eta_4) &= 34.95\% \end{aligned}$$

The mismatch between the data and model output can be explained by unmeasured dynamics, disturbances and unknown external signals. Since the data come from human behavior and in some cases from information collected via questionnaires, this type of mismatch is expected; however, it is observable that the same shape of response could be predicted with the proposed model. For a more formal validation, a semi-physical system identification procedure may be performed, utilizing a complete dataset with more appropriate *a priori* within-person experimental procedures.

2.7 Model Improvements Based on a Physical Activity Behavioral Intervention

Health behavior interventions are intended to move the behavioral status quo of the individual and shift behavior toward more healthful configurations (Hekler *et al.*, 2013b). The way this process is done can affect the success of the intervention significantly. Standardized interventions have been developed and focused on demographical defined groups. However, individual responses diverge considerably creating the necessity of more idiographic approaches. Another important factor is the way results are followed and, therefore, how the intervention components are adapted to changes in real time.

Recent technological developments have allowed a better understanding of behavioral change interventions; they use sensors and techniques, such as phone-based

ecological momentary assessment, to gather context-dependent behavioral and self-reported data. This enables the application of Intensively Adaptive Interventions (IAI), a concept presented by Riley *et al.* (2015b) that includes characterization of human behavior in terms of predictive computational models and the design of the intervention components based on the expected responses and actual measurements of the outcomes in real time.

2.7.1 Description of the Intervention

Models of behavioral theories based on dynamical systems can be used as the framework for IAIs. The low physical activity problem can be represented using Social Cognitive Theory, therefore intervention components can be selected and designed using this approach. The intervention is focused on a simplified version of the SCT model that represents a "behaviorist" articulation of the determinants of behavior (Ferster, 1970; Baum, 2011) including *self-efficacy*. The simplified SCT model considers inventories η_2, η_3, η_4, η_5, η_6, and incorporates additional inputs, as depicted in Fig. 2.18 described later in this paper. The proposed intervention is depicted in Fig. 2.16, where the main goal for the participant is to achieve and sustain the desired level of daily steps by the end of the intervention; this can be reached by systematically delivering the following components:

- *Daily goals* u_8, these can be delivered as an *external cue to action* (ξ_8) to establish quantitatively the desired behavior (e.g., 10,000 steps per day). They can vary according to the intervention objectives or the desired rate of change.

- *Expected points* u_9, delivered as a new input to the model called *outcome expectancy for reinforcement* (ξ_9) connected directly to the *outcome expectancy* (η_2) inventory, allowing the participant to know the daily expected reward points

that will be translated later into specific rewards (e.g., gift cards, gym subscriptions).

- *Granted points* u_{10}, delivered as an additional input to the model called *reinforcement* (u_{10}), that is fed to the *behavioral outcomes* (η_5) inventory, only if the performed behavior $y_4 = \eta_4$ (e.g., steps) is greater or equal than the specified goal u_8. This is achieved through an "If/Then block" that constitutes an inherent nonlinearity within the dynamical system.

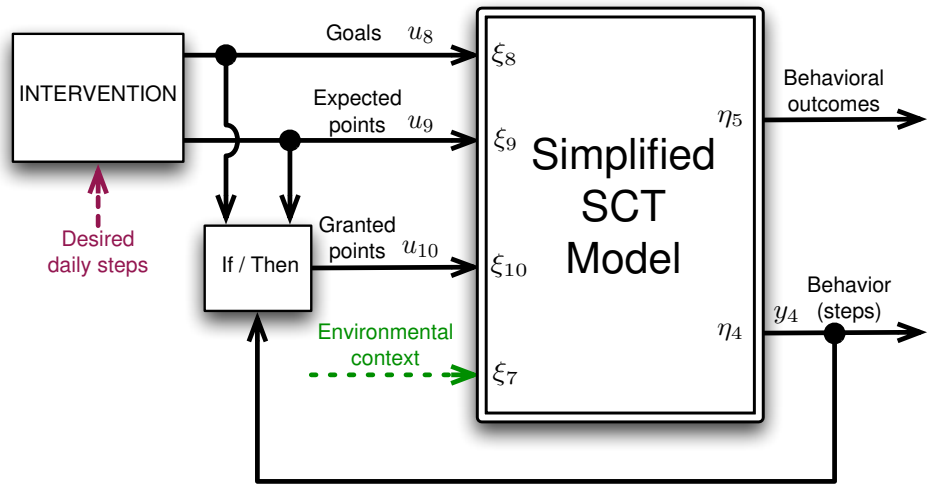

Figure 2.16: Conceptual Representation of the Physical Activity Intervention, Based on a Simplified Version of the SCT Model.

2.7.2 Representing the Ideal Step-Goal Range Feature

From a psychological standpoint, the continuous application of a positive stimulus may lead to a negative response; this response can take the shape of what is called an "inverted U" (Grant and Schwartz, 2011). In the case of a physical activity behavioral intervention using step goals as the main enabler, prior clinical experience (Adams *et al.*, 2013) suggests the existence of an ideal range at any given moment for a step

goal (e.g., if a person walked 7000 steps per day last week, next week an ideal goal range might be 7500-8500 steps). In this context individuals might react negatively to a high goal that they may consider difficult or impossible to reach; this effect can be represented through a steady state equilibrium curve.

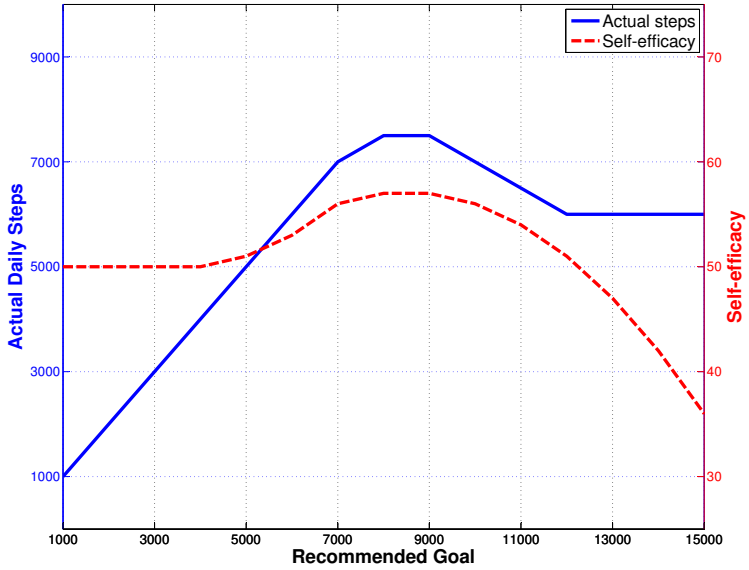

Figure 2.17: Hypothetical Steady State Equilibrium Curve Where the X-Axis Corresponds to the Recommended Goals (ξ_8), and the Y-Axis Gives the Actual Performed Steps (η_4) and *Self-efficacy* (η_3).

Fig. 2.17 illustrates a hypothetical equilibrium curve with numerical indicators implied from real physical activity interventions (King *et al.*, 2013; Adams *et al.*, 2013). The x-axis represents the recommended daily step goals; one of the y-axes represents the achieved average daily steps (e.g., daily average for a full week), while the second axis represents the perceived *self-efficacy* of the individual. A baseline initial behavior of 7000 steps for goals (e.g., steps performed the last week) is assumed; therefore, the ideal range of goals is positioned around that value forming the "inverted U". If the goals are above or below the range then lower achieved steps, and consequently an

inefficient response is expected. This result can be attributed for the higher part of the range to a state of pessimism in the individual caused by such a high goal setting.

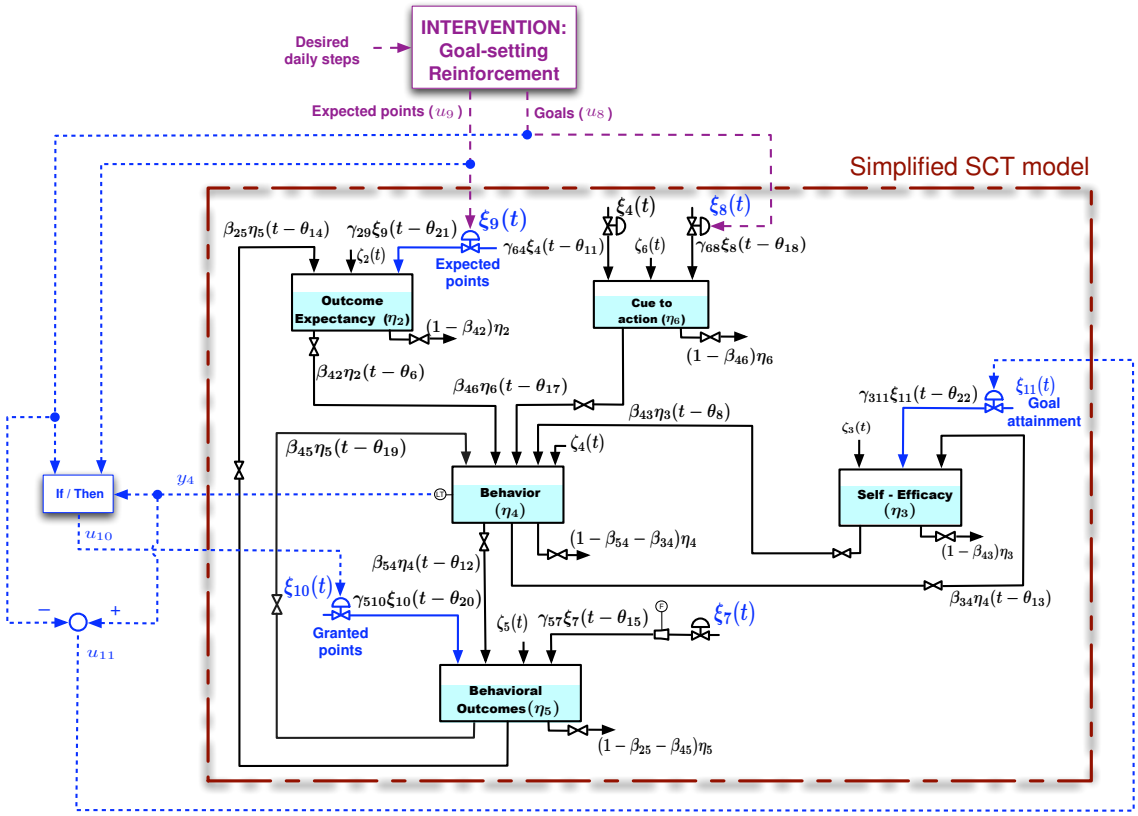

Figure 2.18: Low Physical Activity Intervention Based on the Simplified SCT Model With Reincorporation of the *Self-Efficacy* Inventory η_3 to Implement the Ideal Range Goal-Setting Feature.

The proposed approach to represent the ideal performance range, and hence goal setting, relies on the simplified SCT model. This is illustrated in Fig. 2.18 where the physical activity intervention is affecting the model through inputs: goals (u_8), expected and granted points (u_9, u_{10}), and a new signal called *Goal Attainment* (u_{11}) that gives an indication of the amount of attainment to the established goals as

$$u_{11} = y_4 - u_8 \tag{2.38}$$

This signal is fed into the *self-efficacy* inventory such that if the individual fails to reach a goal, a negative effect will be produced that ultimately will lead to a decrease in performed behavior. The magnitude of this negative effect is quantified through gains γ_{311} and parameter β_{43} .

To show the capability of the proposed approach to achieve an "inverted U" and define the ideal range, a simulation was performed using the model depicted in Fig. 2.18 with goals (u_8) as the unique input, and considering $\theta_i = 0, \zeta_j = 0$ $\forall i, j$. Performing the stability analysis described in Section 2.4.3 and considering the effect from *behavior* (η_4) to *self-efficacy* (η_3), one of the sufficient stability conditions detailed in (2.30) is

$$\beta_{34} < 1 \tag{2.39}$$

Considering that the added signal $u_{11} = y_4 - u_8$ includes a linear dependency on the inventory *behavior* ($y_4 = \eta_4$), the total effect from η_4 to η_3 is now $\beta_{34} + \gamma_{311}$; hence the previously discussed stability condition is modified as

$$\beta_{34} + \gamma_{311} < 1 \tag{2.40}$$

Using the hypothetical representation from Fig. 2.17 and the semi-physical identification procedure described in Section 2.6, the following set of SCT model parameters is selected to represent the ideal range of step-goals feature, and to satisfy the stability sufficient conditions:

- $\tau_2 = 28.26, \tau_3 = 876.07, \tau_4 = 20.19, \tau_5 = 25.98, \tau_6 = 0.06.$
- $\gamma_{29} = 1, \gamma_{64} = 1, \gamma_{68} = 1.01, \gamma_{33} = 1, \gamma_{510} = 1, \gamma_{57} = 1, \gamma_{35} = 1, \gamma_{36} = 1,$ $\gamma_{311} = 0.2.$
- $\beta_{25} = 0.12, \beta_{34} = 0.07, \beta_{42} = 0.27, \beta_{45} = 0.19, \beta_{46} = 0.13, \beta_{43} = 0.06, \beta_{54} = 0.01.$

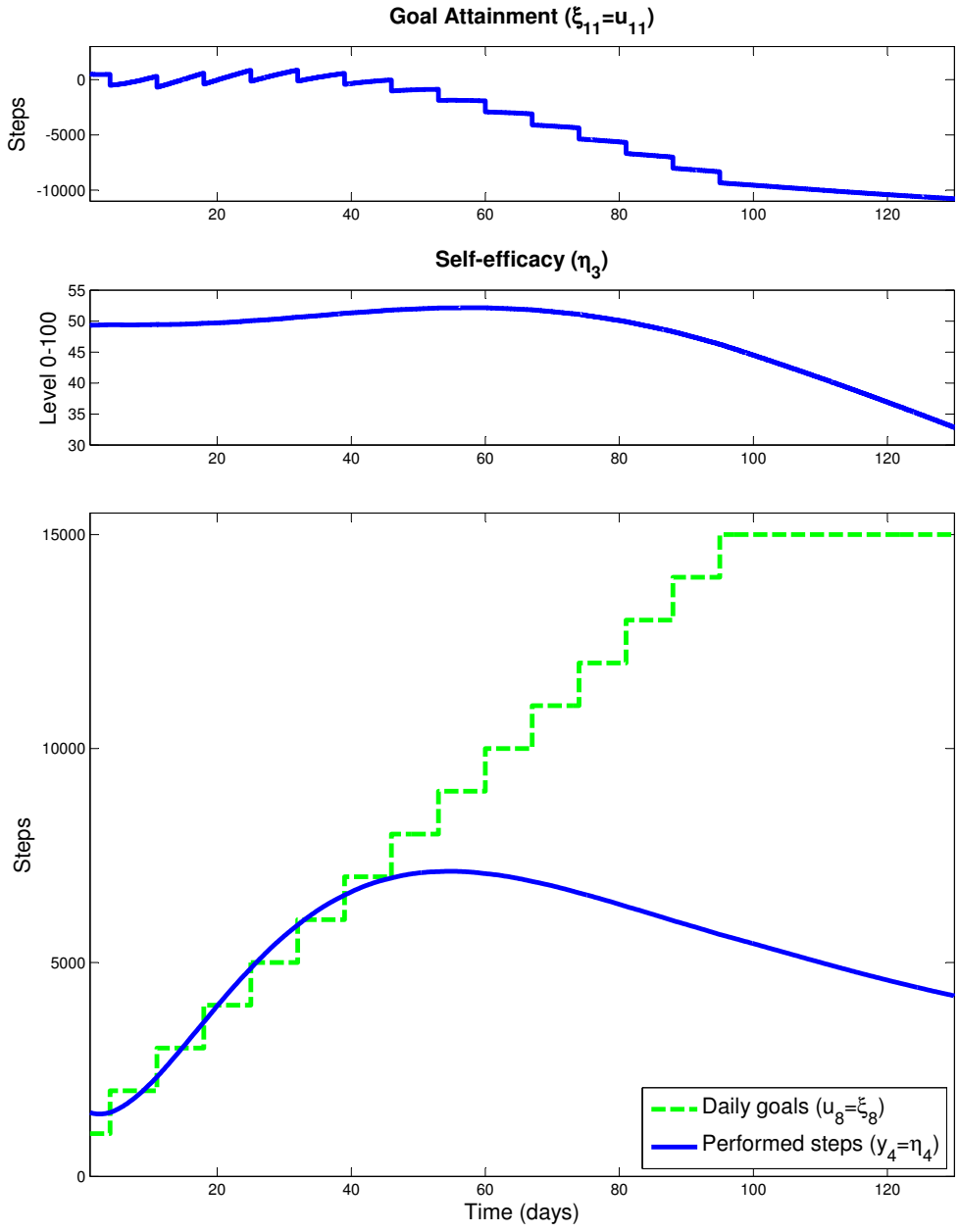

Figure 2.19: Simulation Results for a Physical Activity Behavioral Intervention, Representing the Ideal Range of Step-Goals Feature by Influencing *Self-Efficacy* (η_3) Through the *Goal Attainment* (u_{11}) Signal.

Simulation results are shown in Fig. 2.19. During a few initial cycles, the performed steps approximate the set goal. However, the magnitude of the difference between the goal and the steps increases as observed in the *goal attainment* (u_{11}) signal, causing a considerable reduction in *self-efficacy* (η_3) that eventually leads to a considerable reduction of performed steps ($y_4 = \eta_4$). This approach must be carefully verified via data obtained from system identification experiments, where it is crucial to obtain well validated measurements for *self-efficacy* and the other SCT model constructs.

2.8 Chapter Summary

This chapter describes how Social Cognitive Theory (SCT) can be represented as a control systems model. Fluid analogy concepts were used to represent the dynamic behavior portrayed in the theory; the analogy then was mathematically defined and improved with the addition of a nonlinear section; after that, computational models were created to support visualization and validation efforts. Further, based on the original narrative nature of the theory and the lack of specificity on some of the interrelationships between constructs, especially over time, many challenges to the creation of an effective control system model arose for determining the best representation of SCT from a control systems perspective. A path diagram from Structured Equation Modeling (SEM) was also shown to present the ideas more clearly.

The simulations proved to be valuable for better specifying implicit assumptions made within SCT to ensure better operationalization, for example the scenarios depicted the power of *cue to action* to strongly and rapidly influence behavior, much more so than the cognitive constructs of SCT (e.g., *self-efficacy*, outcome expectancies).

The comparison against the MILES data showed the ability of the model to depict

a real behavioral situation like physical activity. With an appropriate adaptation process, the model could be extended beyond behavioral health scenarios.

Further studies are being developed to test the use and application of this model. The structure of the model must be more thoroughly validated from experimental data using semiphysical modeling principles. System identification techniques can be used to better compare and contrast models; they should include an input design stage that excites the most relevant components of the model.

The simulated scenarios proved the capability of the model to depict the habituation phenomena as it is described in the theory. There are some additional details and approaches involved on the theory, such as overflow of reward structures (*behavioral outcomes*), that could be described with the same strategy used for habituation; furthermore both process could be modeled with more elaborate nonlinear schemes that can improve the accuracy of the model.

A well identified feature for physical activity interventions, called the ideal range of step goals, was incorporated into the model via a measurement of the goal achievement that is directly fed into the *self-efficacy* inventory. Simulations helped to prove the capability of this approach to represent the characteristic "inverted U" response when this condition is activated.

Chapter 3

IDENTIFICATION TEST MONITORING PROCEDURE FOR MULTIVARIABLE SYSTEMS

3.1 Overview

The accuracy of models obtained through system identification depends on the quality of the gathered experimental data and the selected identification method. The effect of external measurement conditions (e.g., noise) on model estimates can be mitigated by judicious input signal design. One of the major challenges in system identification is to obtain experiments that are sufficiently long and/or possess sufficiently high signal to noise ratios such that system identification on the data leads to useful models. Theoretical arguments favor experiments that are infinitely long or have very high input magnitudes; however these conditions are in sharp contrast to practical and economic constraints in real-life applications that demand shorter experiments, constrained input signal magnitudes, and minimal manipulation of the process actuators (Rivera *et al.*, 2003). In particular, problems in process control and adaptive interventions in behavioral health (Rivera, 2012) are application settings where recognizing "plant-friendly" or "patient-friendly" concepts motivate systematic approaches to determining the necessary duration of identification experiments (e.g., which can last months in the case of a behavioral health intervention).

To determine if the experimental data set is sufficiently informative, it is necessary to define reliable indicators of the accuracy of the estimation process, such as statistical uncertainties associated with the estimated parameters. *Identification test monitoring* is a problem postulated by Rivera *et al.* (2003) that proposes an iterative

evaluation and refinement of input signals and experimental execution based on non-parametric methods and uncertainty estimation. To obtain unbiased uncertainty descriptions, periodic deterministic input signals are utilized, with the timespan defined by one signal period defining an examination window for analysis of the identification results. For system identification purposes, the Empirical Transfer Function Estimation (ETFE) (Ljung, 1999) is used; it is an unbiased estimator for LTI systems subject to periodic input signals. To compute statistical uncertainty regions for the ETFE diverse methods have been proposed ((Bayard, 1993; Bayard and Hadaegh, 1994; De Vries and Van den Hof, 1995)); these differ in the level of dependence on *a priori* information available regarding the output noise structure, input design parameters, and process dynamics.

In the first part of this chapter, a basic identification test monitoring procedure is proposed from which the shortest possible experimental dataset resulting in an acceptable model can be identified. The process is applied to a multivariable system where the input signal is designed using a multisinusoidal "zippered" spectrum (Rivera *et al.*, 2009) to obtain independent-in-frequency inputs that enable the identification of individual transfer functions for each input-output combination. Each period of the input signal is considered as the time window from which a statistical uncertainty (using all data from initial to current time) is computed. Stopping criteria for the experiment are defined based on the input-output element(s) of interest and user-defined bounds. The final experimental duration will depend on pre-defined design conditions (e.g., signal period, number of frequencies) and on external and internal factors (e.g., measurement resolution, noise and system dynamics); hence desirable (but not necessarily unique) results are obtained.

In the basic formulation, the outputs are measured after some time to account for the transient effect. An estimate of the system's transient response effect is not

considered because the number of cycles in a multisine signal is the only input design parameter that can be adjusted. Moreover the criterion utilized to stop the experimental execution is solely based on percentage reduction in uncertainty during consecutive iterations. To address these considerations the second part of the chapter presents an enhanced identification test monitoring approach for MIMO systems considering additional types of modifications in the input signal during experimental execution. The additional modifications on the input signal are changes on the signal amplitude and frequency content of the signals. To account for transient responses as a result of changes in amplitude, the Local Polynomial Method (LPM) for periodic signals (Pintelon *et al.*, 2011) is utilized for computing transfer functions and uncertainties. Two variations of the LPM are tested and contrasted: first to reduce the bias in the estimation, the transient LPM (Monteyne *et al.*, 2012) is applied over a set of orthogonal-in frequency excited inputs constructed through the "zippered" spectral design, secondly the fast LPM method (Pintelon *et al.*, 2011) is applied over a set of input signals with a full spectral design allowing a better frequency resolution but increasing the bias on the estimate. The decision to make one or more of the specified modifications relies on operational constraints and user preferences. When the input's frequency content is re-defined, the new frequency grid makes use of harmonic related values to retain a connection with previous estimates. To obtain a complete estimate considering all the modifications performed during the experiment, an aggregate estimator of the transfer functions and uncertainties is developed. Finally, a stopping criterion for the experiment is presented that uses robust stability and robust performance metrics applied to the estimated uncertainty regions to guarantee performance of a closed-loop system achievable from the identification data.

The chapter is organized as follows. Section 3.2 presents a basic identification test monitoring procedure including the input signal design, an uncertainty estimation

procedure, and the proposed stopping criterion. Section 3.3 presents an enhanced identification test monitoring procedure incorporating the possibility of modifications in magnitude and harmonic frequency definition of the input signals. Additionally, an enhanced stopping criterion based on robust control concepts is proposed. Section 3.4 is a simulation study that explores the proposed approaches on a heavy oil fractionator plant model. Section 3.5 gives summary and conclusions of the chapter.

3.2 Basic Identification Test Monitoring Procedure Based on Statistical Uncertainty Estimates

3.2.1 Background and Input Signal Design

Consider a sampled-data multiple-input multiple-output (MIMO) system with $n_u \in \mathbb{N}$ inputs and $n_y \in \mathbb{N}$ outputs that can be described by

$$\boldsymbol{y}(k) = \boldsymbol{G}(q)\boldsymbol{u}(k) + \boldsymbol{v}(k) \tag{3.1}$$

where $\boldsymbol{u} \in \mathbb{R}^{n_u}$ and $\boldsymbol{y} \in \mathbb{R}^{n_y}$ are the input and output vectors respectively, $\boldsymbol{v} \in \mathbb{R}^{n_y}$ is the output disturbance vector and $\boldsymbol{G}(q)$ is the $n_y \times n_u$ transfer function matrix representing the multivariable LTI plant. Each SISO transfer function $G_{[m,n]}(q)$ represents the relationship between an input u_n and an output y_m for $m = 1 \dots n_y$, and $n = 1 \dots n_u$.

Using an output noise model as is illustrated in Fig. 3.1, any output y_m can be represented by the effect of all the n_u inputs and the respective output noise v_m as

$$y_m(k) = G_{[m,1]}(q)u_1(k) + \cdots + G_{[m,n_u]}(q)u_{n_u}(k) + v_m(k), \quad m = 1, \dots, n_y \tag{3.2}$$

Many identification approaches can be used to obtain the transfer function matrix $\boldsymbol{G}(q)$, however frequency domain methods (Bayard, 1993; Bayard and Hadaegh, 1994) offer convenient properties that may result in an appropriate uncertainty es-

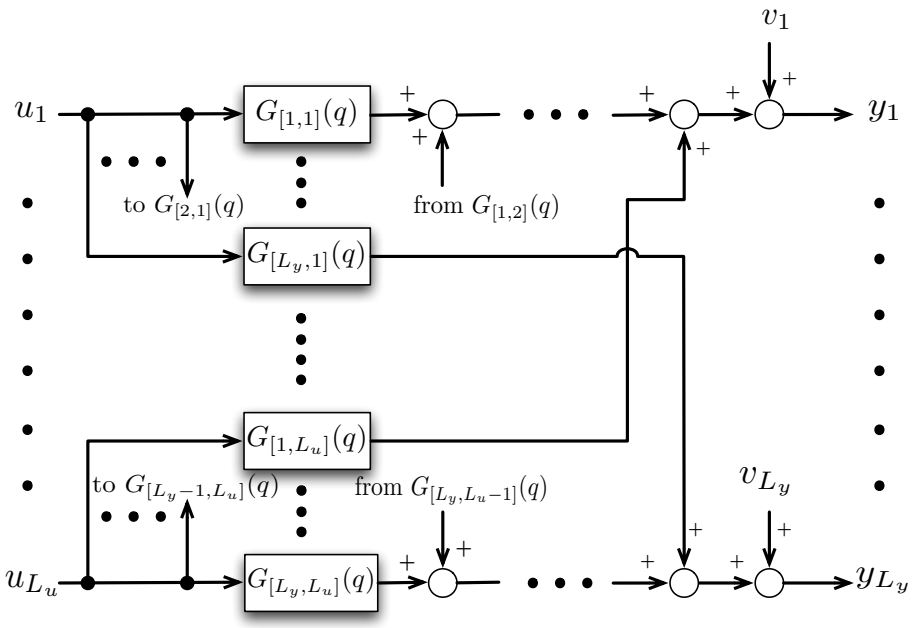

Figure 3.1: Block Diagram for the MIMO System Describing the Effect of an Individual SISO Transfer Function $G_{[m,n]}$ Over the Outputs.

timation. Instead of running n_u independent Single-Input Multiple-Output (SIMO) experiments with n_u different excitation signals, the proposed approach will consist in one experiment where the inputs are acting simultaneously, but each one is excited over an orthogonal grid of frequencies such that each $G_{[m,n]}$ can be independently estimated.

For system identification, the averaged Empirical Transfer Function Estimation (ETFE) method will be used. If the input signals are designed to be periodic (e.g., multisinusoidal signals), uncertainty bounds can be calculated using statistical approaches (Bayard, 1993; De Vries and Van den Hof, 1995; Pintelon and Schoukens, 2012). The general conditions for the existence of the averaged ETFE and the proposed uncertainty bounds are

- The true plant $\boldsymbol{G}(q)$ is exponentially stable, linear and time invariant.

- Each output disturbance noise $v_m(k)$, $m = 1, \ldots, n_y$ can be written as $v_m(k) = H_m(q)a_m(k)$ where $a_m(k)$ is a normalized white Gaussian zero-mean noise sequence, and $H_m(q)$ is a linear filter that can be decomposed as $H_m(q) = \sigma_m \bar{H}_m(q)$ where $\sigma_m < \infty$ is scalar and $\bar{H}_m(q)$ is an stable transfer function.

Multisine inputs are deterministic and periodic signals whose spectrum can be directly specified by the designer. One period of the input u_n can be described by

$$\begin{aligned} u_n(k) &= \lambda_n \sum_{j=1}^{N_s/2} \sqrt{2\alpha_{[n,j]}} \cos(\omega_j k T_s + \phi_{[n,j]}) \\ \omega_j &= \tfrac{2\pi j}{N_s T_s}, \quad k = 1, \ldots, N_s \end{aligned} \tag{3.3}$$

where λ_n is the scaling factor, N_s is the signal period, T_s is the sampling time. For each harmonic: $\alpha_{[n,j]}$ is a factor used to specify the relative power of the harmonic, ω_j is the frequency, and $\phi_{[n,j]}$ is the phase. The input signal will be repeated M cycles such that the total length of the signal is

$$N = N_s M \tag{3.4}$$

The coefficients $\alpha_{[n,j]}$ must be chosen to obtain input signals that are excited orthogonally in frequency. Two signals are orthogonal if a nonzero Fourier coefficient in a specific frequency of one signal implies a zero-valued Fourier coefficient at the same frequency for the other signal; this is called a "zippered" spectra design and was introduced by Rivera *et al.* (2009). If n_s is defined as the total number of independent excited sinusoids considering the n_u inputs, the total number of harmonics n_h can be defined as

$$n_h = n_s \tag{3.5}$$

The spectrum for each signal u_n, $n = 1, \ldots n_u$ can be constructed by specifying each

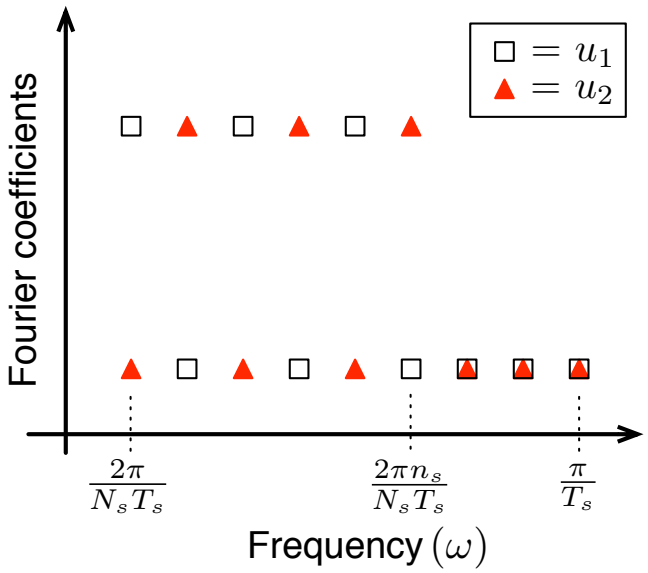

Figure 3.2: Conceptual Representation for a $n_u = 2$ Channel "Zippered" Spectra Design With $n_s = 6$ Independently Excited Sinusoids, Giving $n_h = 6$ Harmonics and Selecting $N_s = 18$.

$\alpha_{[n,j]}$ as

$$\alpha_{[n,j]} = \begin{cases} 1 & \text{if } j = n_u(i-1)+n \quad \text{for } i = 1, 2, \ldots n_s \\ 0 & \text{otherwise} \end{cases} \tag{3.6}$$

A conceptual representation of the zippered design for $n_u = 2$ inputs is presented in Fig. 3.2.

The signal period N_s must be carefully selected to meet the problem requirements; it should be long enough to capture the dynamics of the system, but at the same as short as possible since it will represent the resolution (time decision window) of the monitoring process. A starting point can be to select the required number of sinusoids per channel n_s; if some information is available about the model order and since n_s

represents the number of persistent excitation then

$$\text{Model order} \leq n_s \tag{3.7}$$

The range of usable frequencies is given by (3.3) as

$$\frac{2\pi}{N_s T_s} \leq \omega \leq \frac{2\pi n_s}{N_s T_s} < \frac{\pi}{T_s} \tag{3.8}$$

from where a bound for N_s can be derived as

$$N_s > 2n_s \tag{3.9}$$

therefore the total duration of the experiment N (in terms of sampling instants) is

$$N = N_s M > 2n_s M \tag{3.10}$$

If no further information about the system is available, the minimum period $N_s = 2n_s + 1$ can be selected. If some information is available about the dominant time constants of the system τ_{dom}^L and τ_{dom}^H, frequency bounds ω_* and ω^* can be defined as

$$\frac{1}{\beta_s \tau_{dom}^H} = \omega_* \leq \omega \leq \omega^* = \frac{\alpha_s}{\tau_{dom}^L} \tag{3.11}$$

where α_s and β_s are parameters that respectively specify high and low ranges of interest in the signal. Using a similar procedure to the one developed by Rivera *et al.* (2009), the following bounds can be defined to confirm or modify the values of n_s and N_s

$$\frac{2\pi}{N_s T_s} \leq \omega_* \leq \omega \leq \omega^* \leq \frac{2\pi n_s}{N_s T_s} < \frac{\pi}{T_s} \tag{3.12}$$

from where

$$N_s \geq \frac{2\pi}{\omega_* T_s} \quad \text{and} \quad N_s \leq \frac{2\pi n_s}{\omega^* T_s} \tag{3.13}$$

combining the two sides from (3.12) a bound for the bandwidth can be defined as

$$\omega^* - \omega_* \leq \frac{2\pi}{N_s T_s}(n_s - 1) \tag{3.14}$$

If N_s is replaced with the lower bound from (3.13) then

$$\omega^* - \omega_* \leq \omega_*(n_s - 1) \tag{3.15}$$

$$\frac{\omega^*}{\omega_*} - 1 \leq n_s - 1 \tag{3.16}$$

Consolidating results from (3.16), (3.13), and (3.9) the final bounds can be expressed as

$$n_s \geq \frac{\omega^*}{\omega_*} \tag{3.17}$$

$$\max\left(2n_s, \frac{2\pi}{\omega_* T_s}\right) \leq N_s \leq \frac{2\pi n_s}{\omega^* T_s} \tag{3.18}$$

One option for phase selection is to use the approach of Schroeder (1970), designed to minimize peaking in the time domain as:

$$\phi_{[n,j]} = 2\pi \sum_{c_i=1}^{j} c_i . \alpha_{[n,c_i]} \tag{3.19}$$

If low variability on the input signals is of special importance, a modification can be used based on the crest factor (CF) index; CF is defined by the ratio of the Chebyshev (infinity) norm versus the 2-norm:

$$CF(u_n) = \frac{\ell_\infty(u_n)}{\ell_2(u_n)} \tag{3.20}$$

The crest factor provides a measure of the distribution of the signal values over the input span. A low crest factor indicates that most of the values are located near the maximum and minimum of the sequence, thus avoiding infrequent and comparatively high peak values.

Harmonic phases will be selected to minimize the crest factor of the signal using the approach proposed by Guillaume *et al.* (1991), where an approximation of the

minimization of the Chebyshev norm is proposed by sequentially minimizing the ℓ_p norm for $p = 4, 8, 16, \ldots$ based on Pólya's algorithm which states that:

$$\lim_{p\to\infty} \mathbf{p}_p = \mathbf{p}_\infty \tag{3.21}$$

where $\mathbf{p} = [\phi_{[n,1]} \quad \phi_{[n,2]} \quad \ldots \quad \phi_{[n,n_s]}]^\top$ is the phase vector for (3.3) and $\mathbf{p}_\infty$ is the minimax solution considering that the 2-norm remains invariant with respect to the phases $\phi_{[n,j]}$. This is in general a nonlinear optimization problem and performs better than other crest factor minimization techniques (Guillaume *et al.*, 1991).

3.2.2 Uncertainty Description

3.2.2.1 Transfer Function Estimation

Since each u_n is designed orthogonally in frequency, it is possible to find independent estimates for every transfer function element. Assume that M periods of input/output data $u_n(k)$, $y_m(k)$ are collected and denote the output data from the lth period as

$$\begin{aligned} y_m^l(k) &= y_m(k + (l-1)N_s) \\ k &= 1 \ldots N_s, \quad l = 1 \ldots M \end{aligned} \tag{3.22}$$

The Discrete Fourier Transforms (DFT) for each input and output are defined by

$$U_n(\omega_j) = \frac{1}{\sqrt{N_s}} \sum_{k=1}^{N_s} u_n(k) e^{-i\omega_j k T_s}; \quad n = 1, \ldots, n_u \tag{3.23}$$

$$Y_m^l(\omega_j) = \frac{1}{\sqrt{N_s}} \sum_{k=1}^{N_s} y_m^l(k) e^{-i\omega_j k T_s}; \quad m = 1, \ldots, n_y \tag{3.24}$$

$$\text{for} \quad \omega_j = \tfrac{2\pi j}{N_s T_s}, \quad j = 1, 2 \ldots n_s n_u \tag{3.25}$$

For periodic inputs the ETFE is an unbiased estimation and is defined only for a fixed number of frequencies (Ljung, 1999). The averaged ETFE is computed as

$$\hat{G}_{[m,n]}(\omega_i^n) = \frac{\bar{Y}_m(\omega_i^n)}{U_n(\omega_i^n)} \tag{3.26}$$

$$\text{with} \quad \bar{Y}_m(\omega_i^n) = \frac{1}{M}\sum_{l=1}^{M} Y_m^l(\omega_i^n) \tag{3.27}$$

where $\omega_i^n \in \boldsymbol{W^n}$, and $\boldsymbol{W^n}$ is the frequency grid defined by the zippered design for input n as a subset of the complete grid shown in (3.25), specified by

$$\boldsymbol{W^n} = \{\omega_i^n \in \mathbb{R} \mid \omega_i^n = \tfrac{2\pi[n_u(i-1)+n]}{N_s T_s}, \quad i = 1, 2, \ldots, n_{sch}\} \tag{3.28}$$

and n_{sch} is the total number of harmonics excited per input channel defined as

$$n_{sch} = \frac{n_s}{n_u} \tag{3.29}$$

3.2.2.2 Survey of Statistical Uncertainty Computation Methods

Diverse approaches have been developed for the computation of statistical uncertainties from the ETFE over periodic inputs; the main differences between these are:

- Existence of *a priori* knowledge of the design parameters of the periodic input signal, such that the Fourier coefficients of the spectrum can be derived.
- Existence of *a priori* knowledge of the noise coloring filter $H_m(q)$.
- Requirement that data be collected at periodic steady-state

A first approach presented by Bayard (1993), relies on a simultaneous estimation of the transfer function as a regression problem using a Gauss-Markov formulation, where it is necessary to use the $\alpha_{[n,j]}$ factors from the input spectral definition presented in (3.3). It is assumed that the data is taken at periodic steady-state. The noise coloring filter $H_m(q)$ is known, and σ_m may be either known or unknown. If σ_m is unknown it can be estimated using the regression approach as

$$\hat{\sigma}_m^2 = \frac{\sum_{l=1}^{M}\sum_{i=1}^{n_s}\left|\bar{Y}_m(\omega_i^n) - Y_m^l(\omega_i^n)\right|^2}{N_s(N_s M - 2n_{sch})}, \quad \omega_i^n \in \boldsymbol{W^n} \tag{3.30}$$

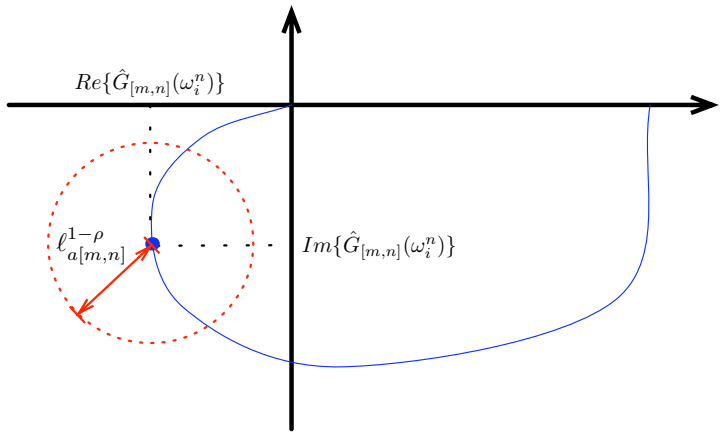

Figure 3.3: Conceptual Representation of the $100 \times (1-\rho)\%$ Confidence Region for $\hat{G}_{[m,n]}(\omega_i^n)$ Over a Nyquist Frequency Response Plot for a Specific Frequency $\omega_i^n \in \boldsymbol{W^n}$.

The confidence region is conceptually illustrated in Fig. 3.3, where it can be seen in a Nyquist plot as a circle centered in $\hat{G}_{[m,n]}(\omega_i^n)$ of radius $\ell^{1-\rho}_{a[m,n]}$ equal to

$$\left[\ell^{1-\rho}_{a[m,n]}(\omega_i^n)\right]^2 = \frac{2\hat{\sigma}_m^2 |\bar{H}_m(\omega_i^n)|^2}{\alpha_{[n,j]} N_s M} F_{1-\rho}(2, N_s M - 2n_{sch}) \tag{3.31}$$

where $\alpha_{[n,j]}$ is given by (3.6), and $F_{1-\rho}(\nu_1, \nu_2)$ is the $100 \times (1-\rho)\%$ percentile of a Fisher distribution with ν_1 and ν_2 degrees of freedom such that

$$Prob\left\{ \left| \hat{G}_{[m,n]}(\omega_i^n) - G_{[m,n]}(\omega_i^n) \right| \leq \ell^{1-\rho}_{a[m,n]}(\omega_i^n) \right\} = 1 - \rho \tag{3.32}$$

An extension for the MIMO case was presented by Bayard and Hadaegh (1994), where an expression of the filter $H_m(q)$ is no longer required. From a practical standpoint this improvement is very important since precise knowledge of the noise structure may be difficult to obtain. However the price to be paid is that results are valid only asymptotically. In this case an estimation of the output noise variance for each

frequency is given as

$$|\hat{H}_m(\omega_i^n)|^2 = \frac{\sum_{l=1}^{M} \left|\bar{Y}_m(\omega_i^n) - Y_m^l(\omega_i^n)\right|^2}{N_s(M-1)} \tag{3.33}$$

The resultant additive uncertainty norm-bound for a $100 \times (1-\rho)\%$ confidence region is

$$\left[\ell_{a[m,n]}^{1-\rho}(\omega_i^n)\right]^2 = \frac{2|\hat{H}_m(\omega_i^n)|^2}{\alpha_{[n,j]} N_s M} F_{1-\rho}(2, 2M-2) \tag{3.34}$$

One minor drawback of this method is that still requires the use of the Fourier coefficients $\alpha_{[n,j]}$ from the multisine definition.

In this work, an uncertainty description that does not require specific knowledge of the noise filter $H_m(q)$ and the input spectral definition will be used. However, it still requires periodic steady-state data. One uncertainty computation method that includes effects of unmodeled dynamics and transient responses can be found in (De Vries and Van den Hof, 1995). It incorporates hard error bounds to deal with the transient response problems while making the estimation more conservative.

3.2.2.3 Additive Uncertainty Calculation

The proposed approach does not require *a priori* information about the input spectra and the noise filter structure, but the data needs to be measured at periodic steady-state. The noise variance is computed from transfer function estimation rather than from the output measurement only. The following expressions are referred to the frequency grid for ω_i^n defined in (3.28). Under the specified conditions it can be shown (Bayard, 1993; Pintelon and Schoukens, 2012) that

$$\frac{|\hat{G}_{[m,n]}(\omega_i^n) - G_{[m,n]}(\omega_i^n)|^2}{\hat{\sigma}^2_{\hat{G}_{[m,n]}}(\omega_i^n)} \sim F(2, 2M-2) \tag{3.35}$$

where $F(\nu_1, \nu_2)$ denotes a Fisher distribution with ν_1 and ν_2 degrees of freedom, and $\hat{\sigma}^2_{\hat{G}_{[m,n]}}(\omega_i^n)$ is the sample variance of the averaged ETFE.

Since the ETFE was obtained from an averaging procedure, and following standard results from probability theory, its variance can be derived from the variance of the real transfer function $G_{[m,n]}$ as

$$\sigma^2_{\hat{G}_{[m,n]}}(\omega_i^n) = \frac{\sigma^2_{G_{[m,n]}}(\omega_i^n)}{M} \tag{3.36}$$

and using sample variances

$$\hat{\sigma}^2_{\hat{G}_{[m,n]}}(\omega_i^n) = \frac{\hat{\sigma}^2_{G_{[m,n]}}(\omega_i^n)}{M} \tag{3.37}$$

the sample variance of $G_{[m,n]}$ can be estimated as

$$\hat{\sigma}^2_{G_{[m,n]}}(\omega_i^n) = \frac{1}{M-1} \frac{\sum_{l=1}^{M} |\bar{Y}_m(\omega_i^n) - Y_m^l(\omega_i^n)|^2}{|U_n(\omega_i^n)|^2} \tag{3.38}$$

from here it follows that

$$\hat{\sigma}^2_{\hat{G}_{[m,n]}}(\omega_i^n) = \frac{1}{M(M-1)} \frac{\sum_{l=1}^{M} |\bar{Y}_m(\omega_i^n) - Y_m^l(\omega_i^n)|^2}{|U_n(\omega_i^n)|^2} \tag{3.39}$$

As was previously noted, the additional division by M is due to averaging in the estimates (Pintelon and Schoukens, 2012).

For a duration of M periods, the $100 \times (1-\rho)\%$ confidence region can be constructed as a circle with center $\hat{G}_{[m,n]}(\omega_i^n)$ and radius $\ell^{1-\rho}_{a[m,n]}(\omega_i^n, M)$ where

$$\left[\ell^{1-\rho}_{a[m,n]}(\omega_i^n, M)\right]^2 = \hat{\sigma}^2_{\hat{G}_{[m,n]}}(\omega_i^n) F_{1-\rho}(2, 2M-2) \tag{3.40}$$

An explicit dependence on the period M in the uncertainty definition has been added for use in the definition of the monitoring process. Estimated uncertainty bounds are asymptotic; small values of M result in conservative estimates.

A multivariable uncertainty computation approach that involves all the transfer function elements can also be specified (Bayard and Hadaegh, 1994); this will constitute a more general but conservative estimate. Model uncertainty constituting the maximum singular value at each frequency grid point with probability $1-\kappa$ can be characterized by

$$Prob\Big\{\overline{\sigma}\big(\hat{\boldsymbol{G}}(\omega_i^n)-\boldsymbol{G}(\omega_i^n)\big)\leq\epsilon^{1-\kappa}(\omega_i^n)\Big\}=1-\kappa \tag{3.41}$$

The well known Frobenious norm bound can be considered over the square of the maximum singular value as

$$\overline{\sigma}\big(\hat{\boldsymbol{G}}(\omega_i^n)-\boldsymbol{G}(\omega_i^n)\big)^2\leq\|\hat{\boldsymbol{G}}(\omega_i^n)-\boldsymbol{G}(\omega_i^n)\|_f^2 \tag{3.42}$$

$$=\sum_{n=1}^{n_u}\sum_{m=1}^{n_y}|\hat{G}_{[m,n]}(\omega_i^n)-G_{[m,n]}(\omega_i^n)|^2 \tag{3.43}$$

Each of the terms in (3.43) can be overbounded to probability $1-\rho$ by

$$\big|\hat{G}_{[m,n]}(\omega_i^n)-G_{[m,n]}(\omega_i^n)\big|^2\leq\big[\ell^{1-\rho}_{a[m,n]}(\omega_i^n,M)\big]^2 \tag{3.44}$$

with $\ell^{1-\rho}_{a[m,n]}(\omega_i^n,M)$ calculated in (3.40). The events in (3.43) are statistically independent since each output is generated from a different Gaussian source and each input is defined orthogonally in frequency; hence the event

$$\overline{\sigma}\big(\hat{\boldsymbol{G}}(\omega_i^n)-\boldsymbol{G}(\omega_i^n)\big)^2\leq\sum_{n=1}^{n_u}\sum_{m=1}^{n_y}\big[\ell^{1-\rho}_{a[m,n]}(\omega_i^n,M)\big]^2\triangleq\big[\epsilon^{1-\kappa}(\omega_i^n,M)\big]^2 \tag{3.45}$$

holds with probability

$$1-\kappa=(1-\rho)^{n_y\cdot n_u} \tag{3.46}$$

3.2.2.4 Extension to a Parallel Connected System

Consider that the system to be identified contains two transfer functions $G_{[m,n]}$ and $S_{[m,n]}$ that operate in parallel over the output as shown in Fig. 3.4; assume also that

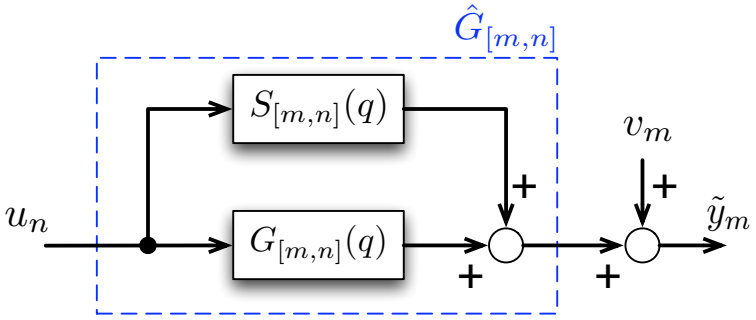

Figure 3.4: Block Diagram of a Modified System Including the Effect of a Transfer Function $S_{[m,n]}(q)$ Connected in Parallel With $G_{[m,n]}(q)$.

individual estimations for each transfer function are required. Regular identification procedures are not able to process the information to obtain independent estimates of $G_{[m,n]}$ and $S_{[m,n]}$. Semi-physical identification methods (e.g., grey box) (Lindskog and Ljung, 1995) can solve the problem by using *a-priori* known partial information of the models, together with the experimental inputs and outputs. Under these conditions it is interesting to check the validity of the calculated uncertainties as indicators of the output noise effect over the estimation.

Considering the original system without the addition of $S_{[m,n]}$ and using (3.1)

$$y_m(k) = G_{[m,n]}(q)u_n(k) + v_m(k) \tag{3.47}$$

$$\begin{gathered} Y_m^l(\omega_i^n) = G_{[m,n]}(\omega_i^n)U_n(\omega_i^n) + V_m^l(\omega_i^n), \\ l = 1, \ldots, M \end{gathered} \tag{3.48}$$

where $V_m^l(\omega_i^n)$ is the DFT for the l^{th} period of the output noise signal $v_m(k)$. The averaged DFT of the output is

$$\bar{Y}_m(\omega_i^n) = \frac{1}{M}\sum_{l=1}^{M}\left[G_{[m,n]}(\omega_i^n)U_n(\omega_i^n) + V_m^l(\omega_i^n)\right] \tag{3.49}$$

$$\bar{Y}_m(\omega_i^n) = G_{[m,n]}(\omega_i^n)U_n(\omega_i^n) + \bar{V}_m(\omega_i^n) \tag{3.50}$$

$$\text{where} \quad \bar{V}_m(\omega_i^n) = \frac{1}{M}\sum_{l=1}^{M} V_m^l(\omega_i^n) \tag{3.51}$$

From (3.39)

$$\hat{\sigma}^2_{\hat{G}_{[m,n]}}(\omega_i^n) = \frac{1}{M(M-1)}\frac{H_m(\omega_i^n)}{|U_n(\omega_i^n)|^2} \tag{3.52}$$

$$\text{with} \quad H_m(\omega_i^n) = \sum_{l=1}^{M} |\bar{Y}_m(\omega_i^n) - Y_m^l(\omega_i^n)|^2 \tag{3.53}$$

substituting (3.48) and (3.50) in (3.53)

$$H_m(\omega_i^n) = \sum_{l=1}^{M} \left|G_{[m,n]}(\omega_i^n)U_n(\omega_i^n) + \bar{V}_m(\omega_i^n) - G_{[m,n]}(\omega_i^n)U_n(\omega_i^n) - V_m^l(\omega_i^n)\right|^2 \tag{3.54}$$

$$H_m(\omega_i^n) = \sum_{l=1}^{M} \left|\bar{V}_m(\omega_i^n) - V_m^l(\omega_i^n)\right|^2 \tag{3.55}$$

By replacing $H_m(\omega_i^n)$ in (3.52) and (3.40) it can be seen that the computed additive uncertainty $\ell^{1-\rho}_{a[m,n]}(\omega_i^n, M)$ depends only on the effect of the output noise $v_m(k)$, and not on $G_{[m,n]}$.

If the system depicted in Fig. 3.4 is now considered including $S_{[m,n]}(q)$ the output is

$$\tilde{y}_m(k) = G_{[m,n]}(q)u_n(k) + S_{[m,n]}(q)u_n(k) + v_m(k) \tag{3.56}$$

Previous derivations are recomputed as

$$\tilde{Y}_m^l(\omega_i^n) = G_{[m,n]}(\omega_i^n)U_n(\omega_i^n) + S_{[m,n]}(\omega_i^n)U_n(\omega_i^n) + V_m^l(\omega_i^n) \tag{3.57}$$

$$\tilde{\bar{Y}}_m(\omega_i^n) = G_{[m,n]}(\omega_i^n)U_n(\omega_i^n) + S_{[m,n]}(\omega_i^n)U_n(\omega_i^n) + \bar{V}_m(\omega_i^n) \tag{3.58}$$

The variance of the ETFE is now

$$\hat{\sigma}^2_{\tilde{\hat{G}}_{[m,n]}}(\omega_i^n) = \frac{1}{M(M-1)}\frac{\tilde{H}_m(\omega_i^n)}{|U_n(\omega_i^n)|^2} \tag{3.59}$$

$$\text{with} \quad \tilde{H}_m(\omega_i^n) = \sum_{l=1}^{M} |\tilde{\bar{Y}}_m(\omega_i^n) - \tilde{Y}_m^l(\omega_i^n)|^2 \tag{3.60}$$

and

$$\tilde{H}_m(\omega_i^n) = \sum_{l=1}^{M} \Big| \big[G_{[m,n]}(\omega_i^n) + S_{[m,n]}(\omega_i^n)\big] U_n(\omega_i^n) + \bar{V}_m(\omega_i^n) - \big[G_{[m,n]}(\omega_i^n) + S_{[m,n]}(\omega_i^n)\big] U_n(\omega_i^n) - V_m^l(\omega_i^n) \Big|^2 \tag{3.61}$$

$$\tilde{H}_m(\omega_i^n) = \sum_{l=1}^{M} \big|\bar{V}_m(\omega_i^n) - V_m^l(\omega_i^n)\big|^2 \tag{3.62}$$

therefore

$$\tilde{H}_m(\omega_i^n) = H_m(\omega_i^n) \tag{3.63}$$

This result shows once again that the computed uncertainty depends only on the portion due to the output noise on y_m. It can serve as a measurement of the output noise effect on the capability of the experimental data set to identify the system adequately.

3.2.2.5 Error-In-Variables Uncertainty Description

In this section the error-in-variables case (Söderström *et al.*, 2007) is considered; this scenario is depicted in Fig. 3.5 for an specific input-output element $G_[m, n]$, where both inputs and outputs are corrupted by external noise as

$$u_n(k) = u_n^0(k) + x_n(k) \tag{3.64}$$

$$y_m(k) = y_m^0(k) + v_m(k) \tag{3.65}$$

u_n^0 and u_n are the designed input and the measured input respectively, while x_n is the input measurement noise. The measured output y_m is defined as shown in (3.2) with

$$y_m^0(k) = G_{[m,1]}(q)u_1^0(k) + \cdots + G_{[m,n_u]}(q)u_{n_u}^0(k) \tag{3.66}$$

Such circumstances may exist when the input signal is not fully designed by the user, but has an underlying periodic character and can be measured. Uncertainty bounds

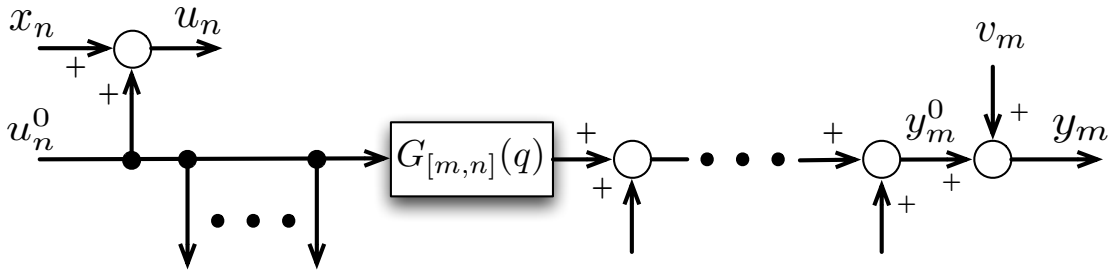

Figure 3.5: Block Diagram Showing the Error-In-Variable Setting for Input n and Output m of a MIMO System.

can still be computed; however, calculating the estimation variance must consider the variability on the input measurement. The l^{th} period of the n^{th} measured input signal is

$$\begin{aligned} u_n^l(k) &= u_n(k + (l-1)N_s) \\ k &= 1 \dots N_s, \quad l = 1 \dots M \end{aligned} \tag{3.67}$$

and its DTF is defined as

$$\begin{aligned} U_n^l(\omega_j) &= \frac{1}{\sqrt{N_s}} \sum_{k=1}^{N_s} u_n^l(k) e^{-i\omega_j k T_s}; \quad n = 1, \dots, n_u \\ \text{for} \quad \omega_j &= \tfrac{2\pi j}{N_s T_s}, \quad j = 1, 2 \dots n_s n_u \end{aligned} \tag{3.68}$$

for $\omega_i^n \in \boldsymbol{W^n}$ the mean value of U_n is

$$\bar{U}_n(\omega_i^n) = \frac{1}{M} \sum_{l-1}^{M} U_n^l(\omega_i^n) \tag{3.69}$$

and the ETFE is now

$$\hat{G}_{[m,n]}(\omega_i^n) = \frac{\bar{Y}_m(\omega_i^n)}{\bar{U}_n(\omega_i^n)} \tag{3.70}$$

The sample variances and covariance of U_n and Y_m are

$$\hat{\sigma}^2_{U_n}(\omega_i^n) = \frac{1}{M-1} \sum_{l=1}^{M} \left| \bar{U}_n(\omega_i^n) - U_n^l(\omega_i^n) \right|^2 \tag{3.71}$$

$$\hat{\sigma}^2_{Y_m}(\omega_i^n) = \frac{1}{M-1}\sum_{l=1}^{M}\left|\bar{Y}_m(\omega_i^n) - Y_m^l(\omega_i^n)\right|^2 \tag{3.72}$$

$$\hat{\sigma}^2_{Y_m U_n}(\omega_i^n) = \frac{1}{M-1}\sum_{l=1}^{M}\left[\left(\bar{Y}_m(\omega_i^n) - Y_m^l(\omega_i^n)\right)\cdot\overline{\left(\bar{U}_n(\omega_i^n) - U_n^l(\omega_i^n)\right)}\right] \tag{3.73}$$

It can be shown (Pintelon and Schoukens, 2012) that the sample variance of the ETFE for this case can be computed as

$$\hat{\sigma}^2_{\hat{G}_{[m,n]}}(\omega_i^n) = \frac{|\hat{G}_{[m,n]}(\omega_i^n)|^2}{M}\left(\frac{\hat{\sigma}^2_{Y_m}(\omega_i^n)}{|\bar{Y}_m(\omega_i^n)|^2} + \frac{\hat{\sigma}^2_{U_n}(\omega_i^n)}{|\bar{U}_n(\omega_i^n)|^2} - 2\,\mathrm{Re}\left\{\frac{\hat{\sigma}^2_{Y_m U_n}(\omega_i^n)}{\bar{Y}_m(\omega_i^n)\overline{\bar{U}_n(\omega_i^n)}}\right\}\right) \tag{3.74}$$

and the additive uncertainty $\ell^{1-\rho}_{a[m,n]}(\omega_i^n, M)$ can be computed using (3.40) again.

Note that if no noise exists in the input (i.e., the input is measured as designed), then $\bar{U}_n(\omega_i^n) = U_n^l(\omega_i^n)(l = 1, \ldots, M) = U_n(\omega_i^n)$; therefore $\hat{\sigma}^2_{U_n}(\omega_i^n) = 0$, $\hat{\sigma}^2_{Y_m U_n}(\omega_i^n) = 0$, and equation (3.74) is transformed into (3.39).

3.2.3 Derivation of a Monitoring Procedure

As noted in the Overview section, the goal is to find the shortest experiment that is sufficiently informative based on a specified uncertainty level. The monitoring procedure is performed by incrementing the number of periods M one at a time (starting from $M = 2$ because of averaged ETFE), such that with each increment on M the total duration of the experiment will be $N_s T$ time units longer.

Using a worst-case criterion, a maximum additive uncertainty is computed over the frequency grid for ω_i^n defined in (3.28) for each input/output element as

$$\tilde{\ell}_{a[m,n]}(M) = \max_{\omega_i^n \in \boldsymbol{W^n}}\left[\ell^{1-\rho}_{a[m,n]}(\omega_i^n, M)\right], \quad M = 2, 3\ldots \tag{3.75}$$

Uncertainty values by themselves are not meaningful for the monitoring process, instead percentages of reduction in $\tilde{\ell}_{a[m,n]}(M)$ among successive values of M are cal-

culated

$$AV_{[m,n]}(M) = \frac{\tilde{\ell}_{a[m,n]}(M-1) - \tilde{\ell}_{a[m,n]}(M)}{\tilde{\ell}_{a[m,n]}(2)} \times 100 \tag{3.76}$$

$$RV_{[m,n]}(M) = \frac{\tilde{\ell}_{a[m,n]}(M-1) - \tilde{\ell}_{a[m,n]}(M)}{\tilde{\ell}_{a[m,n]}(M-1)} \times 100 \tag{3.77}$$

$$M = 3, 4 \ldots$$

where $AV_{[m,n]}$ is the absolute percentage reduction referred to the first estimate ($M = 2$), and $RV_{[m,n]}$ is the relative percentage reduction referred to the previous value of M.

Depending on the system, the set of all the (m, n) elements of interest can be defined as

$$\begin{gathered} \boldsymbol{O} = \big\{(m \in \mathbb{N}, n \in \mathbb{N}) \mid 1 \leq m \leq n_y, 1 \leq n \leq n_u, \\ \text{effect from input } n \text{ to output } m \text{ is of interest}\big\} \end{gathered} \tag{3.78}$$

This definition allows the use of one or more of the transfer function elements.

Using the worst case scenario criterion, maximum percentages of uncertainty reduction within all input-output directions are defined as

$$AV(M) = \max_{(m,n)\in\boldsymbol{O}} AV_{[m,n]}(M), \quad M = 3, 4 \ldots \tag{3.79}$$

$$RV(M) = \max_{(m,n)\in\boldsymbol{O}} RV_{[m,n]}(M), \quad M = 3, 4 \ldots \tag{3.80}$$

The stopping criterion will determine when the percentage changes on uncertainties have reached a predefined minimum bound for a determined amount of continuous iterations, and therefore the experiment can be stopped. If B_{AV} and B_{RV} are defined as the maximum allowed percentages of reduction in the last n_{Mi} consecutive unitary increments of M, then the stopping criterion can be

$$\begin{gathered} \text{Stop at } M = Q - 1 \text{ when} \\ AV(Q-r) \leq B_{AV} \quad \text{and} \quad RV(Q-r) \leq B_{RV} \\ \text{for } r = 1, \ldots, n_{Mi} \text{ consecutive iterations} \end{gathered} \tag{3.81}$$

Lower values of B_{AV} and B_{RV}, or a higher n_{Mi}, will result in more accurate but longer experiments.

Maximum additive uncertainty for the general multivariable case can also be computed using the bound $\epsilon^{1-\kappa}(\omega_i^n, M)$, defined in (3.45)

$$\tilde{\epsilon}(M) = \max_{\omega_i^n \in \boldsymbol{W^n}} \left[\epsilon^{1-\kappa}(\omega_i^n, M)\right], \quad M = 2, 3 \dots \tag{3.82}$$

and percentages of uncertainty reduction can be redefined for $M = 3, 4 \dots$ as

$$AV(M) = \frac{\tilde{\epsilon}(M-1) - \tilde{\epsilon}(M)}{\tilde{\epsilon}(2)} \times 100 \tag{3.83}$$

$$RV(M) = \frac{\tilde{\epsilon}(M-1) - \tilde{\epsilon}(M)}{\tilde{\epsilon}(M-1)} \times 100 \tag{3.84}$$

Based on the definitions in (3.83) and (3.84), the stopping criteria presented in (3.81) can be used.

3.3 Enhanced Identification Test Monitoring Procedure Relying on Uncertainty Estimates

3.3.1 Background

Consider the sampled-data multiple-input multiple-output (MIMO) system presented in Section 3.2.1 with $n_u \in \mathbb{N}$ inputs and $n_y \in \mathbb{N}$ outputs, and described by

$$\boldsymbol{y}(k) = \boldsymbol{G}(q)\boldsymbol{u}(k) + \boldsymbol{v}(k) \tag{3.85}$$

where $\boldsymbol{u} \in \mathbb{R}^{n_u}$ and $\boldsymbol{y} \in \mathbb{R}^{n_y}$ are the input and output vectors respectively, $\boldsymbol{v} \in \mathbb{R}^{n_y}$ is the output disturbance vector and $\boldsymbol{G}(q)$ is the $n_y \times n_u$ transfer function matrix representing the multivariable LTI plant. Each SISO transfer function $G_{[m,n]}(q)$ represents the relationship between an input u_n and an output y_m for $m = 1 \dots n_y$, and $n = 1 \dots n_u$.

To perform the proposed identification test monitoring procedure, uncertainties are obtained through the computation of frequency domain transfer function estimates. The conditions assumed for the validity of the proposed uncertainty computation method are repeated here for clarity:

- The true plant $\boldsymbol{G}(q)$ is exponentially stable, linear and time-invariant.
- The output disturbance noise $v_m(k)$, $m = 1, \ldots, n_y$ can be written as $v_m(k) = H_m(q)a_m(k)$ where $a_m(k)$ is a normalized white Gaussian zero-mean noise sequence. $H_m(q)$ is a linear filter that can be decomposed as $H_m(q) = \sigma_m \bar{H}_m(q)$ where $\sigma_m < \infty$ is scalar and $\bar{H}_m(q)$ is a stable transfer function.

Random phase multisine input signals are used again as these allow direct specification of the frequency spectrum by the user, independent of the selected transfer function computational method. The monitoring procedure considered in this section allows changes on the input signals during experimental execution. These changes can be in amplitude, and/or frequency content of the signals. The Empirical Transfer Function Estimates (ETFE) method used in Section 3.2.2 did not account for transient effects due to the on-the-go input signal modifications, and hence this step has to be re-examined.

3.3.1.1 The Local Polynomial Method

The Local Polynomial Method (LPM; Pintelon *et al.* (2010)) is used to compute transfer functions in the frequency domain considering the system and noise transient (leakage) errors as a function of the frequency. This is done by approximating locally the frequency response function and the transient errors with a low degree polynomial. If N samples of the system outputs, disturbed by filtered white noise $v(k)$, are measured with a sampling time T_s, then the basic assumption of the LPM for MIMO

systems is that the output spectra satisfy

$$Y(\omega_j) = \boldsymbol{G}(\omega_j)U(\omega_j) + T(\omega_j) + V(\omega_j) \tag{3.86}$$

where:

- $Y(\omega_j) \in \mathbb{R}^{n_y}$ is the discrete Fourier transform (DFT) of the noisy N samples of the n_y outputs.
- $\boldsymbol{G}(\omega_j)$ is the $n_y \times n_u$ true frequency response transfer function matrix of the system.
- $U(\omega_j) \in \mathbb{R}^{n_u}$ is the DFT of the true N samples of the n_u inputs.
- $T(\omega_j) \in \mathbb{R}^{n_y}$ is the total system and noise transient term.
- $V(\omega_j) \in \mathbb{R}^{n_y}$ is the MIMO output noise.
- $\omega_j = \frac{2\pi j}{NT_s}$, $j = 1, \ldots, N$.

Since the transient and the transfer function terms are assumed to be smooth functions of the frequency, they can be locally approximated by low-order polynomials:

$$T(\omega_{j+r}) = T(\omega_j) + \sum_{s=1}^{R} t_s(j) r^s + \mathcal{O}_T \tag{3.87}$$

$$\boldsymbol{G}(\omega_{j+r}) = \boldsymbol{G}(\omega_j) + \sum_{s=1}^{R} \boldsymbol{g}_s(j) r^s + \mathcal{O}_G \tag{3.88}$$

where $\mathcal{O}_T = N^{-1/2}\mathcal{O}((r/N)^{R+1})$ and $\mathcal{O}_G = \mathcal{O}((r/N)^{R+1})$ are the remainders of the Taylor series expansions around ω_j of order $R+1$ for T and $\boldsymbol{G}$, as is explained with more details in (Pintelon *et al.*, 2010).

Two variants of the LPM are considered in the proposed monitoring process: LPM for arbitrary excitations for transition cycles when only one period of the signals is available, and LPM for periodic excitations when two or more periods of data are available.

3.3.1.2 LPM for Arbitrary Excitations

This approach is used only immediately after a change (amplitude or frequency content) on the input signal has occurred, and only one period of the signal is available. The vector of unknown parameters is

$$\boldsymbol{\Theta}_{A,j} = [\boldsymbol{G}(\omega_j) \quad \boldsymbol{g}_1(j) \cdots \boldsymbol{g}_R(j) \quad T(\omega_j) \quad t_1(j) \cdots t_R(j)] \tag{3.89}$$

where $\boldsymbol{\Theta}_{A,j} \in \mathcal{C}^{n_y \times (R+1)(n_u+1)}$. To estimate $\boldsymbol{G}(\omega_j)$, the method considers n_A neighboring frequencies around each side of w_j, then by combining (3.86), (3.87) and (3.88) the folowing expressions are derived:

$$\boldsymbol{Y}_{A,j} = \boldsymbol{\Theta}_{A,j}\boldsymbol{K}_{A,j} + \boldsymbol{V}_{A,j} \tag{3.90}$$

$$\text{with} \quad \boldsymbol{Y}_{A,j} = [Y(\omega_{j-n_A}) \cdots Y(\omega_j) \cdots Y(\omega_{j+n_A})] \tag{3.91}$$

$$\boldsymbol{V}_{A,j} = [V(\omega_{j-n_A}) \cdots V(\omega_j) \cdots V(\omega_{j+n_A})] \tag{3.92}$$

$$\boldsymbol{K}_{A,j} = \begin{bmatrix} p(-n_A) \otimes U(\omega_{j-n_A})^T & p(-n_A) \\ \vdots & \vdots \\ p(0) \otimes U(\omega_j)^T & p(0) \\ \vdots & \vdots \\ p(n_A) \otimes U(\omega_{j+n_A})^T & p(n_A) \end{bmatrix}^T \tag{3.93}$$

$$\boldsymbol{V}_{A,j} = [V(\omega_{j-n_A}) \cdots V(\omega_j) \cdots V(\omega_{j+n_A})] \tag{3.94}$$

$$p(r) = [1 \quad r^1 \quad \cdots \quad r^R] \tag{3.95}$$

where $\boldsymbol{Y}_{A,j}, \boldsymbol{V}_{A,j} \in \mathcal{C}^{n_y \times 2n_A+1}$, $\boldsymbol{K}_{A,j} \in \mathcal{C}^{(R+1)(n_u+1)\times 2n_A+1}$, and $\otimes$ is the operator for the Kronecker product. Using a linear least squares (LLS) approximation an estimate of $\boldsymbol{\Theta}_{A,j}$ at ω_j is

$$\hat{\boldsymbol{\Theta}}_{A,j} = \boldsymbol{Y}_{A,j}\boldsymbol{K}_{A,j}^H(\boldsymbol{K}_{A,j}\boldsymbol{K}_{A,j}^H)^{-1} \tag{3.96}$$

where $\boldsymbol{X}^H$ denotes the Hermitian transpose of $\boldsymbol{X}$. From here

$$\hat{\boldsymbol{G}}(\omega_j) = \hat{\boldsymbol{\Theta}}_{A,j} \begin{pmatrix} \boldsymbol{I}_{n_u \times n_u} \\ \boldsymbol{0}_{R(n_u+1)+1 \times n_u} \end{pmatrix} \tag{3.97}$$

The number of frequency points used for the local estimation at each frequency ω_j is $2n_A + 1$, as can be observed in (3.91) – (3.94). This band becomes assymetrical when ω_j is close to the boundaries causing larger estimation errors (Pintelon *et al.*, 2010). For higher values of R, the matrix $\boldsymbol{K}_{A,j}$ can become ill conditioned. Based on the dimension of $\boldsymbol{K}_{A,j}$ the number of degrees of freedom is defined as

$$df_A = 2n_A + 1 - (R+1)(n_u + 1) \tag{3.98}$$

This term quantifies the number of independent noise residuals in

$$\hat{\boldsymbol{V}}_{A,j} = \boldsymbol{Y}_{A,j} - \hat{\boldsymbol{\Theta}}_{A,j} \boldsymbol{K}_{A,j} \tag{3.99}$$

from where an estimate of the noise covariance matrix can be found as

$$\hat{\boldsymbol{C}}_V(\omega_j) = \frac{1}{df_A} \hat{\boldsymbol{V}}_{A,j} \hat{\boldsymbol{V}}_{A,j}^H \tag{3.100}$$

To compute uncertainty bounds a sufficient condition (Pintelon *et al.*, 2010) is

$$df_A \geq n_y \tag{3.101}$$

The parameters must be carefully selected to accomplish (3.101) using the minimum possible n_A and an acceptable value for R ($R = 2$ is often a good selection (Pintelon *et al.*, 2010)).

An estimate for the transfer function covariance matrix can be defined as

$$\hat{\boldsymbol{C}}_{\hat{\boldsymbol{G}}}(\omega_j) = \overline{\boldsymbol{S}^H \boldsymbol{S}} \otimes \hat{\boldsymbol{C}}_V(\omega_j) \tag{3.102}$$

where $\overline{X}$ represents the complex conjugate of X, and

$$\boldsymbol{S} = \boldsymbol{K}_{A,j}^H (\boldsymbol{K}_{A,j} \boldsymbol{K}_{A,j}^H)^{-1} \begin{pmatrix} \boldsymbol{I}_{n_u \times n_u} \\ \boldsymbol{0}_{R(n_u+1)+1 \times n_u} \end{pmatrix} \tag{3.103}$$

3.3.1.3 LPM for Periodic Excitations

This approach is used during the monitoring process when M periods ($M \geq 2$) of the input signals are available. Because of the presence of more than one period, the DFT of the output signals includes frequencies where the inputs are excited and others non-excited. The main assumption is that the system and noise transient errors are present at both excited and non-excited frequencies, while the steady state system response is only present at the excited ones, as depicted in Fig. 3.6. Given the assumed Gaussian nature of the noise and the smoothed-in-frequency nature of the transient response, the method is divided in two parts: an estimation of the transient response based on the non-excited lines, followed by the computation of the system transfer function over the excited lines (Pintelon *et al.*, 2011).

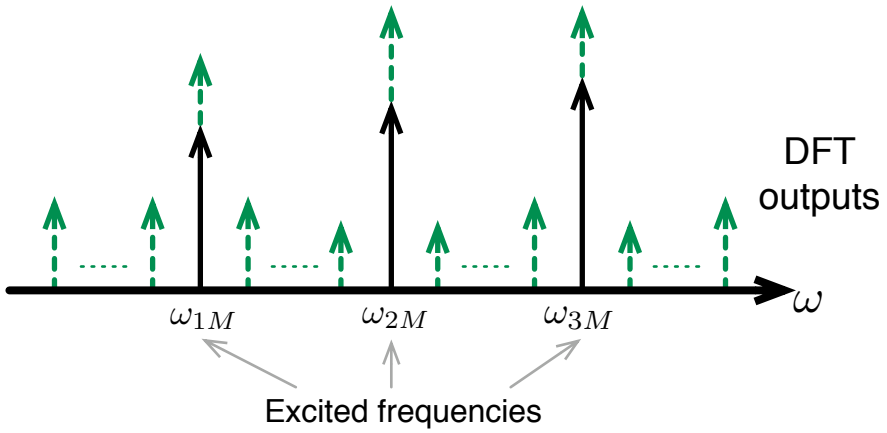

Figure 3.6: Excited and Non-Excited Frequency Components According to the Periodic LPM, Where Solid Lines Correspond to the System Response and Dashed Lines are the Transient and Noise Contributions.

Non-excited frequencies

Using the complete M periods for the DFT computation, the excited frequencies correspond to ω_{jM} for $j = 1, \cdots, N$. The steady state system response is zero at

the non-excited frequencies ω_{jM+r} for $r = \pm 1, \cdots, \pm(M-1)$, hence at those points (3.86) can be reduced as

$$Y(\omega_{jM+r}) = T(\omega_{jM+r}) + V(\omega_{jM+r}) \tag{3.104}$$

The transient term at those frequencies is approximated as

$$T(\omega_{jM+r}) = T(\omega_{jM}) + \sum_{s=1}^{R} t_s(j) r^s + \mathcal{O}_{Tne} \tag{3.105}$$

where $\mathcal{O}_{Tne} = (MN)^{-1/2}\mathcal{O}((r/(MN))^{R+1})$ is the remainder that is explained with details in (Pintelon *et al.*, 2011). The estimation is performed using $2n_T$ non-excited frequencies around the excited frequency ω_{jM}, resulting in the following equations:

$$\boldsymbol{Y}_{T,jM} = \boldsymbol{\Theta}_{T,jM}\boldsymbol{K}_{T,jM} + \boldsymbol{V}_{T,jM} \tag{3.106}$$

$$\text{with} \quad \boldsymbol{Y}_{T,jM} = [Y(\omega_{jM-r_{n_T}}) \cdots Y(\omega_{jM+r_{n_T}})] \tag{3.107}$$

$$\boldsymbol{\Theta}_{T,jM} = [T(\omega_{jM}) \quad t_1(jM) \cdots t_R(jM)] \tag{3.108}$$

$$\boldsymbol{V}_{T,jM} = [V(\omega_{jM-r_{n_T}}) \cdots V(\omega_{jM+r_{n_T}})] \tag{3.109}$$

$$\boldsymbol{K}_{T,jM} = [p(-r_{n_T})^T \cdots p(r_{n_T})^T] \tag{3.110}$$

where $\boldsymbol{Y}_{T,jM}, \boldsymbol{V}_{T,jM} \in \mathcal{C}^{n_y \times 2n_T}$, $\boldsymbol{\Theta}_{T,jM} \in \mathcal{C}^{n_y \times R+1}$, $\boldsymbol{K}_{T,jM} \in \mathcal{C}^{R+1 \times 2n_T}$, and $p(r)$ as was defined in (3.95). Using the same LLS estimator the vector of unknowns is approximated as

$$\hat{\boldsymbol{\Theta}}_{T,jM} = \boldsymbol{Y}_{T,jM}\boldsymbol{K}_{T,jM}^H(\boldsymbol{K}_{T,jM}\boldsymbol{K}_{T,jM}^H)^{-1} \tag{3.111}$$

from where the noise and system transient response is obtained as

$$\hat{T}(\omega_{jM}) = \hat{\boldsymbol{\Theta}}_{T,jM}\begin{pmatrix} 1 \\ \\ \mathbf{0}_{R\times 1} \end{pmatrix} \tag{3.112}$$

Based on the dimension of $\boldsymbol{K}_{T,jM}$ the number of degrees of freedom is $df_T = 2n_T - (R+1)$. This term quantifies the number of independent noise residuals in

$$\hat{\boldsymbol{V}}_{T,jM} = \boldsymbol{Y}_{T,jM} - \hat{\boldsymbol{\Theta}}_{T,jM}\boldsymbol{K}_{T,jM} \tag{3.113}$$

from where an estimate of the noise covariance matrix can be found as

$$\hat{\boldsymbol{C}}_{V_T}(\omega_{jM}) = \frac{1}{df_T}\hat{\boldsymbol{V}}_{T,jM}\hat{\boldsymbol{V}}_{T,jM}^H \tag{3.114}$$

To ensure that the noise covariance estimate has the same rank as its real counterpart, the condition

$$df_T \geq n_y + n_u \tag{3.115}$$

must be satisfied. With the derived estimates of the transient response at the excited frequencies, a transient-free estimate of the output DFT at those frequencies can be defined as

$$\hat{Y}(\omega_{jM}) = Y(\omega_{jM}) - \hat{T}(\omega_{jM}) \tag{3.116}$$

The next step is to compute the transfer function response at the excited frequencies. Two different approaches related to different input signal design methods are explored. The choice between these depends on the operational conditions and constraints of the system.

Excited frequencies using the fast method

The fast method (Pintelon *et al.*, 2011; Pintelon and Schoukens, 2012) for computing the frequency domain transfer function requires one single experiment with M periods. The different input signals are uncorrelated but these can be excited at the same frequencies. At any of the excited frequencies the system and noise transient free output spectra can be represented as

$$\hat{Y}(\omega_{jM}) = \boldsymbol{G}(\omega_{jM})U(\omega_{jM}) + V(\omega_{jM}) \tag{3.117}$$

Since the transfer function matrix is a smooth function of the frequency, it can be approximated at the excited frequencies as

$$\boldsymbol{G}(\omega_{(j+r)M}) = \boldsymbol{G}(\omega_{jM}) + \sum_{s=1}^{R}\boldsymbol{g}_s(j)r^s + \mathcal{O}_{Ge} \tag{3.118}$$

where $\mathcal{O}_{Ge} = \mathcal{O}((r/N)^{R+1})$. If $2n_G + 1$ frequencies are now considered around each excited frequency, the estimation equations are

$$\hat{\boldsymbol{Y}}_{G,jM} = \boldsymbol{\Theta}_{G,jM}\boldsymbol{K}_{G,jM} + \boldsymbol{V}_{G,jM} \tag{3.119}$$

$$\hat{\boldsymbol{Y}}_{G,jM} = [\hat{Y}(\omega_{(j-n_G)M}) \cdots \hat{Y}(\omega_{jM}) \cdots \hat{Y}(\omega_{(j+n_G)M}] \tag{3.120}$$

$$\boldsymbol{\Theta}_{G,jM} = [G(\omega_{jM}) \quad g_1(jM) \cdots g_R(jM)] \tag{3.121}$$

$$\boldsymbol{V}_{G,jM} = [V(\omega_{(j-n_G)M}) \cdots V(\omega_{jM}) \cdots V(\omega_{(j+n_G)M})] \tag{3.122}$$

$$\boldsymbol{K}_{G,jM} = [p(-n_G)^T \otimes U(\omega_{(j-n_G)M}) \cdots p(n_G)^T \otimes U(\omega_{(j+n_G)M})] \tag{3.123}$$

where $\hat{\boldsymbol{Y}}_{G,jM}, \boldsymbol{V}_{G,jM} \in \mathcal{C}^{n_y \times 2n_G+1}$, $\boldsymbol{\Theta}_{G,jM} \in \mathcal{C}^{n_y \times (R+1)n_u}$, $\boldsymbol{K}_{G,jM} \in \mathcal{C}^{(R+1)n_u \times 2n_G+1}$, and $p(r)$ as was defined in (3.95). The LLS estimate of the unknown variables and the correspondent transfer function matrix are

$$\hat{\boldsymbol{\Theta}}_{G,jM} = \hat{\boldsymbol{Y}}_{G,jM}\boldsymbol{K}_{G,jM}^H(\boldsymbol{K}_{G,jM}\boldsymbol{K}_{G,jM}^H)^{-1} \tag{3.124}$$

$$\hat{\boldsymbol{G}}(\omega_{jM}) = \hat{\boldsymbol{\Theta}}_{G,jM}\begin{pmatrix} \boldsymbol{I}_{n_u \times n_u} \\ \boldsymbol{0}_{Rn_u \times n_u} \end{pmatrix} \tag{3.125}$$

The number of degrees of freedom, the noise residuals and the noise covariance matrix are

$$df_G = 2n_G + 1 - (R+1)n_u \tag{3.126}$$

$$\hat{\boldsymbol{V}}_{G,jM} = \hat{\boldsymbol{Y}}_{G,jM} - \hat{\boldsymbol{\Theta}}_{G,jM}\boldsymbol{K}_{G,jM} \tag{3.127}$$

$$\hat{\boldsymbol{C}}_{V_G}(\omega_{jM}) = \frac{1}{df_G}\hat{\boldsymbol{V}}_{G,jM}\hat{\boldsymbol{V}}_{G,jM}^H \tag{3.128}$$

The estimated covariance matrix of the transfer function computation is

$$\hat{\boldsymbol{C}}_{\hat{\boldsymbol{G}}}(\omega_{jM}) = \overline{\boldsymbol{S}_G^H\boldsymbol{S}_G} \otimes \hat{\boldsymbol{C}}_{V_G}(\omega_{jM}) \tag{3.129}$$

$$\boldsymbol{S}_G = \boldsymbol{K}_{G,jM}^H(\boldsymbol{K}_{G,jM}\boldsymbol{K}_{G,jM}^H)^{-1}\begin{pmatrix} \boldsymbol{I}_{n_u \times n_u} \\ \boldsymbol{0}_{Rn_u \times n_u} \end{pmatrix} \tag{3.130}$$

The definition of the matrix $\hat{\boldsymbol{Y}}_{G,jM}$ in (3.120) assumes that n_G frequencies are available around the estimated frequency, which is not the case at the left and right borders of the frequency band. In those cases the required $2n_G + 1$ frequency points are considered asymmetrically starting from the left or the right border respectively; the problem is that now the frequency interval used for estimation is not centered in the frequency of interest and hence the bias error at those frequencies is larger than other cases as is shown in (Pintelon and Schoukens, 2012); this problem is called the border effect.

Excited frequencies using the transient method

Both fast and transient methods estimate the noise and system transient response assuming that it can be locally approximated by a polynomial around the non-excited frequencies; however, the transient method (Monteyne *et al.*, 2012) does not use a polynomial approximation for the computation of the transfer function matrix at the excited frequencies. The computation starts from the corrected value of the output spectrum in (3.116), and relies on the ETFE for each input-output component as

$$\begin{gathered} \hat{G}_{[m,n]}(\omega_{jM}) = \frac{\hat{Y}_{[m]}(\omega_{jM})}{U_{[n]}(\omega_{jM})} \\ \text{for} \quad n = 1, \cdots, n_u, \quad m = 1, \cdots, n_y \end{gathered} \tag{3.131}$$

This method requires that each signal is defined in a frequency grid that is orthogonal with respect to each of the other input signals. The estimated variance of each transfer function computation is

$$\hat{\sigma}^2_{\hat{G}_{[m,n]}}(\omega_{jM}) = \frac{\hat{C}_{V_T[m,m]}(\omega_{jM})}{|U_{[n]}(\omega_{jM})|^2} \tag{3.132}$$

with $\hat{\boldsymbol{C}}_{V_T}(\omega_{jM})$ calculated in (3.114). The main advantage of this method compared to the robust LPM (Pintelon *et al.*, 2011) is that it requires only one experiment, and avoids the bias introduced by the polynomial assumption of the transfer function.

3.3.2 Input Signal Design

The experimental design relies on deterministic and periodic multisine signals. The formulation includes the possibility to perform changes on the amplitude and/or the fundamental frequency content of the signals. To accommodate these changes each of the n_u different input signals is constructed as sequence of multi-sinusoidal signals where the amplitude, number of periods, and the fundamental frequency may differ for each signal in the sequence. L is the number of signals in the sequence.

One period of the l^{th} signal in the sequence for the n^{th} input can be represented for $k = 1, \cdots, N_s$ as

$$\begin{aligned} u_{n,l}(k) &= \lambda_{n,l} \sum_{j=1}^{N_s/2} \sqrt{2\alpha_{n,l,j}} \cos(\omega_j k T_s + \phi_{n,l,j}) \\ \omega_j &= \frac{2\pi j}{N_s T_s}, \quad l = 1, \cdots, L \end{aligned} \tag{3.133}$$

where $\lambda_{n,l}$ is the amplitude scaling factor for each signal, T_s is the sampling period, N_s is the number of samples in one period, $\alpha_{n,l,j}$ is a factor used to specify the relative power at the frequency ω_j, and $\phi_{n,l,j}$ is the phase for each harmonic. Additionally n_s is the total number of sinusoids excited considering all the inputs with $n_s \leq N_s/2$, and M_l is the number of periods in the l^{th} signal. For the experimental design focused on the monitoring process, it is assumed that the first signal in the sequence ($l = 1$) represents the general fundamental frequency. Using the procedure shown in Section 3.2.1, N_s and n_s can be defined by

$$n_s \geq \frac{\omega^*}{\omega_*}, \quad \max\left(2n_s, \frac{2\pi}{\omega_* T_s}\right) \leq N_s \leq \frac{2\pi n_s}{\omega^* T_s} \tag{3.134}$$

with

$$\frac{1}{\beta_s \tau_{dom}^H} = \omega_* \leq \omega \leq \omega^* = \frac{\alpha_s}{\tau_{dom}^L} \tag{3.135}$$

where τ_{dom}^{L} and τ_{dom}^{H} are the dominant time constants of the system, and α_s and β_s are parameters that respectively specify high and low ranges of interest in the signal. Harmonic phases $\phi_{[n,j]}$ are selected to minimize the signal crest factor using the approach proposed by Guillaume *et al.* (Guillaume *et al.*, 1991).

Two different variations will be tested and contrasted. The first design incorporates an orthoghonal-in-frequency approach and is used in conjunction with the transient LPM method. The second variation considers all the inputs excited at the same frequencies and it relies on the fast LPM method for transfer function and uncertainty computations.

3.3.2.1 Input Signals With "Zippered" Design

The transient method for computing transfer functions and uncertainties requires input signals designed such that only one channel is excited at each frequency; this is performed using an orthogonal-in-frequency "zippered" spectra design (Rivera *et al.*, 2009). Construction of this orthogonal spectra is done by carefully selecting the Fourier coefficients $\alpha_{n,l,j}$, such that if one of them is nonzero for one input channel at a given frequency, then all the coefficients for the other input channels at the same frequency are equal to 0. This approach was tested for the basic monitoring procedure in Section 3.2. Here the experimental design is augmented considering the same "zippered" spectra but incorporating modifications on the harmonic frequency content and the amplitude of the signals.

Changes on the amplitude of the signals

All the input signals must satisfy the following operational condition:

$$\begin{gathered} u_n^{min} \leq u_{n,l}(k) \leq u_n^{max} \\ n = 1, \cdots, n_u \quad l = 1, \cdots, L \end{gathered} \tag{3.136}$$

According to the requirements of the monitoring process, and for the l^{th} signal of the sequence, the scale factor $\lambda_{n,l}$ can be increased or decreased such that the condition

$$u_{n,l}^{min} \leq u_{n,l}(k) \leq u_{n,l}^{max} \tag{3.137}$$

is satisfied with

$$\min\left(u_{n,1}^{min}, \cdots, u_{n,L}^{min}\right) \geq u_{n}^{min} \tag{3.138}$$

$$\max\left(u_{n,1}^{max}, \cdots, u_{n,L}^{max}\right) \leq u_{n}^{max} \tag{3.139}$$

for $n = 1, \cdots n_u$.

Changes on the harmonic frequency content

This approach was previously presented for SISO systems in (Steenis and Rivera, 2010; Steenis, 2009), here it is extended for the MIMO case. In order to compute transfer functions and uncertainties over a subset of the original frequency grid, a harmonic relation must exist between the fundamental frequencies of the different signals in the sequence. The number of samples per period of one of the inputs (in our case u_{n_u}) for each signal in the sequence is defined as $N_{s,l}$, and should be related to N_s by a power of two; however to maintain the "zippered" definition of the spectra a larger separation is required as is illustrated in Fig. 3.7 for $n_u = 2$. $S_{h,l}$ is the harmonic reduction step between the initial ($l = 1$) and the l^{th} signal in the sequence; the first plot corresponds to the initial sequence with no harmonic reduction ($S_{h,l} = 0$), and showing the zippered effect only.

Based on the desired harmonic reduction step at the l^{th} signal of the sequence, the theoretical number of samples per period for u_{n_u}, and the number of independent sinusoids excited per channel ($n_{s,l}$) are

$$N_{s,l} = \frac{N_s}{n_u 2^{S_{h,l}}}, \qquad n_{s,l} = \frac{n_s}{n_u 2^{S_{h,l}}} \tag{3.140}$$

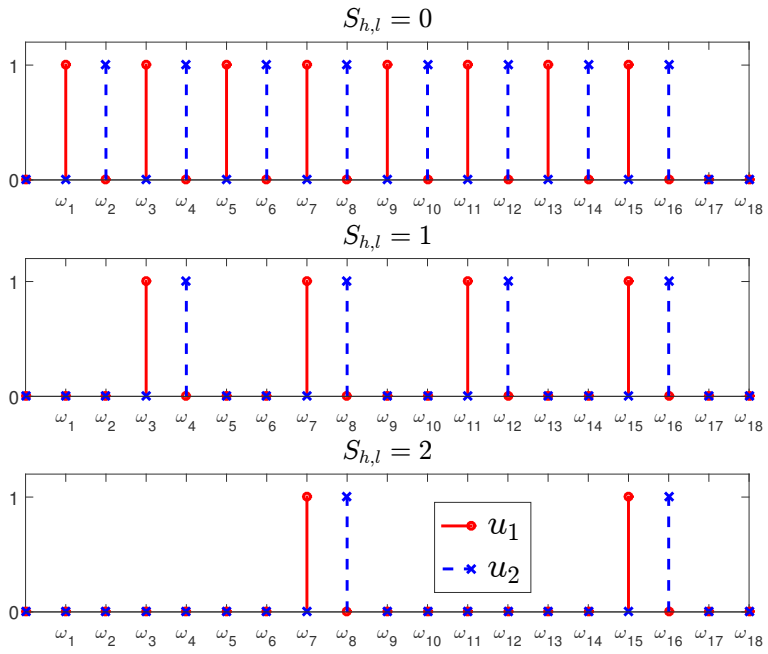

Figure 3.7: Conceptual Representation of the Desired "Zippered" and Harmonic Related Spectra for $n_u = 2$ Input Signals. The X-Axis Represents the Harmonic Frequencies ω_j While the Y-axis Represents the Fourier Coefficients $\alpha_{n,l,j}$.

From here the spectrum for each input signal u_n, $n = 1, \cdots, n_u$ is constructed by defining

$$\alpha_{n,l,j} = \begin{cases} 1 & \text{if } j = n_u(2^{S_{h,l}} i - 1) + n, \quad \text{for } i = 1, \cdots, n_{s,l} \\ 0 & \text{otherwise} \end{cases} \tag{3.141}$$

It is important to notice that for the l^{th} signal of the sequence, only the input channel u_{n_u} ($n_u = 2$ in Fig. 3.7) maintains a specific harmonic relation to the fundamental frequency defined by N_s. The remaining input channels are constructed using (3.141) that defines specific frequency shifts with respect to u_{n_u}. Hence, the only way of having a grid definition including all the utilized frequencies is to keep the total number of samples fixed to N_s for all the signals in the sequence.

During the initial signal of the sequence, the scale factor $\lambda_{n,1}$ is computed such

that

$$u_{n,1}^{min} \leq u_{n,1}(k) \leq u_{n,1}^{max} \tag{3.142}$$

is satisfied. The l^{th} signal of the sequence has the same number of samples N_s but less frequencies excited per channel, hence the idea is to keep the power of the entire signal constant with respect to the initial one; this is done by increasing the contribution of the signal at the remaining frequencies. It can be shown that the power spectral density of the multisine signal defined in (3.133) for the initial ($l = 1$) signal in the sequence is

$$P_{n,1} = \sum_{j=1}^{n_s} \frac{\lambda_{n,1}^2 \beta_{n,l,j}^2}{2} = n_{s,1} \lambda_{n,1}^2 \tag{3.143}$$

with $\beta_{n,l,j} = \sqrt{2\alpha_{n,l,j}}$ and $\alpha_{n,l,j} = 1$ at the $n_{s,1}$ excited frequencies. For the l^{th} signal of the sequence

$$P_{n,l} = \sum_{j=1}^{n_{s,l}} \frac{\lambda_{n,l}^2 \beta_{n,l,j}^2}{2} = n_{s,l} \lambda_{n,l}^2 \tag{3.144}$$

Hence by considering $P_{n,1} = P_{n,l}$ and substituting (3.140) we obtain

$$\lambda_{n,l} = \lambda_{n,1} \sqrt{2^{S_{h,l}}} \tag{3.145}$$

The computed inputs must satisfy the conditions imposed in (3.136) – (3.139).

3.3.2.2 Input Signals With Full Design

For this case the designed input signals and their respective outputs are used in conjunction with the fast LPM approach. This method assumes that the transfer function matrix can be approximated by a low order polynomial around the excited frequencies. Given this basic structure, the "zippered" definition of the excited frequencies for each input is no longer required. This condition opens the possibility of

a better frequency resolution, however the price to pay is the presence of bias in the estimation since the ETFE is no longer utilized.

The multisine definition presented in (3.133) is still used, but now for $k = 1, \cdots, N_{s,l}$ where $N_{s,l}$ is the number of samples per period in the l^{th} signal of the sequence. Independent realizations of the different inputs u_n are required; this can be achieved by using periodic shifted versions of the entries of one multisine realization, or the use of Hadamard or orthogonal multisines as is explained in (Pintelon *et al.*, 2011). Changes on the amplitude of the signals are handled in the same way as was described for the zippered signals in Section 3.3.2.1.

With this approach, reductions on the harmonic frequency content represent actual decreases on the length of the signal. If $S_{h,l}$ is again the harmonic reduction step for the l^{th} signal of the sequence, then $N_{s,l}$ is the number of samples per period , and $n_{s,l}$ is the number of excited frequencies that are harmonically related to the parameters from the initial signal; they are computed as

$$N_{s,l} = \frac{N_s}{2^{S_{h,l}}}, \qquad n_{s,l} = \frac{n_s}{2^{S_{h,l}}} \tag{3.146}$$

The spectrum of the harmonic related signals should consider frequencies excited at the $2^{S_{h,l}}$ harmonics of the fundamental signal. This is done by defining the Fourier coefficients to be equal to 0 at the frequencies that does not correspond to the specified harmonic reduction as is illustrated in Fig. 3.8. The Fourier coefficient are defined as

$$\alpha_{n,l,j} = \begin{cases} 1 & \text{if } j = 2^{S_{h,l}} i \quad \text{for } i = 1, \cdots, n_{s,l} \\ 0 & \text{otherwise} \end{cases} \tag{3.147}$$

If the only modification of a new signal in the sequence is the harmonic frequency contain (and hence its length), then the values of the parameters $\lambda_{n,l}$ must be selected to exhibit the same maximum and minimum amplitudes as the previous signal. In this case the power of the signal is not held constant after the change.

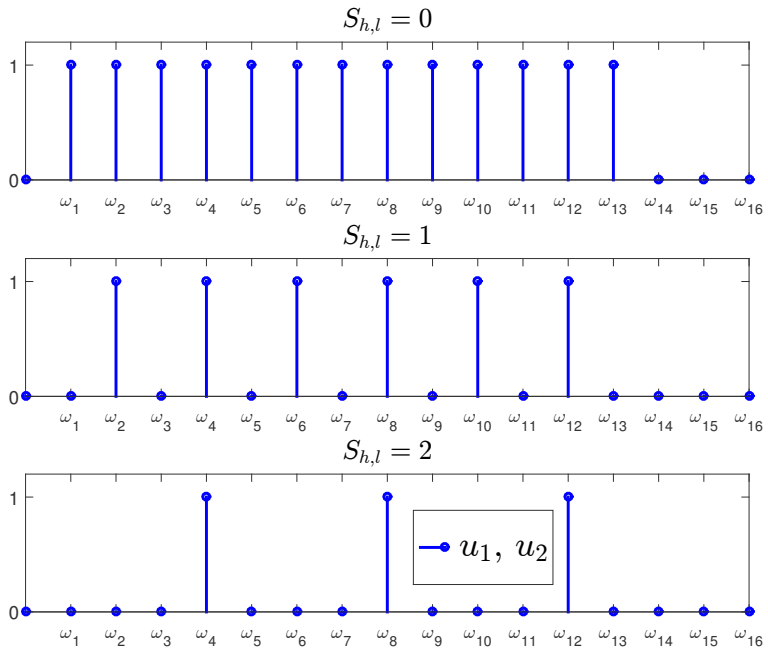

Figure 3.8: Conceptual Representation of the Desired Harmonic Related Spectra for $n_u = 2$ Input Signals With the Full Design. The X-Axis Represents the Harmonic Frequencies ω_j While the Y-Axis Represents the Fourier Coefficients $\alpha_{n,l,j}$.

3.3.3 Transfer Function and Uncertainty Computation

The l^{th} signal of the sequence for $l = 1, \cdots, L$ is implemented using M_l periods, and noisy samples of the n_y outputs are collected. Uncertainty bounds rely on the computation of the variance of the transfer function estimates computed with the selected method.

"Zippered" Signals

Signals designed with the "zippered" power spectrum are analyzed and the transfer functions for each input output component are obtained using the transient method described in Section 3.3.1.3 . Equation (3.132) gives the estimated variance of each transfer function computation. The transfer function estimates are valid for the

following frequency grid for each input and each signal of the sequence:

$$\boldsymbol{W^z}_{n,l} = \{\omega_{n,l,i} \in \mathbb{R} \mid \omega_{n,l,i} = \frac{2\pi[n_u(2^{S_{h,l}}i-1)+n]}{N_s T_s}, \quad i = 1, 2, \ldots, n_{s,l}\} \tag{3.148}$$

Full Signals

Transfer function matrices from signals with the full power spectrum are computed using the fast method described in Section 3.3.1.3. The considered frequency grid for these estimates is

$$\boldsymbol{W^f}_{n,l} = \{\omega_{n,l,i} \in \mathbb{R} \mid \omega_{n,l,i} = \frac{2\pi[2^{S_{h,l}}i]}{N_s T_s}, \quad i = 1, 2, \ldots, n_{s,l}\} \tag{3.149}$$

Equation (3.129) gives the estimated covariance matrix of the transfer function computation. This estimate is computed considering

$$\hat{\boldsymbol{C}}_{\hat{\boldsymbol{G}}}(\omega_{n,l,i}) = Cov\Big(vec\big(\hat{\boldsymbol{G}}(\omega_{n,l,i})\big)\Big) \tag{3.150}$$

$$\text{with } vec\big(\hat{\boldsymbol{G}}(\omega_{n,l,i})\big) = \begin{pmatrix} \hat{G}_{[1,1]} \\ \hat{G}_{[2,1]} \\ \vdots \\ \hat{G}_{[n_y,n_u]} \end{pmatrix} \tag{3.151}$$

where $vec\big(\hat{\boldsymbol{G}}(\omega_{n,l,i})\big) \in \mathcal{C}^{n_y n_u}$, and $\hat{\boldsymbol{C}}_{\hat{\boldsymbol{G}}}(\omega_{n,l,i}) \in \mathcal{C}^{n_y n_u \times n_y n_u}$ can be represented as

$$\hat{\boldsymbol{C}}_{\hat{\boldsymbol{G}}}(\omega_{n,l,i})| = \begin{pmatrix} \hat{\sigma}^2_{\hat{G}_{[1,1]}} & \hat{\sigma}_{\hat{G}_{[1,1]},\hat{G}_{[2,1]}} & \cdots & \hat{\sigma}_{\hat{G}_{[1,1]},\hat{G}_{[n_y,1]}} \\ \hat{\sigma}_{\hat{G}_{[2,1]},\hat{G}_{[1,1]}} & \hat{\sigma}^2_{\hat{G}_{[2,1]}} & \cdots & \hat{\sigma}_{\hat{G}_{[2,1]},\hat{G}_{[n_y,1]}} \\ \vdots & & & \vdots \\ \hat{\sigma}_{\hat{G}_{[n_y,n_u]},\hat{G}_{[1,1]}} & \hat{\sigma}_{\hat{G}_{[n_y,n_u]},\hat{G}_{[2,1]}} & \cdots & \hat{\sigma}^2_{\hat{G}_{[n_y,n_u]}} \end{pmatrix} \tag{3.152}$$

From where the estimated variance of the transfer function computation for each input output component is

$$diag\big(|\hat{\boldsymbol{C}}_{\hat{\boldsymbol{G}}}(\omega_{n,l,i})|\big) = \big(\hat{\sigma}^2_{\hat{G}_{[1,1]}} \quad \cdots \quad \hat{\sigma}^2_{\hat{G}_{[n_y,n_u]}}\big)^T \tag{3.153}$$

The following definitions are valid for $\omega_{n,l,i} \in \boldsymbol{W}_{n,l}$ defined as

$$\boldsymbol{W}_{n,l} = \begin{cases} \boldsymbol{W}^{\boldsymbol{z}}{}_{n,l} & \text{for signals with "zippered" spectra} \\ \boldsymbol{W}^{\boldsymbol{f}}{}_{n,l} & \text{for signals with full spectra} \end{cases} \tag{3.154}$$

The LPM method for periodic signals described in Section 3.3.1.3 assumes that more than two periods of the input/output data are available. That is not the case when a change in amplitude or frequency content, resulting from the monitoring procedure, has just been applied and only data for one period is available. For these transition cases the LPM method for arbitrary excitation described in Section 3.3.1.2 is applied for $\omega_{n,l,i} \in \boldsymbol{W}_{n,l}$, and using (3.97) and (3.102) to find the estimated variance of the transfer function with the same procedure described in (3.150) – (3.153).

Assuming that the signal-to-noise ratio of the inputs is larger than 20 dB (Pintelon and Schoukens, 2012), then the circular $100 \times (1-\rho)\%$ confidence region such that

$$Prob\Big\{ \big| \hat{G}_{[m,n]}(\omega_{n,l,i}) - \mathbb{E}\{\hat{G}_{[m,n]}(\omega_{n,l,i})\} \big| \leq \ell^{1-\rho}_{a[m,n]}(\omega_{n,l,i}) \Big\} = 1-\rho \tag{3.155}$$

can be constructed via a circular complex Gaussian approximation with a radius

$$\ell^{1-\rho}_{a[m,n]}(\omega_{n,l,i}) = \sqrt{-\ln \rho}\ \ \hat{\sigma}_{\hat{G}_{[m,n]}}(\omega_{n,l,i}) \tag{3.156}$$

These estimates are asymptotically valid as the total length of the input $N_s M_l$ increases (Pintelon *et al.*, 2010). A more general MIMO uncertainty bound can be computed considering the maximum singular value at each frequency with a probability $1-\kappa$ such that

$$Prob\Big\{ \overline{\sigma}\big(\hat{\boldsymbol{G}}(\omega_{n,l,i}) - \boldsymbol{G}(\omega_{n,l,i})\big) \leq \epsilon^{1-\kappa}(\omega_{n,l,i}) \Big\} = 1-\kappa \tag{3.157}$$

The bound can be computed relying on the Frobenious norm over the square of the maximum singular values as was shown in Section 3.2.2.3 with

$$\overline{\sigma}\big(\hat{\boldsymbol{G}}(\omega_{n,l,i}) - \boldsymbol{G}(\omega_{n,l,i})\big)^2 \leq \sum_{n=1}^{n_u} \sum_{m=1}^{n_y} \big[\ell^{1-\rho}_{a[m,n]}(\omega_{n,l,i}, M_l)\big]^2 \triangleq \big[\epsilon^{1-\kappa}(\omega_{n,l,i}, M_l)\big]^2 \tag{3.158}$$

where a specific dependence on the number of periods M_l, for each signal of the sequence, has been added. Since each source of output noise is assumed to come from a different Gaussian realization and the inputs are excited independently the probabilities are related by

$$1 - \kappa = (1 - \rho)^{n_y n_u} \tag{3.159}$$

3.3.4 Identification Test Monitoring Procedure

The main idea for identification test monitoring is to assess the quality of the data in terms of its capability for identification purposes after each cycle of a periodic signal. If a pre-specified stopping criterion is not satisfied, then the content and character of the input for the next period might be altered depending on different conditions. Assume that the total number of samples of the experiment has a maximum bound

$$N_{total} = \sum_{l=1}^{L} N_s M_l \leq N_{max} \tag{3.160}$$

for the "zippered" signals, and

$$N_{total} = \sum_{l=1}^{L} N_{s,l} M_l \leq N_{max} \tag{3.161}$$

for the full signals. Three different types of actions are considered:

1. **Add an additional period of the identical signal**. This is recommended when the actual total number of samples is considerably less than N_{max}.

2. **Apply a signal with higher amplitude**. An increase in the input signal amplitude is recommended if the uncertainty is decreasing slowly, and the maximum bounds defined in (3.136) are still not reached.

3. **Apply a signal with different harmonic related frequency content**. The harmonic content of the signal can be modified if a better understanding of the system is achieved and the power of the input can be emphasized over frequencies of interest. This step can be applied when uncertainty is decreasing slowly and the maximum number of samples N_{max} is close to be reached.

The action to be performed for the subsequent period must be judiciously selected for each case depending on the operational constraints of the system, the level of noise experienced, and user preferences.

3.3.4.1 Aggregate Computation of Uncertainty

The additive uncertainty bound defined in (3.156) is valid for the l^{th} signal of the sequence; hence an aggregate computation is needed considering all the L signals. This computation is implemented over a common frequency grid among all the signals in the sequence that is defined by the signal with the highest harmonic reduction step. If we define

$$l_{agg} = \{1 \leq l \leq L \mid S_{h,l} = \max(S_{h,1}, \cdots, S_{h,L})\} \tag{3.162}$$

then the frequency grid of the aggregate estimate is defined for each $\omega_{n,i} \in \boldsymbol{W}_{n,l_{agg}}$. The total number of periods per each signal is

$$M = \sum_{l=1}^{L} M_l \tag{3.163}$$

The transfer function estimate of the complete experiment can be represented by a weighted sum of the different independent estimates $\hat{G}_{[m,n]}(\omega_{n,l,i}, M_l)$ for each signal in the sequence as

$$\hat{G}_{[m,n]}(\omega_{n,i}, M) = \frac{\sum_{l=1}^{L} w_{l[m,n]}(\omega_{n,l,i}) \hat{G}_{[m,n]}(\omega_{n,l,i}, M_l)}{\sum_{l=1}^{L} w_{l[m,n]}(\omega_{n,l,i})} \tag{3.164}$$

where each $w_{l[m,n]}(\omega_{n,l,i})$ is a frequency dependent weight. By using the Lagrange multipliers method, it can be shown that the weights that minimize the variance of the total estimate are equal to the reciprocal of the variance of the estimate at the specified frequency for the l^{th} signal in the input sequence:

$$w_{l[m,n]}(\omega_{n,l,i}) = \frac{1}{\hat{\sigma}^2_{\hat{G}_{[m,n]}}(\omega_{n,l,i})} \tag{3.165}$$

The resultant variance of the weighted mean estimation (Hogg and Craig, 1978) is

$$\hat{\sigma}^2_{\hat{G}_{[m,n]}}(\omega_{n,i}) = \frac{1}{\sum_{l=1}^{L} \frac{1}{\hat{\sigma}^2_{\hat{G}_{[m,n]}}(\omega_{n,l,i})}} \tag{3.166}$$

Relying on (3.156) and (3.158), the resultant total uncertainty bounds are computed as

$$\ell^{1-\rho}_{a[m,n]}(\omega_{n,i}, M) = \sqrt{-\ln \rho}\ \hat{\sigma}_{\hat{G}_{[m,n]}}(\omega_{n,i}) \tag{3.167}$$

$$\left[\epsilon^{1-\kappa}(\omega_{n,i}, M)\right]^2 = \sum_{n=1}^{n_u} \sum_{m=1}^{n_y} \left[\ell^{1-\rho}_{a[m,n]}(\omega_{n,i}, M)\right]^2 \tag{3.168}$$

3.3.4.2 Stopping Criterion Based on Robustness Metrics

The purpose here is to define a stopping criterion that provides a basis to halt or continue the test, based on robust control ideas. An unstructured additive uncertainty $\boldsymbol{L_a}$ is assumed over the estimated plant transfer function $\tilde{\boldsymbol{G}}$, connected in a closed loop configuration with a controller $\boldsymbol{C}$ as is illustrated in Fig. 3.9, where d' is a disturbance input and w_P is a performance scalar weight.

The bound $\bar{\ell}_a$ is interpreted as a scalar weight on a normalized additive perturbation $\boldsymbol{\Delta_a}(s)$, where the total perturbation $\boldsymbol{L_a}(s)$ is

$$\boldsymbol{L_a}(s) = \bar{\ell}_a \boldsymbol{\Delta_a}(s), \quad \bar{\sigma}(\boldsymbol{\Delta_a}(\omega)) \leq 1 \quad \forall \omega \tag{3.169}$$

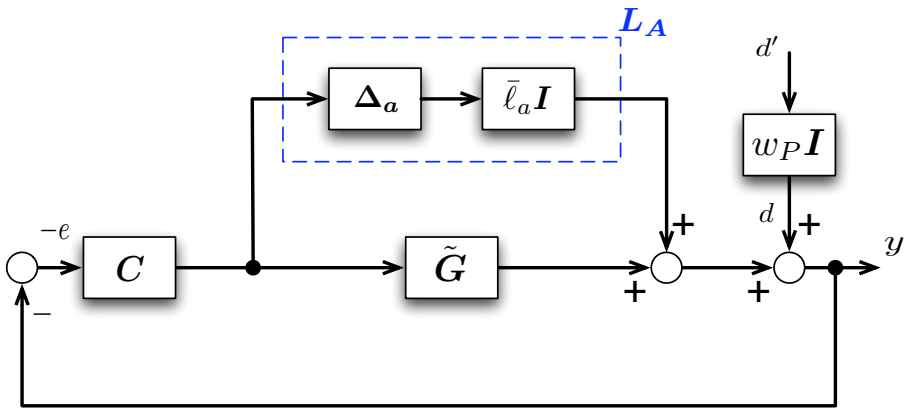

Figure 3.9: Closed-Loop Representation of the System Describing a Single Unstructured Additive Uncertainty.

The magnitude of the perturbation can be measured in terms of the bound over the maximum singular values as

$$\bar{\sigma}(\boldsymbol{L_a}) \leq \bar{\ell}_a(\omega), \quad \forall\omega \tag{3.170}$$

The estimated sensitivity $\tilde{\boldsymbol{E}}$, and complementary sensitivity $\tilde{\boldsymbol{H}}$ of the system are

$$\tilde{\boldsymbol{E}} = (I + \tilde{\boldsymbol{G}}\boldsymbol{C})^{-1} \tag{3.171}$$

$$\tilde{\boldsymbol{H}} = \tilde{\boldsymbol{G}}\boldsymbol{C}(\boldsymbol{I} + \tilde{\boldsymbol{G}}\boldsymbol{C})^{-1} \tag{3.172}$$

$$\text{and} \quad \tilde{\boldsymbol{E}} + \tilde{\boldsymbol{H}} = \boldsymbol{I} \tag{3.173}$$

Considering the robust performance problem described by Morari and Zafiriou (1989) for the system depicted in Fig. 3.9, a H_∞ performance specification is presented such that the controller is designed to minimize the worst normalized output error y resulting from any disturbance input d through the sensitivity function $\boldsymbol{E}$ as

$$\min_{\boldsymbol{C}} \|\boldsymbol{E}w_P\|_\infty = \min_{\boldsymbol{C}} \sup_{\omega} \bar{\sigma}\big(\boldsymbol{E}w_P\big) \tag{3.174}$$

where the weight w_P can be designed to be low at low frequencies, to have a minimum bandwidth, and to limit the magnitude of the sensitivity operator avoiding distur-

bance amplification. The H_∞ performance requirement (Morari and Zafiriou, 1989) is written as

$$\bar{\sigma}\big(\boldsymbol{E}w_P\big) < 1, \quad \forall\omega \tag{3.175}$$

The sensitivity operator $\boldsymbol{E}$ can be expressed in terms of the estimated sensitivity $\tilde{\boldsymbol{E}}$ and complementary sensitivity $\tilde{\boldsymbol{H}}$ as

$$\boldsymbol{E} = \tilde{\boldsymbol{E}}\big(\boldsymbol{I} + \boldsymbol{L_a}\tilde{\boldsymbol{G}}^{-1}\tilde{\boldsymbol{H}}\big)^{-1} \tag{3.176}$$

from where

$$\bar{\sigma}\Big(\tilde{\boldsymbol{E}}\big(\boldsymbol{I} + \boldsymbol{L_a}\tilde{\boldsymbol{G}}^{-1}\tilde{\boldsymbol{H}}\big)^{-1}w_P\Big) < 1$$
$$\bar{\sigma}\big(\tilde{\boldsymbol{E}}w_P\big)\bar{\sigma}\big(\boldsymbol{I} + \boldsymbol{L_a}\tilde{\boldsymbol{G}}^{-1}\tilde{\boldsymbol{H}}\big)^{-1} < 1$$

Using the properties of the singular values (Skogestad and Postlethwaite, 2005) the following expressions are obtained

$$\bar{\sigma}\big(\tilde{\boldsymbol{E}}w_P\big) < \underline{\sigma}\big(\boldsymbol{I} + \boldsymbol{L_a}\tilde{\boldsymbol{G}}^{-1}\tilde{\boldsymbol{H}}\big)$$
$$\bar{\sigma}\big(\tilde{\boldsymbol{E}}w_P\big) < 1 - \bar{\sigma}\big(\boldsymbol{L_a}\tilde{\boldsymbol{G}}^{-1}\tilde{\boldsymbol{H}}\big)$$
$$\bar{\sigma}\big(\tilde{\boldsymbol{E}}w_P\big) + \bar{\sigma}\big(\boldsymbol{L_a}\tilde{\boldsymbol{G}}^{-1}\tilde{\boldsymbol{H}}\big) < 1$$

Utilizing this result and the defined bound $\bar{\ell}_a$, a sufficient condition for robust performance can be defined (Morari and Zafiriou, 1989) as

$$\bar{\sigma}\big(\tilde{\boldsymbol{E}}w_P\big) + \bar{\sigma}\big(\tilde{\boldsymbol{G}}^{-1}\tilde{\boldsymbol{H}}\big)\bar{\ell}_a < 1, \quad \forall\omega \tag{3.177}$$

The performance weighting function w_P is designed to shape the sensitivity $\boldsymbol{E}$ of the closed-loop system using the following representation (Skogestad and Postlethwaite, 2005):

$$w_P = \frac{s/M_P + \omega_B}{s + \omega_B A_P} \tag{3.178}$$

Fig. 3.10 shows a typical plot of $1/|w_P|$, where the upper bound on the sensitivity $|\boldsymbol{E}|$ is equal to $A_P \leq 1$ at low frequencies, and $M_P \geq 1$ at high frequencies. The asymptotic response is equal to 1 at the frequency ω_B.

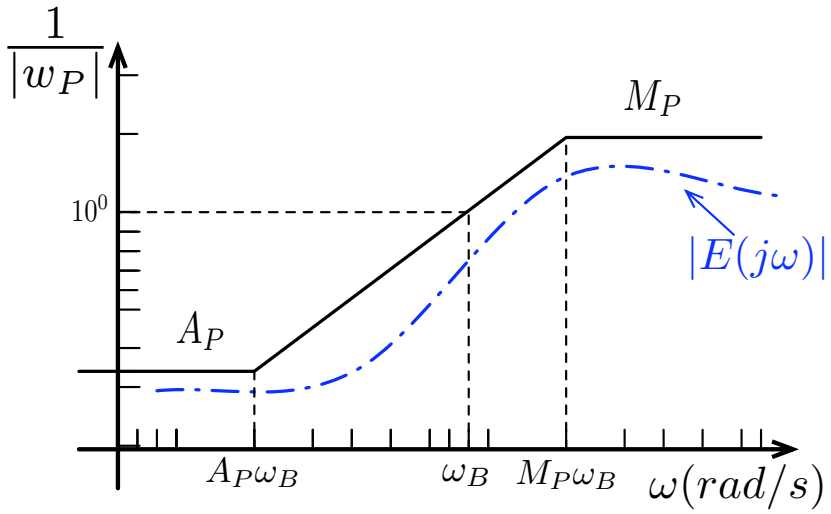

Figure 3.10: Inverse Performance Weight $1/|w_P|$ Used for Robust Performance Test According to (3.178).

To obtain a general representation for the complementary sensitivity function, the controller is defined using a multivariable Q-parametrization/Internal Model Control (IMC) representation (Morari and Zafiriou, 1989) as

$$\boldsymbol{C} = \boldsymbol{Q}(\boldsymbol{I} - \tilde{\boldsymbol{G}}\boldsymbol{Q})^{-1} \quad \text{with } \boldsymbol{Q} = \tilde{\boldsymbol{Q}}\boldsymbol{F} \tag{3.179}$$

The values of $\tilde{\boldsymbol{Q}}$ and $\boldsymbol{F}$ are defined as follows: $\boldsymbol{G}$ can be factorized into an invertible portion $\boldsymbol{G}_-$ that is stable and causal, and a nononvertible part $\boldsymbol{G}_+$ as $\boldsymbol{G} = \boldsymbol{G}_+\boldsymbol{G}_-$ from where $\tilde{\boldsymbol{Q}} = {\boldsymbol{G}_-}^{-1}$ is defined. For robustness purposes the controller is augmented

with a set of decoupled low-pass filters represented by $\boldsymbol{F}$, whose basic structure is

$$\boldsymbol{F} = \begin{pmatrix} f_1(s) & 0 & \cdots & 0 \\ 0 & f_2(s) & \cdots & 0 \\ \vdots & \vdots & \ddots & \vdots \\ 0 & 0 & \cdots & f_v(s) \end{pmatrix} \tag{3.180}$$

where each filter can be defined using a Type 1 representation as

$$f_i(s) = \frac{1}{(\lambda_i s + 1)^n}, \quad i = 1, \cdots, v \tag{3.181}$$

Using the IMC representation, and assuming a zero plant model mismatch, the complementary sensitivity can be represented as

$$\tilde{\boldsymbol{H}} = \tilde{\boldsymbol{G}}\boldsymbol{Q} = \boldsymbol{G}_+\boldsymbol{F} \tag{3.182}$$

from where the robust performance condition presented in (3.177) can be written as

$$\bar{\sigma}\big(\tilde{\boldsymbol{E}} w_P\big) + \bar{\sigma}\big(\tilde{\boldsymbol{G}}^{-1}\boldsymbol{G}_+\boldsymbol{F}\big)\bar{\ell}_a(\omega) \leq 1, \quad \forall\omega \tag{3.183}$$

If the system contains only minimum phase elements, then the matrix $\boldsymbol{G}_+$ in (3.183) is unity, leading to a robust performance condition that only depends in the plant estimate and the computed uncertainty bounds.

For the monitoring procedure the total plant estimate and the MIMO uncertainty bound described in (3.164) and (3.168) are substituted as $\tilde{\boldsymbol{G}}$ and $\bar{\ell}_a$ respectively in (3.183), yielding to the following robust performance condition for M total periods of experimental execution:

$$\begin{gathered} RPi(\omega_{n,i}, M) \leq 1, \quad \forall\omega_{n,i} \in \boldsymbol{W}_{n,l_{agg}} \\ RPi(\omega_{n,i}, M) = \bar{\sigma}\big(\tilde{\boldsymbol{E}} w_P\big) + \bar{\sigma}\big(\hat{\boldsymbol{G}}^{-1}\boldsymbol{G}_+\boldsymbol{F}\big)\epsilon^{1-\kappa}(\omega_{n,i}, M) \\ \text{with} \quad \tilde{\boldsymbol{E}} = \boldsymbol{I} - \boldsymbol{G}_+\boldsymbol{F} \end{gathered} \tag{3.184}$$

from which a stopping criterion can be defined as:

$$\text{Stop after } M \text{ total number of periods if}$$

$$RPi(\omega_{n,i}, M) \leq 1 \tag{3.185}$$

$$\forall \omega_{n,i} \in \boldsymbol{W}_{n,l_{agg}}, \text{ during the last } n_{Mi} \text{ iterations.}$$

The proposed criterion also incorporates a verification of the robust performance condition accomplishment for more than one consecutive iteration. To improve the closed loop response the tuning parameters $\lambda_i,\ i = 1, \cdots, v$ are selected for each iteration as the values that minimize the maximum robust performance index among all the frequencies, hence

$$\lambda_1, \cdots, \lambda_v = \lambda_1^*, \cdots, \lambda_v^* \tag{3.186}$$

where $\lambda_1^*, \cdots, \lambda_v^*$ are those values obtained after solving the following optimization problem:

$$\min_{\lambda_1, \cdots, \lambda_v} \left(\max_{\omega_{n,i} \in \boldsymbol{W}_{n,l_{agg}}} RPi(\omega_{n,i}, M) \right) \tag{3.187}$$

3.4 Simulation Study

A linear time invariant 2×2 MIMO system, consisting of a subset of the Shell Heavy-Oil Fractionator plant model (Prett and Garcia, 1988) is considered with the following plant model:

$$\boldsymbol{G}(s) = \begin{bmatrix} \frac{4.05}{50s+1} e^{-27s} & \frac{1.77}{60s+1} e^{-28s} \\ \frac{5.39}{50s+1} e^{-18s} & \frac{5.72}{60s+1} e^{-14s} \end{bmatrix} \tag{3.188}$$

where the physical inputs and outputs are

$$\boldsymbol{u}(k) = \begin{bmatrix} u_1(k) \\ u_2(k) \end{bmatrix} = \begin{bmatrix} \text{Top Draw} \\ \text{Side Draw} \end{bmatrix} \tag{3.189}$$

$$\boldsymbol{y}(k) = \begin{bmatrix} y_1(k) \\ y_2(k) \end{bmatrix} = \begin{bmatrix} \text{Top End Point} \\ \text{Side End Point} \end{bmatrix} \tag{3.190}$$

Bounds are imposed on the inputs such that

$$\begin{gathered} -0.5 \leq u_n(k) \leq 0.5 \\ n = 1, 2 \quad k = 1, \ldots, N_s \end{gathered} \tag{3.191}$$

The sampling time is fixed to $T = 4$ min; based on *a priori* knowledge of the system, $\tau_{dom}^H = \tau_{dom}^L = 60$ and $\alpha_s = 2$, $\beta_s = 3$ are considered. Using (3.11) $\omega_* = 0.0056 \frac{rad}{min}$ and $\omega_* = 0.033 \frac{rad}{min}$ are obtained, and using (3.17) the following bound for n_s is obtained

$$n_s \geq 6 \tag{3.192}$$

To achieve an adequate persistence of excitation level $n_s = 32$ is selected; using (3.18) the following bounds for N_s are defined

$$282.74 \leq N_s \leq 1507.97 \tag{3.193}$$

from where $N_s = 512$ is chosen.

3.4.1 Basic Identification Test Monitoring Procedure

In this section a simulation study is implemented to test the basic identification test monitoring procedure presented in Section 3.2. Scaling factors λ_n are selected to comply with (3.191), and phases $\phi_{[n,j]}$ are estimated to minimize the crest factor using Guillaume's approach (Guillaume *et al.*, 1991). For simulation purposes Gaussian output noise is assumed for $v_1(k)$ and $v_2(k)$ with $v_1 \sim \mathcal{N}(0, 1)$ and $v_2 \sim \mathcal{N}(0, 0.3)$; Fig. 3.11 depicts the designed inputs and the simulated outputs for $M = 2$ periods.

According to the basic identification test monitoring formulation it is assumed that the direction of interest is from input u_2 to output y_1 hence

$$\boldsymbol{O} = \big\{[1, 2]\big\} \tag{3.194}$$

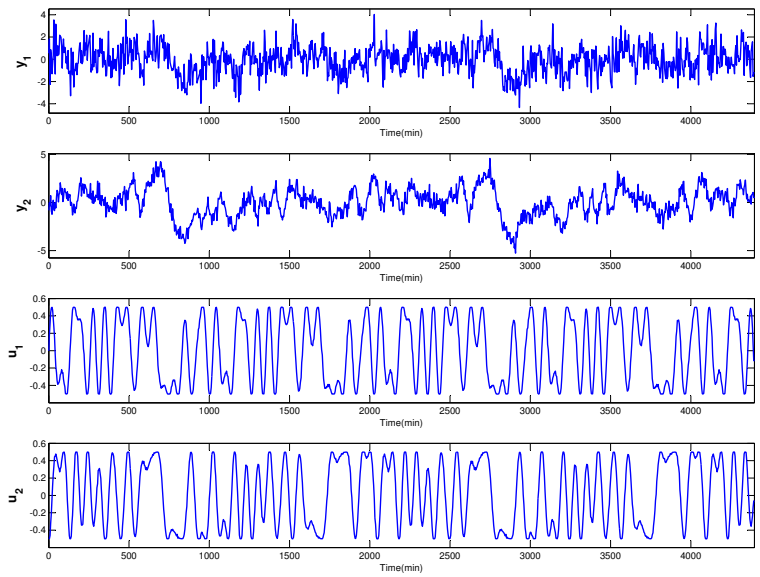

Figure 3.11: Simulation Results for the Model Defined in (3.188) With $M = 2$ Periods of Input Signals and Considering $v_1 \sim \mathcal{N}(0, 1)$ and $v_2 \sim \mathcal{N}(0, .3)$.

Transfer functions and statistical additive uncertainties for a $100 \times (1 - \rho)\%$ with $\rho = 0.5$ confidence region, are computed following the procedure described in section 3.2.2. Data is considered after 75 samples to allow for transient response. Fig. 3.12 shows Nyquist frequency response plots of the ETFE in the direction $[1, 2]$ for $M = 15$ periods. Uncertainty bounds are drawn as circles around each estimation, and 100 replications with different realizations of the same type of noise are plotted to verify the computed uncertainties.

This simulation experiment was developed from a known definition of the plant model. Hence for validation purposes the mean absolute error between the real plant and the ETFE over the n_s frequencies, and for each input-output direction can be defined as:

$$\bar{e}_{[m,n]}(M) = \frac{1}{n_s} \sum_{i=1}^{n_s} \left| G_{[m,n]}(\omega_i^n) - \hat{G}_{[m,n]}(\omega_i^n, M) \right| \tag{3.195}$$

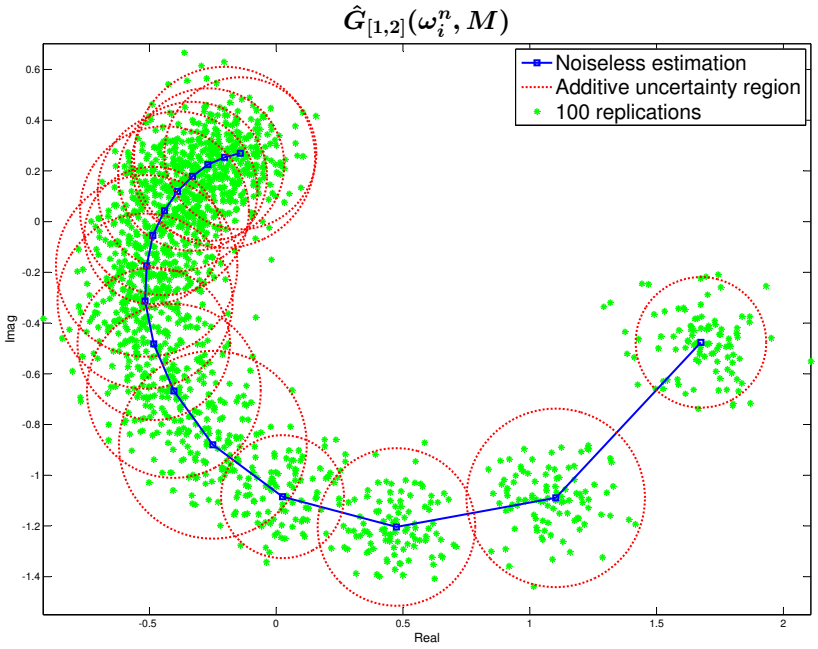

Figure 3.12: Additive Uncertainties $\ell_{a[1,2]}^{1-\rho}(\omega_i^n, M)$ Drawn as Circles Around the ET-FEs for $\hat{G}_{[1,2]}$, with $\rho = 0.5$, $\sigma_1^2 = 1$, $\sigma_2^2 = 0.3$, $M = 15$ Periods and Showing 100 Replications With Different Noise Realizations.

and expressed in percentage variation:

$$\%\bar{e}_{[m,n]}(M) = \frac{1}{n_s}\sum_{i=1}^{n_s}\frac{\left|G_{[m,n]}(\omega_i^n) - \hat{G}_{[m,n]}(\omega_i^n, M)\right|}{\left|G_{[m,n]}(\omega_i^n)\right|} \times 100 \tag{3.196}$$

Fig. 3.13 shows estimations of $\tilde{\ell}_{a[m,n]}(M)$, $AV_{[m,n]}(M)$, and $RV_{[m,n]}(M)$ for $M = 1, \ldots 11$ and for all the input-output elements. For validation purposes, the percentage mean error $\%\bar{e}_{[m,n]}(M)$ is also shown. In both cases special emphasis is placed on the specified direction of interest $[1, 2]$.

The following stopping criterion according to (3.81) is proposed: the experiment should finalize when the decrease in the additive uncertainty is consistently lower than 2% with respect to the initial estimation and 15% with respect to the previous iteration ($B_{AV} = 2\%$ and $B_{RV} = 15\%$). These conditions should persist for at least

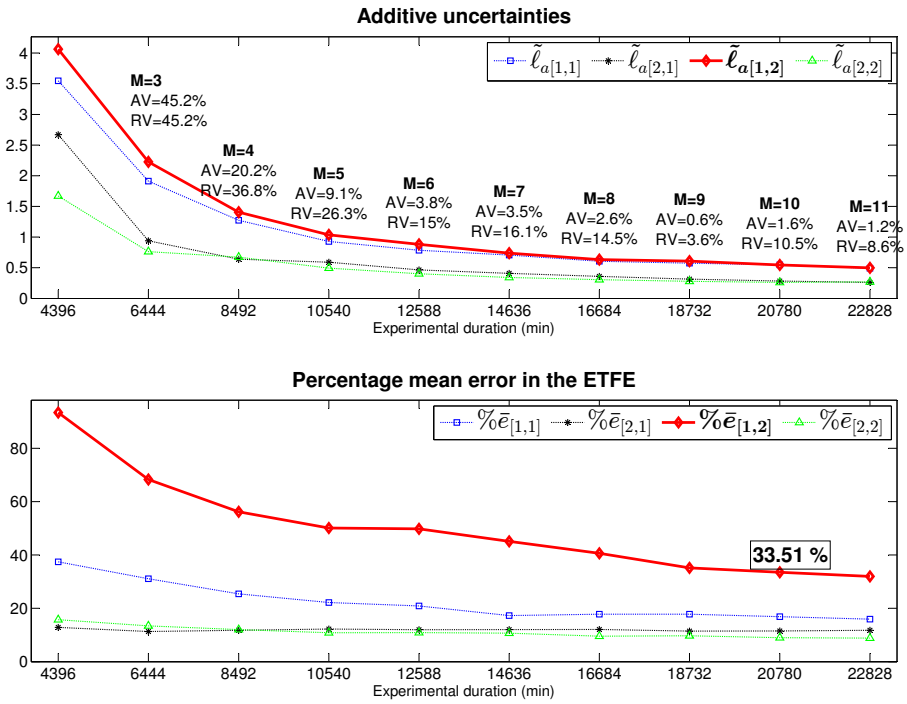

Figure 3.13: Illustration of the Monitoring Procedure With Estimates Made for $M = 1, \ldots 11$, $m = 1, 2$ and $n = 1, 2$ and Showing Values of $\tilde{\ell}_{a[m,n]}(M)$, $AV_{[m,n]}(M)$, $RV_{[m,n]}(M)$, and $\%\bar{e}_{[m,n]}(M)$.

two iterations ($n_{Mi} = 2$). From Fig. 3.13, it can be observed that the conditions are accomplished at $M = 10$ periods with a duration of 20780 minutes, resulting in $\tilde{\ell}_{a[1,2]}(10) = 0.545$, $AV_{[1,2]}(10) = 1.6\%$, $RV_{[1,2]}(10) = 10.5\%$, and $\%\bar{e}_{[1,2]}(10) = 33.51\%$. Fig. 3.14 shows the resultant ETFEs for all the input-output elements with their respective percentage mean errors. If more accurate results are desired bounds B_{AV} and B_{RV} should be reduced and/or n_{Mi} should be increased. This will cause considerable increases in the final length of the experiment.

To test the repeatability of the monitoring process, the same experiment is replicated 10 times with different realizations of the same Gaussian output noise. Results are shown in Fig. 3.15 for the element of interest $[1, 2]$, where a reduction trend can be

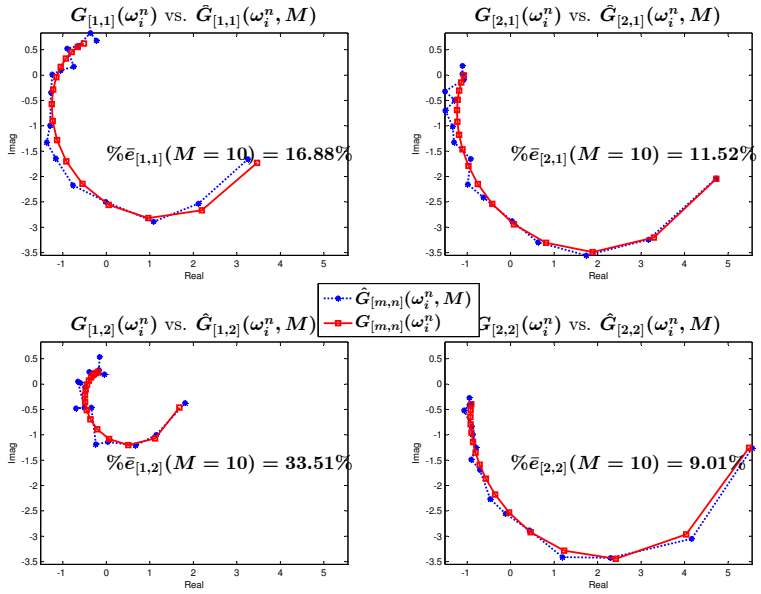

Figure 3.14: Nyquist Plots of ETFEs $\hat{G}_{[m,n]}(\omega_i^n, M)$ for all the Input Output Elements Compared to the Simulation Plant $G_{[m,n]}(\omega_i^n)$, Including the Percentage Mean Error $\%\bar{e}_{[m,n]}(M)$ After Stopping the Experiment at $M = 10$ Periods.

observed in both the uncertainties and the mean error with increments in the number of periods M. With $M = 10$ cycles mean errors vary from 29.56% to 42.7%; slightly improvements will occur with further increments of M.

The performance of the monitoring process over different types of noise will be tested. Equation (3.197) is an autoregressive noise whose effect is specified by the coefficients ϕ and σ_n^2.

$$v_n(k) = \phi v_n(k-1) + a_t, \quad a_t \sim \mathcal{N}(0, \sigma_n^2) \tag{3.197}$$

A simulation using autoregressive noise is performed with $\sigma_1^2 = 0.2$, $\sigma_2^2 = 0.1$ and $\phi = 0.6$. If the same stopping criterion is applied ($B_{AV} = 2\%, B_{RV} = 15\%$, and $n_{Mi} = 2$) the experiment ends at $M = 10$ periods with $\%\bar{e}_{[1,2]}(M) = 34.12\%$. However, if the bound on the relative uncertainty decrease is reduced to $B_{RV} = 3\%$ then the

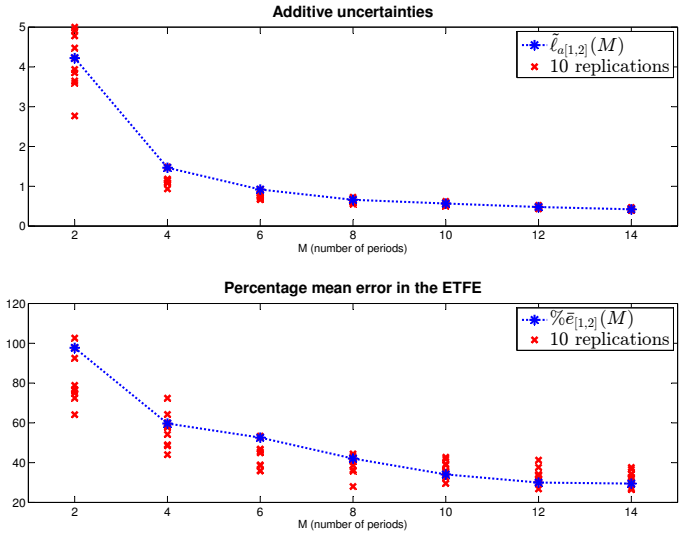

Figure 3.15: Estimated Additive Uncertainties for 10 Replications of Gaussian Output Noise With $\sigma_1^2 = 1$ and $\sigma_2^2 = 0.3$ for $M = 2, \ldots, 14$. Percentage Mean Errors for Each Case are Also Shown.

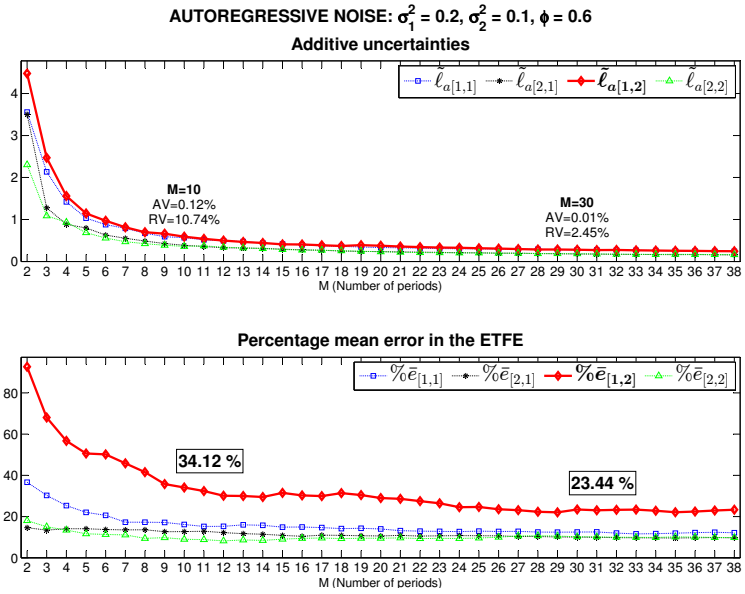

Figure 3.16: Monitoring Procedure Assuming an Autoregressive Output Noise With $\sigma_1^2 = 0.2$, $\sigma_2^2 = 0.1$ and $\phi = 0.6$, Including Uncertainty Estimates and Percentage Mean Error Computations.

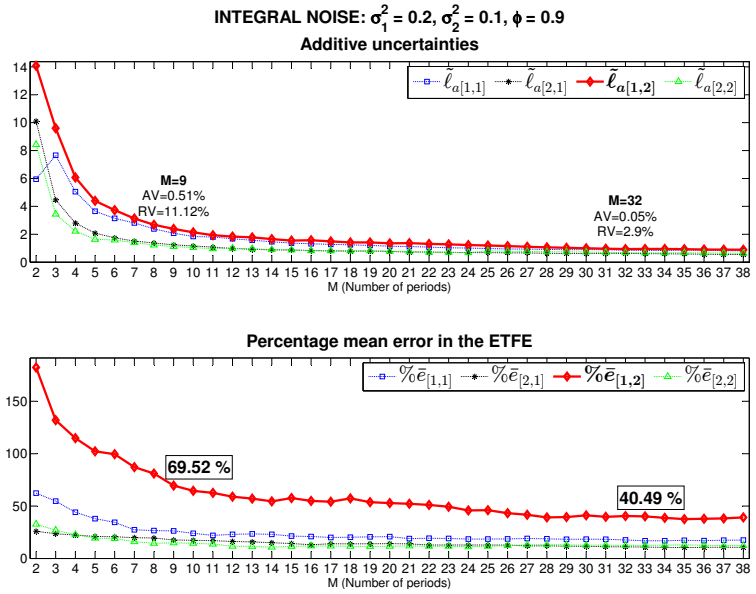

Figure 3.17: Monitoring Procedure Assuming an Integral Output Noise With $\sigma_1^2 = 0.2$, $\sigma_2^2 = 0.1$, and $\phi = 0.9$ Including Uncertainty Estimations and Percentage Mean Error Computations.

experiment stops at $M = 30$ periods with $\%\bar{e}_{[1,2]}(M) = 23.44\%$, as can be observed in Fig. 3.16.

A more autoregressive noise structure, resembling integrative effects, is tested by using (3.197) with $\sigma_1^2 = 0.2$, $\sigma_2^2 = 0.1$ and $\phi = 0.9$ to reproduce the random walk effect. Results are shown in Fig. 3.17. If $B_{RV} = 15\%$ is considered, the experiment stops at $M = 9$ with an error of $\%\bar{e}_{[1,2]}(M) = 69.52\%$; using $B_{RV} = 3\%$ the experiment stops at $M = 32$ with $\%\bar{e}_{[1,2]}(M) = 40.49\%$. Better results can be achieved with lower values of B_{RV}, however the mean error still remains high. To complement the performance analysis, Fig. 3.18 shows uncertainty estimates and mean errors for 10 different replications of the autoregressive and integral noise for $M = 2, 12, 22, \ldots, 62$. Considerable reductions in both uncertainty levels and mean errors can be observed as M increases.

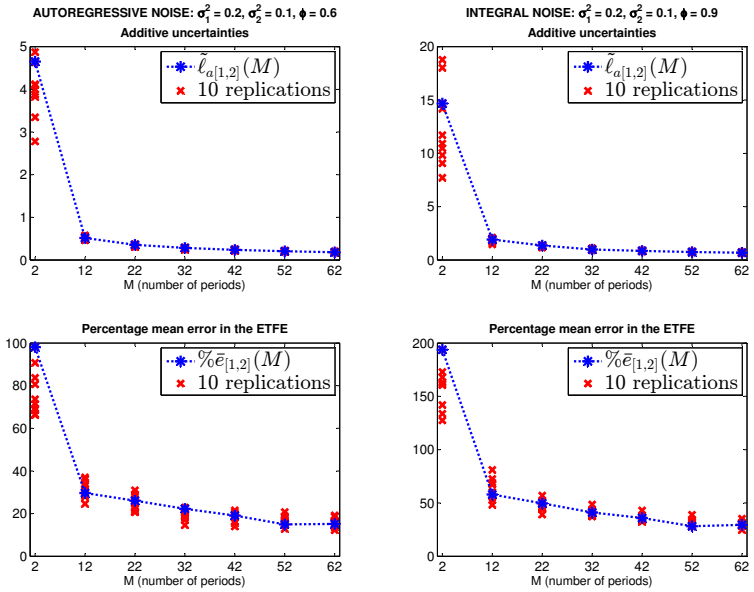

Figure 3.18: Estimated Additive Uncertainties for 10 Replications of Autoregressive and Integral Noise for $M = 2, \ldots, 62$. Percentage Mean Errors for Each Case are Also Shown.

3.4.2 Enhanced Identification Test Monitoring Procedure

The enhanced identification test monitoring procedure described in Section 3.3 is now tested through a simulation experiment. The same referential MIMO system and operational conditions described in (3.188) – (3.193) are considered. Gaussian output noise is assumed for $v_1(k)$ and $v_2(k)$ with $v_1 \sim \mathcal{N}(0,1)$ and $v_2 \sim \mathcal{N}(0,0.3)$.

For validation purposes the mean absolute error between the real plant and the transfer function estimate is computed over all the frequencies as

$$\bar{e}(M) = \frac{1}{n_{s,l_{agg}}} \sum_{i=1}^{n_{s,l_{agg}}} \bar{\sigma}\big(\boldsymbol{G}(\omega_{n,i}) - \hat{\boldsymbol{G}}(\omega_{n,i}, M)\big) \tag{3.198}$$

The noninvertible matrix $\boldsymbol{G}_+$ used in the computation of the robust stability index in (3.184) is computed using dynamic decoupling ideas that minimize control errors for plants with significant delays. This is done using the following theorem proposed

by Holt and Morari (1985):

Theorem 1 *The diagonal* $\boldsymbol{G}_+^d$ *matrix with the smallest delay terms such that the multivariable IMC controller* $\tilde{\boldsymbol{Q}} = \boldsymbol{G}_-^{-1} = \boldsymbol{G}^{-1}\boldsymbol{G}_+$ *is realizable has the form*

$$\boldsymbol{G}_+^d = diag(r_{ii}, \cdots, r_{jj}, \cdots, r_{nn}) \tag{3.199}$$

where

$$r_{jj} = e^{-s \max_i \left(max\left(0,(\hat{q}_{ij} - \hat{p}_{ij})\right)\right)} \tag{3.200}$$

and $\hat{p}_{ij}$ *is the minimum delay in the numerator of element* ij *of* $\boldsymbol{G}^{-1}$*, and* $\hat{q}_{ij}$ *is the minimum delay in the denominator of element* ij *of* $\boldsymbol{G}^{-1}$*.*

Using Theorem 1 with the model described in (3.188), and assuming that *a priori* information about the delays is available, the resultant matrix and filter are

$$\boldsymbol{G}_+ = \begin{pmatrix} e^{-27s} & 0 \\ 0 & e^{-14s} \end{pmatrix}, \quad \boldsymbol{F} = \begin{pmatrix} \frac{1}{\lambda_1 s+1} & 0 \\ 0 & \frac{1}{\lambda_2 s+1} \end{pmatrix} \tag{3.201}$$

The maximum robust stability indexes among all frequencies for each cycle are computed as

$$RPi_{max}(M) = \max_{\omega_{n,i} \in \boldsymbol{W}_{n,l_{agg}}} RPi(\omega_{n,i}, M) \tag{3.202}$$

To find the values for the parameters λ_1 and λ_2 according to (3.187) a simple exhaustive search is performed varying each λ_i from 10 to 100 with increments of 2 units, and then finding the values of λ_1^* and λ_2^* that combined result in the minimum value for $RPi_{max}(M)$. An example of the proposed search process is illustrated in Fig. 3.19.

The performance weighting function w_P is defined using (3.178) considering $A_P = 10^{-3}$ and $M_P = 2$. By observing the defined asymptotic frequency bands in Fig. 3.10,

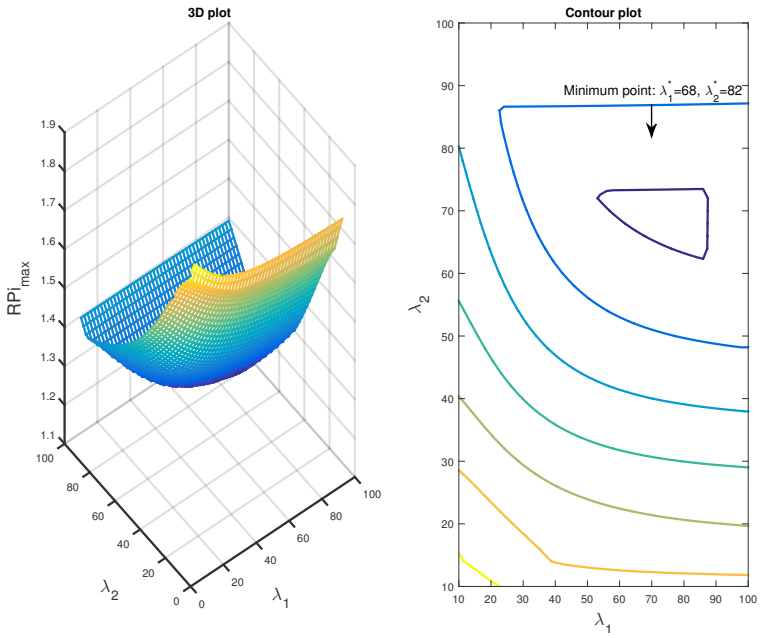

Figure 3.19: Illustration of the Proposed Simple Search Procedure for the Values λ_1^* and λ_2^* That Minimizes RPi_{Max}.

and considering again the dominant time constant of $\tau_{dom} = 60$ then

$$M_P\omega_b \approx \frac{1}{\tau_{dom}}, \quad \omega_b = \frac{1}{M_P\tau_{dom}} = 0.0083 \tag{3.203}$$

The simulation is performed, input-output data is analyzed, uncertainty bounds are computed with $\rho = 0.05$, and $\kappa = 0.1855$ giving a confidence level of 81.45% using (3.159) for the MIMO estimate. Two different simulation studies are performed and contrasted to evaluate the "zippered" and full spectral input signal design structures.

3.4.2.1 Simulation Results Using "Zippered" Signals

The "zippered" input signal design procedure described in Section 3.3.2.1 is applied. Fig. 3.20 illustrates the resulting input and output signals for $M = 2$ cycles.

Uncertainty computations are performed using the transient LPM, assuming $R =$

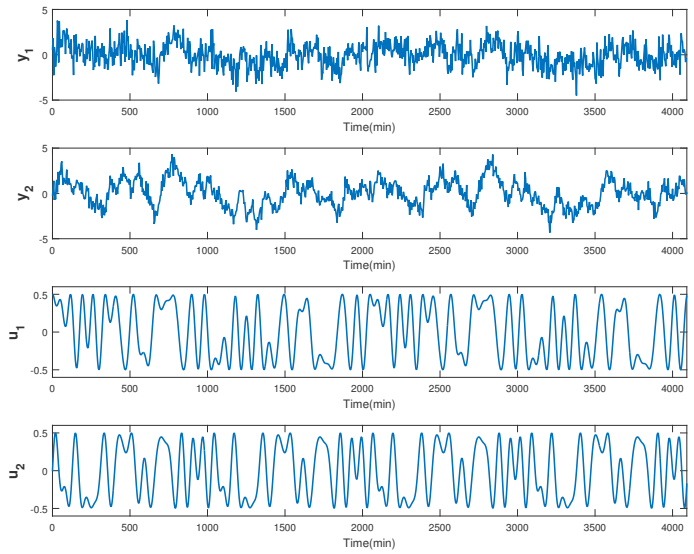

Figure 3.20: Simulation of Input Signals Designed With the "Zippered" Method and the Resulting Output Signals for $M = 2$ Cycles With $\sigma_1^2 = 1$ and $\sigma_2^2 = 0.3$.

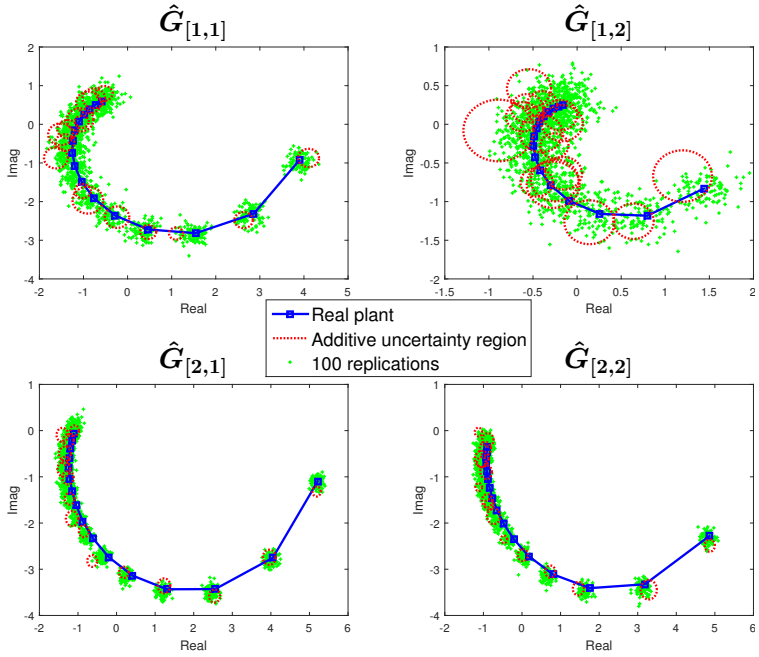

Figure 3.21: Additive Uncertainties for the "Zippered" Design Drawn as Circular Regions Around Each Real Transfer Function Response, Showing Different Transfer Function Estimates for 100 Realizations of the Same Gaussian Noise.

2, and $n_T = 6$ resulting in $df_T = 5$. Fig. 3.21 illustrates the computed additive uncertainty regions drawn as circles around the real values of the transfer functions. New estimates of the transfer functions for each frequency are also presented using 100 different realizations of the same type of noise.

Results for a maximum of $M = 16$ periods of the same input signals with no modifications are shown in Fig. 3.22. The upper plot shows results for the robust performance test while the lower plot shows a validation perspective through the computation of the mean error. The proposed stopping criterion described in (3.185) is evaluated considering $n_{Mi} = 2$ consecutive iterations. It can be observed that the desired conditions are met, and the experiment can be stopped after $M = 11$ periods with a total length of 22528 minutes. The mean error at that point is $\bar{e}(11) = 0.31$ what represents a reduction of 48% compared to the error estimate at $M = 2$ cycles.

Different types of modifications in the input signals are tested. Fig. 3.23 and Fig. 3.24 present simulation results including changes on the amplitude and the fundamental frequency of the inputs signals for $M = 3$ cycles.

Results for the monitoring procedure are shown in Fig. 3.25 where the dotted line represents increments on the amplitude of the signals after $M = 6$ cycles considering $u_1^{min} = u_2^{min} = -1$, and $u_1^{max} = u_2^{max} = 1$. If the same stopping criterion is considered, the test is now accomplished earlier and the experiment can be stopped after $M = 8$ cycles with a total duration of 16384 minutes. This type of modification assumes that the amplitude operational constraints of the signals have not been reached yet. The dashed line in Fig. 3.25 represents a change on the frequency harmonic content of the input signals after $M = 6$ cycles, considering a harmonic step reduction of $S_{h,l} = 1$. If the stopping criterion is evaluated again, the experiment can be halted after $M = 9$ cycles with a total duration of 18432 minutes. The type of modification in

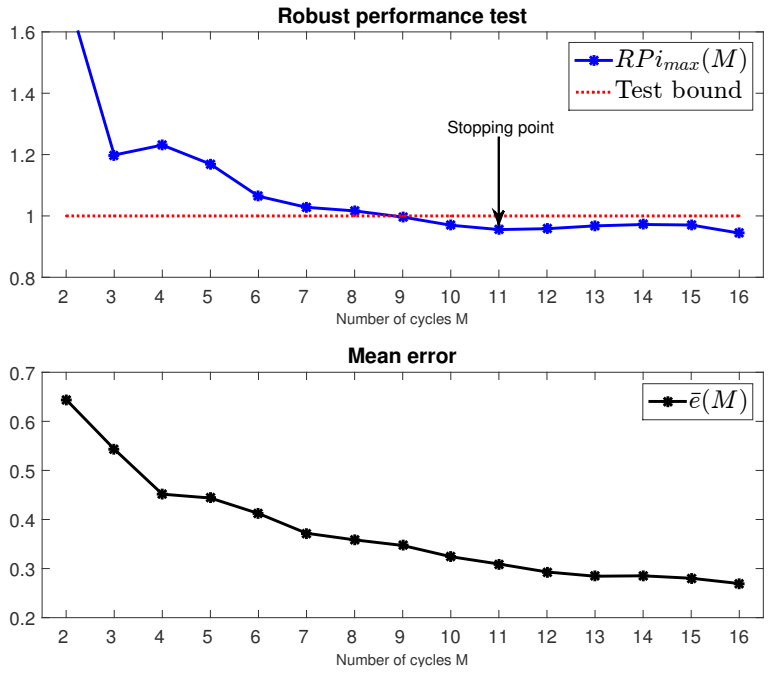

Figure 3.22: Illustration of the Monitoring Process for $M = 1, \cdots, 16$ Cycles of the Same Input Signals With no Modifications. Uncertainties and Robust Performance Indexes Are Computed for $\rho = 0.05$

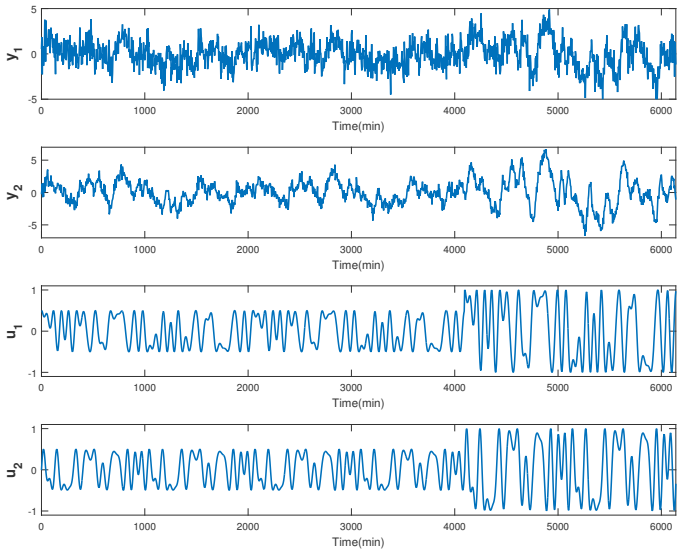

Figure 3.23: Simulation of the "Zippered" Experiment Considering a Total of $M = 3$ Cycles, and Including a Change on the Input Amplitude After $M = 2$ Cycles.

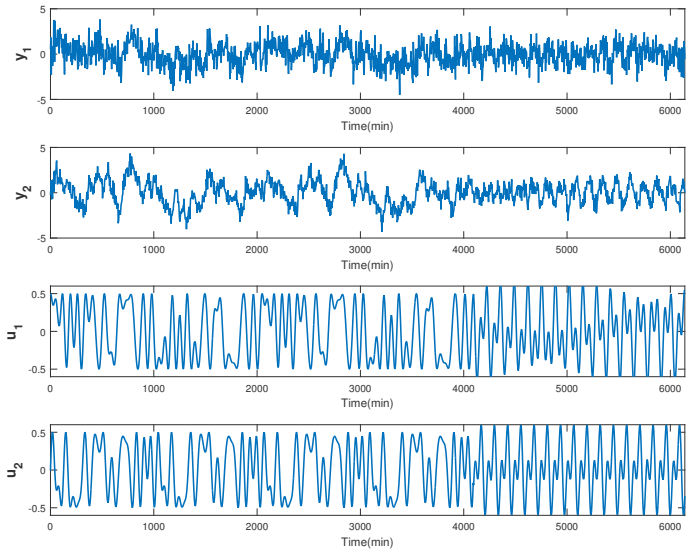

Figure 3.24: Simulation of the "Zippered" Experiment Considering a Total of $M = 3$ Cycles, and Including a Change on the Fundamental Frequency of the Inputs After $M = 2$ Cycles.

the input signals depends on the available resources and user preferences; however all modifications lead to improvements in the useful for identification of the experiment.

The performance of the proposed monitoring process is tested through the application of 10 independent realizations of the same Gaussian noise with $v_1 \sim \mathcal{N}(0, 1)$ and $v_2 \sim \mathcal{N}(0, 0.3)$. Results are shown in Fig. 3.26 where each simulation exhibits information regarding the robust stability test and validation through the computation of the mean error when only the number of cycles is increased.

Fig. 3.27 depicts results using an autoregressive noise structure represented by

$$v_n(k) = \phi v_n(k-1) + a_t, \quad a_t \sim \mathcal{N}(0, \sigma_n^2) \tag{3.204}$$

The left-side plots represent a full autoregressive structure considering $\phi = 0.6$, $\sigma_1^2 = 0.2$, and $\sigma_2^2 = 0.1$. The right-side plots represent a more integral noise action with a higher autoregressive factor of $\phi = 0.9$, $\sigma_1^2 = 0.2$, and $\sigma_2^2 = 0.1$. As expected the

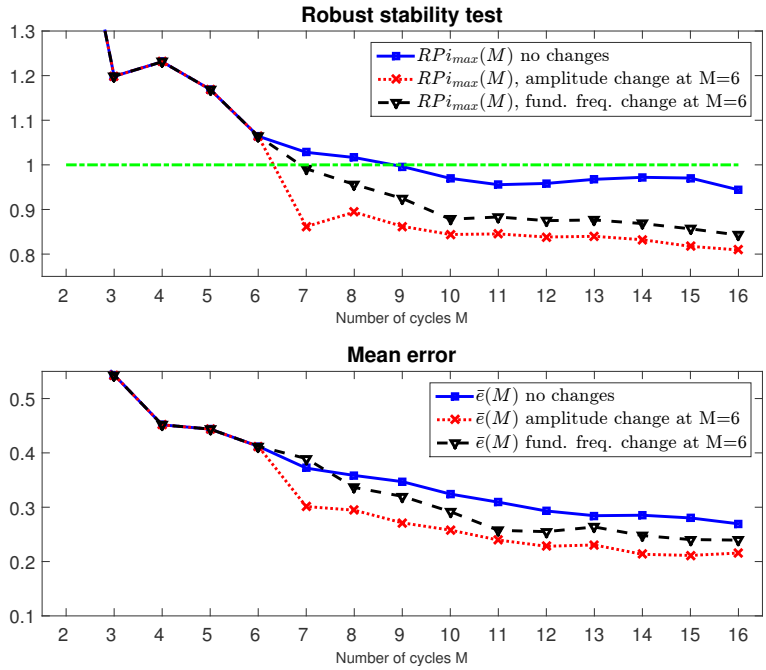

Figure 3.25: Illustration of the Monitoring Process for $M = 1, \cdots, 16$ Cycles Considering Changes in the Amplitude and the Frequency Content of the Input Signals After $M = 6$ Cycles.

simulation shows a decrease tendency on the robust performance index RPi_{max} as the number of period increases that is consistent with the mean error reduction. An error and uncertainty reduction pattern is observed for the different types of noise. Integral noise demands more excitation power from the inputs at low frequencies; hence the ability to reduce the uncertainty is lower.

3.4.2.2 Simulation Results Using Full Signals

The input signal design procedure presented in Section 3.3.2.2 considering the full frequency band and the fast LPM for uncertainty computations, is implemented. Fig. 3.28 presents the simulated inputs and outputs considering the same Gaussian noise representation described in the previous section for $M = 2$ periods with $\sigma_1^2 = 1$

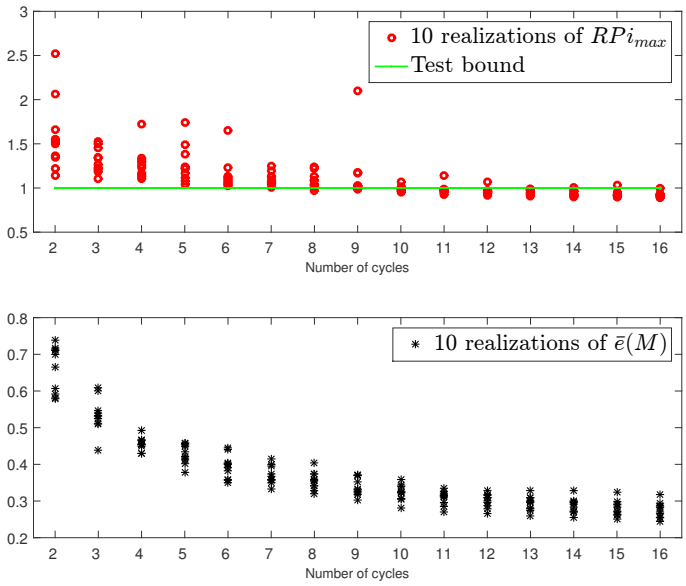

Figure 3.26: Ten Computations of the Robust Performance Index and the Absolute Mean Error Relying on the "Zippered" Design Generated From Different Realizations of Gaussian Noise With $\sigma_1^2 = 1$, and $\sigma_2^2 = 0.3$.

and $\sigma_2^2 = 0.3$. Uncertainty computations are performed using the fast LPM approach, considering $R = 2$, $n_T = 4$, and $df_T = 5$ for the non-excited frequencies, and $R = 3$, $n_G = 6$, and $df_G = 5$ for the excited frequencies. Fig. 3.29 illustrates the computed additive uncertainties drawn as circular regions over a Nyquist plot and including 100 replications utilizing the same noise structure but with different realizations for $M = 11$ cycles. Considerable bias and higher variability, especially at the border frequencies can be observed as expected. To avoid problems due the border effect described in Section 3.3.1.3, the uncertainties computed for the two shorter and the two higher frequencies in the grid are neglected as is illustrated in Fig. 3.30.

The monitoring process is performed and results for a maximum of $M = 16$ cycles are shown in Fig. 3.31, where the upper plot again represents the robust performance index contrasted with test bound presented in (3.185). The lower plot presents vali-

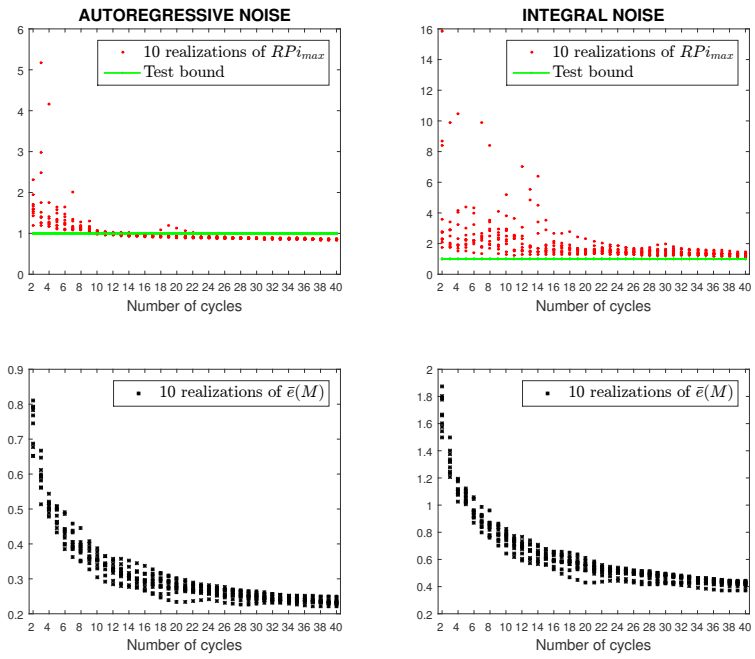

Figure 3.27: Illustration of 10 Independent Computations of RPi_{Max} and $\bar{e}$ Using Different Noise Structures for the "Zippered" Design: 1) Autoregressive With $\phi = 0.6$, $\sigma_1^2 = 0.2$, and $\sigma_2^2 = 0.1$. 2) Integral With $\phi = 0.9$, $\sigma_1^2 = 0.2$, and $\sigma_2^2 = 0.1$.

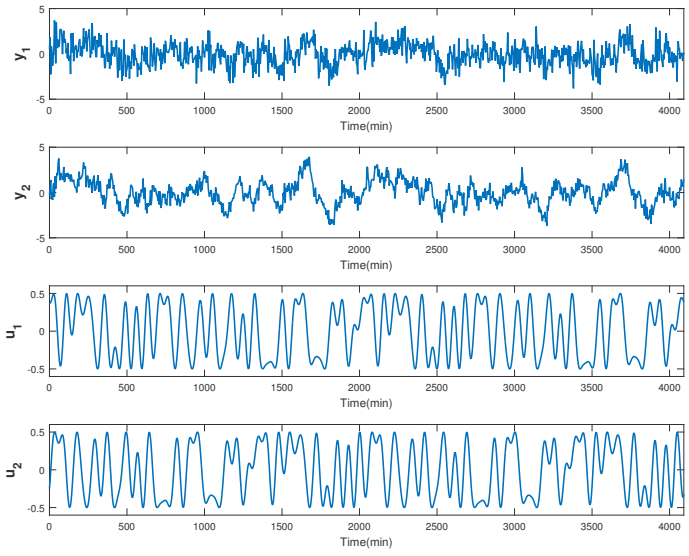

Figure 3.28: Simulation of Input Signals Designed With the Full Method and the Resulting Output Signals for $M = 2$ Cycles With $\sigma_1^2 = 1$ and $\sigma_2^2 = 0.3$.

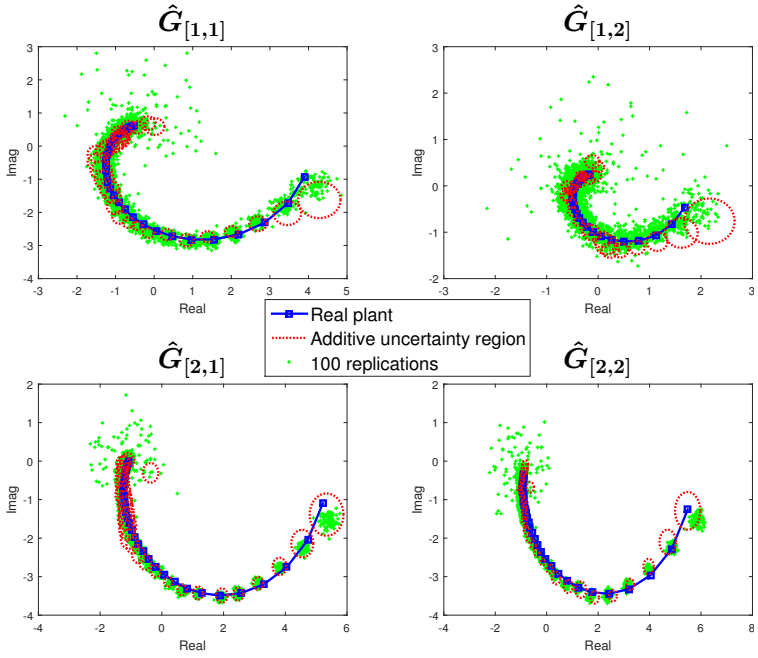

Figure 3.29: Additive Uncertainties for the Full Design Drawn As Circular Regions Around Each Real Transfer Function Response, Showing Different Transfer Function Estimates for 100 Realizations of the Same Gaussian Noise.

dation results through the computation of the absolute mean error using (3.198). It can be observed that using the proposed stopping criterion considering accomplishment of the test for $n_{Mi} = 2$ consecutive iterations, the experiment can be halted after $M = 12$ iterations with a total duration of 24576 minutes, and a mean error of $\bar{e}(12) = 0.314$. The same experiment is repeated utilizing 10 different realizations of the same Gaussian noise; results are presented in Fig. 3.32 where the reduction tendency can be observed with higher variability. The different types of input signal modifications are again tested for the full design, including changes on the amplitude and the fundamental frequency content. Results are presented in Fig. 3.33 depicting changes in the amplitude of the input signals to $u_1^{min} = u_2^{min} = -1$, $u_1^{max} = u_2^{max} = 1$, and a harmonic step reduction to $S_{h,l} = 1$. Best results in both the robust perfor-

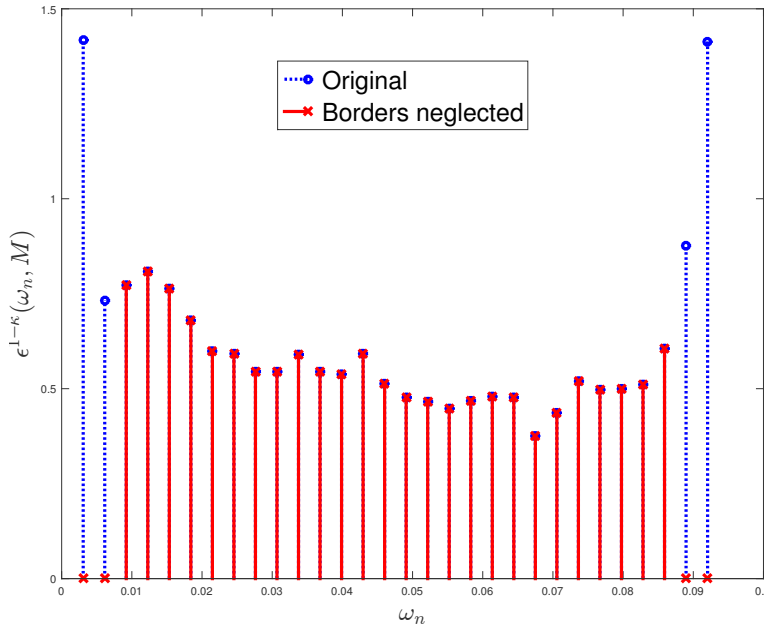

Figure 3.30: Original Additive Uncertainties $\epsilon^{1-\kappa}(\omega_n, M)$ Computed Using the Full Design for $M = 3$ Cycles, With Corresponding Reduction to Neglect the Border Effect.

mance index and the mean error are obtained when the input signal amplitude is increased. If the fundamental frequency of the input signal is modified, a slight increment in the absolute mean error can be observed. This issue is later compensated when the total number of iterations increases. This error is attributed to an increment on the bias of the transfer function estimate that occurs when the total number of samples (N_s) is reduced (Pintelon *et al.*, 2011) as a consequence of the change in the harmonic frequency content.

Finally the performance of the procedure is tested using different realizations of the autoregressive noise structure presented in (3.204). Results are presented in Fig. 3.34 where the left-side plots represent a regular autoregressive structure considering $\phi = 0.6$, $\sigma_1^2 = 0.2$, and $\sigma_2^2 = 0.1$, and the right-side plots represent a more autoregressive

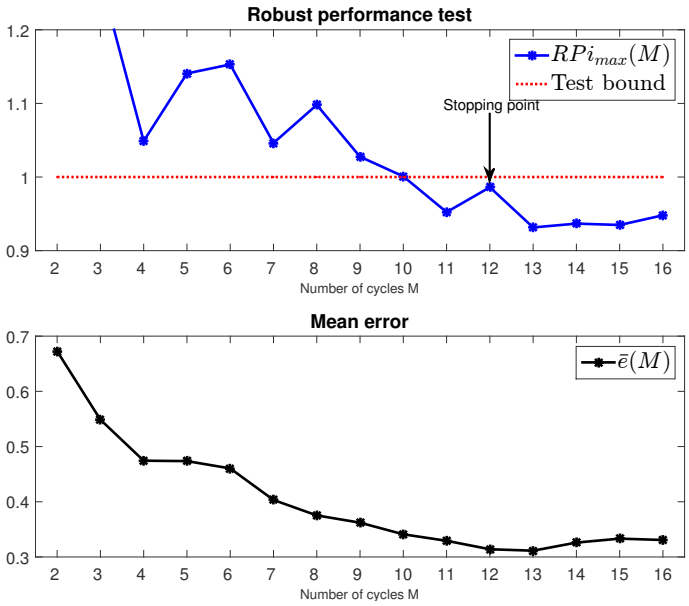

Figure 3.31: Illustration of the Monitoring Process for $M = 1, \cdots, 16$ Cycles of the Same Input Signals With No Modifications. Uncertainties and Robust Performance Indexes Are Computed for $\rho = 0.05$.

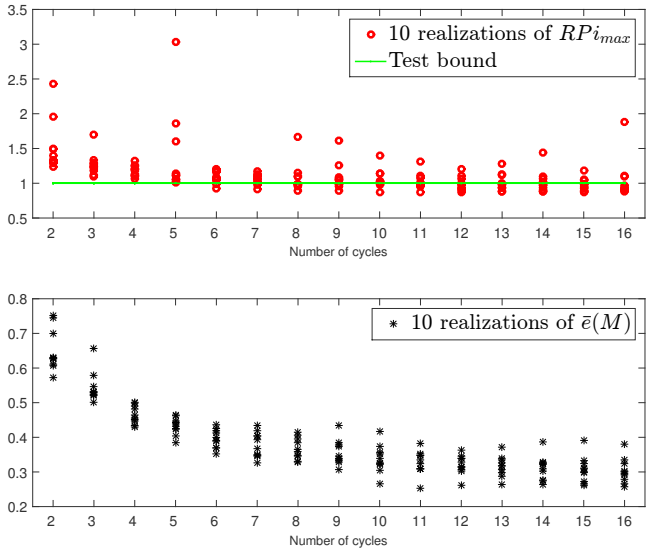

Figure 3.32: Ten Computations of the Robust Performance Index and the Absolute Mean Error Relying on the Full Design Generated From Different Realizations of Gaussian Noise With $\sigma_1^2 = 1$, and $\sigma_2^2 = 0.3$.

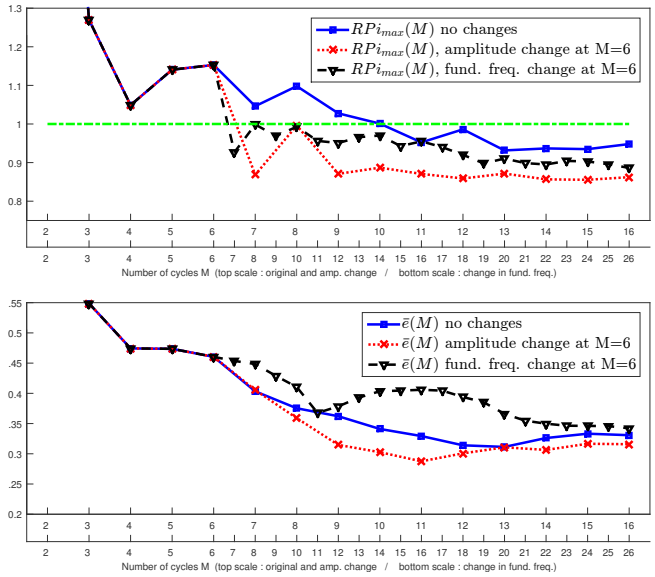

Figure 3.33: Illustration of the Monitoring Process for $M = 1, \cdots, 16$ Cycles Considering Changes in the Amplitude and the Frequency Content of the Input Signals After $M = 6$ Cycles.

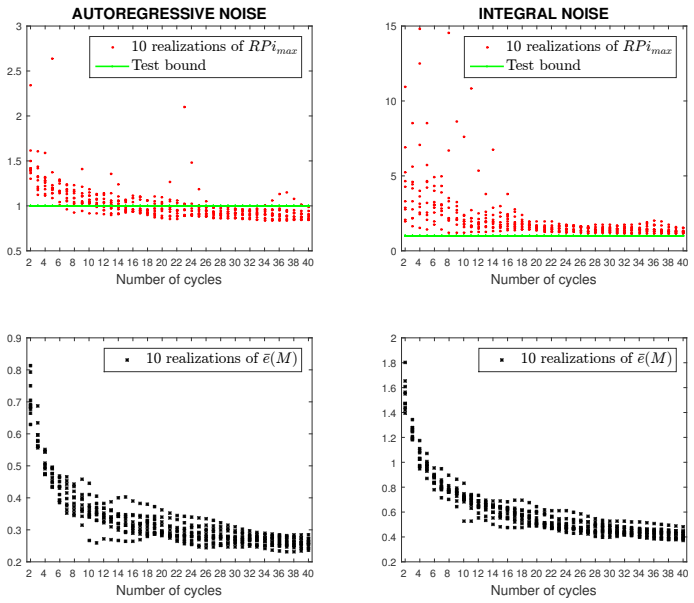

Figure 3.34: Illustration of 10 Independent Computations of RPi_{Max} and $\bar{e}$ Using Different Noise Structures for the Full Design: 1) Autoregressive With $\phi = 0.6$, $\sigma_1^2 = 0.2$, and $\sigma_2^2 = 0.1$. 2) Integral With $\phi = 0.9$, $\sigma_1^2 = 0.2$, and $\sigma_2^2 = 0.1$.

(integrative) noise action with $\phi = 0.9$, $\sigma_1^2 = 0.2$, and $\sigma_2^2 = 0.1$. For the regular autoregressive case it can be observed that the test bound is accomplished in most of the cases after 25 cycles with a considerable reduction in the mean error. For the integral case there is a reduction in the error and in the performance index, however the test conditions are hardly barely satisfied. A modification of performance weights or a relaxation on the test conditions may be needed.

3.5 Chapter Summary

This chapter presents an identification test monitoring procedure that determines the shortest possible experiment in terms of the problem definitions (e.g., N_s, n_s), and at the same time with data that is sufficiently informative for identification purposes. Different formulations of the problem are presented and contrasted.

A basic approach that assumes data measured at steady state is initially presented. Simulations show that bounds B_{AV}, B_{RV}, and n_{Mi} cannot be rigidly defined; user intervention is important for their adjustment in real time. Because of the multivariable nature of the system and the use of "zippered" power spectrums, the total duration of the experiment N is affected by the number of inputs n_u as was shown in (3.10); however the same dependence would have existed, if n_u independent SIMO experiments had been designed instead. The uncertainty computation method can be applied to different situations where no *a priori* knowledge of the noise structure is available, and also when the input signal is not designed by the user but is periodic in nature and can be measured. Multivariable uncertainty computation leads to results that are valid for all the input/output elements. In practical applications and for identification purposes the worst case scenario criterion may give acceptable results, as the simulation results suggest. The disadvantage of the basic method is that it requires output signals measured at steady state to account for transient responses;

hence no modifications can be performed to the input signals during the experimental execution.

An enhanced identification test monitoring methodology was also proposed. An evaluation is accomplished after each input period, from which three possible actions are proposed: increasing the length of the experiment (by adding another cycle), increasing the amplitude of the signal, or adjusting the frequency content of excitation in the signal. To account for the transient effect caused by these modifications, the Local Polynomial Method (LPM) was adopted for the transfer function and uncertainty computation. Two variants of the LPM were tested, first the transient LPM using "zippered" multisine input signals, and the fast LPM method using input signals defined for the full frequency band of interest. There is a trade between these approaches: the zippered design offers a less conservative and more accurate definition of uncertainties and robust performance index, while the full method offers a better frequency resolution and hence possible smaller time intervals. Simulations proved that the "zippered" design exhibits a better performance in terms of bias error and variability of the estimation. The experiment ends when a predefined criterion based on robust performance metrics is satisfied.

Simulations demonstrated the ability of the identification test monitoring procedure to identify an appropriate moment to halt the experiment. Increasing the amplitude of the input signal is a effective means for improving the experiment; however because of operational constraints this is not always possible. A second alternative is to modify how power is distributed over frequency in the input signal, increasing its contribution at some frequencies while keeping the total power constant. This was accomplished in the paper by redistributing harmonic excitation content. Ultimately, the decision to take after each evaluation point will depend on operational constraints and user preferences.

Chapter 4

DESIGN OF OPEN-LOOP BEHAVIORAL INTERVENTIONS RELYING ON SYSTEM IDENTIFICATION IDEAS

4.1 Overview

As noted in Chapter 1, physical inactivity is a serious behavioral problem that contributes to a high number of mortalities in the U.S. each year (Mokdad *et al.*, 2004). The use of emerging technologies, such as smartphones and wearable sensors, is enabling the application of novel mobile and wireless (mHealth) interventions (Hekler *et al.*, 2013b) that lend themselves to a systematic and mathematically rigorous approach. The results are interventions that rely on highly intensive measurement of outcomes of interest to make decisions on intervention treatment components and dosages that are opportunely delivered; hence these interventions are referred to in the literature as *Intensively Adaptive Interventions* (IAI; Riley *et al.* (2015b)).

In order to design optimal interventions through the use of effective feedback (and/or feedforward) controllers, it is necessary to obtain an adequate model that properly represents the dynamical nature of the system. As noted in Chapter 2, Social Cognitive Theory (SCT) (Bandura, 1977, 1986) is a highly prevalent and generally well-regarded conceptual framework within behavioral science that has been used to design a variety of behavioral interventions. The developed dynamical model of SCT will be used to represent the dynamic nature of the low physical activity behavioral problem.

In this work, the term "plant" refers to a human behavioral system defined as a dynamical model based on SCT. IAIs can address the problem of low physical activity in

sedentary individuals, using SCT as the conceptual framework. If these interventions are to be based on control systems engineering principles, then an appropriate estimation of the behavioral dynamics should be obtained first. A semi-physical system identification procedure is proposed to search and refine the individual SCT model parameters. One important goal of the experimental input design is to satisfy identification requirements such as persistent excitation and at the same time keep the variations within user-defined, "patient-friendly" (Deshpande *et al.*, 2012) constraints. An additional challenge in behavioral intervention settings is to obtain outputs that are consistent with the goals and the practical demands of the intervention.

In this chapter an input signal design will be proposed, together with an estimation procedure, that provides an adequate plant model and at the same time enables accomplishing desired behavioral outcomes during the course of the experiment. The proposed strategy will consider the construction of two open-loop experiments with different inputs. The first one is referred to as an *informative* experiment. It is designed based on *a priori* knowledge from behavior change theory and previous experience with behavioral interventions. This experiment will provide basic preliminary information on the dynamics of the system and lead to an initial model.

Two different alternatives for the informative experiment will be presented; the first one relies on random signals generated within user-defined bounds, with the goal to achieve the required amount of daily steps per week (e.g., 10,000). The second alternative will propose a design procedure with the shortest possible duration, that correspondingly allows inferring the important dynamical properties of the system. This will be done using the approach presented in Chapter 3 testing both, the basic and enhanced identification test monitoring methods. This result has important practical implications in behavioral interventions, given that systematic approaches for determining experimental duration in single-subject /"idiographic" experiments

are not well-understood. Under the assumption that noise in the signals is the major source of uncertainty in the estimation, a deterministic periodic input signal can be employed to analyze and extract frequency domain information that can be used in the computation of probabilistic uncertainty descriptions. In the basic method the required uncertainty bounds are estimated relying on a non-parametric averaged Empirical Transfer Function Estimates (ETFE). The enhanced approach relies on the Local Polynomial Method (LPM) to compute transfer functions and uncertainties, allowing the incorporation of changes in the amplitude or the frequency content of the input signals. To obtain independent computations of each input-output transfer function of the MIMO system for both methods, the input design will consider a multisinusoidal "zippered" spectra (Rivera *et al.*, 2009) and will include a "patient-friendly" selection of phases.

The second experiment is an *optimized* experiment that will use the results from the informative experiment, to shape the behavioral outcomes to a desired pattern. It is designed by solving a formal optimization problem that searches for the best inputs, considering the estimated preliminary model and expected performance requirements. Both experimental designs will consider internal logic conditions that are present in a behavioral situation, and will be properly specified.

The chapter is organized as follows: Section 4.2 presents a description of the components and decision algorithms that form part of the physical activity intervention. It also describes general design constraints, and details about the proposed grey-box estimation. Section 4.3 describes the design of the informative experiment, including input signal generation through pseudo-random signals and using an identification test monitoring procedure. Section 4.4 explore the design of the optimized experiment as a constrained optimization problem. Section 4.5 shows a simulation study and results using the proposed procedure. Section 4.6 gives summary and conclusions

of the chapter.

4.2 Description of the Physical Activity Intervention and the System Identification Problem

The main purpose of the intervention is to promote physical activity, e.g., walking/running, among inactive adults age 21 years and older, with a specific goal of reaching 10,000 steps per day on average per week. Social Cognitive Theory (SCT; Bandura (1986)) can be used to represent this problem. SCT is an extensively used conceptual and theoretical framework for behavioral interventions, including physical activity (Bandura, 1998).

4.2.1 Simplified SCT Model

In Chapter 2, a dynamical interpretation of SCT was developed, based on a fluid analogy that describes the interrelationships among psychosocial variables. SCT describes a human agency perspective of *behavior* (η_4) in which individuals proactively self-reflect, self-regulate, and self-organize (Bandura, 1989). The intervention is focused on one of the internal loops within the SCT model, that represents a "behaviorist" articulation of the determinants of behavior (Ferster, 1970; Baum, 2011). This is depicted in Fig. 4.1, through a simplified version of the SCT model where coefficients ξ_i represent the main inputs, η_i are the outputs, γ_{ij} and β_{ij} represent the interrelation among the different constructs, ζ_i are external disturbances, and θ_i are delay times.

For the simplified version of the SCT model, applied to the physical activity problem, the most important constructs include *behavior* (η_4) that is the action of interest (e.g., amount of performed daily steps), *outcome expectancy* (η_2) that is the perceived likelihood that performing a given behavior will result in certain *behavioral outcomes* (η_5) (e.g., weight reduction); these outcomes are greatly influenced by the *environ-*

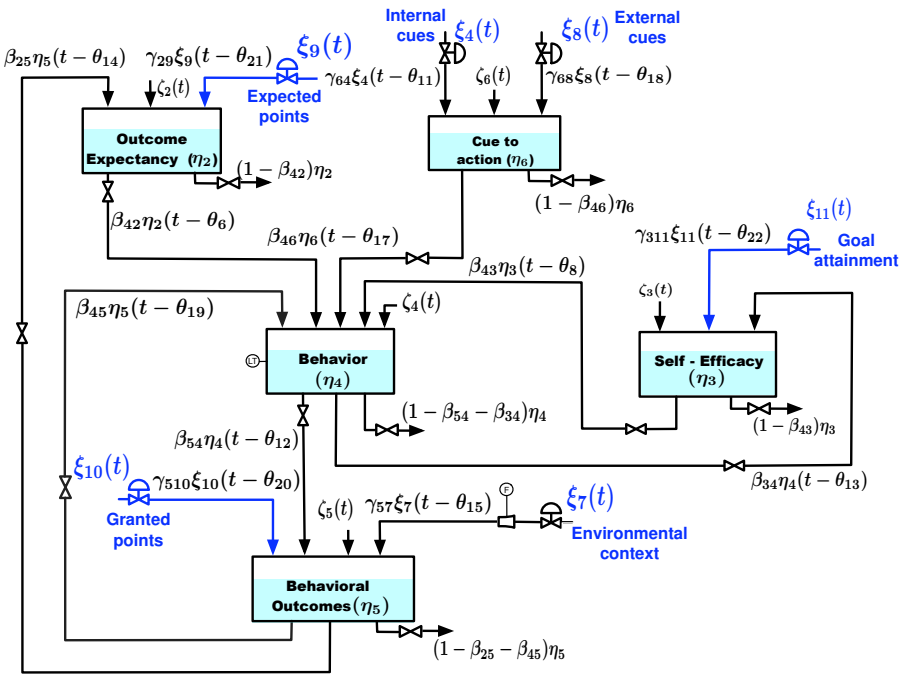

Figure 4.1: Fluid Analogy for a Simplified Version of the SCT Model Developed in Chapter 2.

mental context (ξ_7) in which the behavior occurs (e.g., weather). Outcome expectancy is often conceptualized as a predisposition for engaging in any given behavior that is triggered by a *cue to action* (η_6) that can be internal (ξ_4) or external (ξ_8) (e.g daily goal-setting). For the proposed intervention, three additional inputs are included:

- *Outcome expectancy (OE) for reinforcement* (ξ_9) (i.e., expected daily reward points).

- *Reinforcement* (ξ_{10}) (i.e., received daily reward points resulting from a successful behavior).

- *Goal attainment* (ξ_{11}) computed as the difference between the daily goal and the actual performed behavior, affecting *self-efficacy*. This signal is used to represent the ideal step-goal range feature described in Section 2.7.2, where

individuals might react negatively to too high a goal that they consider difficult to reach.

Based on the described analogy and assuming first-order dynamics for each inventory, the following equations for the simplified SCT model are developed:

$$\tau_2 \frac{d\eta_2}{dt} = \gamma_{29}\xi_9(t-\theta_{21}) + \beta_{25}\eta_5(t-\theta_{14}) - \eta_2(t) + \zeta_2(t) \tag{4.1}$$

$$\tau_3 \frac{d\eta_3}{dt} = \gamma_{311}\xi_{11}(t-\theta_{22}) + \beta_{34}\eta_4(t-\theta_{13}) - \eta_3(t) + \zeta_3(t) \tag{4.2}$$

$$\begin{aligned}\tau_4 \frac{d\eta_4}{dt} =& \beta_{42}\eta_2(t-\theta_6) + \beta_{43}\eta_3(t-\theta_8) + \beta_{46}\eta_6(t-\theta_{17}) + \beta_{45}\eta_5(t-\theta_{19}) \\ & - \eta_4(t) + \zeta_4(t)\end{aligned} \tag{4.3}$$

$$\tau_5 \frac{d\eta_5}{dt} = \gamma_{57}\xi_7(t-\theta_{15}) + \gamma_{510}\xi_{10}(t-\theta_{20}) + \beta_{54}\eta_4(t-\theta_{12}) - \eta_5(t) + \zeta_5(t) \tag{4.4}$$

$$\tau_6 \frac{d\eta_6}{dt} = \gamma_{64}\xi_4(t-\theta_{11}) + \gamma_{68}\xi_8(t-\theta_{18}) - \eta_6(t) + \zeta_6(t) \tag{4.5}$$

As was described in Chapter 2, it is possible (based on data or prior knowledge) to use higher-order differential equations to describe the behavior, or to add nonlinear features (such as habituation).

IAI components can be delivered by decision algorithms (i.e., controllers) to influence behavior and, consequently, the other SCT constructs. The goal in this chapter is to formulate an intervention that can be designed beforehand in an open-loop setting for identification purposes.

4.2.2 Intervention Components

In order to design effective intervention controllers, a "sufficiently good"/adequate plant model is required. Since the main hypothesis of this work is that physical activity interventions can be represented through SCT, the use of a dynamical model per Section 4.2 as *a priori* structural information is assumed. Fig. 4.2 depicts the interaction of the open-loop intervention over the simplified SCT model through the

following components:

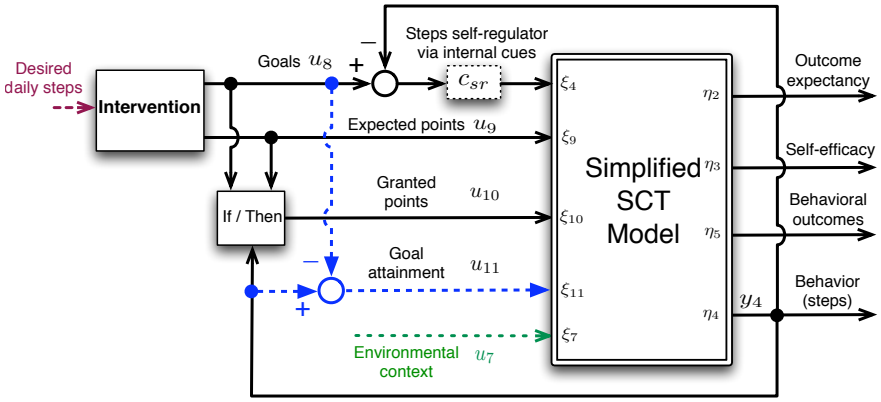

Figure 4.2: Conceptual Diagram for the Proposed Intervention to Influence Behavior and Other Constructs Represented by the Simplified SCT Model. Input/output Symbols ξ_i and η_i are Used for Modeling and Simulation, While u_i and y_i are Used for Formulations of the Informative and Optimized Experiments.

- *Daily goals* (u_8), to establish the desired amount of daily steps (e.g., 10,000).
- *Expected points* (u_9), as an outcome expectancy for reinforcement (ξ_9) that lets the participant know the daily expected reward points.
- *Granted points* (u_{10}), as a reinforcement (ξ_{10}) through an "If/Then" block that delivers the announced expected points ($u_{10} = u_9$) only if the performed steps (y_4) are greater or equal than the specified goal (u_8).

The intervention is implemented using an SCT model enhanced with individualized self-regulation via internalized cues. In the work of Carver and Scheier (1998) self-regulation mechanisms for human behavior are expressed as feedback control systems, where individuals take self-corrective adjustments to stay on track for a defined goal. To represent self-regulation process we rely on a controller that makes adjustments to *internal cues* (ξ_4) based on the discrepancies between the set goal (u_8) and

the measured outcome (y_4). The controller must allow for a partial level of setpoint tracking that allows the rest of the intervention components (e.g., points) to also influence for changes in the output. Internal model control (IMC; Morari and Zafiriou (1989)) is used to formulate a self-regulator via internalized cues relying on the transfer function p_{44} from input ξ_4 to output η_4 computed from the SCT model. Fig. 4.3 is the block diagram representing the IMC design structure, where p_{44} is the plant, $\tilde{p}_{44}$ is the nominal model, d is an external disturbance, p_d is the disturbance model, and q_{sr} is the self-regulator (expressed in q-parametrization form).

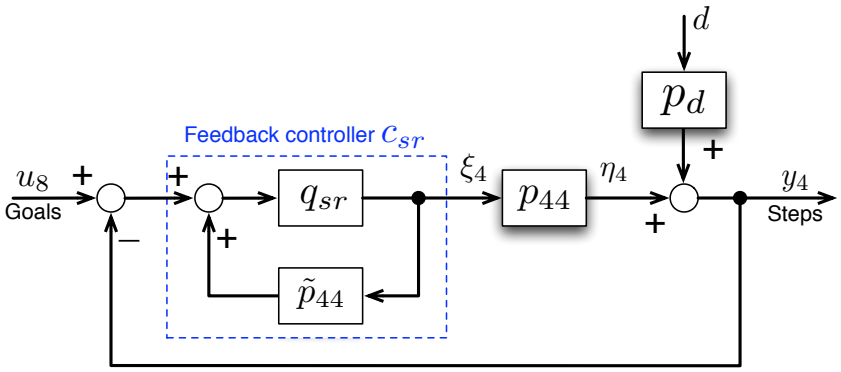

Figure 4.3: Block Diagram Representing the IMC Design Structure for the Self-Regulator Via Internalized Cues.

The closed-loop relationships between variables in Fig. 4.3 are given by

$$y_4 = \frac{p_{44}q_{sr}}{1+(p_{44}-\tilde{p}_{44})q_{sr}}u_8 + \frac{(1-\tilde{p}_{44}q_{sr})p_d}{1+(p_{44}-\tilde{p}_{44})q_{sr}}d \tag{4.6}$$

$$\xi_4 = \frac{q_{sr}}{1+(p_{44}-\tilde{p}_{44})q_{sr}}u_8 - \frac{p_d q_{sr}}{1+(p_{44}-\tilde{p}_{44})q_{sr}}d \tag{4.7}$$

In the absence of plant-model mismatch ($p_{44} = \tilde{p}_{44}$) these reduce to

$$y_4 = p_{44}q_{sr}u_8 + (1-\tilde{p}_{44}q_{sr})p_d d \tag{4.8}$$

$$\xi_4 = q_{sr}u_8 - p_d q_{sr} d \tag{4.9}$$

Assuming that the dominant effect on the output is obtained from the time constant of the behavior inventory (τ_4), the nominal model is considered as

$$\tilde{p}_{44} = \frac{\beta_{46}\gamma_{64}}{\tau_4 s + 1} \approx \frac{\eta_4}{\xi_4} \tag{4.10}$$

It is desirable to have a controller that makes the process output follow its setpoint and reject all disturbances. According to the IMC formulation, the self-regulator is defined as

$$q_{sr} = \tilde{p}_{44}^{-1} f_{sr} = \tilde{p}_{44}^{-1} \frac{K_{sr}}{\lambda s + 1} \tag{4.11}$$

where a Type I filter f_{sr} is used to ensure properness of the final control system. The representation of the self-regulator as a classical feedback controller is

$$c_{sr} = \frac{q_{sr}}{1 - \tilde{p}_{44} q_{sr}} = \frac{K_{sr}}{\beta_{46}\gamma_{64}} \frac{\tau_4 s + 1}{\lambda s + 1 - K_{sr}} \tag{4.12}$$

The performance of the self-regulator is characterized by the value of the parameter λ that reflects the closed-loop speed of response, and the parameter K_{sr} that ranges from 0 to 1, with 1 representing perfect integral action.

The proposed intervention considers only variables that are potentially measurable in a preliminary study, hence *internal cues* (ξ_4), *outcome expectancy* (η_2), and *cue to action* (η_6) are not considered. Based on previous experimental studies using smartphones (King *et al.*, 2013; Adams *et al.*, 2013), measurements will be taken daily. The basic choice of inputs and outputs for identification corresponds to those that will be used by the intervention as was depicted in Fig. 4.2. The inputs (e.g., goals, reward points) should be delivered to the participant through the smartphone and the outputs will also be collected in the phone (e.g., steps via the internal pedometer).

Proper measurement is crucial for success of the identification procedure, and the following steps must be followed to guarantee reliability of the information: observational studies, equipment selection, software development, prototyping, test design,

among others. In behavioral health, this activity falls under the topic of *ecological momentary assessment* (Shiffman *et al.*, 2008).

4.2.3 Grey-Box Parameter Estimation

Parameter estimation is done through semi-physical modeling, a technique that takes into account physical insight about the system (Lindskog and Ljung, 1995). In this sense a grey-box parameter estimation procedure (Ljung, 1999) should be applied, where input-output data from an experiment under real-life circumstances must be collected. Grey-box parameter estimation relies on two sources of information to estimate the required model: prior knowledge of the system (in this case the SCT dynamical model), and experimental data (Lindskog and Ljung, 1995; Bohlin, 1994). This technique allows the use of a specific state space structure, where the value of a set of unknown model parameters must be estimated.

To find a state space representation of the system for identification purposes, differential Equations (4.1) - (4.5) are used together with the representation of the self-regulator c_{sr} that adds a new state referred as η_7. Considering only signals from Fig. 4.2 with no disturbances or delays ($\zeta_i = 0$, $\theta_i = 0$, $\forall i$), the following structure is obtained:

$$\begin{aligned} \dot{\boldsymbol{x}}_{\boldsymbol{p}}(t) &= \boldsymbol{A}(\boldsymbol{\theta_p})\boldsymbol{x_p}(t) + \boldsymbol{B}(\boldsymbol{\theta_p})\boldsymbol{u_p}(t) + \boldsymbol{K}\boldsymbol{e}(t) \\ \boldsymbol{y_p}(t) &= \boldsymbol{C}\boldsymbol{x_p}(t) + \boldsymbol{v}(t) \end{aligned} \tag{4.13}$$

where $\boldsymbol{e}$ and $\boldsymbol{v}$ are uncertainties, $\boldsymbol{x_p}$ is the state vector, $\boldsymbol{u_p}$ the input vector, $\boldsymbol{y_p}$ the output vector and $\boldsymbol{\theta_p}$ is a vector of the unknown model parameters defined as

$$\boldsymbol{x_p} = [\eta_2 \quad \eta_3 \quad \eta_4 \quad \eta_5 \quad \eta_6 \quad \eta_7]^\top \tag{4.14}$$

$$\boldsymbol{u_p} = [u_7 \quad u_8 \quad u_9 \quad u_{10}]^\top \tag{4.15}$$

$$\boldsymbol{y_p} = [y_2 \quad y_3 \quad y_4 \quad y_5]^\top \tag{4.16}$$

$$\boldsymbol{\theta_p} = [\tau_2 \quad \tau_3 \quad \tau_4 \quad \tau_5 \quad \tau_6 \quad \beta_{25} \quad \beta_{34} \quad \beta_{42} \quad \beta_{43} \quad \beta_{45} \quad \beta_{46} \quad \beta_{54}$$
$$\gamma_{57} \quad \gamma_{64} \quad \gamma_{29} \quad \gamma_{510} \quad \gamma_{311} \quad K_{sr} \quad \lambda]^\top \tag{4.17}$$

Considering that the *goal attainment* signal can be represented within the state space representation via $u_{11} = y_4 - u_8$, the state-space system matrices are

$$\boldsymbol{A}(\boldsymbol{\theta_p}) = \begin{pmatrix} -\frac{1}{\tau_2} & 0 & 0 & \frac{\beta_{25}}{\tau_2} & 0 & 0 \\ 0 & -\frac{1}{\tau_3} & \frac{\beta_{34}+\gamma_{311}}{\tau_3} & 0 & 0 & 0 \\ \frac{\beta_{42}}{\tau_4} & \frac{\beta_{43}}{\tau_4} & -\frac{1}{\tau_4} & \frac{\beta_{45}}{\tau_4} & \frac{\beta_{46}}{\tau_4} & 0 \\ 0 & 0 & \frac{\beta_{54}}{\tau_5} & -\frac{1}{\tau_5} & 0 & 0 \\ 0 & 0 & -\frac{\gamma_{64} M_{sr} \tau_4}{\tau_6} & 0 & -\frac{1}{\tau_6} & \frac{\gamma_{64} M_{sr}(1-N_{sr}\tau_4)}{\tau_6} \\ 0 & 0 & -1 & 0 & 0 & -N_{sr} \end{pmatrix} \tag{4.18}$$

$$\boldsymbol{B}(\boldsymbol{\theta_p}) = \begin{pmatrix} 0 & 0 & \frac{\gamma_{29}}{\tau_2} & 0 \\ 0 & -\frac{\gamma_{311}}{\tau_3} & 0 & 0 \\ 0 & 0 & 0 & 0 \\ \frac{\gamma_{57}}{\tau_5} & 0 & 0 & \frac{\gamma_{510}}{\tau_5} \\ 0 & \frac{\gamma_{64} M_{sr} \tau_4}{\tau_6} & 0 & 0 \\ 0 & 1 & 0 & 0 \end{pmatrix} \tag{4.19}$$

$$\boldsymbol{C} = \begin{pmatrix} 1 & 0 & 0 & 0 & 0 & 0 \\ 0 & 1 & 0 & 0 & 0 & 0 \\ 0 & 0 & 1 & 0 & 0 & 0 \\ 0 & 0 & 0 & 1 & 0 & 0 \end{pmatrix} \tag{4.20}$$

$$\text{with} \quad M_{sr} = \frac{K_{sr}}{\gamma_{64}\beta_{46}\lambda}, \quad \text{and} \quad N_{sr} = \frac{1 - K_{sr}}{\lambda}.$$

The actual dimensions of the $\boldsymbol{C}$ matrix depend on the available measurement outputs. To estimate $\boldsymbol{\theta_p}$ the well-known prediction-error identification methods (PEM; Ljung

(1999)) will be used. The one-step ahead prediction error of the system is

$$\boldsymbol{\varepsilon}(t, \boldsymbol{\theta_p}) = \boldsymbol{y_p}(t) - \hat{\boldsymbol{y}}_{\boldsymbol{p}}(t|t-1, \boldsymbol{\theta_p}) \tag{4.21}$$

where $\hat{\boldsymbol{y}}_{\boldsymbol{p}}(t|t-1, \boldsymbol{\theta_p})$ is the predicted output based on estimated models.

4.2.4 General Design Constraints

In the ensuing formulations, $N \in \mathbb{N}$ will be referred as the number of measurements in days and signals $\boldsymbol{u_n} \in \mathbb{R}^N$ and $\boldsymbol{y_m} \in \mathbb{R}^N$ as vectors containing the design inputs and outputs respectively, where n and m are the considered input and output indexes.

For input signal design, only a subset of the inputs and outputs used for subsequent parameter estimation will be considered. The design inputs are *goal-setting* (u_8) and *expected points* ($\xi_9 = u_9$), *Environmental context* (ξ_7) will not be used because it is an external variable that, while measurable, cannot be manipulated by the user. The input design procedure must consider the presence of an "If/Then" decision block as was depicted in Fig. 4.2, which delivers daily points (i.e., makes $\xi_{10} = u_{10} = u_9$) only if the actual behavior ($y_4 = \eta_4$) meets or exceeds the daily goal (u_8). For the optimized experiment, the main interest is to shape the participant's "behavior" ($y_4 = \eta_4$). Therefore, it will be the only output considered in this formulation, however other outputs are also considered for identification purposes.

Input design must be implemented under strict clinical constraints (also called "patient friendly"). Therefore, the following general constraints must be considered:

1. Bounds must be imposed on the magnitude of the intervention components

$$u_n^{min}(k) \leq u_n(k) \leq u_n^{max}(k), \quad k = 1, \ldots, N \tag{4.22}$$

where $\boldsymbol{u_n^{min}}$,$\boldsymbol{u_n^{max}} \in \mathbb{R}^N$ are vectors containing the minimum and maximum allowed daily value for each input, where in absence of any additional constraint

$$u_n^{min}(k) = Z_n^{min}, \quad k = 1, \ldots, N \tag{4.23}$$

$$u_n^{max}(k) = Z_n^{max}, \quad k = 1, \ldots, N \tag{4.24}$$

2. The inputs are constrained to have a maximum move size MS_n that may depend on the type of intervention

$$\Delta u_n(k) = \big|u_n(k) - u_n(k-1)\big|, \quad k = 2, \ldots, N \tag{4.25}$$

$$\Delta u_n(k) \leq MS_n, \quad k = 2, \ldots, N \tag{4.26}$$

3. A minimum switching time $T_{sw} \in \mathbb{N}$ can also be imposed to the system to avoid excessive changes in the intervention components

$$\begin{gathered} u_n(k) - u_n(k+j) = 0, \quad j = 1, \ldots, T_{sw} - 1 \\ \forall k = 1 + l.T_{sw}, \quad l = 0, 1, ... \\ k + T_{sw} - 1 \leq N \end{gathered} \tag{4.27}$$

4. In addition, any input $\boldsymbol{u_n}$ can be constrained for a late start at day D_n as

$$u_n(k) = 0, \qquad k = 1, \ldots, D_n - 1 \tag{4.28}$$

4.3 Informative Experimental Design

The primary goal of the informative experiment is to gain insights about the basic dynamics of the system. Two different approaches are tested: first an input signal design using a randomized signal generation strategy, and a design using deterministic multisine input signals aimed to the application of identification test monitoring ideas presented in Chapter 3.

4.3.1 Randomized Signal Generation

Since little is currently known *a priori* regarding the dynamical system properties of a physical activity IAI, an initial approach would be to use constrained yet

standard input signals (i.e., random, RBS, PRBS, multisine) with sufficient excitation. However, this could cause undesired variations on the participant's behavior. Therefore, an initial judicious experiment will be developed; the proposed inputs will rely on an *a priori* study (King *et al.*, 2013; Adams *et al.*, 2013), designed to produce data according to an expected profile, combined with the mentioned standard input signals that will facilitate capturing the dynamical relationships among variables. The input signals to be designed are *goal-setting* (u_8) and *available points* (u_9), the signal *granted points* (u_{10}) will be internally generated by the "if/then" block, as was described in Fig. 4.2.

Assuming that the individual starts the experiment with an average value of daily steps called baseline (B_s), the vector *goal-setting* ($\boldsymbol{u_8}$), will take samples from a discrete uniform distribution, that represents an increment of 0%, 20%, 40%, 60%, 80% or 100% of B_s, such that

$$W = \{w_1, \ldots, w_6\} = \{B_s, 1.2B_s, 1.4B_s, 1.6B_s, 1.8B_s, 2B_s\} \tag{4.29}$$

$$P(u_8(k) = w_i) = \frac{1}{6}, \quad , \forall w_i \in W, \quad k = 1, \ldots, N \tag{4.30}$$

where $P(\cdot)$ represents an event probability. The vector *available points* ($\boldsymbol{u_9}$) will take a set of random uniform values from 100, 300 or 500 such that

$$Z = \{z_1, z_2, z_3\} = \{100, 300, 500\} \tag{4.31}$$

$$P(u_9(k) = z_i) = \frac{1}{3}, \quad , \forall z_i \in Z, \quad k = 1, \ldots, N \tag{4.32}$$

The inputs must comply with the constraints described by Equations (4.22) - (4.28). The randomization of the variables supports the orthogonal delivery of information required by the identification technique. Having specified these input signals, the informative experiment must be executed. The collected input-output data will be used in the grey-box parameter estimation procedure described in Section 4.2.3. As a

result, an initial *informative model* with all the parameter values defined, is obtained which represents a preliminary version of the system's model, and forms the basis for subsequent optimization.

4.3.2 Multisine Signal Generation

A second approach for the design of the informative experiment will attempt to obtain input signals with the shortest possible duration, and at the same time with sufficient information for identification purposes. As was described in Chapter 3, this process relies on uncertainty bounds computations based on transfer function estimates. It is important to highlight that semi-physical methods (i.e., grey box) will be still used to identify the SCT model parameters; transfer function estimates will be used only for uncertainty computations to determine the effect of noise over the estimation process.

The proposed uncertainty bounds will be calculated using frequency domain methods, and multisinusoidal signals will be employed. The design procedure was completely described in Chapter 3, some details are repeated here for clarity. Two of the presented approaches are adapted for the physical activity intervention: the basic identification test monitoring method using ETFE, and the enhanced method using the transient LPM for transfer function computations.

4.3.2.1 Basic Identification Test Monitoring Method

This approach relies on uncertainty computations from transfer function estimates obtained using the Empirical Transfer Function Estimate (ETFE) method and multisinusoidal signals with a "zippered" frequency spectrum. Multisine inputs are deterministic, periodic signals whose spectrum can be directly specified by the designer.

The input u_n $(n = 8, 9)$ can be described as

$$u_n(k) = \lambda_n \sum_{j=1}^{N_s/2} \sqrt{2\alpha_{[n,j]}} \cos(\omega_j k T_s + \phi_{[n,j]})$$
$$\omega_j = \tfrac{2\pi j}{N_s T_s}, \quad k = 1, \ldots, N_s \tag{4.33}$$

where λ_n is the scaling factor, N_s is the period, T_s is the sampling time. For each harmonic: $\alpha_{[n,j]}$ is a factor used to specify the relative power of the harmonic, ω_j is the frequency, and $\phi_{[n,j]}$ is the phase. Coefficients λ_n are chosen based on the input constraints described in (4.22).

Factors $\alpha_{[n,j]}$ are chosen to obtain input signals that are excited orthogonally in frequency. If n_u is the number of design inputs ($n_u = 2$ for this case), and n_s is the total amount of independently excited sinusoids, then the total number of harmonics is n_s and the "zippered" spectrum for each signal u_n can be constructed by specifying

$$\alpha_{[n,j]} = \begin{cases} 1 & \text{if } j = n_u(i-1) + (n-7), \quad \text{for } i = 1, 2, \ldots n_s \\ 0 & \text{otherwise} \end{cases} \tag{4.34}$$

The resulting bound for N_s is

$$N_s \geq 2n_s \tag{4.35}$$

The input signals will be repeated for M cycles such that the total duration of the experiment is N_s M days. The period N_s represents the decision time window for the monitoring process that is expected to be as short as possible; therefore, the bound defined in (4.35) can be used to estimate N_s assuming an initial guess for n_s. If *a priori* information is available about the system dynamics, it can be used to refine the estimates of n_s and N_s as was described in Section 3.2.1. Phases ϕ will be selected to minimize the crest factor of the signal using the approach proposed by Guillaume *et al.* (1991).

Transfer Function and Uncertainty Estimation

The proposed estimation procedure considers a multivariable system subject to output noise, where the effect of each independent transfer function is given by

$$y^*(k) = P^*(q)u^*(k) + v^*(k) \tag{4.36}$$

where $u^*(k)$ and $y^*(k)$ are any given pair of inputs and outputs, $P^*(q)$ is the respective sampled-data transfer function, and $v^*(k)$ is the output noise.

Uncertainty bounds are calculated from an averaged Empirical Transfer Function Estimate (ETFE). In the work of Bayard (1993), a statistical uncertainty computation is developed; however it requires *a priori* knowledge of the noise structure which can be difficult to obtain in behavioral settings. The uncertainty computation used in this work (Pintelon and Schoukens, 2012) does not require prior knowledge of the noise structure. The price to be paid for this flexibility is that the uncertainty bounds are only valid asymptotically. The conditions for the existence of the averaged ETFE and the proposed uncertainty bounds are:

- Each true plant $P^*(q)$ is exponentially stable, linear and time invariant.
- Disturbance $v^*(k)$ can be written as filtered white noise with finite order moments, and is independent from the input $u^*(k)$ and the output $y^*(k)$.

To obtain the ETFEs it is necessary to represent the individual transfer functions for the identification problem described in section 4.2.2. Fig. 4.4 represents an equivalent block diagram for the behavioral intervention based on the simplified SCT model and the proposed self-regulation block considering the design inputs u_8, u_9, and assuming that the only measured outputs are y_4 and y_5. Transfer functions from each input n to each output m are represented by $P_{[m,n]}(q)$.

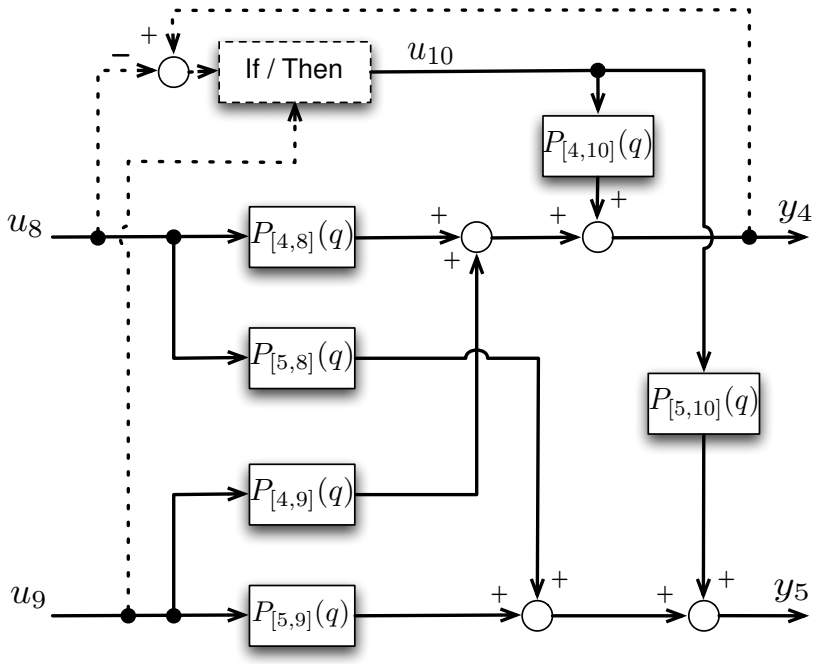

Figure 4.4: Block Diagram for the Physical Activity Behavioral Intervention Based on the Simplified SCT Model, Using Independent Transfer Functions for Each Input/output Element.

The two independent inputs are u_8 and u_9; u_{10} is generated within the "If/Then" block as is illustrated in Fig. 4.5. The outputs with available measurements are y_4 and y_5.

Since u_8 and u_9 are designed orthogonally in frequency, it becomes possible to find independent estimates of each directional transfer function. One of the conditions for uniqueness in the ETFE is to have a linear time invariant model such that periodic inputs result in periodic outputs; for the behavioral problem this condition is generally accomplished by the SCT model but is violated by the nonlinearity associated with the "If/Then" block. The outputs, however, are still periodic and therefore transfer functions can still be estimated, but these will be valid only for a given input realization.

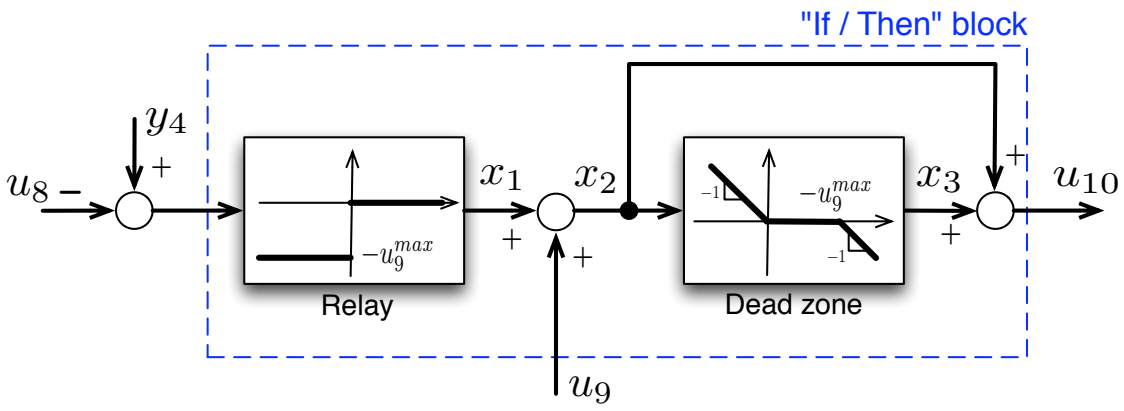

Figure 4.5: Representation of the "If/Then" Block, Using Relay-Type and Dead-Zone Nonlinearities.

In this work semi-physical identification will be used to obtain the model parameters, hence transfer functions are computed only as means to estimate uncertainties, which computation is based mostly in the variability due to the output noise $v^*(k)$ and not in the transfer function dependent term $P^*(q)u^*(k)$ resulting in adequate uncertainty bounds as was demonstrated in Section 3.2.2.4. The periodicity of the outputs can be verified from Fig. 4.5: y_4 can be assumed periodic, then the input to the relay $(y_4 - u_8)$ is periodic and the signal x_1 is also periodic; by the same analysis x_2, x_3 and u_{10} are also periodic and considering the linearity of the SCT model, y_5 and y_4 are confirmed to be periodic.

Consider that M periods of input/output data $u_n(k)$, $y_m(k)$ are collected and denoting the output data from the lth period as

$$\begin{aligned} y_m^l(k) &= y_m(k + (l-1)N_s) \\ k &= 1 \ldots N_s, \quad l = 1 \ldots M \end{aligned} \tag{4.37}$$

The output noise setting described in (4.36) can be represented by

$$y_m(k) = G_{[m,n]}(q)u_n(k) + v_m(k) \tag{4.38}$$

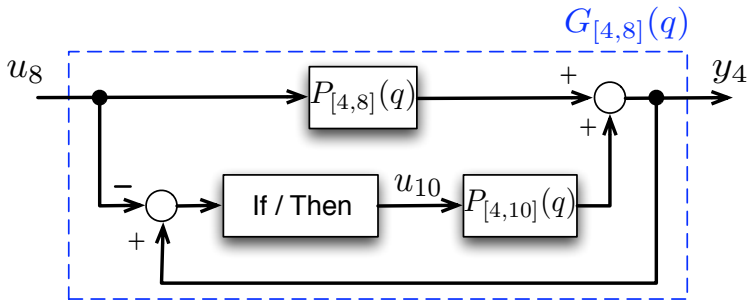

Figure 4.6: Block Diagram for the Transfer Function $G_{[4,8]}(q)$ From u_8 to y_4 Neglecting the Effect of u_9.

where $v_m(k)$ is the output disturbance noise, $n = 8, 9$ $m = 4, 5$, and each $G_{[m,n]}(q)$ is the total SISO equivalent transfer function from input n to output m including the "If/Then" block as is illustrated in Fig. 4.6 for the transfer function $G_{[4,8]}(q)$.

The averaged ETFE is computed as

$$\hat{G}_{[m,n]}(\omega_i^n) = \frac{\bar{Y}_m(\omega_i^n)}{U_n(\omega_i^n)} \tag{4.39}$$

$$\text{with} \quad \bar{Y}_m(\omega_i^n) = \frac{1}{M}\sum_{l=1}^{M} Y_m^l(\omega_i^n) \tag{4.40}$$

where $\omega_i^n \in \boldsymbol{W^n}$, and $\boldsymbol{W^n}$ is the frequency grid defined by the zippered design for input n as a subset of the complete frequency grid, specified by

$$\boldsymbol{W^n} = \{\omega_i^n \in \mathbb{R} \mid \omega_i^n = \tfrac{2\pi[n_u(i-1)+(n-7)]}{N_s T_s}, \quad i = 1, 2, \ldots, n_s\} \tag{4.41}$$

$U_n(\omega_j)$ and $Y_m^l(\omega_j)$ are the DFTs for one period of the input u_n and the l^{th} period of the output y_m^l, respectively.

The following expressions refer to the frequency grid for ω_i^n defined in (4.41). Under the specified conditions it can be shown (Bayard, 1993; Pintelon and Schoukens, 2012) that

$$\frac{|\hat{G}_{[m,n]}(\omega_i^n) - G_{[m,n]}(\omega_i^n)|^2}{\hat{\sigma}^2_{\hat{G}_{[m,n]}}(\omega_i^n)} \sim F(2, 2M-2) \tag{4.42}$$

where $F(\nu_1, \nu_2)$ denotes a Fisher distribution with ν_1 and ν_2 degrees of freedom, and $\hat{\sigma}^2_{\hat{G}_{[m,n]}}(\omega_i^n)$ is the sample variance of the averaged ETFE approximated by

$$\hat{\sigma}^2_{\hat{G}_{[m,n]}}(\omega_i^n) = \frac{1}{M(M-1)} \frac{\sum_{l=1}^{M} |\bar{Y}_m(\omega_i^n) - Y_m^l(\omega_i^n)|^2}{|U_n(\omega_i^n)|^2} \tag{4.43}$$

the additional division by M is due to the averaging effect in the estimation (Pintelon and Schoukens, 2012). The $100 \times (1-\rho)\%$ confidence region can be constructed as a circle with center $\hat{G}_{[m,n]}(\omega_i^n)$ and radius $\ell^{1-\rho}_{a[m,n]}(\omega_i^n, M)$ where

$$\left[\ell^{1-\rho}_{a[m,n]}(\omega_i^n, M)\right]^2 = \hat{\sigma}^2_{\hat{G}_{[m,n]}}(\omega_i^n) F_{1-\rho}(2, 2M-2) \tag{4.44}$$

$F_{1-\rho}(2, 2M-2)$ is the $100 \times (1-\rho)\%$ percentile of an $F(2, 2M-2)$-distributed random variable such that

$$Prob\Big\{ \big|\hat{G}_{[m,n]}(\omega_i^n) - G_{[m,n]}(\omega_i^n)\big| \leq \ell^{1-\rho}_{a[m,n]}(\omega_i^n, M) \Big\} = 1 - \rho \tag{4.45}$$

These estimated uncertainty bounds are asymptotic for M; for low values of M can be considered as conservative estimates.

Monitoring procedure

The goal is to find the shortest experiment that is sufficiently informative based on the estimated uncertainties. The monitoring procedure described in Section 3.2.3 is performed by incrementing the number of periods M one at a time, starting from $M = 2$ (because of averaged ETFE), such that with each increment on M the total duration of the experiment will be N_s days longer. For each input-output direction a maximum additive uncertainty is computed over the frequency grid for ω_i^n defined in (4.41)

$$\tilde{\ell}_{a[m,n]}(M) = \max_{\omega_i^n \in \boldsymbol{W^n}} \left(\ell^{1-\rho}_{a[m,n]}(\omega_i^n, M)\right), M = 2, 3 \ldots \tag{4.46}$$

Percentage reduction in $\tilde{\ell}_{a[m,n]}(M)$ among consecutive values of M is calculated as:

$$AV_{[m,n]}(M) = \frac{\tilde{\ell}_{a[m,n]}(M-1) - \tilde{\ell}_{a[m,n]}(M)}{\tilde{\ell}_{a[m,n]}(2)} \times 100 \tag{4.47}$$

$$RV_{[m,n]}(M) = \frac{\tilde{\ell}_{a[m,n]}(M-1) - \tilde{\ell}_{a[m,n]}(M)}{\tilde{\ell}_{a[m,n]}(M-1)} \times 100 \tag{4.48}$$

$$M = 3, 4 \ldots$$

where $AV_{[m,n]}$ is the absolute percentage reduction referred to the first estimation, and $RV_{[m,n]}$ is the relative percentage reduction referred to the previous value of M.

Depending on the type of intervention the set of all the input-output directions of interest is

$$\boldsymbol{O} = \{(m,n) \mid \text{ effect from input } n \text{ to output } m \text{ is of interest}\} \tag{4.49}$$

The maximum percentages of uncertainty reduction are

$$AV(M) = \max_{(m,n)\in\boldsymbol{O}} AV_{[m,n]}(M), \quad M = 3, 4 \ldots \tag{4.50}$$

$$RV(M) = \max_{(m,n)\in\boldsymbol{O}} RV_{[m,n]}(M), \quad M = 3, 4 \ldots \tag{4.51}$$

The stopping criterion will determine when the uncertainties have reached predefined bounds in the last n_{Mi} consecutive iterations, and therefore the experiment can be stopped. If B_{AV} and B_{RV} are defined as the maximum allowed percentages of reduction, then the stopping criterion can be posed as

$$\begin{gathered} \text{Stop at } M = Q - 1 \text{ when} \\ AV(Q-r) \leq B_{AV} \quad \text{and} \quad RV(Q-r) \leq B_{RV} \\ \text{for } r = 1, \ldots, n_{Mi} \text{ consecutive iterations} \end{gathered} \tag{4.52}$$

Lower values of B_{AV} and B_{RV}, or a higher n_{Mi}, will result in more accurate but longer experiments.

A more general but conservative MIMO approach can also be specified. Model uncertainty constituting the maximum singular value at each frequency grid point with probability $1-\kappa$ can be characterized by

$$Prob\Big\{\overline{\sigma}\big(\hat{\boldsymbol{G}}(\omega_i^n)-\boldsymbol{G}(\omega_i^n)\big)\leq\epsilon^{1-\kappa}(\omega_i^n)\Big\}=1-\kappa \tag{4.53}$$

By using the Frobenious norm, the bounds can be computed as

$$\overline{\sigma}\big(\hat{\boldsymbol{G}}(\omega_i^n)-\boldsymbol{G}(\omega_i^n)\big)^2\leq\sum_{n=1}^{n_u}\sum_{m=1}^{n_y}\big[\ell_{a[m,n]}^{1-\rho}(\omega_i^n,M)\big]^2\triangleq\big[\epsilon^{1-\kappa}(\omega_i^n,M)\big]^2 \tag{4.54}$$

that holds with probability

$$1-\kappa=(1-\rho)^{n_y\cdot n_u} \tag{4.55}$$

From here a maximum additive uncertainty for the MIMO case is computed as

$$\tilde{\epsilon}(M)=\max_{\omega_i^n\in\boldsymbol{W^n}}\big[\epsilon^{1-\kappa}(\omega_i^n,M)\big],\quad M=2,3\ldots \tag{4.56}$$

Percentages of uncertainty reduction are redefined as

$$AV(M)=\frac{\tilde{\epsilon}(M-1)-\tilde{\epsilon}(M)}{\tilde{\epsilon}(2)}\times 100 \tag{4.57}$$

$$RV(M)=\frac{\tilde{\epsilon}(M-1)-\tilde{\epsilon}(M)}{\tilde{\epsilon}(M-1)}\times 100 \tag{4.58}$$

Based on these definitions, the stopping criteria presented in (4.52) can still be used.

4.3.2.2 Enhanced Identification Test Monitoring Method

The main idea of the enhanced formulation for the identification test monitoring procedure is to incorporate on-the-go modifications of the input signal content to improve the performance of the identification process. The allowed modifications are in the amplitude and harmonic frequency content of the input signals. This is possible through the application of the Local Polynomial Method (LPM) to estimate

frequency domain transfer functions and uncertainties taking into account the natural transient effect of the system.

To accommodate the proposed modifications, each of the $n_u = 2$ different input signals is constructed as sequence of multi-sinusoids where the amplitude, number of periods, and the fundamental frequency may differ for each signal in the sequence. L is the number of signals in the sequence. One period of the l^{th} signal in the sequence for the input u_n $(n = 8, 9)$ can be represented for $k = 1, \cdots, N_s$ as

$$\begin{aligned} u_{n,l}(k) &= \lambda_{n,l} \sum_{j=1}^{N_s/2} \sqrt{2\alpha_{n,l,j}} \cos(\omega_j k T_s + \phi_{n,l,j}) \\ \omega_j &= \frac{2\pi j}{N_s T_s}, \quad l = 1, \cdots, L \end{aligned} \tag{4.59}$$

where $\lambda_{n,l}$ is the amplitude scaling factor for each signal, T_s is the sampling period, N_s is the number of samples in one period, $\alpha_{n,l,j}$ is a factor used to specify the relative power at the frequency ω_j, and $\phi_{n,l,j}$ is the phase for each harmonic. Additionally n_s is the total number of sinusoids excited considering all the inputs with $n_s \leq N_s/2$, and M_l is the number of periods in the l^{th} signal. For the experimental design focused on the monitoring process, it is assumed that the first signal in the sequence $(l = 1)$ represents the fundamental frequency. Harmonic phases $\phi_{[n,j]}$ are selected to minimize the signal crest factor using the approach proposed by Guillaume *et al.* (1991).

Transfer functions and uncertainties computed utilizing the transient method with "zippered" spectra (because of its reduced estimation bias properties) were discussed in Chapter 3. The experimental design is augmented considering the same "zippered" spectra but incorporating modifications on the harmonic frequency content and the amplitude of the signals.

Changes on the amplitude of the signals

Input signals must satisfy the following operational condition:

$$\begin{aligned} u_n^{min} \leq u_{n,l}(k) \leq u_n^{max} \\ n = 8, 9 \quad l = 1, \cdots, L \end{aligned} \tag{4.60}$$

According to the requirements of the monitoring process, and for the l^{th} signal of the sequence, the scale factor $\lambda_{n,l}$ can be increased or decreased such that the condition

$$u_{n,l}^{min} \leq u_{n,l}(k) \leq u_{n,l}^{max} \tag{4.61}$$

is satisfied with

$$\min\left(u_{n,1}^{min}, \cdots, u_{n,L}^{min}\right) \geq u_n^{min} \tag{4.62}$$

$$\max\left(u_{n,1}^{max}, \cdots, u_{n,L}^{max}\right) \leq u_n^{max} \tag{4.63}$$

for $n = 8, 9$.

Changes on the harmonic frequency content

A harmonic relation must exist between the fundamental frequencies of the different signals in the sequence. For the input u_9 the number of samples per period for the l^{th} signal in the sequence is defined as $N_{s,l}$. To have a harmonic relation, this quantity should be related to N_s by a power of two; however to maintain the "zippered" definition of the spectra an additional frequency shift must be implemented as was illustrated in Fig. 3.7. $S_{h,l}$ is the harmonic reduction step between the initial ($l = 1$) and the l^{th} signal in the sequence; hence $S_{h,1} = 0$.

Based on the desired harmonic reduction step at the l^{th} signal of the sequence, the theoretical number of samples per period for u_{n_u}, and the number of independent sinusoids excited per channel ($n_{s,l}$) are

$$N_{s,l} = \frac{N_s}{n_u 2^{S_{h,l}}}, \qquad n_{s,l} = \frac{n_s}{n_u 2^{S_{h,l}}} \tag{4.64}$$

where the division by n_u was included to create additional frequency space for the "zippered" definition of signals. From here the spectrum for each input signal u_n, $n = 8, 9$ is constructed by defining

$$\alpha_{n,l,j} = \begin{cases} 1 & \text{if } j = n_u(2^{S_{h,l}} i - 1) + n - 7 \\ & \text{for } i = 1, \cdots, n_{s,l} \\ 0 & \text{otherwise} \end{cases} \tag{4.65}$$

It is important to notice that for the l^{th} signal of the sequence only the input channel u_9 maintains a specific harmonic relation to the fundamental frequency defined by N_s. The remainder input channels are constructed using (4.65) that defines specific frequency shifts with respect to u_9. Hence, the only way of having a grid definition including all the utilized frequencies is to keep the total number of samples N_s for all the signals in the sequence.

For the physical activity behavioral intervention problem the sampling time is one day ($T_s = 1$). For an effective experiment, the time decision window (i.e., number of samples per period N_s) must not be too long, hence the total number of excited frequencies n_s must be short too. In Section 3.3.2.1 the scale factors $\lambda_{n,l}$ were chosen to keep constant the power of the signal after a change in the harmonic content. For this case that action is not practical given the proposed low number of excited frequencies (n_s); hence the scale factors are chosen to maintain the minimum and maximum values established in the previous signal of the sequence as

$$\text{Choose } \lambda_{n,l} \text{ such that } u_{n,l}^{min} = u_{n,l-1}^{min}, \quad u_{n,l}^{max} = u_{n,l-1}^{max}, \quad \text{for } n = 8, 9 \tag{4.66}$$

Transfer Function and Uncertainty Computation

Signals designed with the "zippered" power spectrum are analyzed and the transfer functions for each input output component are obtained using the transient

method described in Section 3.3.1.3, where the transient estimate of the output DFT $\hat{Y}_{[m]}(\omega_{n,l,i})$ is computed using (3.104) – (3.116). The transfer function estimate for the n^{th} input and m^{th} output element is

$$\begin{gathered}\hat{G}_{[m,n]}(\omega_{n,l,i}) = \frac{\hat{Y}_{[m]}(\omega_{n,l,i})}{U_{[n]}(\omega_{n,l,i})} \\ \text{for} \quad n = 1, \cdots, n_u, \quad m = 1, \cdots, n_y\end{gathered} \tag{4.67}$$

with the following estimated variance for each transfer function computation:

$$\hat{\sigma}^2_{\hat{G}_{[m,n]}}(\omega_{n,l,i}) = \frac{\hat{C}_{V_T[m,m]}(\omega_{n,l,i})}{|U_{[n]}(\omega_{n,l,i})|^2} \tag{4.68}$$

where $\hat{C}_{V_T[m,m]}$ is defined in (3.114). The complete procedure is described in Section 3.3.1.3.

The transfer function estimates are valid for the following frequency grid for each input and each signal of the sequence:

$$\boldsymbol{W}_{n,l} = \{\omega_{n,l,i} \in \mathbb{R} \mid \omega_{n,l,i} = \tfrac{2\pi[n_u(2^{S_{h,l}}i-1)+n-7]}{N_s T_s}, \quad i = 1, 2, \ldots, n_{s,l}\}, \quad n = 8, 9 \tag{4.69}$$

Assuming that the signal-to-noise ratio of the inputs is larger than 20 dB, then the circular $100 \times (1-\rho)\%$ confidence region (Pintelon and Schoukens, 2012) such that

$$Prob\Big\{\big|\hat{G}_{[m,n]}(\omega_{n,l,i}) - \mathbb{E}\{\hat{G}_{[m,n]}(\omega_{n,l,i})\}\big| \leq \ell^{1-\rho}_{a[m,n]}(\omega_{n,l,i})\Big\} = 1-\rho \tag{4.70}$$

can be constructed via a circular complex Gaussian approximation with a radius

$$\ell^{1-\rho}_{a[m,n]}(\omega_{n,l,i}) = \sqrt{-\ln\rho}\ \ \hat{\sigma}_{\hat{G}_{[m,n]}}(\omega_{n,l,i}) \tag{4.71}$$

A more general MIMO uncertainty bound can be computed considering the maximum singular value at each frequency with a probability $1-\kappa$ such that

$$Prob\Big\{\overline{\sigma}\big(\hat{\boldsymbol{G}}(\omega_{n,l,i}) - \boldsymbol{G}(\omega_{n,l,i})\big) \leq \epsilon^{1-\kappa}(\omega_{n,l,i})\Big\} = 1-\kappa \tag{4.72}$$

The bound can be computed relying on the Frobenious norm over the square of the maximum singular values as

$$\overline{\sigma}\big(\hat{\boldsymbol{G}}(\omega_{n,l,i}) - \boldsymbol{G}(\omega_{n,l,i})\big)^2 \leq \sum_{n=1}^{n_u}\sum_{m=1}^{n_y}\left[\ell^{1-\rho}_{a[m,n]}(\omega_{n,l,i}, M_l)\right]^2 \triangleq \left[\epsilon^{1-\kappa}(\omega_{n,l,i}, M_l)\right]^2 \quad (4.73)$$

Since each source of output noise is assumed to come from a different Gaussian realization and the inputs are excited independently the probabilities are related by

$$1 - \kappa = (1-\rho)^{n_y n_u} \quad (4.74)$$

Computation of a Robust Performance Index

The stopping criterion is designed relying on robust control ideas and utilizing the structure presented in Section 3.3.4.2. The closed loop representation shown in Fig. 3.9 yields to the definition of the estimated sensitivity $\tilde{\boldsymbol{E}}$, and complementary sensitivity $\tilde{\boldsymbol{H}}$ of the system as

$$\tilde{\boldsymbol{E}} = (I + \tilde{\boldsymbol{G}}\boldsymbol{C})^{-1} \quad (4.75)$$

$$\tilde{\boldsymbol{H}} = \tilde{\boldsymbol{G}}\boldsymbol{C}(\boldsymbol{I} + \tilde{\boldsymbol{G}}\boldsymbol{C})^{-1} \quad (4.76)$$

$$\text{and} \quad \tilde{\boldsymbol{E}} + \tilde{\boldsymbol{H}} = \boldsymbol{I} \quad (4.77)$$

The magnitude of the perturbation can be measured in terms of the bound over the maximum singular values as

$$\bar{\sigma}(\boldsymbol{L_a}) \leq \bar{\ell}_a(\omega), \quad \forall\omega \quad (4.78)$$

The controller is designed to minimize the worst normalized output error resulting from any disturbance input in the H_∞ sense, through the sensitivity function $\boldsymbol{E}$ as

$$\min_{\boldsymbol{C}} \|\boldsymbol{E}w_P\|_\infty = \min_{\boldsymbol{C}} \sup_{\omega} \bar{\sigma}\big(\boldsymbol{E}w_P\big) \quad (4.79)$$

The H_∞ performance requirement (Morari and Zafiriou, 1989) is usually written as

$$\bar{\sigma}\big(\boldsymbol{E}w_P\big) < 1, \quad \forall\omega \quad (4.80)$$

from where the following expression can be derived as was shown in Section 3.3.4.2:

$$\bar{\sigma}\big(\tilde{\boldsymbol{E}}w_P\big) + \bar{\sigma}\big(\boldsymbol{L_a}\tilde{\boldsymbol{G}}^{-1}\tilde{\boldsymbol{H}}\big) < 1 \tag{4.81}$$

Utilizing this result and the defined bound $\bar{\ell}_a$, a sufficient condition for robust performance can be defined (Morari and Zafiriou, 1989) as

$$\bar{\sigma}\big(\tilde{\boldsymbol{E}}w_P\big) + \bar{\sigma}\big(\tilde{\boldsymbol{G}}^{-1}\tilde{\boldsymbol{H}}\big)\bar{\ell}_a < 1, \quad \forall\omega \tag{4.82}$$

The performance weighting function w_P is designed to shape the sensitivity $\boldsymbol{E}$ of the closed-loop system using the following representation (Skogestad and Postlethwaite, 2005):

$$w_P = \frac{s/M_P + \omega_B}{s + \omega_B A_P} \tag{4.83}$$

For the closed loop proposed structure the controller is defined using a multivariable Q-parametrization/Internal Model Control (IMC) representation (Morari and Zafiriou, 1989) as

$$\boldsymbol{C} = \boldsymbol{Q}(\boldsymbol{I} - \tilde{\boldsymbol{G}}\boldsymbol{Q})^{-1} \quad \text{with } \boldsymbol{Q} = \tilde{\boldsymbol{Q}}\boldsymbol{F} \tag{4.84}$$

The values of $\tilde{\boldsymbol{Q}}$ and $\boldsymbol{F}$ are defined as follows: $\boldsymbol{G}$ can be factorized into an invertible portion $\boldsymbol{G}_-$ that is stable and causal, and a nononvertible part $\boldsymbol{G}_+$ as $\boldsymbol{G} = \boldsymbol{G}_+\boldsymbol{G}_-$ from where $\tilde{\boldsymbol{Q}} = {\boldsymbol{G}_-}^{-1}$ is defined. For robustness purposes the controller is augmented with a set of low-pass filters $\boldsymbol{F}$, whose basic structure is

$$\boldsymbol{F} = diag\{f_1(s), \cdots, f_v(s)\} \tag{4.85}$$

where each filter can be defined using a Type 1 representation as

$$f_i(s) = \frac{1}{(\lambda_i s + 1)^n} \tag{4.86}$$

Using the IMC representation, and assuming a zero plant model mismatch, the complementary sensitivity can be represented as

$$\tilde{\boldsymbol{H}} = \tilde{\boldsymbol{G}}\boldsymbol{Q} = \boldsymbol{G}_{+}\boldsymbol{F} \tag{4.87}$$

from where the robust performance condition presented in (4.82) can be written as

$$\bar{\sigma}\big(\tilde{\boldsymbol{E}}w_P\big) + \bar{\sigma}\big(\tilde{\boldsymbol{G}}^{-1}\boldsymbol{G}_{+}\boldsymbol{F}\big)\bar{\ell}_a(\omega) \leq 1, \quad \forall\omega \tag{4.88}$$

If the system contains only minimum phase elements, then the matrix $\boldsymbol{G}_{+}$ in (4.88) is unity, leading to a robust performance condition that only depends in the plant estimate and the computed uncertainty bounds.

By substituting the computed transfer function and uncertainties for the l^{th} signal in the sequence, the following robust performance condition for M_l periods of experimental execution is obtained:

$$\begin{gathered} RPi(\omega_{n,l,i}, M_l) \leq 1, \quad \forall\omega_{n,l,i} \in \boldsymbol{W}_{n,l} \\ RPi(\omega_{n,l,i}, M_l) = \bar{\sigma}\big(\tilde{\boldsymbol{E}}w_P\big) + \bar{\sigma}\big(\hat{\boldsymbol{G}}^{-1}\boldsymbol{G}_{+}\boldsymbol{F}\big)\epsilon^{1-\kappa}(\omega_{n,l,i}, M_l) \\ \text{with} \quad \tilde{\boldsymbol{E}} = \boldsymbol{I} - \boldsymbol{G}_{+}\boldsymbol{F} \end{gathered} \tag{4.89}$$

The tuning parameters λ_i, $i = 1, \cdots, v$ are selected for each iteration as the values that minimize the maximum robust performance index among all the frequencies as was shown in Section 3.3.4.2.

Aggregate response for all the L signals in the sequence

Consider that the total number of samples of the experiment is

$$N_{total} = \sum_{l=1}^{L} N_s M_l \leq N_{max} \tag{4.90}$$

After the application of one input signal period, three different types of actions are considered:

1. **Add an additional period of the identical signal**. This is recommended when the actual total number of samples is considerably less than N_{max}.

2. **Apply a signal with higher amplitude**. An increase in the input signal amplitude is recommended if the uncertainty is decreasing slowly, and the maximum bounds defined in (4.60) are still not reached.

3. **Apply a signal with different harmonic related frequency content**. The harmonic content of the signal can be modified if a better understanding of the system is achieved and the power of the input can be emphasized over frequencies of interest. This step can be applied when uncertainty is decreasing slowly and the maximum number of samples N_{max} is close to be reached.

The action to be performed for the subsequent period must be judiciously selected for each case depending on the operational constraints of the system, the level of noise experienced, and user preferences.

The additive uncertainty bound defined in (4.73), and the robust performance index from (4.89) are valid for the l^{th} signal of the sequence; hence an aggregate computation is needed considering all the L signals in the sequence. This computation is implemented over a common frequency grid among all the signals in the sequence that is defined by the signal with the highest harmonic reduction step. If we define

$$l_{agg} = \{1 \leq l \leq L \mid S_{h,l} = \max(S_{h,1}, \cdots, S_{h,L})\} \tag{4.91}$$

then the frequency grid of the aggregate estimate is defined for each $\omega_{n,i} \in \boldsymbol{W}_{n,l_{agg}}$. The total number of periods of the experiment is

$$M = \sum_{l=1}^{L} M_l \tag{4.92}$$

The transient LPM to compute frequency domain transfer functions utilizes an ETFE approach for the excited frequencies. In Section 4.3.2.1 the block diagram for

the physical activity behavioral problem was described in terms of a non-linear representation of the "If/Then" block that is active for each of the input-output transfer function elements. Even in the presence of the specified nonlinearity, the transfer function response remained the same while the inputs were unaltered. That is not the case for the enhanced method which incorporates sequential changes on the input signal content. Hence the computation of a single and unique aggregate transfer function is not meaningful from the physical standpoint; however the computed additive uncertainty bounds are still valid, since under the assumed conditions the transient LPM approach is an unbiased transfer function estimator (Monteyne *et al.*, 2012).

To prove that the computation of the proposed bounds $\epsilon^{1-\kappa}(\omega_{n,l,i}, M_l)$ is independent of the values of the computed transfer functions $\hat{G}_{[m,n]}(\omega_{n,l,i})$, the equations used for additive uncertainties are shown again

$$\left[\epsilon^{1-\kappa}(\omega_{n,l,i}, M_l)\right]^2 = \sum_{n=1}^{n_u}\sum_{m=1}^{n_y}\left[\ell^{1-\rho}_{a[m,n]}(\omega_{n,l,i}, M_l)\right]^2 \tag{4.93}$$

$$\ell^{1-\rho}_{a[m,n]}(\omega_{n,l,i}) = \sqrt{-\ln\rho}\ \hat{\sigma}_{\hat{G}_{[m,n]}}(\omega_{n,l,i}) \tag{4.94}$$

from here is clear that additive uncertainty estimates depend on the values of the sample variances of the estimated transfer functions $\hat{\sigma}_{\hat{G}_{[m,n]}}(\omega_{n,l,i})$ for $m = 4, 5$, and $n = 8, 9$, that are computed using

$$\hat{\sigma}^2_{\hat{G}_{[m,n]}}(\omega_{n,l,i}) = \frac{\hat{C}_{V_T[m,m]}(\omega_{n,l,i})}{|U_{[n]}(\omega_{n,l,i})|^2} \tag{4.95}$$

where $\hat{C}_{V_T[m,m]}(\omega_{n,l,i})$ is the (m, m) element of the noise covariance matrix from the non-excited frequency analysis of the LPM for periodic excitations method presented in Section 3.3.1.3, using a Taylor series expansion of order $R + 1$ and using $2n_T$ non-excited frequencies ω^*_j around each excited frequency $\omega_{n,l,i}$. Hence the sample

variance of the transfer function estimate is now

$$\hat{\sigma}^2_{\hat{G}_{[m,n]}}(\omega_{n,l,i}) = \frac{\frac{1}{df_T}\sum_{j=1}^{2n_T} |Y_{[m]}(\omega_j^*) - \hat{Y}_{[m]}(\omega_j^*)|^2}{|U_{[n]}(\omega_{n,l,i})|^2} \tag{4.96}$$

where $df_T = 2n_T - (R+1)$ is the number of degrees of freedom of the LPM estimate, $U_{[n]}$, $Y_{[m]}$, and $\hat{Y}_{[m]}$ are the DFT of the input u_n, output y_m and the estimate of y_m respectively at the specified frequencies. Considering the "zippered" definition of the inputs, the DFT of the sampled output y_m at the non-excited frequencies can be written as

$$Y_{[m]}(\omega_j^*) = T_{[m]}(\omega_j^*) + V_{[m]}(\omega_j^*) \tag{4.97}$$

where $T_{[m]}(\omega_j^*)$ is the system and noise transient term, and $V_{[m]}(\omega_j^*)$ is the output noise component. According to the LPM formulation the estimated DFT of the output y_m at the non-excited points is

$$\hat{Y}_{[m]}(\omega_j^*) = \hat{T}_{[m]}(\omega_j^*) \tag{4.98}$$

hence by replacing (4.97) and (4.98) in (4.96), the following expression is obtained

$$\hat{\sigma}^2_{\hat{G}_{[m,n]}}(\omega_{n,l,i}) = \frac{\frac{1}{df_T}\sum_{j=1}^{2n_T} |(T_{[m]}(\omega_j^*) - \hat{T}_{[m]}(\omega_j^*)) + V_{[m]}(\omega_j^*)|^2}{|U_{[n]}(\omega_{n,l,i})|^2} \tag{4.99}$$

Under the LPM specified conditions $\hat{T}_{[m]}$ is an unbiased estimator of the system transient and noise term $T_{[m]}$ (Pintelon and Schoukens, 2012), hence the sample variance of the transfer function estimate can be reduced to

$$\hat{\sigma}^2_{\hat{G}_{[m,n]}}(\omega_{n,l,i}) \approx \frac{\frac{1}{df_T}\sum_{j=1}^{2n_T} |V_{[m]}(\omega_j^*)|^2}{|U_{[n]}(\omega_{n,l,i})|^2} \tag{4.100}$$

Therefore the estimated additive uncertainty bounds shown in (4.93) do not depend on the values of the estimated transfer functions, and they can still be used in the

monitoring process. Utilizing this result, the resultant aggregate variance of the transfer function estimation considering all the L signals in the sequence is

$$\hat{\sigma}^2_{\hat{G}_{[m,n]}}(\omega_{n,i}) = \frac{1}{\sum_{l=1}^{L} \frac{1}{\hat{\sigma}^2_{\hat{G}_{[m,n]}}(\omega_{n,l,i})}} \tag{4.101}$$

Relying on (4.93) and (4.94), the resultant total uncertainty bounds are computed as

$$\ell^{1-\rho}_{a[m,n]}(\omega_{n,i}, M) = \sqrt{-\ln \rho}\ \hat{\sigma}_{\hat{G}_{[m,n]}}(\omega_{n,i}) \tag{4.102}$$

$$\left[\epsilon^{1-\kappa}(\omega_{n,i}, M)\right]^2 = \sum_{n=1}^{n_u} \sum_{m=1}^{n_y} \left[\ell^{1-\rho}_{a[m,n]}(\omega_{n,i}, M)\right]^2 \tag{4.103}$$

Monitoring Procedure

The general stopping criterion is defined using the same ideas described in Section 4.3.2.1 for the basic identification test monitoring case. For each input-output element a maximum MIMO additive uncertainty is computed for $\omega_{n,i} \in \boldsymbol{W}_{n,l_{agg}}$

$$\tilde{\epsilon}(M) = \max_{\omega_{n,i} \in \boldsymbol{W}_{n,l_{agg}}} \left[\epsilon^{1-\kappa}(\omega_{n,i}, M)\right], \quad M = 2, 3 \ldots \tag{4.104}$$

Percentages of uncertainty reduction among consecutive values of M are calculated as

$$AV(M) = \frac{\tilde{\epsilon}(M-1) - \tilde{\epsilon}(M)}{\tilde{\epsilon}(2)} \times 100 \tag{4.105}$$

$$RV(M) = \frac{\tilde{\epsilon}(M-1) - \tilde{\epsilon}(M)}{\tilde{\epsilon}(M-1)} \times 100 \tag{4.106}$$

$$\text{for } M = 2, 3, \cdots$$

where $AV(M)$ is the absolute percentage reduction referred to the first estimation ($M = 2$), and $RV(M)$ is the relative percentage reduction referred to the previous value of M. With these definitions the stopping criterion can be posed as

$$\text{Stop at } M = Q - 1 \text{ when}$$

$$AV(Q-r) \leq B_{AV} \quad \text{and} \quad RV(Q-r) \leq B_{RV} \tag{4.107}$$

$$\text{for } r = 1, \ldots, n_{Mi} \text{ consecutive iterations}$$

where B_{AV} and B_{RV} are the predetermined required bounds over the absolute and relative variations, and n_{Mi} is the number of consecutive iterations where the previous condition must be accomplished.

When more than two signals in the sequence are present ($L \geq 2$) robust performance ideas cannot be applied directly in the definition of the stopping criterion, because each signal in the sequence results in a different transfer function $\hat{G}_{[m,n]}$. However an intuitive weighted mean of the computed robust performance index for the different L signals in the sequence can be defined. For the l^{th} signal of the sequence the robust performance index RPi is

$$RPi(\omega_{n,l,i}, M_l) = \bar{\sigma}\big(\tilde{\boldsymbol{E}} w_P\big) + \bar{\sigma}\big({\hat{\boldsymbol{G}}_l}^{-1} \boldsymbol{G}_+ \boldsymbol{F}\big)\epsilon^{1-\kappa}(\omega_{n,l,i}, M_l) \tag{4.108}$$

where a specific dependence on l in $\hat{\boldsymbol{G}}_l$ has been added to highlight the fact that the transfer function estimates are not the same for the different l signals of the sequence, due to the performed changes on their input signal content. The computed MIMO additive uncertainty bound $\epsilon^{1-\kappa}(\omega_{n,l,i}, M_l)$ from (4.93) is directly influenced by the additive uncertainty bounds for each input output element whose computation is independent of the estimated transfer function; hence the following weights are proposed for $\omega_{n,l,i} \in \boldsymbol{W}_{n,l}$:

$$w_{RP}(\omega_{n,l,i}, M_l) = \frac{1}{[\epsilon^{1-\kappa}(\omega_{n,l,i}, M_l)]^2} \tag{4.109}$$

from where the approximate aggregated robust performance index for $\omega_{n,i} \in \boldsymbol{W}_{n,l_{agg}}$ is computed as

$$\widetilde{RPi}(\omega_{n,i}, M) = \frac{\sum_{l=1}^{L} w_{RP}(\omega_{n,l,i}, M_l) RPi(\omega_{n,l,i}, M_l)}{\sum_{l=1}^{L} w_{RP}(\omega_{n,l,i}, M_l)} \tag{4.110}$$

from where the stopping criterion can be redefined as

$$\text{Stop after } M \text{ total number of periods if}$$
$$\widetilde{RPi}(\omega_{n,i}, M) \leq 1 \tag{4.111}$$
$$\forall \omega_{n,i} \in \boldsymbol{W}_{n,l_{agg}}, \text{ during the last } n_{Mi} \text{ iterations.}$$

This stopping criterion can be accurately used when there is one signal in the sequence ($L = 1$) and only additional periods of the identical signal were added. When changes in the input signal content are applied ($L \geq 2$) the stopping criterion presented in (4.107) is a more accurate representation, however (4.111) is a rational intuitive option that can be considered too.

4.4 Design of the Optimized Experiment

The primary goal of the optimized experiment is to delineate a judiciously-selected protocol for allowing intervention features to be systematically activated, deactivated and reactivated, taking into account an improved understanding of the behavior change process brought about by the informative experiment. The inputs will be optimally designed to follow a weekly set point which inherently will include some variations. One of the challenges in the optimized input signal design is to consider the natural feedback involved in the reinforcement strategy, represented by the "If / Then" block showed in Fig. 4.2.

Only a subset of the inputs and outputs used in the semi-physical identification will be used in this formulation. The considered inputs correspond to the independent signals: goals (u_8), available reward points (u_9), and the resultant signal (through the "If/Then" block) reward points (u_{10}). The final interest of the behavioral intervention is to shape the participant's behavior, therefore y_4 will be the unique considered output. To account for this new input/output profile the following state space repre-

sentation is used:

$$\begin{aligned} \dot{\boldsymbol{x}}_{\boldsymbol{O}}(t) &= \boldsymbol{A}_{\boldsymbol{O}}\boldsymbol{x}_{\boldsymbol{O}}(t) + \boldsymbol{B}_{\boldsymbol{O}}\boldsymbol{u}_{\boldsymbol{O}}(t) \\ \boldsymbol{y}_{\boldsymbol{O}}(t) &= \boldsymbol{C}_{\boldsymbol{O}}\boldsymbol{x}_{\boldsymbol{O}}(t) + \boldsymbol{D}_{\boldsymbol{O}}\boldsymbol{u}_{\boldsymbol{O}}(t) \end{aligned} \tag{4.112}$$

where $\boldsymbol{x}_{\boldsymbol{O}}$ is the state vector, $\boldsymbol{u}_{\boldsymbol{O}}$ is the input vector, and $\boldsymbol{y}_{\boldsymbol{O}}$ is the output vector defined as

$$\boldsymbol{x}_{\boldsymbol{O}} = \begin{bmatrix} \eta_2 & \eta_3 & \eta_4 & \eta_5 & \eta_6 & \eta_7 \end{bmatrix}^\top \tag{4.113}$$

$$\boldsymbol{u}_{\boldsymbol{O}} = \begin{bmatrix} u_8 & u_9 & u_{10} & y_{4ini} - u_{8ini} \end{bmatrix}^\top \tag{4.114}$$

$$\boldsymbol{y}_{\boldsymbol{O}} = y_4 \tag{4.115}$$

Variables y_{4ini} and u_{8ini} are the initial values for the inputs y_4 and u_8 respectively, that must be considered in the definition of the output using a transfer function, and in the construction of the signal u_{11}.

The state-space system matrices are

$$\boldsymbol{A}_{\boldsymbol{O}} = \begin{pmatrix} -\frac{1}{\tau_2} & 0 & 0 & \frac{\beta_{25}}{\tau_2} & 0 & 0 \\ 0 & -\frac{1}{\tau_3} & \frac{\beta_{34}+\gamma_{311}}{\tau_3} & 0 & 0 & 0 \\ \frac{\beta_{42}}{\tau_4} & \frac{\beta_{43}}{\tau_4} & -\frac{1}{\tau_4} & \frac{\beta_{45}}{\tau_4} & \frac{\beta_{46}}{\tau_4} & 0 \\ 0 & 0 & \frac{\beta_{54}}{\tau_5} & -\frac{1}{\tau_5} & 0 & 0 \\ 0 & 0 & -\frac{\gamma_{64}M_{sr}\tau_4}{\tau_6} & 0 & -\frac{1}{\tau_6} & \frac{\gamma_{64}M_{sr}(1-N_{sr}\tau_4)}{\tau_6} \\ 0 & 0 & -1 & 0 & 0 & -N_{sr} \end{pmatrix} \tag{4.116}$$

$$\boldsymbol{B}_{\boldsymbol{O}} = \begin{pmatrix} 0 & \frac{\gamma_{29}}{\tau_2} & 0 & 0 \\ -\frac{\gamma_{311}}{\tau_3} & 0 & 0 & \frac{\gamma_{34}}{\tau_3} \\ 0 & 0 & 0 & 0 \\ 0 & 0 & \frac{\gamma_{510}}{\tau_5} & 0 \\ \frac{\gamma_{64}M_{sr}\tau_4}{\tau_6} & 0 & 0 & 0 \\ 1 & 0 & 0 & 0 \end{pmatrix} \tag{4.117}$$

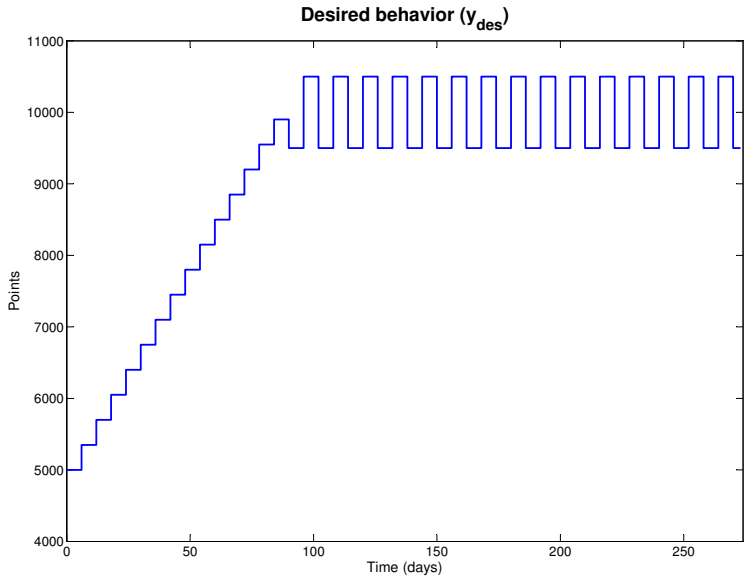

Figure 4.7: Realization of the Desired Behavior (y_{des}) to be Used in the Formulation of the Optimized Experiment, With a Starting Baseline of $5,000$ Steps, and a Duration of 273 Days.

$$\boldsymbol{C_O} = \begin{pmatrix} 0 & 0 & 1 & 0 & 0 & 0 \end{pmatrix} \tag{4.118}$$

$$\boldsymbol{D_O} = \begin{pmatrix} 0 & 0 & 0 \end{pmatrix} \tag{4.119}$$

$$\text{with} \quad M_{sr} = \frac{K_{sr}}{\gamma_{64}\beta_{46}\lambda}, \quad \text{and} \quad N_{sr} = \frac{1 - K_{sr}}{\lambda}.$$

To formulate the optimization problem for $N \in \mathbb{N}$ days, $\boldsymbol{u}_8, \boldsymbol{u}_9, \boldsymbol{u}_{10} \in \mathbb{R}^N$ represent the intervention inputs, $\boldsymbol{y_{des}} \in \mathbb{R}^N$ is a vector containing the desired set point for behavior (i.e., number of daily steps per each week) that is generated using an increment of 350 steps every six days starting from the baseline, until the main goal of 10,000 daily steps is achieved, after which a variation of $\pm$ 500 steps from the 10,000 mark is applied. A realization of this signal for 273 days with a starting baseline of 5,000 steps is shown in Fig. 4.7.

The signal $\boldsymbol{y_4} \in \mathbb{R}^N$ represents the output "behavior" (η_4), if $\boldsymbol{u_T} \in \mathbb{R}^{3N} = [\boldsymbol{u_8}^\top \quad \boldsymbol{u_9}^\top \quad \boldsymbol{u_{10}}^\top]^\top$ is considered, then $\boldsymbol{y_4}$ can be generated by a linear time-invariant system as

$$\boldsymbol{y_4} = \boldsymbol{G} \cdot \boldsymbol{u_T} + \boldsymbol{y_{ini}} \tag{4.120}$$

where $\boldsymbol{G} \in \mathbb{R}^{N \times 3N}$ is the Toeplitz matrix of system impulse responses that was estimated using the state space structure defined in Equations (4.112) - (4.119) with the model parameters obtained from the informative experiment, and $\boldsymbol{y_{ini}} \in \mathbb{R}^N$ is a vector with all its elements equal to the initial value of the output signal.

The problem statement is as follows:

$$\min_{\boldsymbol{u}_8, \boldsymbol{u}_9, \boldsymbol{u}_{10}} \sum_{k=1}^{N} \left[y_4(k) - y_{des}(k) \right]^2 \tag{4.121}$$

subject to constraints per Equations (4.22) - (4.28) and per Equations (4.122) - (4.129) next described. Bounds must be imposed to the output y_4

$$y_4^{min} \leq y_4(k) \leq y_4^{max}, \quad k = 1, \ldots, N \tag{4.122}$$

To force the condition imposed by the "If/Then" block (meaning that at a given day k, the points are delivered only when the output $y_4(k)$ is greater than the applied goal $u_8(k)$), a big-M reformulation (Williams, 2013) is applied where a carefully selected constant is added to convert a logic constraint to another one describing the same feasible set. A set of auxiliary binary variables $\boldsymbol{\delta}$ is introduced such that

$$\delta(k) \in \{0, 1\}, \quad k = 1, \ldots, N \tag{4.123}$$

where $\delta(k) = 1$ represents that the goal for the day k has been accomplished. To represent the dependence of $\boldsymbol{\delta}$ on $\boldsymbol{y_4}$ and $\boldsymbol{u_8}$ at every day k, the following constraints are added:

$$y_4(k) - u_8(k) \leq \delta(k)[y_4^{max} - u_8^{min}(k)] \tag{4.124}$$

$$y_4(k) - u_8(k) \geq [1 - \delta(k)][y_4^{min} - u_8^{max}(k)] \tag{4.125}$$
$$k = 1, \ldots, N$$

If the goal is achieved, $y_4(k)$ is greater than $u_8(k)$ and the difference is a positive number less than $y_4^{max} - u_8^{min}(k)$, therefore the only way to accomplish Equation (4.124) is by making $\delta(k) = 1$. On the other hand if the goal is not achieved $y_4(k) - u_8(k)$ is a negative number greater than $y_4^{min} - u_8^{max}(k)$ therefore the condition $\delta(k) = 0$ must be imposed to satisfy Equation (4.125).

At day $k + 1$ the granted points must be equal to available points the day before ($u_{10}(k + 1) = u_9(k)$), if the goal was achieved ($\delta(k) = 1$)

$$u_9(k) - u_{10}(k + 1) \leq [1 - \delta(k)][u_9^{max}(k) - u_{10}^{min}(k + 1)] \tag{4.126}$$
$$u_9(k) - u_{10}(k + 1) \geq [1 - \delta(k)][u_9^{min}(k) - u_{10}^{max}(k + 1)] \tag{4.127}$$
$$k = 1, \ldots, N - 1$$

The following constraints state that at day $k + 1$ the input $u_{10}(k + 1)$ must be zero, if the goal was not achieved the day before ($\delta(k) = 0$):

$$u_{10}(k + 1) \geq \delta(k) u_{10}^{min}(k + 1) \tag{4.128}$$
$$u_{10}(k + 1) \leq \delta(k) u_{10}^{max}(k + 1) \tag{4.129}$$
$$k = 1, \ldots, N - 1$$

The proposed constrained optimization problem must be solved as a mixed integer quadratic problem (MIQP). The experiment must be executed with the new designed inputs and new data should be collected. Since prior insight of the system was used during the optimization, the output is expected to exhibit a shape of increasing activity more in line with a designed physical activity intervention and also a better approximation of the real plant is expected.

4.5 Simulation Study

The proposed system identification procedure will be tested over a reference "simulation plant" for the physical activity behavioral situation based on the SCT model, which parameters are selected to resemble results from a previous intervention development experiment using intensive data and mobile devices (King *et al.*, 2013; Adams *et al.*, 2013). The selected SCT model parameters are

- $\tau_2 = 40, \tau_3 = 30, \tau_4 = 0.8, \tau_5 = 2, \tau_6 = 0.5$
- $\gamma_{29} = 2.5, \gamma_{311} = 0.4, \gamma_{57} = 1, \gamma_{510} = 0.6, \gamma_{68} = 1, \gamma_{64} = 1.5$
- $\beta_{25} = 0.5, \beta_{34} = 0.2, \beta_{42} = 0.3, \beta_{43} = 0.9, \beta_{45} = 0.5, \beta_{46} = 0.9, \beta_{54} = 0.6$
- $K_{sr} = 0.8, \lambda = 1$

Delays (θ_i) are considered zero, environmental context (ξ_7) is considered as an autoregressive signal described by

$$\xi_7(k) = \phi_7 \xi_7(k-1) + a(k), \quad a(k) \sim \mathcal{N}(0, \sigma_7^2) \tag{4.130}$$

with $\phi_7 = 0.7$ and $\sigma_7^2 = 9$. Uncertainties (ζ_i) in all the inventories are represented as Gaussian signals with $\zeta_i(k) \sim \mathcal{N}(0, 10), \quad \forall i$. Output measurement noises are Gaussian with $v_4(k) \sim \mathcal{N}(0, \sigma_4^2)$, $v_5(k) \sim \mathcal{N}(0, \sigma_5^2)$, and considering $\sigma_4^2 = 300000$, $\sigma_5^2 = 500$.

4.5.1 Fixed Time Random Signal Experiments

Fixed duration of the experiment is assumed in this section, therefore the informative experiment will be implemented using the randomized generation described in Section 4.3.1.The simulation will be projected for 273 days (Prochaska and DiClemente, 1983), (approx. 9 months) to obtain sufficient data for analysis. Based

on previous studies (King *et al.*, 2013; Adams *et al.*, 2013) and the desired goal of achieving 10,000 daily steps, a baseline (B_s) of 5,000 steps is selected, and signals u_8 and u_9 are computed as was described in equations (4.29) - (4.32). Design constraints described in Equations (4.22) through (4.28) are considered with the values listed in Table 4.1.

Table 4.1: Constant Values of Design Constraints for Informative and Optimized Experiments.

Input u_n	**Min. value** Z_n^{min}	**Max. value** Z_n^{max}	**Start day** D_n	**Max. move** MS_n
u_8	5000	10000	8	5000
u_9	100	500	15	500
u_{10}	0	500	15	500
$Tsw = 1$				

A realization of these signals is shown in Fig. 4.8 as well as the output signal behavior ($y_{sim} = y_4$) obtained by evaluating the simulation plant. Since this experiment occurs in open-loop, the resulting behavior exhibits an initial increment and later a non-settling pattern with random elements that does not achieve the main goal of 10,000 steps during the whole experiment.

With the resulting data, the described grey-box parameter estimation procedure is implemented in MATLAB via the functions `idgrey` and `greyest`. The following conditions are included in the estimation based on considerations from the SCT model (β_i) and general assumed bounds (τ_i and γ_i):

$$0.1 \leq \tau_i \leq 200, \qquad \forall \tau \tag{4.131}$$

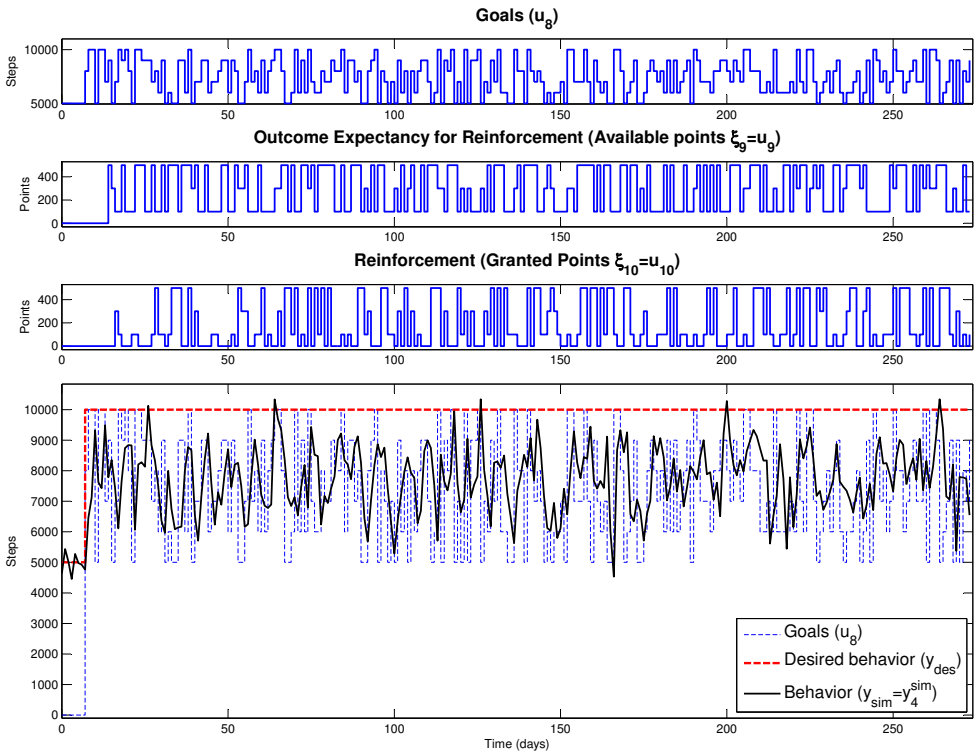

Figure 4.8: Input/output Data for the Fixed Time Informative Experiment Using Random Inputs Within Clinical Constraints.

$$0.1 \leq \beta_i \leq 0.9, \qquad \forall \beta \tag{4.132}$$

$$0.1 \leq \gamma_i \leq 100, \qquad \forall \gamma \tag{4.133}$$

with the following specific constraints:

$$\beta_{34} \leq 0.3, \quad \gamma_{311} \leq 0.3 \tag{4.134}$$

enforced by the stability condition presented in (2.40). Conditions for the parameters of the self-regulator visa internalized cues are

$$0.01 \leq K_{sr} \leq 1, \quad 0.1 \leq \lambda \leq 50 \tag{4.135}$$

For crossvalidation purposes a different set of inputs shown in Fig. 4.9a is generated and evaluated in the simulation plant for a period of 90 days. These inputs are applied

to the identified model and the goodness of fit for each output is calculated via

$$\%fit_m = 100\left(1 - \frac{\|\boldsymbol{y_m} - \hat{\boldsymbol{y}}_{\boldsymbol{m}}\|}{\|\boldsymbol{y_m} - \text{mean}(\boldsymbol{y_m})\|}\right) \tag{4.136}$$

where $\boldsymbol{y_m} \in \mathbb{R}^N$ is the evaluated output ($m = 4, 5$) from the simulation plant (real model) and $\hat{\boldsymbol{y}}_{\boldsymbol{m}} \in \mathbb{R}^N$ is the simulated output value from the identified model. Fitting results are 39.94% for behavior and 61.49% for behavioral outcomes as is shown in Fig. 4.9b.

The informative preliminary model then serves as a basis for an optimized experiment with the purpose of both getting a better estimate of the plant while satisfying "participant-friendly" experimental conditions. Values for the optimization constraints described in Equations (4.22) - (4.28), are listed in Table 4.1; the constraints defined in Equations (4.122) through (4.129) are also considered with $y_4^{min} = 0$ and $y_4^{max} = 11,000$.

The optimization algorithm is coded in MATLAB with a YALMIP (J. Löfberg, 2004) interface and solved via a MIQP problem using CPLEX (ILOG CPLEX Optimization Studio, 2013) as the solver. Fig. 4.10 shows the estimated optimized inputs together with the output of the system, when these inputs are applied to the reference simulation plant. The pattern of the resulting behavior is now following a similar shape to the set point; however responses from the simulation plant are skewed because of the errors in the model from the informative experiment.

A new grey-box parameter estimation procedure is conducted with this new set of data, using the same conditions declared in Equations (4.131) - (4.133) and using the parameter values obtained in the informative identification as the initial values. The obtained fits are 44.09% for behavior and 64.18% for behavioral outcomes. Cross-validation results for both the informative and optimized experiment are shown in Fig.4.11.

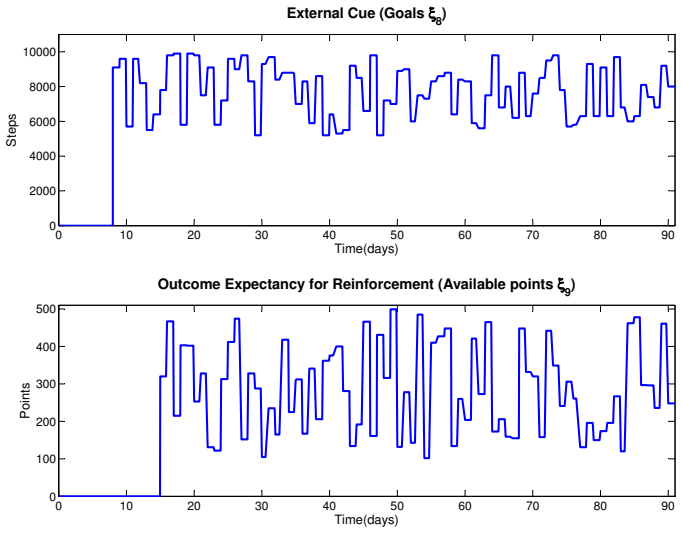

(a) Cross-Validation Input Signals.

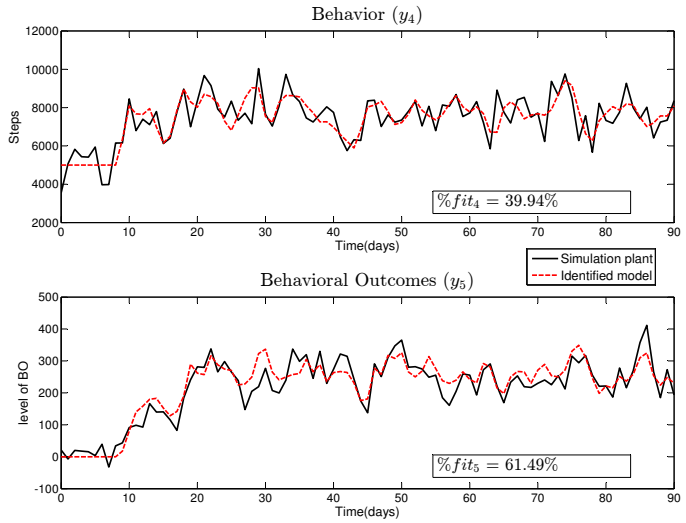

(b) Cross-Validation Output Signals.

Figure 4.9: Cross-Validation Results Comparing the Simulation Plant With the Identified Model From the Informative Experiment.

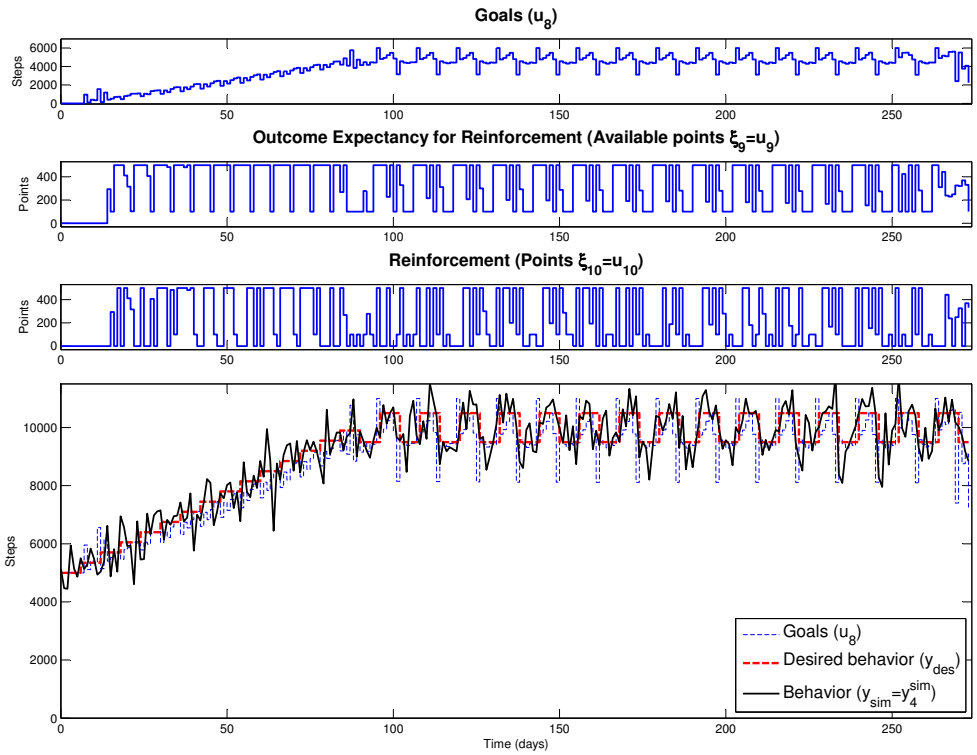

Figure 4.10: Input/output Data for the Fixed Time Optimized Experiment.

To assess the "patient-friendly" requirements for both experiments a series of metrics are computed. The move sizes of the designed inputs Δu_8 and Δu_9 are calculated using Equation (4.25); the particular interest is in their mean ($\overline{\Delta} u_n$) and standard deviation ($S_{\Delta u_n}$)

$$\overline{\Delta} u_n = \frac{1}{N-1} \sum_{k=2}^{N} \Delta u_n(k) \tag{4.137}$$

$$S_{\Delta u_n} = \sqrt{\frac{\sum_{k=2}^{N} [\Delta u_n(k) - \overline{\Delta} u_n]^2}{N-2}} \tag{4.138}$$

The signal u_{10} is not considered because during simulation it is internally generated by the model. To measure the goodness of the simulated behavior compared to the

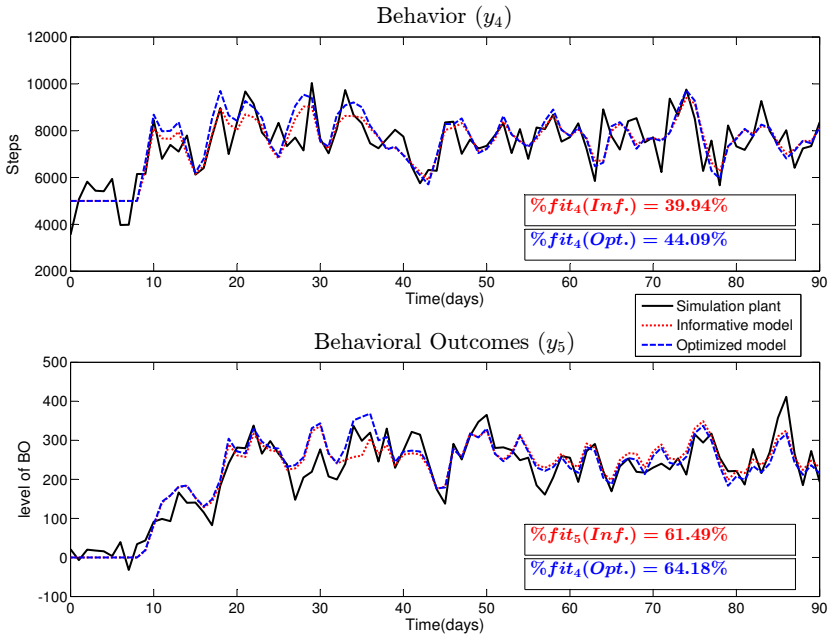

Figure 4.11: Cross-Validation Results Comparing the Simulation Plant With the Identified Model From the Informative and Optimized Experiments.

desired steps for each experiment, the simulation error is defined as

$$e_{sim}(k) = |y_{des}(k) - y_{sim}(k)|, \quad k = 1, \ldots, N \tag{4.139}$$

where $\boldsymbol{y_{des}}$ and $\boldsymbol{y_{sim}}$ are taken from the simulation results of each experiment for the output behavior (y_4) as was shown in Figs. 4.8 and 4.10 respectively. The deviation of the simulation error with respect to zero can also be computed as

$$S_{e_{sim}} = \sqrt{\frac{\sum_{k=1}^{N} [e_{sim}(k)]^2}{N-1}} \tag{4.140}$$

Values of the specified metrics from the informative and optimized experiments are shown in Table 4.2. It can be observed that input signals from the optimized experiment exhibit less variability and lower mean values than those from the informative experiment; furthermore, the error mean and standard deviation are lower in the op-

timized case, signifying that the optimized experiment achieved an output that more closely resembles the desired behavior.

Table 4.2: Performance Metrics Comparison of Input/output Signals From Informative and Optimized Experiments.

Metric	**Informative**	**Optimized**
$\overline{\Delta}u_8$ (steps)	1875.5	575.92
$S_{\Delta u_8}$ (steps)	1475	605.08
$\overline{\Delta}u_9$ (points)	184.98	161.83
$S_{\Delta u_9}$ (points)	177.69	171.63
$\overline{e}_{sim}$ (steps)	2262.8	519.25
$S_{e_{sim}}$ (steps)	2472.6	666.86

4.5.2 Monitoring Process

The identification test monitoring process will be performed over the simulation plant defined in Section 4.5 with daily measurements ($T_s = 1$). Disturbances and output noises have the same definitions with $\zeta_i(k) \sim \mathcal{N}(0, 10)\ \forall i$, $v_4(k) \sim \mathcal{N}(0, \sigma_4^2)$, $v_5(k) \sim \mathcal{N}(0, \sigma_5^2)$, with $\sigma_4^2 = 300000$ and $\sigma_5^2 = 500$.

4.5.2.1 Basic Identification Test Monitoring Procedure

Multisinusoidal signals will be generated for u_8 and u_9 using (4.33). The sampling time of the process is one day; hence the number of frequencies and samples per period cannot be large to avoid a long decision window for the monitoring process. With that in mind and assuming that none *a priori* information about the plant

is available $n_s = 8$ is chosen; using (4.35) the period is selected as $N_s = 18$ days. Coefficients $\alpha_{[n,j]}$ will be computed via (4.34), λ_n coefficients are computed according to the bounds described in (4.22) and Table 4.1. For phase selection the minimum crest factor method (Guillaume *et al.*, 1991) is used. Simulation results are shown in Fig. 4.12 for $M = 5$ periods.

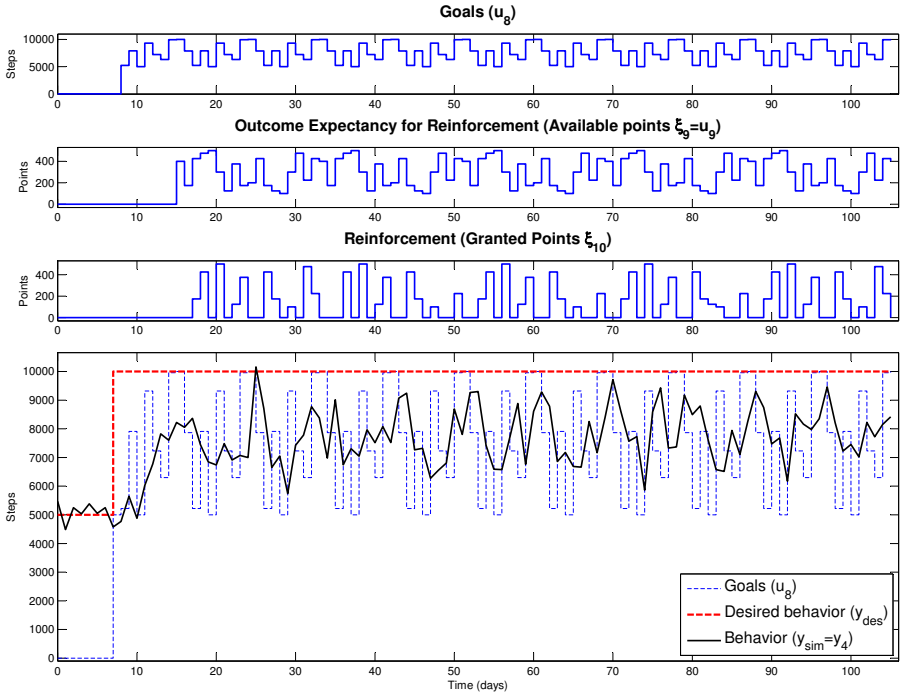

Figure 4.12: Simulation Results Using the "Simulation Plant" and the Designed Multisine With "Zippered" Spectra Signals for M=5 Periods.

Identification data is considered starting from day 15 to allow for transient effects. Uncertainty bounds with 95% of confidence ($\rho = 0.05$) are calculated as was described on Section 4.3.2.1. Fig. 4.13 shows the estimated Nyquist plots for the transfer functions $\hat{G}_{[4,8]}$, $\hat{G}_{[4,9]}$, $\hat{G}_{[5,8]}$, and $\hat{G}_{[5,8]}$ defined in Section 4.3.2.1, where circumferences of radius $\ell^{1-\rho}_{a[m,n]}(\omega^n_i)$ are drawn around each frequency transfer function estimate to illustrate additive uncertainties. One hundred replications of each $\hat{G}_{[m,n]}$ with different

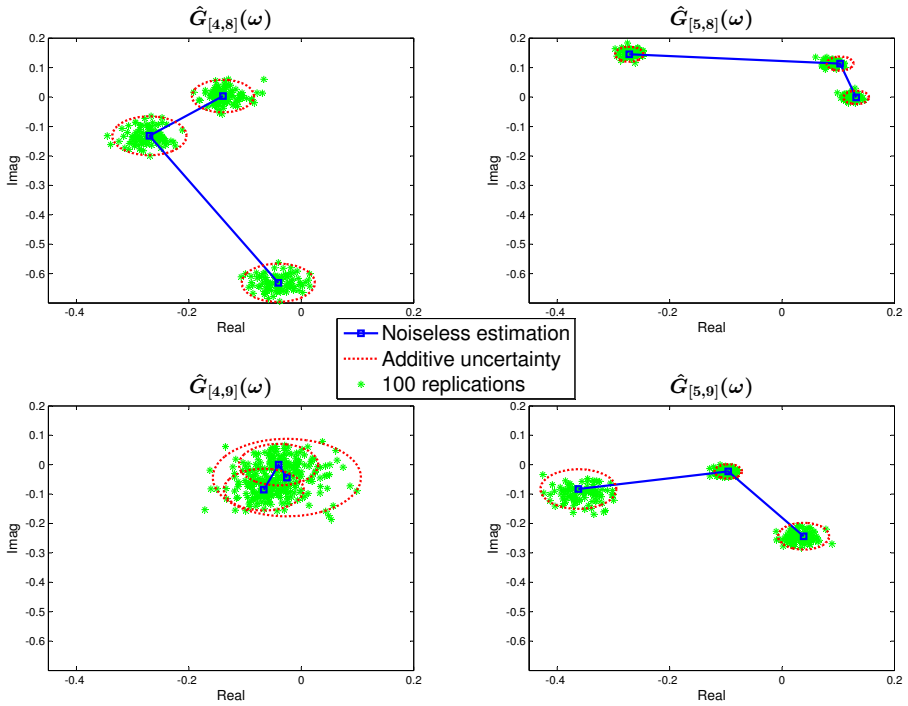

Figure 4.13: Nyquist Plot of $\hat{G}_{[m,n]}(\omega)$ ($n = 8, 9$ and $m = 4, 5$) for $N_s = 18$, $n_s = 8$ and $M = 50$ Periods, With 95% Additive Uncertainty Bounds Drawn as Circumferences Over Each Frequency Estimate and Showing 100 Replications.

noise realizations are plotted to observe the asymptotic properties of the uncertainty estimates for $M = 50$ periods.

For this behavioral intervention the main modeling interest is in the effect of "goal settings" (u_8) to "steps" (y_4), therefore $\boldsymbol{O}$ is defined as:

$$\boldsymbol{O} = \{(4, 8)\} \tag{4.141}$$

To evaluate the monitoring process Fig. 4.14 shows additive uncertainties for an increasing number of periods M. Plots for $\tilde{\ell}_{a[m,n]}(M)$ for the four possible input-output elements are shown with special emphasis in $\tilde{\ell}_{a[4,8]}(M)$. The figure also shows the percentage of fit of the model to the same cross-validation data set used in Section 4.5.1 computed according to (4.136). Percentages of reduction $AV_{[4,8]}(M)$ and $RV_{[4,8]}(M)$

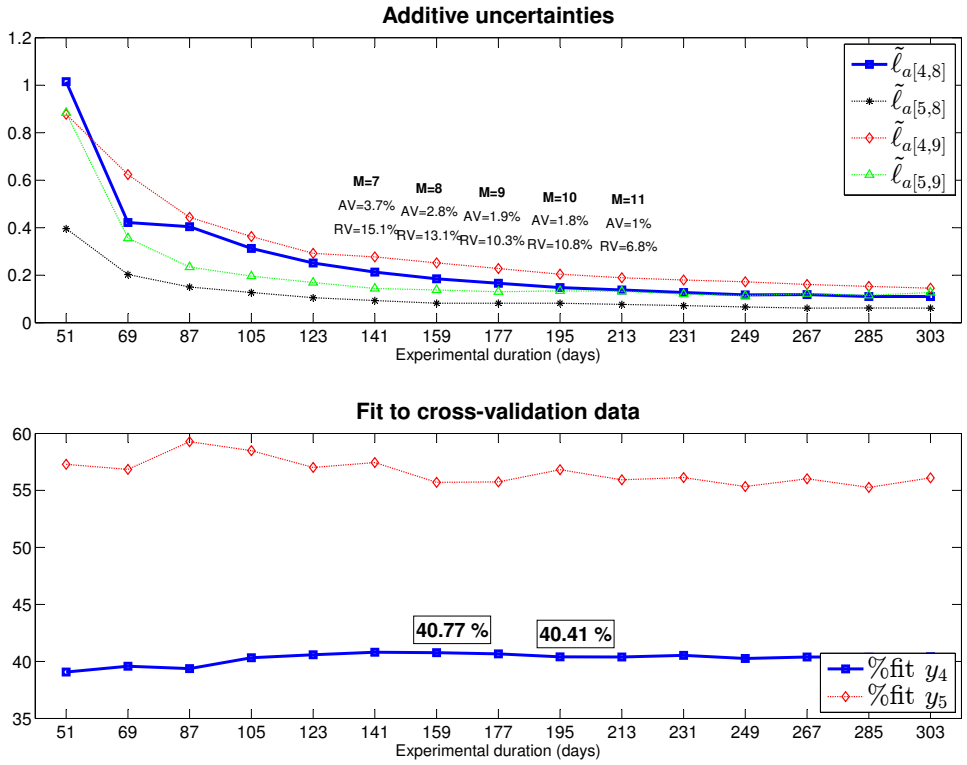

Figure 4.14: Additive Uncertainty Bound Estimates $\tilde{\ell}_{a[m,n]}(M)$ With Percentages of Variation for $M = 3, \ldots, 16$. Percentages of fit to a Cross-Validation Data set for y_4 and y_5 are Also Plotted. Results are Computed Only for the Input/output Direction of Interest $[4, 8]$.

for some values of M are shown in the graphic; a complete list of these values for all the iterations is shown in Table 4.3.

The stopping criterion defined in (4.52) is evaluated considering $B_{AV} = 2\%$, $B_{RV} = 15\%$ and $n_{Mi} = 2$, that are the same values used in Section 3.4; from here it can be concluded that the experiment could be stopped at $M = 10$ with $AV_{[4,8]} = 1.8\%$, $RV_{[4,8]} = 10.8\%$ giving a $\%fit_4 = 40.41\%$ and a total duration of 195 days. If more relaxed bounds are selected (e.g., $B_{AV} = 5\%$), $B_{RV} = 20\%$ and $n_{Mi} = 2$), the monitoring process is stopped at $M = 8$ with $AV_{[4,8]} = 2.8\%$, $RV_{[4,8]} = 13.1\%$, and a

Table 4.3: Monitoring Indexes of the Informative Experiment for the Input/output Direction of Interest $[4, 8]$.

$\boldsymbol{M}$	**3**	**4**	**5**	**6**	**7**	**8**	**9**
$AV_{[4,8]}(\%)$	58.4	1.8	9	6.1	3.7	2.8	1.9
$RV_{[4,8]}(\%)$	58.4	4.3	22.5	19.8	15.1	13.1	10.3
$\boldsymbol{M}$	**10**	**11**	**12**	**13**	**14**	**15**	**16**
$AV_{[4,8]}(\%)$	1.8	1	1.1	1	-0.1	0.8	0
$RV_{[4,8]}(\%)$	10.8	6.8	8	7.9	-0.9	6.8	6

$\%fit_4 = 40.77\%$ with a total duration of 159 days; this indicates, as was mentioned earlier, that by relaxing the bounds shorter experiments are obtained.

To demonstrate the repeatability of the process, Fig. 4.15 shows estimates of $\tilde{\ell}_{a[4,8]}(M)$ and $\%fit_4$ for a set of 10 different realizations of the same output Gaussian noise for y_4 and y_5 with $\sigma_4^2 = 300000$, $\sigma_5^2 = 500$. A reduction tendency in the uncertainty estimation variability, and an increment in the percentage of fit can be observed. The stopping criterion resulting in $M = 8$ and 159 days will give acceptable estimates with higher fits for different noise realizations. In Table 4.3 some negative values are observed in the percentages of uncertainty reduction; these are caused by increments in the additive uncertainty estimation resulting from the randomized nature of the noise signals; however the expected decreasing trend in the uncertainty estimation can be clearly observed in Fig. 4.15.

To evaluate the performance of the uncertainty estimation over different noise conditions, Fig. 4.16 shows plots of the uncertainty estimates for increments on M with 10 replications of two different structures of noise based on an autoregressive

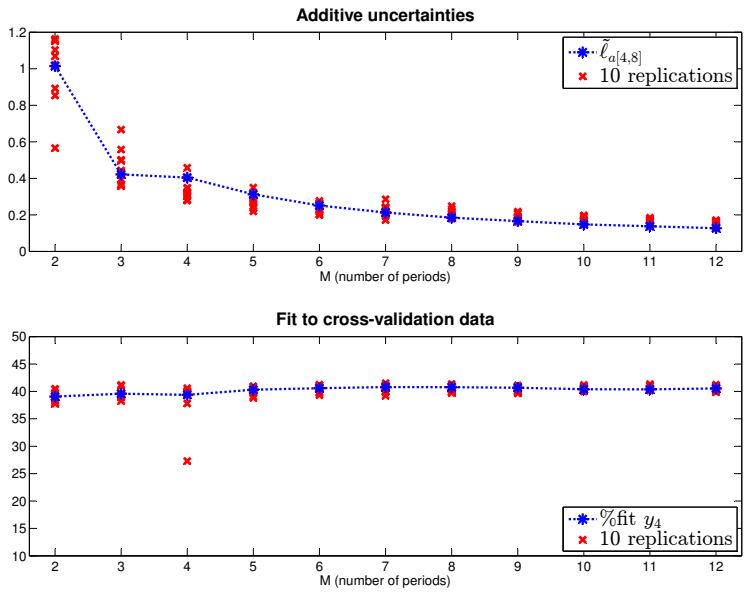

Figure 4.15: Estimates of $\tilde{\ell}_{a[4,8]}(M)$ and $\%fit_4$ for a set of 10 Different Realizations of Output Gaussian Noise $v_4(k)$ and $v_5(k)$ With $\sigma_4^2 = 300000$, $\sigma_5^2 = 500$.

form represented by

$$v_4(k) = \phi v_4(k-1) + a_t, \quad a_t \sim \mathcal{N}(0, \sigma_4^2) \tag{4.142}$$

A more integral representation of noise is obtained when the value of ϕ is closer to 1. Simulations include different realizations of noise, considering only the output y_4 ($v_5(k) = 0$). Considering the noise structure of (4.142), first autoregressive noise is tested with $\sigma_4^2 = 300000$ and $\phi = 0.7$, and then integral noise is also evaluated with $\sigma_4^2 = 300000$, and $\phi = 0.9$. In both cases the asymptotic properties in the uncertainty estimations can be observed. Fits to cross-validation data exhibit more variability than the Gaussian case. In general reducing uncertainty for integral noise is a more difficult task to accomplish, and requires more input power.

Finally, results obtained from the informative experiment derived using the basic monitoring process are used to construct an optimized experiment. The total dura-

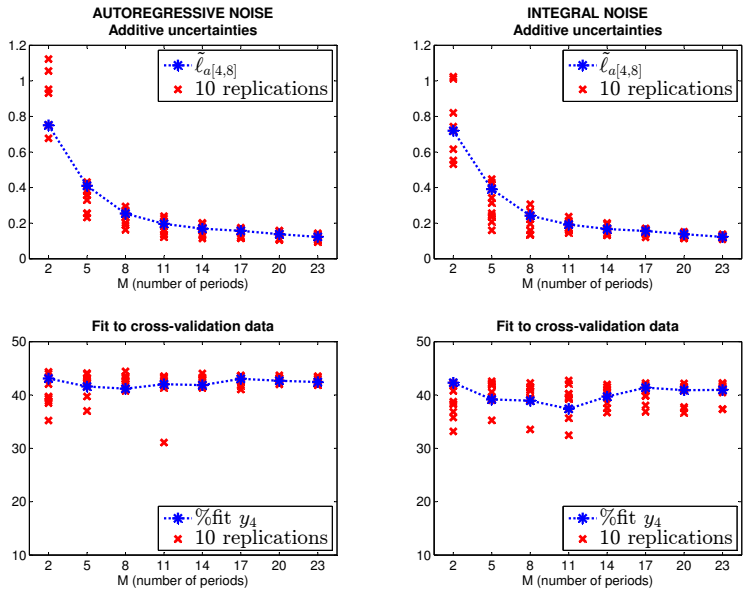

Figure 4.16: Estimates of $\tilde{\ell}_{a[4,8]}(M)$ and $\%fit_4$ for a set of 10 Different Realizations of two Types of Noise for $v_4(k)$: Autoregressive With $\sigma_4^2 = 300000$, $\phi = 0.7$, and Integral With $\sigma_4^2 = 300000$, and $\phi = 0.9$.

tion of the optimized experiment is set for 273 days since there are no guarantees that the new experiment with non-periodic inputs exhibits the same properties on uncertainties compared to the one obtained through the monitoring procedure. The same parameters defined in Section 4.5.1 are used and the obtained input-output signals are shown in Fig. 4.17. The same set of cross-validation data is used and resulting fits are 45.4% for behavior and 60.56% for outcome expectancy; validation plots for both informative and optimized experiments are shown in Fig. 4.18.

The statistical metrics defined in equations (4.137) – (4.140) are computed and shown in Table 4.4. The optimized input signals again show less variability and the output resembles more to the desired output.

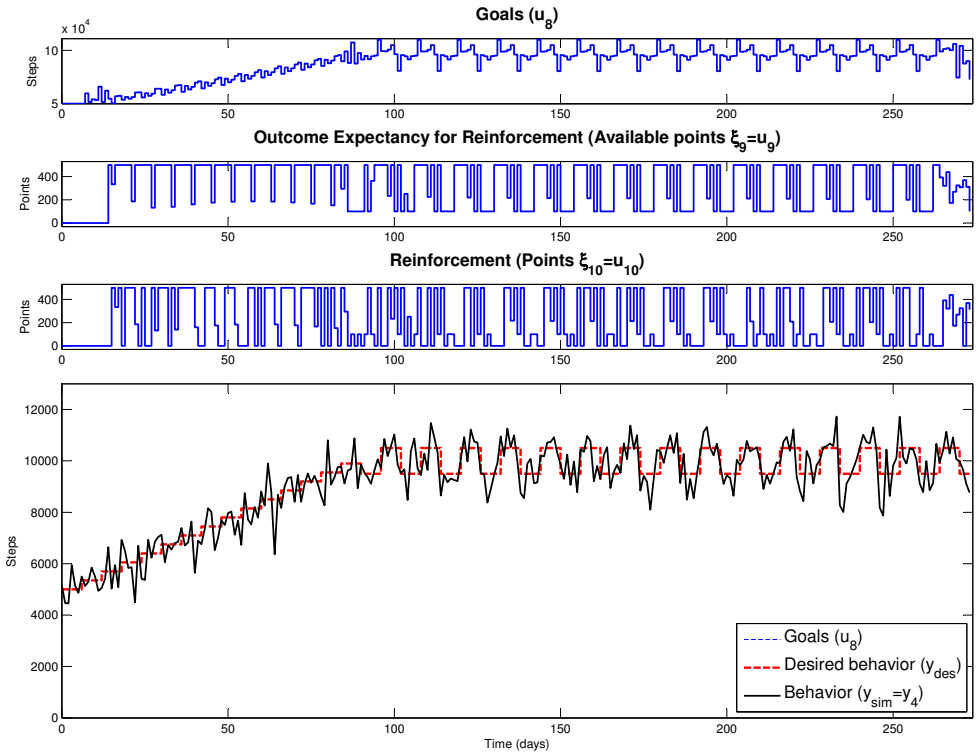

Figure 4.17: Input/output Data for the Optimized Experiment Derived From the Basic Monitoring Procedure.

Table 4.4: Performance Metrics Comparison of Input/output Signals From Informative and Optimized Experiments Resulting From the Basic Monitoring Process.

Metric	**Informative**	**Optimized**
$\overline{\Delta}u_8$ (steps)	2283.4	612.29
$S_{\Delta u_8}$ (steps)	1299.2	572.51
$\overline{\Delta}u_9$ (points)	145.64	153.68
$S_{\Delta u_9}$ (points)	96.96	175.97
$\overline{e}_{sim}$ (steps)	4837.8	3802.6
$S_{e_{sim}}$ (steps)	4768.5	3914.5

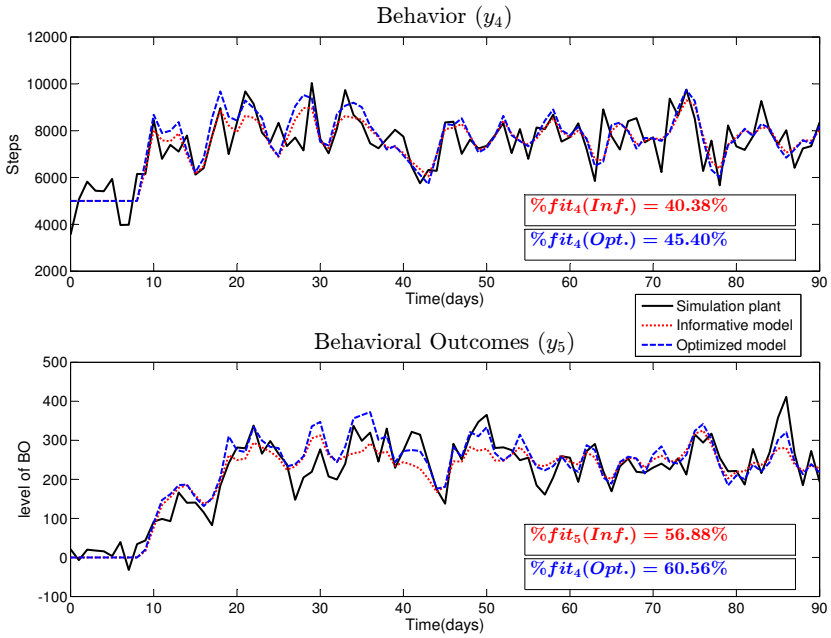

Figure 4.18: Cross-Validation Results Comparing the Simulation Plant With the Identified Model From the Informative and Optimized Experiments Resulting From the Basic Monitoring Process.

4.5.2.2 Enhanced Identification Test Monitoring Procedure

In this section the enhanced identification test monitoring process is tested through a simulation study. Input signals u_8 and u_9 are designed as multisinusoidal elements according to (4.59), and relying on the "zippered" definition of the frequency grid presented in (4.65) for the L different signals in the sequence for each input. The total number of signals in the sequence L depends on the number of implemented changes in the input signal content. Input design parameters are selected using the same criteria of the basic monitoring simulation study, resulting in $n_s = 8$, $N_s = 18$ and λ_n computed to satisfy the conditions described in (4.22) and Table 4.1. Noise conditions are those described at the beginning of Section 4.5.2. Fig. 4.19 shows a simulation of the designed inputs and resultant outputs for $M = 5$ periods of the

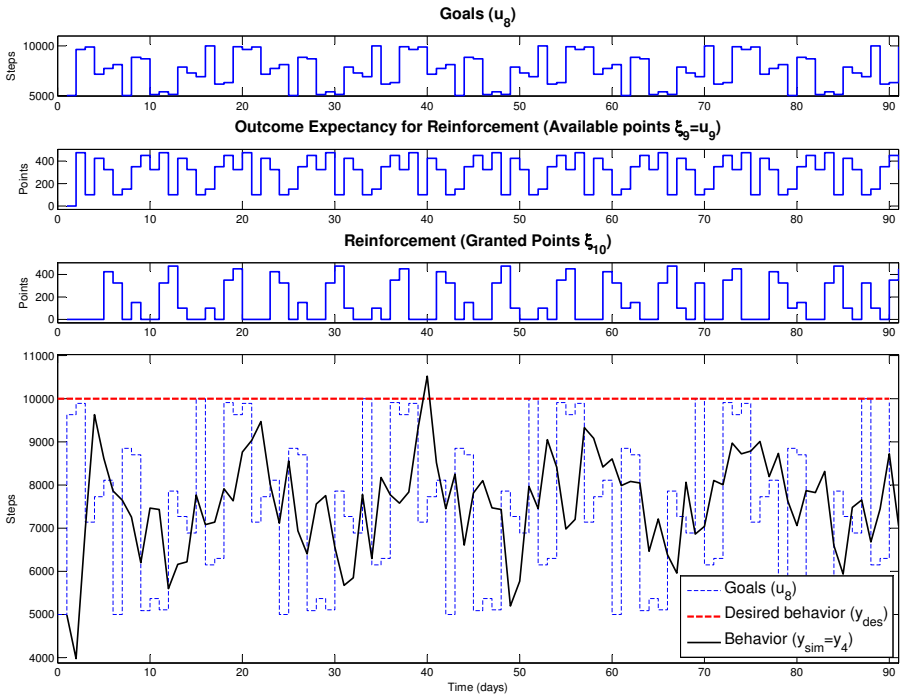

Figure 4.19: Simulation Results Using the "Simulation Plant" and the Designed Multisine With "Zippered" Spectra Signals for M=5 Periods to be Used in the Enhanced Monitoring Process.

same input signals.

Transfer functions and additive uncertainties are computed using the transient LPM approach with 95% of confidence ($\rho = 0.05$) . To test the reliability of these uncertainty computations, Fig. 4.20 shows the additive uncertainties $\ell_{a[m,n]}(\omega_{n,l,i})$ for each input-output element drawn as circular regions centered in the noiseless estimate of the transfer function for each frequency $\omega_{n,l,i}$ of the grid. 100 replications of the estimation process are performed with different realizations of the same Gaussian noise definition.

The enhanced monitoring process is tested initially for the case when only additional periods of the same signal are applied at the end of each cycle, with no changes

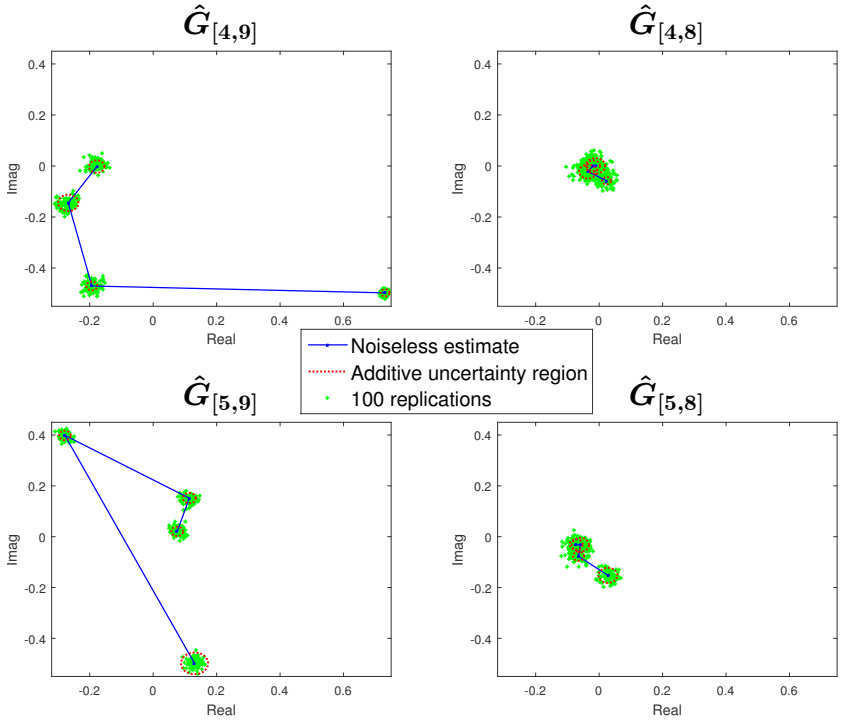

Figure 4.20: Additive Uncertainties $\ell_{a[m,n]}(\omega_{n,l,i})$ Correspondent to Each Frequency Transfer Function Estimate, Drawn as Circular Regions Around Each Noiseless Estimate, With 100 Replications of the Same Gaussian Noise ($\sigma_4^2 = 300000$ and $\sigma_5^2 = 500$) for the Enhanced Monitoring Process.

in amplitude or frequency content. In this case the approximate robust performance index is an accurate estimate ($RPi = \widetilde{RPi}$); hence the stopping criterion based on robust performance metrics is utilized. Assuming that no delays are present, the considered matrices $\boldsymbol{G}_+$, and $\boldsymbol{F}$ in (4.108) are

$$\boldsymbol{G}_+ = \begin{pmatrix} 1 & 0 \\ 0 & 1 \end{pmatrix}, \quad \boldsymbol{F} = \begin{pmatrix} \frac{1}{\lambda_1 s+1} & 0 \\ 0 & \frac{1}{\lambda_2 s+1} \end{pmatrix} \tag{4.143}$$

Values of tuning parameters λ_1 and λ_2 are found by solving

$$\min_{\lambda_1,\lambda_2} \left(\max_{\omega_{n,l,i} \in \boldsymbol{W}_{n,l}} RPi(\omega_{n,l,i}, M_l) \right) \tag{4.144}$$

This is performed through a simple exhaustive search, where each λ_i varies from 10 to 100 with increments of 2 units. For testing purposes, the maximum approximate robust performance index among all frequencies is computed as

$$\widetilde{RPi}_{max}(M) = \max_{\omega_{n,i} \in \boldsymbol{W}_{n,l_{agg}}} \widetilde{RPi}(\omega_{n,i}, M) \tag{4.145}$$

Results are shown in Fig. 4.21 where the stopping criterion from (4.111) is accomplished after $M = 12$ cycles with a duration of 216 days and a cross-validation fit of 39.25%.

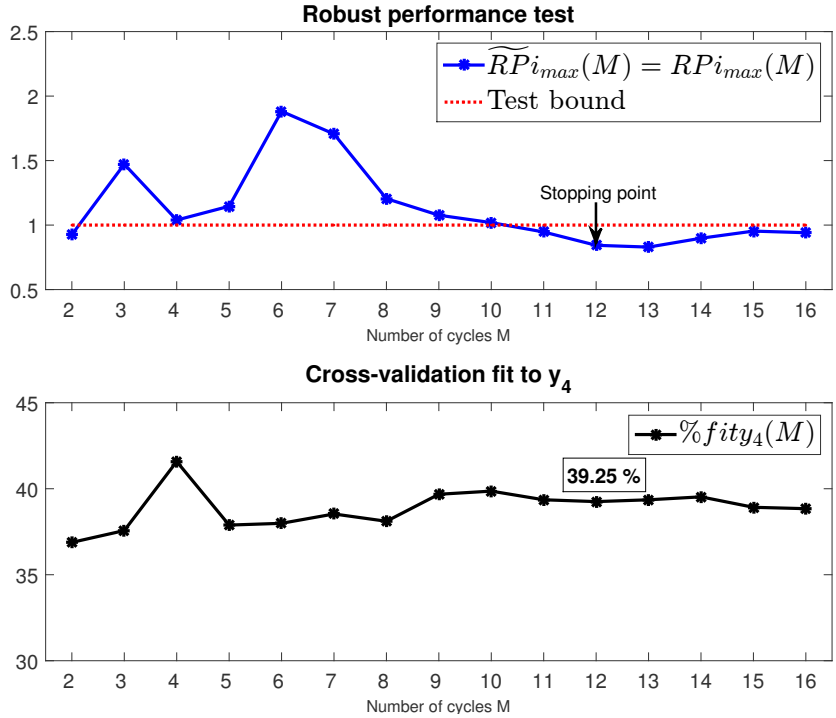

Figure 4.21: Evaluation of the Enhanced Identification Test Monitoring Process for a Simulation Plant With no Changes in the Amplitude and/or Frequency Content of the Input Signals, at Each Cycle $M = 1, \cdots, 16$.

The method is tested for the two different types of modifications on the input signal content: higher amplitude, and different harmonic related frequency content, under

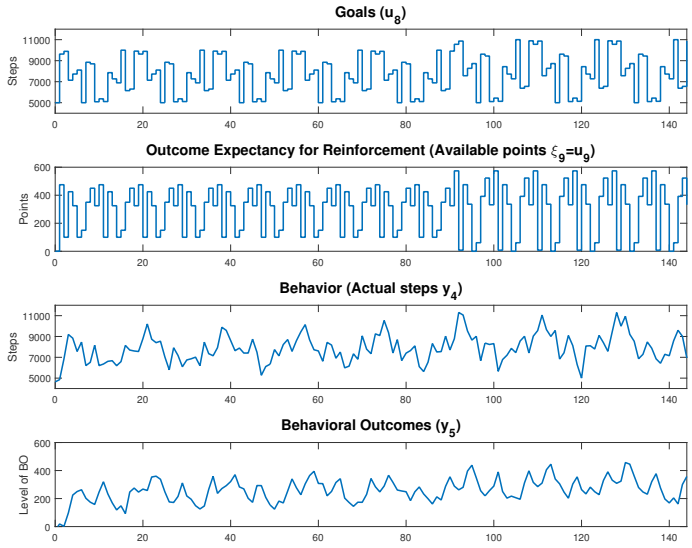

(a) Increase on the Amplitude.

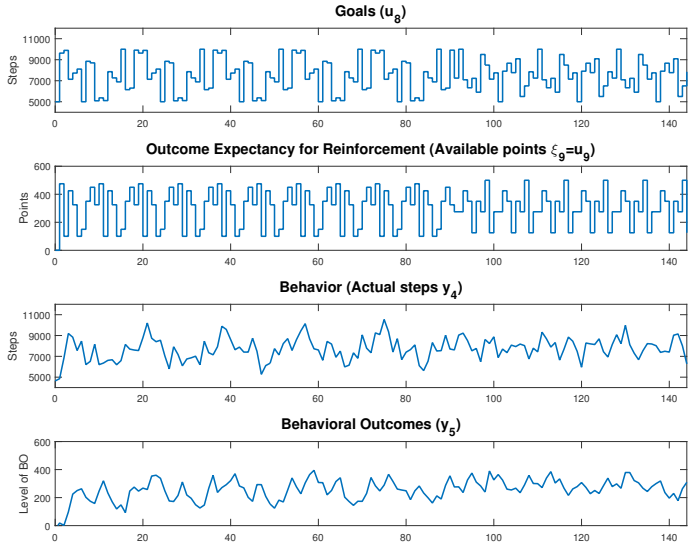

(b) Change on the Frequency Content.

Figure 4.22: Illustration of the Different Types of Changes in the Inputs Signal Content for the Enhanced Monitoring Method After $M = 5$ Cycles With a Total of $M = 8$ Cycles.

realistic constraints. The first case represents an increase in the amplitude of the input signals after $M = 5$ cycles. The maximum daily goal is incremented to 11000 steps per day, the minimum number of available points is now 0 and the maximum number of points is increased to 600 as is illustrated in Fig. 4.22a for a total of $M = 8$ cycles. The second case represents a change on the harmonic related frequency content of the inputs signals. For both inputs the consider harmonic reduction step after $M = 5$ cycles is from $S_{h,1} = 0$ to $S_{h,2} = 1$ for $L = 2$, as was defined in (4.64) – (4.66). A simulation of the input-output signals for $M = 8$ cycles is shown in Fig. 4.22b.

Monitoring results are presented in Fig. 4.23 for the two mentioned cases and the initial case with no modifications in the signals. The first plot represents the maximum additive uncertainty $\tilde{\epsilon}(M)$ as is computed in (4.104). The second plot presents computations of the approximate robust performance index and its respective test according to (4.110) – (4.111), and the third plot presents again fits to a different cross-validation data set.

The increment on amplitude represents the best improvement for identification purposes. The maximum additive uncertainty is reduced and the robust performance test is now accomplished after $M = 8$ cycles. Checking cross-validation results it can be observed that percentage fits increase at higher rates and they reach the desired values faster. If the stopping criterion from (4.107) is now considered with $B_{AV} = 2\%$, $B_{RV} = 15\%$, and $n_{Mi} = 2$ the experiment can be halt after $M = 11$ cycles as is shown in Table 4.5.

When modifications in the harmonic frequency content of the input signals are implemented, improvements on identification results are also observed. Now the robust performance test indicates that the experiment can stop after $M = 9$ cycles, with better percentages of fit. Also the stopping criterion from (4.107) considering $B_{AV} = 2\%$, $B_{RV} = 15\%$, and $n_{Mi} = 2$ indicates that the experiment can be halted

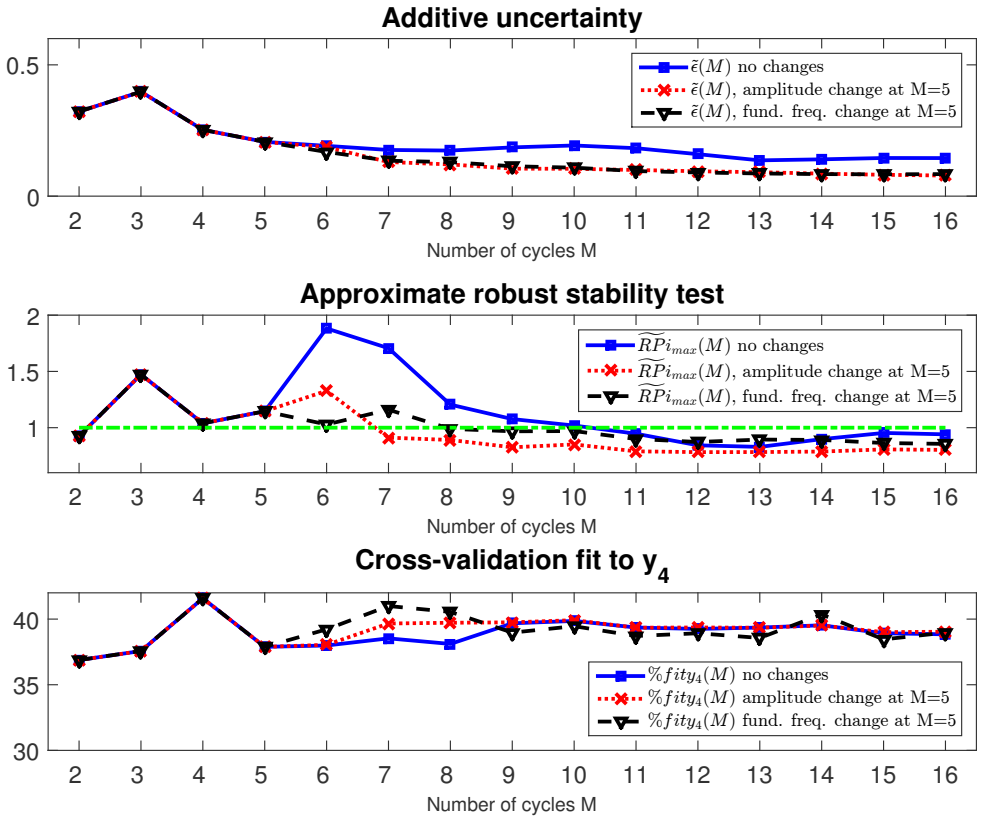

Figure 4.23: Illustration of the Enhanced Identification Test Monitoring Method, Testing all the Possible Actions Over the Input Signals After $M = 5$ Cycles: no Changes, Increments on the Amplitude, and Changes on the Harmonic Related Frequencies for $M = 1, \cdots, 16$.

after $M = 13$ cycles as is detailed in Table 4.6. The stopping criterion based on percentage uncertainty reductions is more conservative since it computes a MIMO metric based on singular values, and it uses the maximum value over all the frequency grid.

The performance of the process is tested now utilizing 10 replications of different noise structures: The original Gaussian noise with $\sigma_4^2 = 300000$, $\sigma_5^2 = 500$, and the autoregressive structure of (4.142). Initially the pure autoregressive case is considered

Table 4.5: Percentages of Uncertainty Reduction According to (4.105) – (4.106) for Increments on the Amplitude of the Input Signals.

$\boldsymbol{M}$	**3**	**4**	**5**	**6**	**7**	**8**	**9**
$AV(\%)$	-23.39	44.97	14.27	6.32	17.5	2.85	5
$RV(\%)$	-23.39	36.44	18.2	9.85	30.26	7.07	13.34
$\boldsymbol{M}$	**10**	**11**	**12**	**13**	**14**	**15**	**16**
$AV(\%)$	0.16	1.39	1.52	1.11	1.71	1.36	0.9
$RV(\%)$	0.5	4.31	4.92	3.76	6.03	5.1	3.55

Table 4.6: Percentages of Uncertainty Reduction According to (4.105) – (4.106) for Changes on the Frequency Content of the Input Signals.

$\boldsymbol{M}$	**3**	**4**	**5**	**6**	**7**	**8**	**9**
$AV(\%)$	-23.39	44.97	14.27	11.93	10.35	1.67	4.86
$RV(\%)$	-23.39	36.44	18.2	18.6	19.81	3.98	12.08
$\boldsymbol{M}$	**10**	**11**	**12**	**13**	**14**	**15**	**16**
$AV(\%)$	1.69	4.04	1.66	1.16	0.76	0.24	-0.25
$RV(\%)$	4.79	11.99	5.59	4.15	2.84	0.93	-0.98

with $\sigma_4^2 = 300000$ and $\phi = 0.7$, then a more integral noise configuration with $\sigma_4^2 = 300000$, and $\phi = 0.9$ is applied. Results are shown in Fig. 4.24a and Fig. 4.24b. For all cases the robust performance test is eventually accomplished after some iterations. The percentage fits are more variable for the autoregressive and integral cases that demand more power from the inputs.

With the obtained informative model utilizing $M = 12$ cycles, the optimized experiment is implemented again with a fixed duration of 273 days. The obtained inputs and the resultant simulated outputs are shown in Fig. 4.25. The same set of cross-validation data is used and resulting fits are 42.41% for behavior and 64.65% for outcome expectancy; validation plots for both informative and optimized experiments are shown in Fig. 4.26.

Patient-friendlessness indexes from inputs-output data are again computed an tabulated in Table 4.7 according to equations (4.137) – (4.140). Once again improvements resulting from the optimized experiment can be observed in percentage fits and in the reduced variability of input-output data.

4.6 Chapter Summary

In this chapter a system identification procedure has been described which includes both experimental (input signal) design and grey-box (semi-physical) parameter estimation for a physical activity intervention described by a dynamical systems model for Social Cognitive Theory (SCT). Input signal design is performed in two stages: one called the informative where signals are designed using either a randomized technique or an identification test monitoring process, and an optimized experiment where signals are designed to improve the response of the intervention from a behavioral standpoint, and to obtain an acceptable model for the system.

In the informative stage different input signal design strategies were presented.

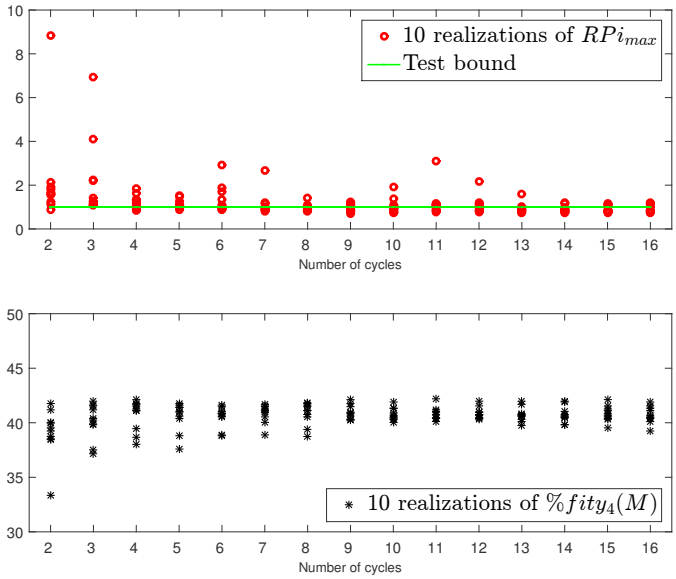

(a) Gaussian Noise.

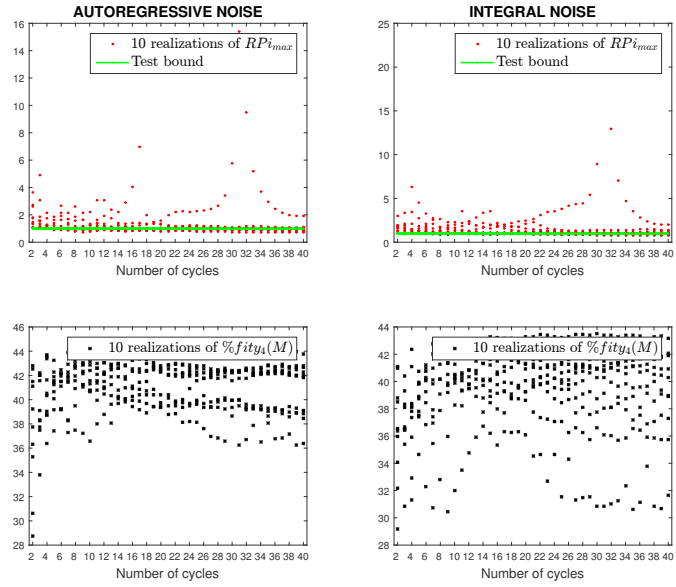

(b) Autoregressive and Integral Noise.

Figure 4.24: Ten Replications of the Enhanced Monitoring Process for Different Noise Structures, Including Gaussian With $\sigma_4^2 = 300000$, $\sigma_5^2 = 500$, Autoregressive With $\sigma_4^2 = 300000$ and $\phi = 0.7$, and Integral With $\sigma_4^2 = 300000$, and $\phi = 0.9$.

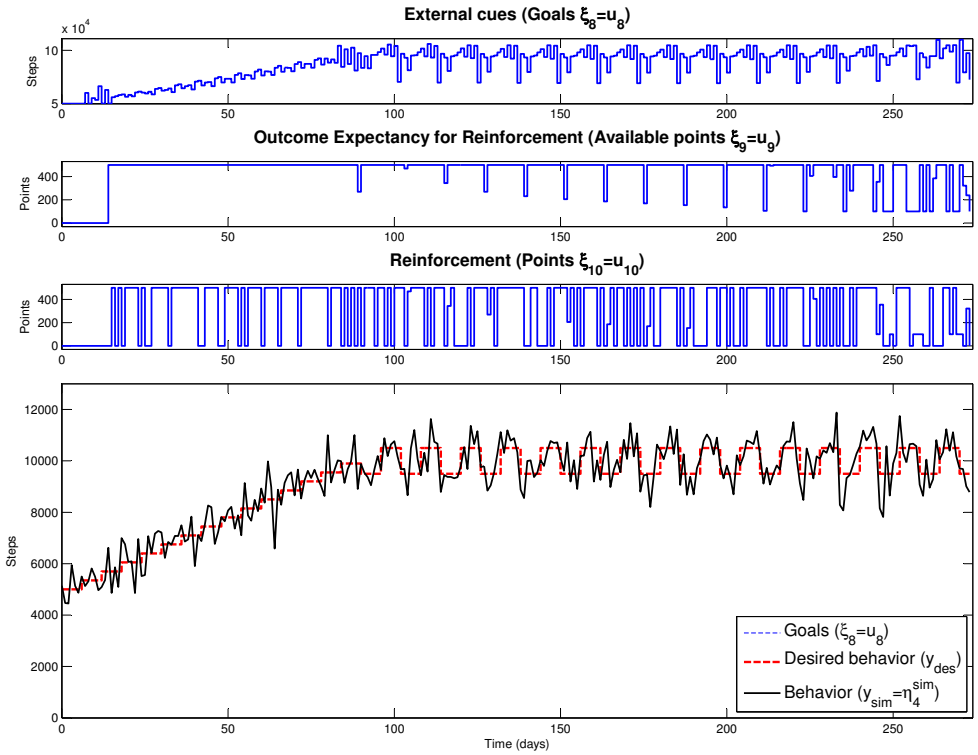

Figure 4.25: Input/output Data for the Optimized Experiment Derived From the Enhanced Monitoring Process.

Table 4.7: Performance Metrics Comparison of Input/output Signals From Informative and Optimized Experiments Resulting From the Enhanced Monitoring Process.

Metric	**Informative**	**Optimized**
$\overline{\Delta}u_8$ (steps)	1684.6	958.72
$S_{\Delta u_8}$ (steps)	1534.7	934.57
$\overline{\Delta}u_9$ (points)	184.84	54.526
$S_{\Delta u_9}$ (points)	104.85	124.16
$\overline{e}_{sim}$ (steps)	4810.6	3681.8
$S_{e_{sim}}$ (steps)	4748.4	3787

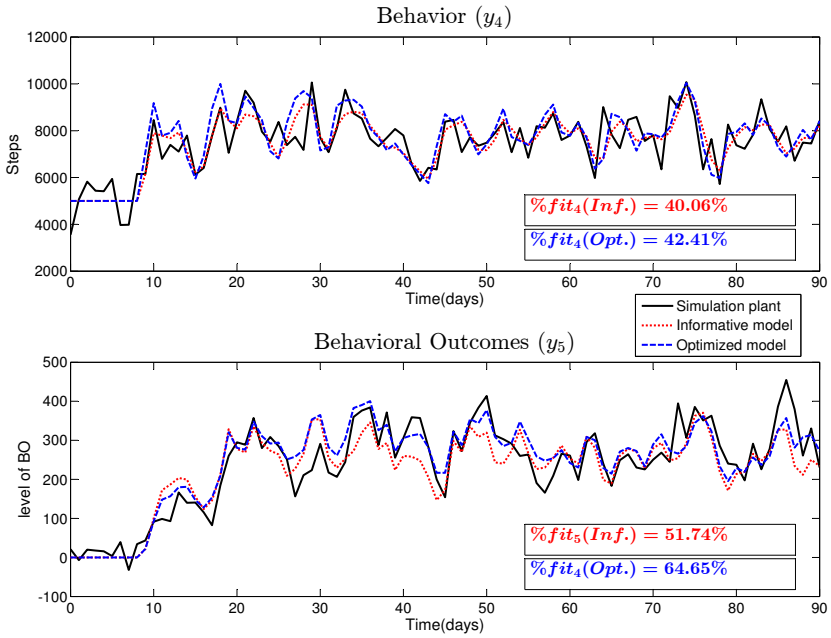

Figure 4.26: Cross-Validation Results Comparing the Simulation Plant With the Identified Model From the Informative and Optimized Experiments Resulting From the Enhanced Monitoring Process.

First a fixed time randomized generation of input signals subject to operational amplitude constraints. As a second alternative, a monitoring approach is designed to find the shortest possible experiment that is "good enough" for identification purposes; this was done through the computation of asymptotic statistical uncertainties that are accurate for a large number of periods M, and conservative otherwise. Initially a basic monitoring procedure was proposed where an evaluation of the signal quality is performed every period yielding to the decision to halt the experiment or to aggregate an additional period of the same signal. This transfer function based estimation procedure enabled the specification of input-output directions of interest for the identification problem. Finally and enhanced monitoring method is presented which incorporates the possibility to perform changes in the amplitude or in the har-

monic frequency content of the input signals. The proposed experimental stopping criterion relies on robust performance ideas. For the optimized experiment it was shown that the design of the required inputs within practical operating limitations can be formulated as a feasible constrained optimization problem.

Independent simulation studies are presented for each input signal design approach. For the fixed time case, an acceptable percentage of fit can be observed, even in the presence of external disturbances. In the informative experiment a set of data exhibiting high variability is obtained (Fig. 4.8); in the optimized experiment the variability in the data is reduced (Fig. 4.10) while obtaining a model that displays a higher level of predictive ability. It is important to highlight the fact that the input/output signals from the optimized experiment showed a better performance in terms of "patient-friendliness" and desired behavior tracking, as could be observed in Table 4.2. The resultant behavior from the optimized experiment strongly depends on the initial results from the informative stage. If the informative estimation results are biased then the optimized output is also expected to be biased, however if the informative experiment succeeds in predicting the variability of the system, a pattern similar to the desired one is expected in the optimized output.

For the basic monitoring process input magnitudes were held constant while the length of the experiment was under periodic evaluation. The simulation study considered the simultaneous effect of noise in all the measured outputs and the presence of disturbance inputs, to resemble a more realistic situation. Simulation results illustrated how by applying the monitoring process, a shorter informative experiment could be defined that still captures the dynamics of the system. Acceptable fits could be obtained (Fig. 4.18) and again good signals in terms of "patient-friendliness" were derived in the optimized stage as is observed in Table 4.4.

Finally the enhanced monitoring process is simulated considering two possible

additional modifications in the input signal content after each periodic evaluation: increments in the amplitude, and changes in the harmonic related frequency content. The proposed stopping criterion incorporates robust performance ideas; however if one of the specified modifications on the input signal content is applied, then a more general criterion based on percentage change of MIMO additive uncertainties can be used. Fig. 4.27 shows a comparison between the basic and the enhanced MIMO uncertainty computation index $\tilde{\epsilon}(M)$ using (4.56) and (4.104), considering the same "zippered" input signal. As expected the enhanced method provides a more conservative measurement of uncertainties; both methods present similar uncertainty reduction tendencies when the length of the experiment is increasing. One advantage of the enhanced method is that it does not require to wait until the signal has reached its steady state; hence the evaluation can be started earlier. The use of the enhanced method also enables the possibility of on-the-go modifications in the input signal content.

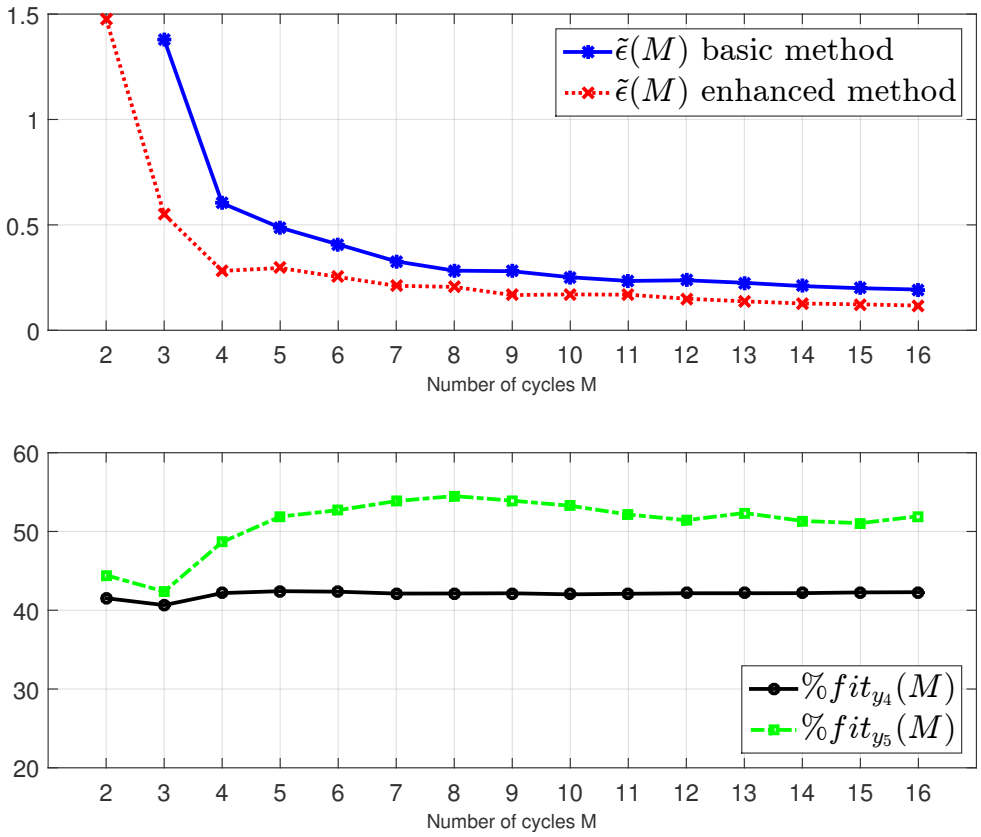

Figure 4.27: Comparison Between the Computed MIMO Additive Uncertainties $\tilde{\epsilon}(M)$ for the Basic and Enhanced Monitoring Procedures Applied Over the Same Input Signals.

Chapter 5

DESIGN OF CLOSED-LOOP BEHAVIORAL INTERVENTIONS USING HYBRID MODEL PREDICTIVE CONTROL

5.1 Overview

A variety of serious health conditions, among them breast and colon cancer, obesity, diabetes, and cardiovascular disease, are linked to physical inactivity (McGinnis *et al.*, 2002). For breast cancer in particular, estimates suggest that the risk of developing this disease can be reduced by 20-30% by engaging in 30-60 minutes of moderate-intensity physical activity (PA) per day (Clague and Bernstein, 2012). However, most researcher-developed mHealth PA interventions have only been evaluated in short-term pilots (e.g., 4 weeks to 6 months) with modest effects (Payne *et al.*, 2015) and require an assessment of their effectiveness under real-world conditions that include maintenance. There is a need for interventions that can cost-effectively scale, adapt to each person's changing needs, and provide support as long as needed. Most evidence-based PA interventions are delivered by a person, thus limiting scalability, data-driven adaptability, and long-term use (Marcus *et al.*, 2006). Almost all interventions, including digital ones, are designed for fixed durations, which is problematic when circumstances, health conditions, or goals change. Previous evidence supports the notion that PA is a highly variable behavior, with the general trend of individuals moving towards less PA (Rauner *et al.*, 2015). There is a need for interventions that provide treatment when necessary, quietly monitor when not needed, and re-emerge when a relapse is imminent.

In previous chapters a dynamical model for Social Cognitive Theory (SCT) (Ban-

dura, 1986) was developed using fluid analogies to represent the different constructs of the theory and their interactions. Using an open-loop PA intervention as a reference, a set of system identification experiments at an idiographic (i.e., single subject) level have been designed to search and refine the model parameters and for validation purposes. Relying on these ideas a pilot mHealth intervention called "Just Walk" is currently being tested (Hekler, 2015), this intervention provides daily "ambitious but doable" step goals and reinforcements (i.e., points) for achieving goals.

In this chapter, the purpose is to develop a decision algorithm for a closed-loop mHealth Intensively Adaptive Intervention (IAI; Riley *et al.* (2015b)) to promote PA (measured in terms of daily steps) among sedentary adults. To achieve successful outcomes of the intervention in the long term, two phases are included: a behavioral initiation training stage where individuals are progressively driven to a healthy status through the introduction of daily step goals and rewards, and a maintenance training phase where rewards are gradually decreased based on the enhanced capacity of individuals to continuing engaging in the required behavior. The decision framework for the intervention relies on a Hybrid Model Predictive Control (HMPC) formulation (Nandola and Rivera, 2013); in general model predictive controllers have proved their effectiveness on multivariable problems with operational constraints in diverse application areas. HMPC-based solutions have recently been considered in behavioral health settings (Deshpande *et al.*, 2014a; Dong *et al.*, 2013; Timms *et al.*, 2014d). As the basis for decision policies, they enable optimization of intervention dosages in the presence of interaction between continuous and discrete signals that are commonplace in behavioral interventions.

The HMPC-based decision policy presented here relies on a mixed logical dynamical (MLD) framework to describe discrete sets of goals and rewards as the intervention components. It is also used to represent the logical process of awarding rewards only

if daily goals are achieved. The formulation employs a three degree-of-freedom modality to independently adjust the speeds of set-point tracking, measured disturbance rejection and unmeasured disturbance rejection. Controller reconfiguration through the manipulation of penalty weights is proposed to address the transition between the initiation and maintenance phases. Simulation results showing a hypothetical scenario for a PA intervention are presented to illustrate the benefits of the proposed approach in addressing the hybrid nature of the system, set point tracking, disturbance rejection, and the transition between the two stages of the intervention.

This chapter is organized as follows. Section 5.2 describes the different components and conditions of the intervention. Section 5.3 presents details about the formulation of the HMPC based adaptive intervention, including the discrete and logical constraints and the controller reconfiguration to support the maintenance stage. Section 5.4 presents a simulation study to test the performance of the controller under conditions of disturbances. Section 5.5 gives a summary and conclusions of the chapter.

5.2 Adaptive Closed-Loop Behavioral Intervention Based on SCT

The main purpose of the proposed intervention is to promote physical activity among sedentary individuals, with the specific goal of achieving 10,000 steps per day (or +3,000 steps/day more than baseline) on a weekly average. The goal will be reached via the design and implementation of an effective intervention for behavior change that is theoretically grounded on Social Cognitive Theory (SCT) (Bandura, 1986). In Chapter 4 a dynamical model of SCT for the low physical activity problem was developed relying on a fluid analogy that depicts the constructs and their interrelationships described by the theory. As in the open-loop case, the closed-loop intervention relies on the simplified version of the SCT model representing a "be-

haviorist" articulation of the determinants of behavior (Ferster, 1970), depicted in Fig. 4.1. Assuming first order dynamics, the model is described by the set of differential equations (4.1) – (4.5).

The proposed closed-loop behavioral adaptive intervention is depicted in Fig. 5.1, where the amount of performed daily steps is measured by the signal y_4. It relies on the systematic delivery of the following components, based on the actual performance of individuals:

- *Daily goals* u_8, to establish in a quantitative form the desired behavior (e.g., $10,000$ steps per day).

- *Expected points* u_9, the announced daily reward points that will be granted to individuals if they achieve the daily goal.

- *Granted points* u_{10}, given every day if individuals reach the set goal; this feature is represented by the "If/Then" block. Points can later be exchanged for tangible rewards (e.g., gift cards).

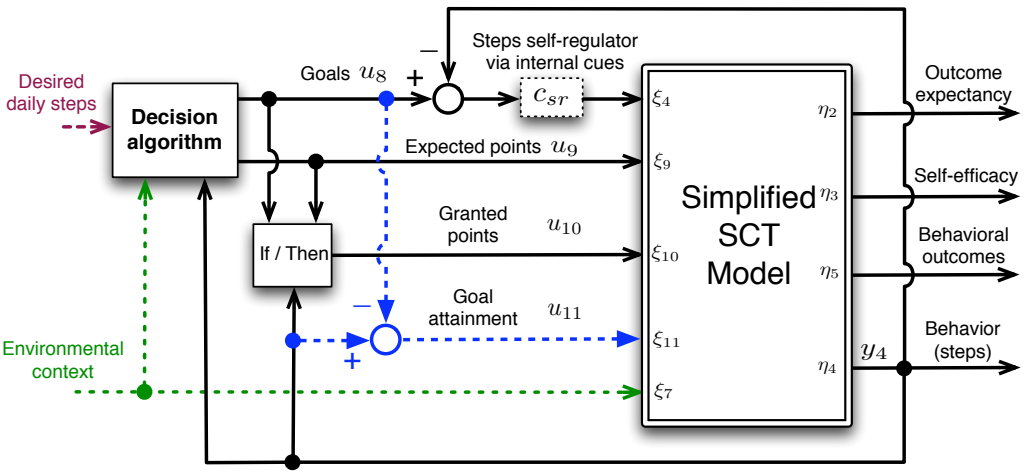

Figure 5.1: Conceptual Representation of the Closed-Loop Behavioral Adaptive Intervention, Based on the Simplified Version of the SCT Model in Fig. 4.1

The intervention is implemented using an SCT model enhanced with individualized self-regulation via internalized cues as was described in Section 4.2.2. Relying on the internal model control approach (IMC; Morari and Zafiriou (1989)) the self-regulator is represented in a classical feedback controller form as

$$c_{sr} = \frac{q_{sr}}{1 - \tilde{p}_{44} q_{sr}} = \frac{K_{sr}}{\beta_{46}\gamma_{64}} \cdot \frac{\tau_4 s + 1}{\lambda s + 1 - K_{sr}} \tag{5.1}$$

where β_{46}, γ_{64}, and τ_4 are part of the SCT model parameters, the transfer function $\tilde{p}_{44}$ represents the effect from input ξ_4 to output η_4, and q_{sr} is the self-regulator expressed in q-parametrization form. The performance of the system is characterized by the value of the parameter λ that reflects the closed-loop speed of response and the parameter K_{sr} that ranges from 0 to 1, with 1 representing perfect integral action.

The signal *goal attainment* (u_{11}) is computed as the difference between the daily goal and the actual performed behavior, affecting *self-efficacy*. This signal is used to represent the ideal step-goal range feature presented in Section 2.7.2, where individuals might react negatively to too high a goal that they consider difficult to reach.

5.3 Formulation of the HMPC-Based Adaptive Intervention

The purpose of the adaptive intervention is to have individuals achieve a desired level of daily steps, while considering some important physical and operational constraints such as:

- Maximum and minimum values for goals and points (u_8, u_9 and u_{10}) depending on physical conditions (e.g., maximum and minimum daily step goals for an individual). Financial limitations lead to bounds on the expected reward points, since these have a direct conversion into monetary value.

- Goals and reward points must be drawn from discrete sets of integer values that

may represent meaningful effects on the intervention. As prior physical activity experiments have pointed (King *et al.*, 2013; Adams *et al.*, 2013) having a fixed set of goals and points could be important to analyze specific aspects of interest on the intervention.

- The intervention may be configured in different stages where some of the inputs may be deactivated or partially activated. For instance, when the behavior has reached the desired level and is successfully sustained, a gradual decrease on rewards may be activated.

The ensuing subsections describe the detailed formulation of the HMPC-based decision policy.

5.3.1 Use of the HMPC framework

The control strategy for intervention design must incorporate the defined requirements and constraints for the physical activity behavioral intervention. A Hybrid Model Predictive Control strategy (HMPC; Nandola and Rivera (2013)) will be further studied and applied to this problem since it incorporates hybrid dynamics through mixed logical dynamical (MLD) representations (Bemporad and Morari, 1999); this feature can be used to represent the natural constraints of the problem. Hybrid dynamical systems consider discrete and continuous events simultaneously; they can be represented by differential (or difference) equations and logical conditions describing their categorical or binary response. The aim of the control design will be directed to the following tasks:

- **Setpoint tracking:** Goals and expected reward points are assigned to obtain the desired amount of daily steps following continuous and discrete constraints.

- **Measured disturbance rejection:** The controller manipulates goals and expected points to mitigate the effect from measured external disturbances (e.g., *environmental context*) using the subsection of the identified SCT model that is related to those signals. For instance if some environmental event (e.g., bad weather) is known *a priori*, then goals or rewards can be adjusted to compensate for that disturbance.

- **Unmeasured disturbance rejection:** Inputs are manipulated to mitigate the effect of unknown and possibly unmodeled external influences. For example, any unexpected situation that may impact the disposition of the individual for physical activity (e.g., sickness of a family member, sudden party invitation) can be mitigated by adjustments on goals or points by the controller.

Model predictive control (MPC; Camacho and Bordons (2004)) is a controller formulation where the current values of the manipulated variables (i.e., inputs) are determined in real time as the solution of an optimal control problem over a horizon of given length. The optimization problem is solved for a move horizon using a model (e.g., the identified SCT model) from where a new set of control moves are obtained; outputs from the system are then computed over the prediction horizon with the current plant state estimate (i.e., output measurement) assumed as the initial state. Only the first calculated moves are applied at each instant; the whole process is then repeated and new control moves are obtained. This receding horizon control strategy is depicted in Fig. 5.2 considering *set goals* (u_8) as the manipulated variable, *actual steps* (y_4) as the controlled variable, and *environmental context* (d_7) as measured disturbance.

The HMPC controller relies on the MLD structure that describes a hybrid linear system including real and integer states, inputs and constraints, and is represented

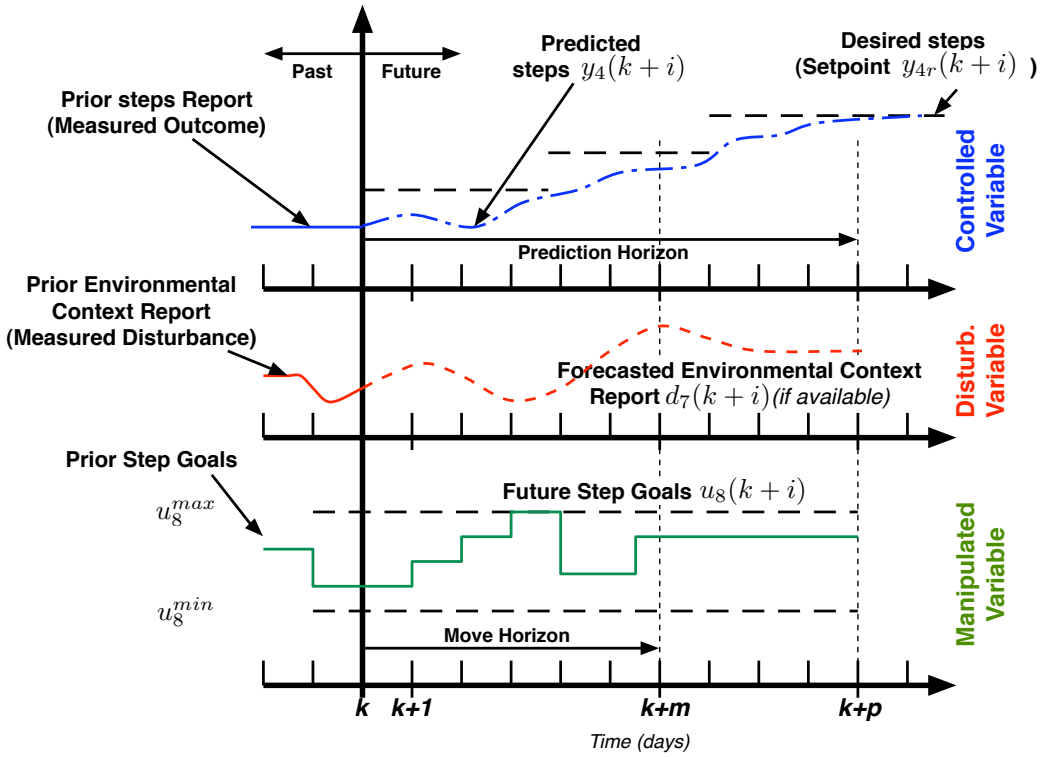

Figure 5.2: Conceptual Application of the Receding Horizon Control Strategy to the Physical Activity Behavioral Problem Considering Step Goals (u_8) as the Input, Actual Steps (y_4) as the Output, and Environmental Context (d_7) as Measured Disturbance.

as

$$x(k+1) = Ax(k) + B_1u(k) + B_2\delta(k) + B_3z(k) + B_dd(k) \tag{5.2}$$

$$y(k+1) = Cx(k+1) + d'(k+1) + v(k+1) \tag{5.3}$$

$$E_2\delta(k) \leq E_5 + E_4y(k) + E_1u(k) - E_3z(k) - E_dd(k) \tag{5.4}$$

where in general $x = [x_c^T \quad x_d^T]^T, x_c \in \mathbb{R}^{n_x^c}, x_d \in \{0,1\}^{n_x^d}$, and $u = [u_c^T \quad u_d^T]^T, u_c \in \mathbb{R}^{n_u^c}, u_d \in \{0,1\}^{n_u^d}$ are systems states and inputs with continuous and discrete elements; $y \in \mathbb{R}^{n_y}$ is the vector of outputs; d, d', and v are measured disturbances,

unmeasured disturbances, and measurement noise respectively. $\delta \in \{0,1\}^{n_\delta}$ and $z \in \mathbb{R}^{n_z}$ are discrete and continuous auxiliary variables that are introduced in order to convert logical and discrete decisions into their equivalent linear inequality constraints represented in (5.4). Variables $n_x = n_x^c + n_x^d$, $n_u = n_u^c + n_u^d$, n_{dist}, and n_y are the total number of states, inputs, measured disturbances, and outputs, respectively. Dimensions of auxiliary variables and the number of linear constraints in (5.4) depend on the specific character of the discrete and logical decisions in the particular hybrid system.

A standard quadratic cost function is used to calculate the decision vector for the optimization problem as

$$\begin{aligned} J \triangleq & \sum_{i=1}^{p} \|y(k+i) - y_r\|_{Q_y}^2 + \sum_{i=0}^{m-1} \|\Delta u(k+i)\|_{Q_{\Delta u}}^2 + \sum_{i=0}^{m-1} \|u(k+i) - u_r\|_{Q_u}^2 \\ & + \sum_{i=0}^{p-1} \|\delta(k+i) - \delta_r\|_{Q_\delta}^2 + \sum_{i=0}^{p-1} \|z(k+i) - z_r\|_{Q_z}^2 \end{aligned} \tag{5.5}$$

where p is the prediction horizon, m is the control (or move) horizon. The matrices $Q_y, Q_{\Delta u}, Q_u, Q_\delta$, and Q_z are the penalty weights on the error, move size, control signal, auxiliary binary variables, and auxiliary continuous variables respectively. The weighted norm of a vector $r = [r_1 \cdots r_n]^T$ can be defined as:

$$\|r\|_{Q_r}^2 = r^T \cdot Q_r \cdot r \tag{5.6}$$

$$\text{with} \quad Q_r = \begin{pmatrix} w_{r_1} & 0 & \cdots & 0 \\ 0 & w_{r_2} & \cdots & 0 \\ \vdots & \vdots & \ddots & \vdots \\ 0 & 0 & \cdots & w_{r_n} \end{pmatrix} \tag{5.7}$$

where each w_{r_i} is the correspondent weight or relative importance of the element r_i. The problem is formulated as a tracking control system where y_r, u_r, δ_r, and z_r are the references for output, input, discrete and continuous auxiliary variables respectively.

The optimization problem consists of finding the sequences of control actions $u(k)$,.., $u(k+m-1)$, $\delta(k)$,.., $\delta(k+p-1)$, and $z(k)$,.., $z(k+p-1)$ that minimize J as

$$\min_{\{[u(k+i)]_{i=0}^{m-1},[\delta(k+i)]_{i=0}^{p-1},[z(k+i)]_{i=0}^{p-1}\}} J \tag{5.8}$$

subject to the mixed integer constraints described in (5.4) and the following various process constraints:

$$y_{min} \leq y(k+i) \leq y_{max}, \quad 1 \leq i \leq p \tag{5.9}$$

$$u_{min} \leq u(k+i) \leq u_{max}, \quad 0 \leq i \leq m-1 \tag{5.10}$$

$$\Delta u_{min} \leq \Delta u(k+i) \leq \Delta u_{max}, \quad 0 \leq i \leq m-1 \tag{5.11}$$

Unmeasured disturbances d' are described as general non-stationary stochastic signals by

$$x_w(k) = A_w x_w(k-1) + B_w w(k-1) \tag{5.12}$$

$$d'(k) = C_w x_w(k) \tag{5.13}$$

where $w(k)$ is a vector of integrated white noise. In this formulation single integrating disturbances are assumed, hence $B_w = C_w = I$ and $A_w = 0_{n_y \times n_y}$ are assumed. These results yields to an augmented representation of the system as

$$\begin{aligned} X(k) =& \mathcal{A}X(k-1) + \mathcal{B}_1\Delta_u(k-1) + \mathcal{B}_2\Delta\delta(k-1) + \mathcal{B}_3\Delta z(k-1) \\ &+ \mathcal{B}_d\Delta d(k-1) + \mathcal{B}_w\Delta w(k-1) \end{aligned} \tag{5.14}$$

$$y(k) = \mathcal{C}X(k) + \nu(k) \tag{5.15}$$

where

$$X(k) = \begin{pmatrix} \Delta x^T(k) & \Delta x_w^T(k) & y^T(k) \end{pmatrix}^T \tag{5.16}$$

$$\mathcal{A} = \begin{pmatrix} A & 0 & 0 \\ 0 & A_w & 0 \\ CA & A_w & I \end{pmatrix} \tag{5.17}$$

$$\mathcal{B}_i = \begin{pmatrix} B_i \\ 0 \\ CB_i \end{pmatrix}, i = 1, 2, 3, d; \quad \mathcal{B}_w = \begin{pmatrix} 0 \\ I \\ I \end{pmatrix}; \quad \mathcal{C} = \begin{pmatrix} 0 & 0 & I \end{pmatrix} \tag{5.18}$$

These equations are used to build a filtered observation $X(k/k)$ and a prediction $\mathcal{Y}(k+1)$ for p steps into the future where

$$\mathcal{Y}(k+1) = \begin{pmatrix} y^T(k+1) & y^T(k+2) & \cdots & y^T(k+p) \end{pmatrix}^T \tag{5.19}$$

A detailed explanation about the formulation of the algorithm including the definition of all the scalar and vectorial coefficients is presented in (Nandola and Rivera, 2013).

The HMPC formulation relies on a three degree-of-freedom tuning process, where setpoint tracking, measured and unmeasured disturbance rejections can be adjusted independently by varying parameters α_r^j, α_d^l and f_a^j from 0 to 1, for $j = 1, \cdots, n_y$, and $l = 1, \cdots, n_{dist}$. This process is depicted in Fig. 5.3, where P and P_d are the multivariable plant and disturbance models, respectively. For setpoint tracking the filter matrix $F(q, \alpha_r)$ is

$$F(q, \alpha_r) = \begin{pmatrix} f(q, \alpha_r^1) & 0 & \cdots & 0 \\ 0 & f(q, \alpha_r^2) & \cdots & 0 \\ \vdots & \vdots & \ddots & \vdots \\ 0 & 0 & \cdots & f(q, \alpha_r^{n_y}) \end{pmatrix} \tag{5.20}$$

where each $f(q, \alpha_r^j)$ is a Type-I discrete-time filter (Morari and Zafiriou, 1989) defined as

$$f(q, \alpha_r^j) = \frac{(1 - \alpha_r^j)q}{q - \alpha_r^j}, \quad j = 1, \cdots, n_y \tag{5.21}$$

The speed of setpoint tracking can be adjusted by manipulating coefficients α_r^j from 0 to 1. The smaller the value for α_r^j, the faster the output response for setpoint tracking.

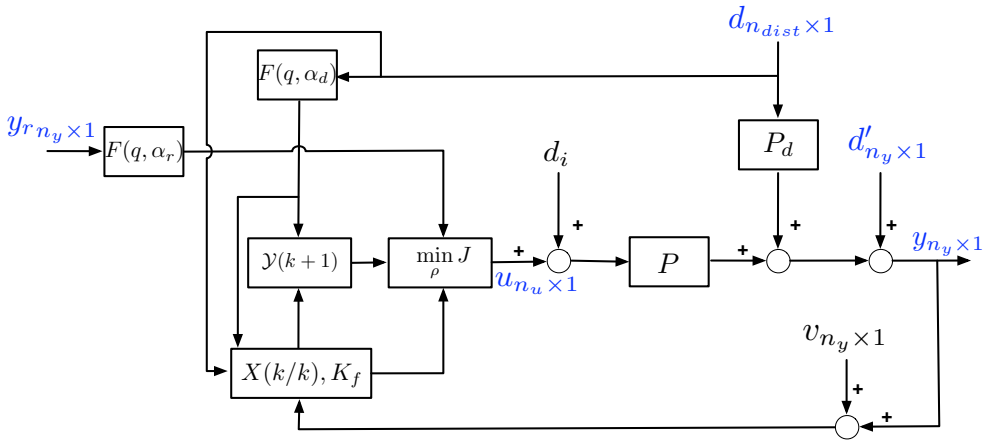

Figure 5.3: Block Diagram Depicting the Three Degree-of-Freedom Tuning Within the HMPC Formulation. P and P_d Are the System Plant Models, $X(k/k)$, K_f is the Observer Block, $\mathcal{Y}(k+1)$ is the Predictor Block, $F(q,\alpha_x), x = r, d$ are the Filters for Reference and Measured Disturbance Signals, and the Block Referred as "min J" is the Optimizer Where ρ is the Vector of Decision Variables.

For measured disturbance rejection the formulation relies on an externally generated forecast that is processed through the filter $F(q,\alpha_d)$. In this work Type-I filters are considered

$$F(q,\alpha_d) = \begin{pmatrix} f(q,\alpha_d^1) & 0 & \cdots & 0 \\ 0 & f(q,\alpha_d^2) & \cdots & 0 \\ \vdots & \vdots & \ddots & \vdots \\ 0 & 0 & \cdots & f(q,\alpha_d^{n_{dist}}) \end{pmatrix} \tag{5.22}$$

$$f(q,\alpha_d^l) = \frac{(1-\alpha_d^l)q}{q-\alpha_d^l}, \quad l = 1,\cdots,n_{dist} \tag{5.23}$$

however a Type-II filter structure should be used if the integrating system dynamics are present (Nandola and Rivera, 2013). Coefficients α_d^l are used to adjust the speed of measured disturbance rejection. These parameters must have values lying between 0 and 1; the lower the value of each α_d^l, the faster the speed of disturbance rejection.

The optimizer uses the model and current measurements $y(k)$ to compute future states through an observer/filter. To achieve the full three degree-of-freedom feature it is necessary to decouple the effects of measured and unmeasured disturbance, hence the augmented state estimator is computed as

$$X_{flt}(k|k) = X_{flt}(k|k-1) + K_f\big(y(k) - \mathcal{C}X(k|k-1)\big) \tag{5.24}$$

where X_{flt} is computed considering the filtered measured disturbance, while X utilizes the unfiltered measured disturbance such that the second term in (5.24) represents the effect of unmeasured disturbance only. The term

$$PE = y(k) - \mathcal{C}X(k|k-1) \tag{5.25}$$

is the prediction error. The process is described with details by Nandola and Rivera (2013).

The observer weights the effect of the unmeasured disturbances through the gain matrix K_f. The optimal value of K_f is computed using the parametrization shown in Lee *et al.* (1994) and Lee and Yu (1994) that enables the independent specification of unmeasured disturbance rejection for each output channel. The closed-loop response of the system is affected by the tuning method, creating a direct link with robust stability and robust performance ideas (Morari and Zafiriou, 1989). K_f is defined as

$$K_f = [0 \quad F_b^T \quad F_a^T]^T \tag{5.26}$$

where

$$F_a = \begin{pmatrix} f_a^1 & 0 & \cdots & 0 \\ 0 & f_a^2 & \cdots & 0 \\ \vdots & \vdots & \ddots & \vdots \\ 0 & 0 & \cdots & f_a^{n_y} \end{pmatrix} \tag{5.27}$$

$$F_b = \begin{pmatrix} (f_a^1)^2 & 0 & \cdots & 0 \\ 0 & (f_a^2)^2 & \cdots & 0 \\ \vdots & \vdots & \ddots & \vdots \\ 0 & 0 & \cdots & (f_a^{n_y})^2 \end{pmatrix} \tag{5.28}$$

Equation (5.28) is formulated under the assumption of white noise. Each f_a^j, $j = 1, \cdots, n_y$ is a tuning parameter that lies between 0 and 1, affecting how the controller reacts to unmeasured disturbances that are present at each output. If one of these coefficients approaches 0, then for that particular output the controller ignores the prediction error correction, and decisions are done mainly based in the model and the controller structure. If parameters f_a^j are close to 1, the controller relies more on prediction errors, which are affected by unmeasured disturbance and unmodeled dynamics, and its action over the inputs can become very aggressive. The clear effect of F_a on the sensitivity and complementary sensitivity functions is discussed in Lee and Yu (1994).

For the closed-loop physical activity intervention the considered input and output vectors are

$$u = [u_8 \quad u_9 \quad u_{10}]^T, \quad n_u = 3 \tag{5.29}$$

$$y = [y_2 \quad y_3 \quad y_4 \quad y_5]^T, \quad n_y = 4 \tag{5.30}$$

Environmental context is considered as the measured disturbance $d = \xi_7$, the unmeasured disturbance is assumed Gaussian and affecting only performed daily steps (i.e., output $y_4 = \eta_4$).

5.3.2 Discrete and Logical Constraints

Discrete and logical features of the physical activity behavioral intervention can be described using the MLD framework. Intervention components take their val-

ues from discrete sets of events, the possible set of step goals is defined as $u_8(k) \in U_8 = \{Cv_1, \cdots, Cv_{n_{u_8}}\}$, and the possible set of available points is $u_9(k) \in U_9 = \{Cv_{n_{u_8}+1}, \cdots, Cv_{n_{u_8}+n_{u_9}}\}$, hence the following logical and continuous auxiliary variables are defined as

$$\delta_j(k) = 1 \Leftrightarrow z_j(k) = Cv_j, \quad j = 1, \cdots, n_{u_8} + n_{u_9} \tag{5.31}$$

This condition is enforced by

$$z_j(k) = Cv_j \delta_j(k), \quad j = 1, \cdots, n_{u_8} + n_{u_9} \tag{5.32}$$

To assure that only one value can be assigned to u_8 and u_9 at each sampling time it is necessary to add the following constraints:

$$\sum_{j=1}^{n_{u_8}} \delta_j(k) = 1, \quad u_8(k) = \sum_{j=1}^{n_{u_8}} z_j(k) \tag{5.33}$$

$$\sum_{j=n_{u_8}+1}^{n_{u_8}+n_{u_9}} \delta_j(k) = 1, \quad u_9(k) = \sum_{j=n_{u_8}+1}^{n_{u_8}+n_{u_9}} z_j(k) \tag{5.34}$$

The effect of all the inputs at any given day will be reflected on the outputs at the following day, hence the number of performed steps $y_4(k)$ is resultant from the goals and points from the previous day $u_8(k-1)$, $u_9(k-1)$, and $u_{10}(k-1)$. According to the proposed intervention depicted in Fig. 5.1, the "If/Then" block is responsible for determining if the points are granted, depending on the fulfillment of daily goals. The auxiliary logical variable δ_{10} is set as true when the performed steps are greater or equal than the goal set the previous day

$$\delta_{10}(k) = 1 \Leftrightarrow y_4(k) \geq u_8(k-1) \tag{5.35}$$

A big-M reformulation is applied to convert logical constraints to a set of linear conditions with the same feasible set. To assign the corresponding value of δ_{10} the

following constraints are considered:

$$y_4(k) - u_8(k-1) \leq \delta_{10}(k)[y_4^{max} - u_8^{min}] \tag{5.36}$$

$$y_4(k) - u_8(k-1) \geq [1 - \delta_{10}(k)][y_4^{min} - u_8^{max}] \tag{5.37}$$

The auxiliary variable z_{10} is used to represent the granted points, hence

$$u_{10}(k) = z_{10}(k) \tag{5.38}$$

At the beginning of every day, goal attainment is verified; if the goals have been met, the points announced the previous day are granted ($u_{10} = u_9$). This is imposed by

$$u_9(k-1) - z_{10}(k) \leq [1 - \delta_{10}(k)][u_9^{max} - u_{10}^{min}] \tag{5.39}$$

$$u_9(k-1) - z_{10}(k) \geq [1 - \delta_{10}(k)][u_9^{min} - u_{10}^{max}] \tag{5.40}$$

If the goals are not achieved, no points are given that day ($u_{10} = 0$)

$$z_{10}(k) \geq \delta_{10}(k) u_{10}^{min} \tag{5.41}$$

$$z_{10}(k) \leq \delta_{10}(k) u_{10}^{max} \tag{5.42}$$

The constraints described by (5.31) - (5.42) are incorporated to the system presented in (5.4) by defining the values for matrices E_1, E_2, E_3, E_4, E_5, and E_d. This is performed using the Hybrid Systems Description Language (HYSDEL; Torrisi and Bemporad (2004)), which is a software tool that helps to the construction of the MLD representation matrices, using a high level description of the logical inputs, states, outputs, and other logical rules.

5.3.3 Maintenance Training Stage

Once the desired goal has been reached and sustained for a predetermined number of days, a maintenance training stage of the intervention is initiated. Here the

HMPC algorithm must be reconfigured so as to maintain the daily performed steps in spite of a reduction of the number of points, and, if needed, reactivating the use of points if a significant relapse occurs. To adapt the HMPC performance to these new considerations, the penalty weights in the objective function are adjusted during the course of the intervention.

During the initiation phase, the main goal is to achieve the required daily steps. The reference output set point is $y_r = [y_{r2} \quad y_{r3} \quad y_{r4} \quad y_{r5}]^T$, where y_{r4} is the desired amount of daily steps (e.g., 10000). Considering vectors u and y defined in (5.29) – (5.30) the following weight matrices Q_u and Q_y are considered in the objective function (5.5) to impose a set point tracking only on the variable y_4 (daily steps)

$$Q_u = \begin{pmatrix} 0 & 0 & 0 \\ 0 & 0 & 0 \\ 0 & 0 & 0 \end{pmatrix}, \quad Q_y = \begin{pmatrix} 0 & 0 & 0 & 0 \\ 0 & 0 & 0 & 0 \\ 0 & 0 & 1 & 0 \\ 0 & 0 & 0 & 0 \end{pmatrix} \tag{5.43}$$

The remaining weight matrices in (5.5) are considered zero-valued.

The maintenance stage is enabled when the goal has been achieved and sustained at least $n_m - 2$ times during the last n_m days. The goal is considered achieved when the difference between the actual steps and the reference is within a predefined tolerance tol_4. A new auxiliary logical variable $\delta_{goal}(k)$, that is not included in the general HMPC formulation per (5.2)-(5.4), is defined as

$$\begin{gathered} \delta_{goal}(k-i) = 1 \Leftrightarrow |y_4(k-i) - y_{r_4}| \leq tol_4 \\ i = 0, \cdots, n_m - 1 \end{gathered} \tag{5.44}$$

hence the second phase is activated at the sample time k if

$$\sum_{i=0}^{n_m-1} \delta_{goal}(k-i) \geq n_m - 2 \tag{5.45}$$

During this phase it is necessary to reconfigure the controller to target a low use of points (u_9). If the target inputs are: $u_r = [u_{r_8} \quad u_{r_9} \quad u_{r_{10}}]^T$, an appropriate value for u_{r_9} must be selected (e.g., $u_{r_9} = 0$ points) and the weight matrix Q_u is changed to

$$Q_u = \begin{pmatrix} 0 & 0 & 0 \\ 0 & w_{u_9} & 0 \\ 0 & 0 & 0 \end{pmatrix} \tag{5.46}$$

The value of w_{u_9} depends on the expected performance of the set point tracking versus the input targeting. The matrix Q_y remains as was defined in (5.43) and the rest of the weight matrices are zero-valued. If at any time k the condition specified in (5.45) is not accomplished (e.g., a relapse), the initiation phase is reactivated.

5.4 Simulation Study

The simulation results presented in this section assume a hypothetical individual with a sedentary lifestyle, performing an average (i.e., baseline) of 5000 steps per day with an intervention starting at day zero. This simulation scenario is considered to resemble the performance observed on previous physical activity interventions with similar components (King *et al.*, 2013). The assumed model parameters are

- $\tau_2 = 40, \tau_3 = 30, \tau_4 = 0.8, \tau_5 = 2, \tau_6 = 0.5$
- $\gamma_{311} = 0.4, \gamma_{29} = 2.5, \gamma_{57} = 1, \gamma_{510} = 0.6, \gamma_{64} = 1.5$
- $\beta_{25} = 0.5, \beta_{34} = 0.2, \beta_{42} = 0.3, \beta_{43} = 0.9, \beta_{45} = 0.5, \beta_{46} = 0.9, \beta_{54} = 0.6$

Delays (θ_i) and internal disturbance parameters (ζ_i) are considered zero. The self-regulator via internalized cues described in (4.12) is considered with $K_{sr} = 0.8$ and $\lambda = 1$. Parameters for the HMPC are as follows: the sampling time is $T_s = 1$ day, the controller horizons are $p = 7$ and $m = 5$ days, maximum and minimum bounds are

$$u_{min} = [5000 \quad 0 \quad 0]^T$$

$$
\begin{aligned}
u_{max} =& [10000 \quad 500 \quad 500]^T \\
\Delta u_{min} =& [-1000 \quad -500 \quad -500]^T \\
\Delta u_{max} =& [1000 \quad 500 \quad 500]^T \\
y_{min} =& [0 \quad 0 \quad 0 \quad 0]^T \\
y_{max} =& [10000 \quad 10000 \quad 12000 \quad 10000]^T
\end{aligned}
$$

The weight matrices are defined as is shown in (5.43) including the reconfigured matrix Q_u described in (5.46) with $w_{u_9} = 0.005$. The categorical values of the intervention components are defined by the sets

$$
\begin{aligned}
U_8 =& \{5000, 6000, 7000, 8000, 9000, 10000\} \\
U_9 =& \{100, 200, 300, 400, 500\}
\end{aligned}
$$

with $n_{u_8} = 6$ and $n_{u_9} = 5$. The unmeasured disturbance is assumed Gaussian with $d'(k) \sim \mathcal{N}(0, 40000)$.

Considering the input/output definitions for this problem, the vectors representing the different tuning parameters according to (5.20), (5.22), and (5.27) are expressed as

$$\alpha_r = [\alpha_r^2 \quad \alpha_r^3 \quad \alpha_r^4 \quad \alpha_r^5]^T \tag{5.47}$$

$$\alpha_d = \alpha_d^4 \tag{5.48}$$

$$f_a = [f_a^2 \quad f_a^3 \quad f_a^4 \quad f_a^5]^T \tag{5.49}$$

To allow for a progressive increase on the performed steps and a fast disturbance rejection the considered tuning parameters are $\alpha_r = [0 \quad 0 \quad 0.96 \quad 0]^T$, $\alpha_d = 0.1$, $f_a = [0 \quad 0 \quad 0.3 \quad 0]^T$.

Initial simulation results are shown in Fig. 5.4 where no plant-model mismatch is assumed. Goals (u_8) and available points (u_9) are generated by the HMPC algorithm.

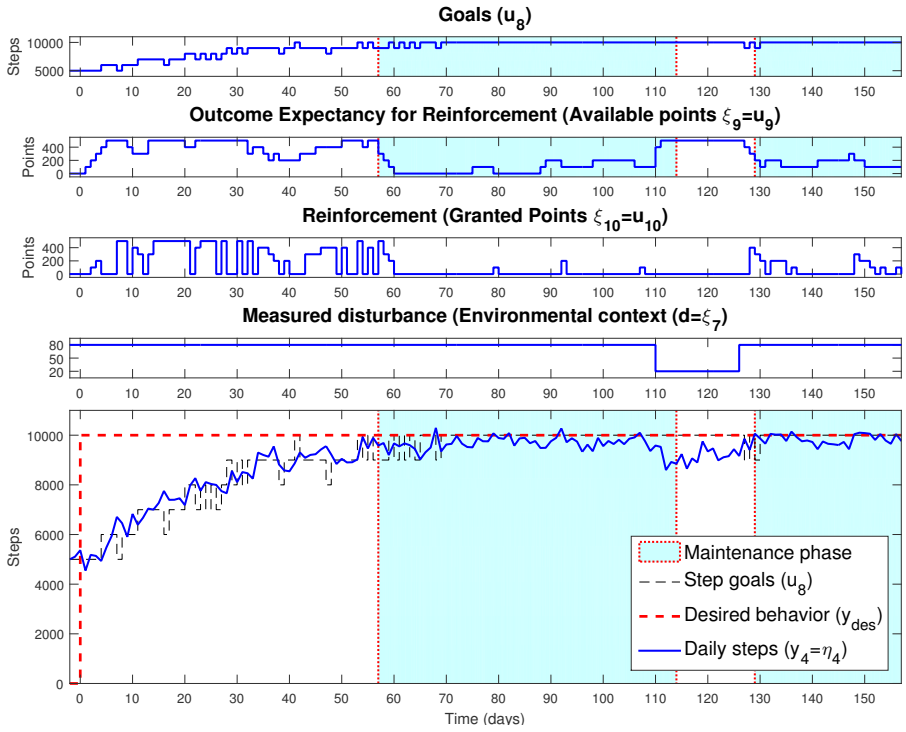

Figure 5.4: Simulation Results for the HMPC Based Adaptive Intervention for a Participant With low Physical Activity, Considering $d'(K) \sim \mathcal{N}(0, 40000)$, $w_{u_9} = 0.005$, $\alpha_r = [0 \quad 0 \quad .96 \quad 0]^T$, $\alpha_d = 0.1$, and $f_a = [0 \quad 0 \quad 0.3 \quad 0]^T$.

It is observed that the value for granted points (u_{10}) is taken from the available points only when the previous day goal is achieved, as was enforced by the MLD constraints. The maintenance stage of the intervention is illustrated via a shaded region; this phase starts when the goal has been achieved for at least 4 times during the last $n_m = 6$ days with a tolerance of $tol_4 = 700$ steps. During this stage a reduction in the amount of available and granted points can be observed. The impact of measured disturbances (e.g., environmental context) is tested via a downward pulse starting at the day 110, and lasting for 15 days, as a result participants tend to reduce their steps and the controller reacts by deactivating the maintenance phase and hence using the points back to compensate any deviation.

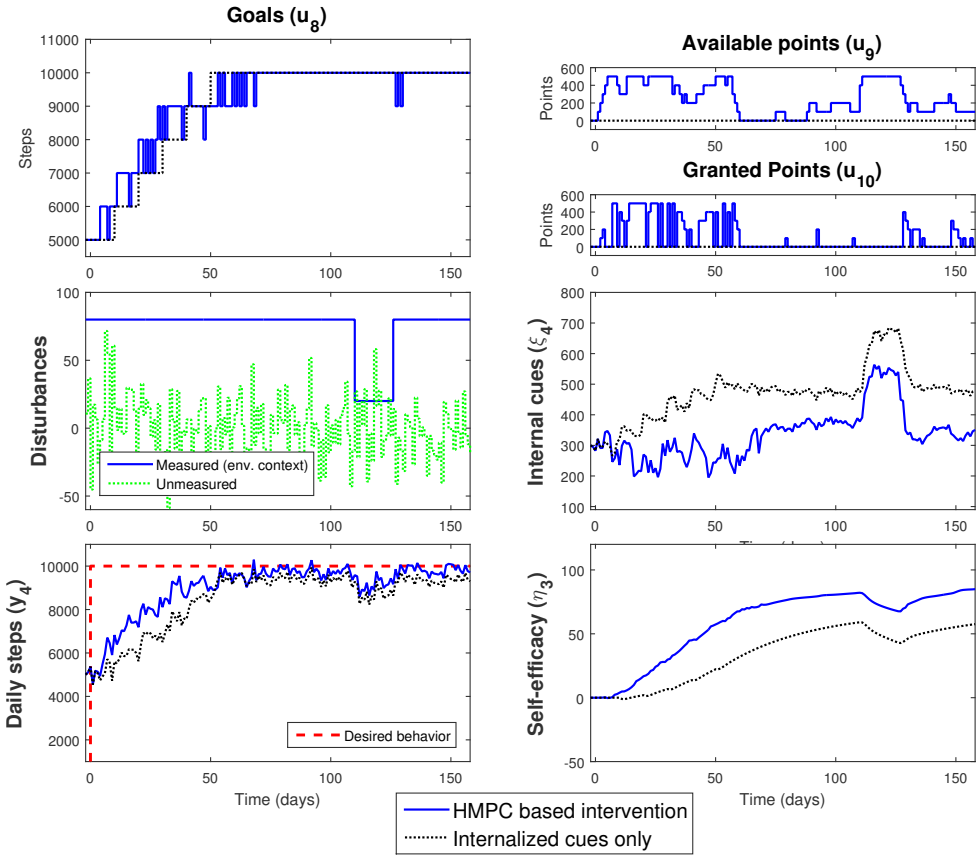

Figure 5.5: Performance of the HMPC Physical Activity Intervention Versus a Self-Regulation via Internalized Cues Case With a Pre-Defined Set of Incremental Step Goals.

Fig. 5.5 shows a comparison between the performance of the HMPC intervention against a second scenario where a set of incremental goals is the only defined input. In this scenario individuals try to attain their goals through the internal self-regulation via internalized cues process. The HMPC intervention displays a better tracking to the final desired behavior of $10,000$ steps; this is achieved through an increase of the individual's *self-efficacy* via the offered and granted rewards. In the HMPC case the higher *self-efficacy* lets the individual require less *internal cues* compared to the internalized cues-only case, and allows the use of fewer points during the

maintenance phase. In both scenarios the self-regulation block tries to compensate differences and/or disturbances by increasing the *internal cues* of individuals.

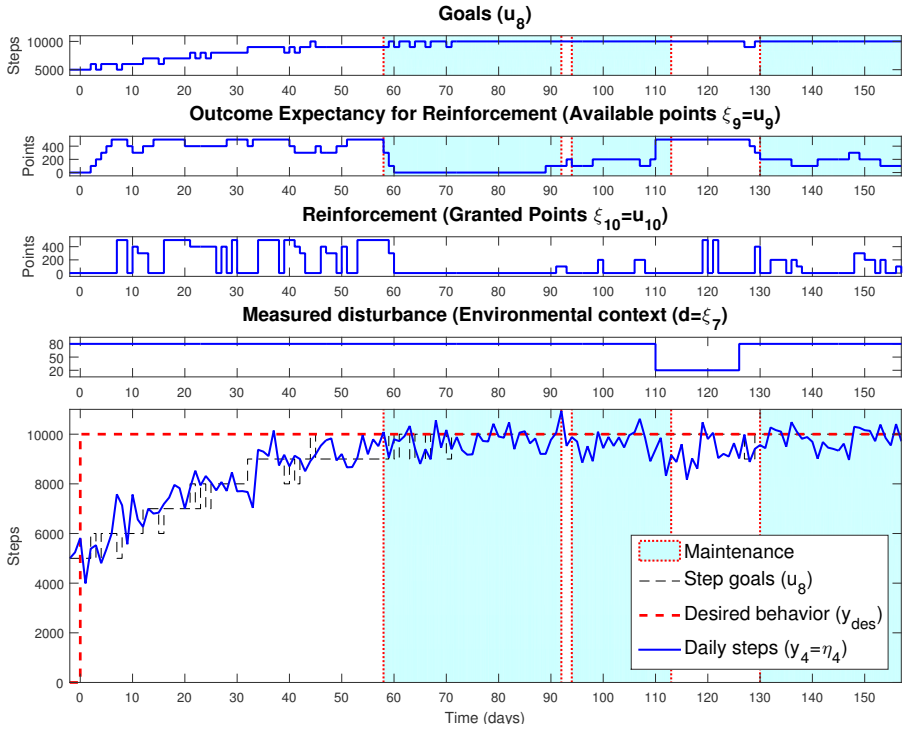

Figure 5.6: Simulation Results for the HMPC Based Adaptive Intervention for a Participant With low Physical Activity, Considering $d'(K) \sim \mathcal{N}(0, 200000)$, $w_{u_9} = 0.005$, $\alpha_r = [0 \quad 0 \quad .96 \quad 0]^t$, $\alpha_d = 0.1$, and $f_a = [0 \quad 0 \quad 0.3 \quad 0]^T$.

The performance of the controller is tested under more aggressive conditions for unmeasured disturbance. Fig. 5.6 shows simulation results using the same conditions and tuning parameters of the previous simulation, with the exception of the unmeasured disturbance that is now Gaussian with $d'(k) \sim \mathcal{N}(0, 200000)$. Good tracking results can be observed with a slighter deviation from the maintenance phase due to the increased level of perturbations. There is an observable increment on the number of available points used to compensate the increased disturbances.

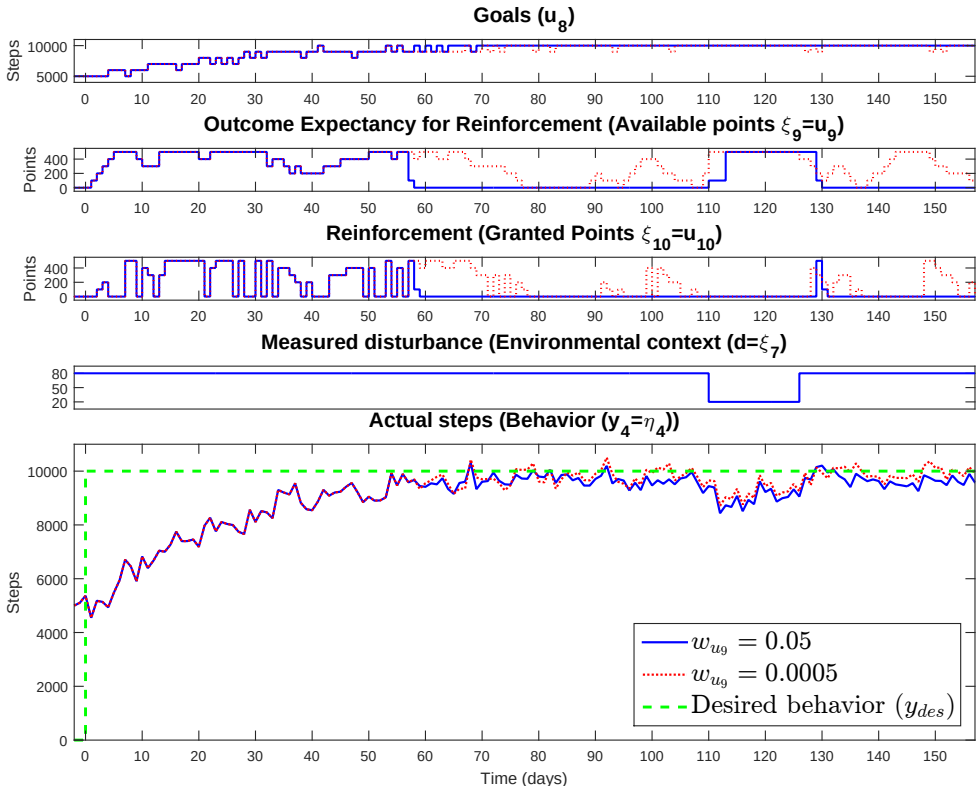

Figure 5.7: Simulation Results for the HMPC Based Adaptive Intervention for a Participant With low Physical Activity, Considering $d'(K) \sim \mathcal{N}(0, 40000)$, $\alpha_r = [0 \quad 0 \quad .96 \quad 0]^T$, $\alpha_d = 0.1$, $f_a = [0 \quad 0 \quad .3 \quad 0]^t$, and two Different Cases for w_{u_9}: $w_{u_9} = 0.05$, and $w_{u_9} = 0.0005$.

The configuration of the maintenance phase is evaluated through the manipulation of the parameter w_{u_9}. Results are shown in Fig. 5.7 for two cases: $w_{u_9} = 0.05$, and $w_{u_9} = 0.0005$. With $w_{u_9} = 0.0005$, an almost total suppression of reward points can be observed during the maintenance phase that starts around day 50. On the other hand, with $w_{u_9} = 0.05$ there is not a considerable reduction of points. In both cases the performance in terms of the output y_4 is similar. Fig. 5.8 shows a detailed comparison between these two cases considering only the interval of time where the maintenance phase is activated for the first name. For the manipulated

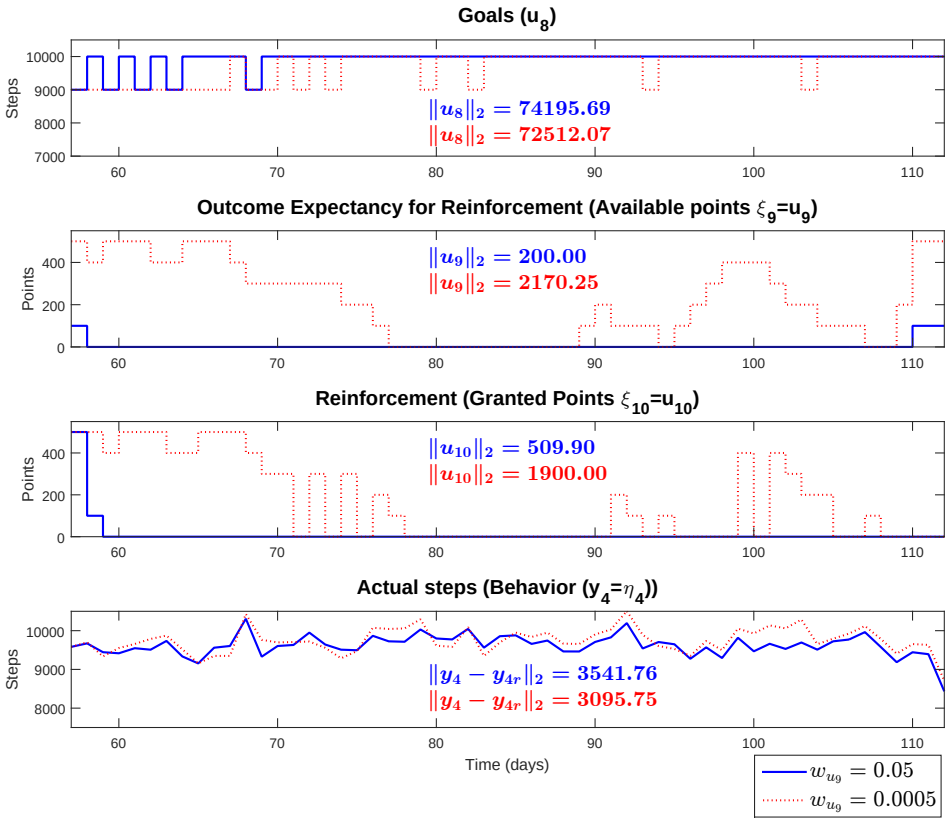

Figure 5.8: More detailed comparison of results from Fig. 5.7 considering only the time interval where the first maintenance phase occurs, and including the computation of 2-norms ($\|u_n\|_2$) for the manipulated inputs and the output *behavior* (u_8, u_9, u_{10}, and y_4) for each value of w_{u_9}.

inputs and the output y_4, 2-norms ($\|u_n\|_2 = \sqrt{u_n^T u_n}$) are computed to contrast the effect of w_{u_9} in terms of provided rewards. As expected, a considerable reduction in the 2-norm of available and granted points can be observed for the case of a higher penalty weight ($w_{u_9} = 0.05$). The performance of the system in term of set goals (u_8) and actual steps (y_4) is similar for both values of w_{u_9}; however, the response of y_4 shows less offset with respect to the reference set point for the case of a lower penalty weight ($w_{u_9} = 0.0005$). The manipulation of parameter w_{u_9} enables the definition of the level of point reductions during the maintenance phase, without affecting the

final behavior. Reinforcing point reductions goes more in the direction of perpetual interventions that is the ultimate goal of the proposed behavioral approach.

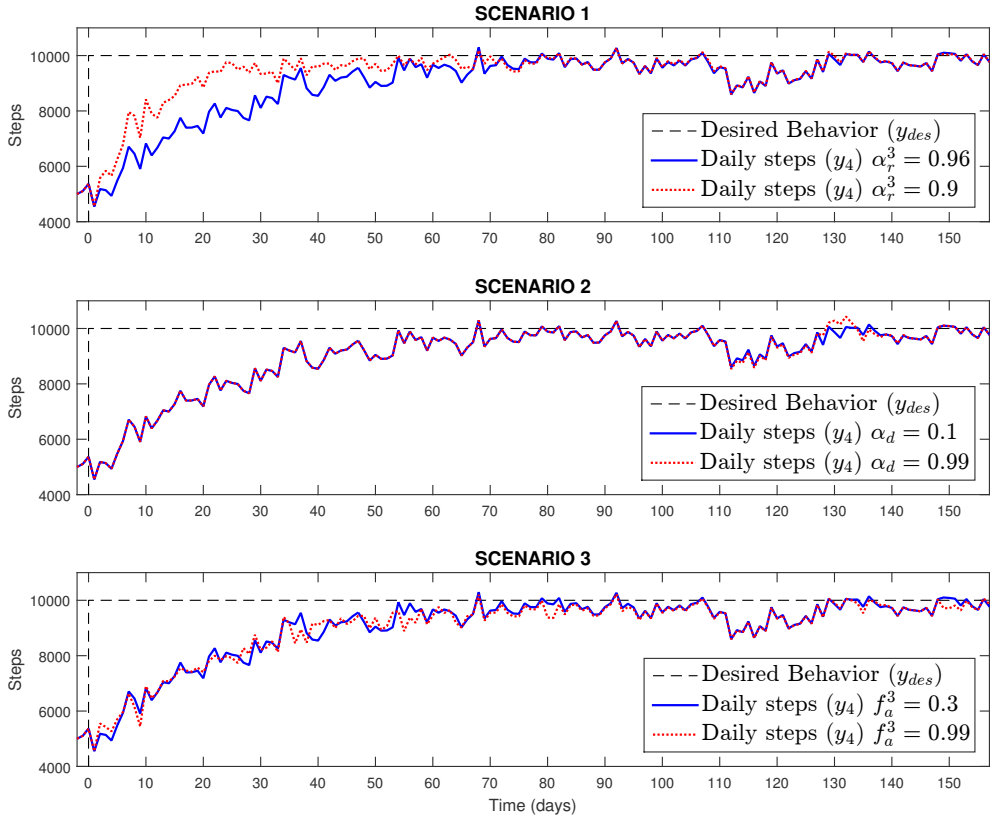

Figure 5.9: Evaluation of the Three Degree-of-Freedom Tuning Procedure Over the Output y_4, Considering Three Different Scenarios.

The three degree-of-freedom tuning procedure is tested in Figures 5.9 and 5.10 All simulations assume the specified general conditions with $d'(k) \sim \mathcal{N}(0, 40000)$. Manipulations are performed on the tuning parameters only, considering their initial values equal to $\alpha_r = [0 \quad 0 \quad 0.96 \quad 0]^T$, $\alpha_d = 0.1$, and $f_a = [0 \quad 0 \quad 0.3 \quad 0]^T$ from where $\alpha_r^3 = 0.96$, and $f_a^3 = 0.3$ are specified. Three different scenarios are constructed as follows:

1. **Scenario 1**: The reference trajectory and setpoint tracking effect is manipulated by reducing the filter constant α_r^3 from 0.96 to 0.9. As a result the output

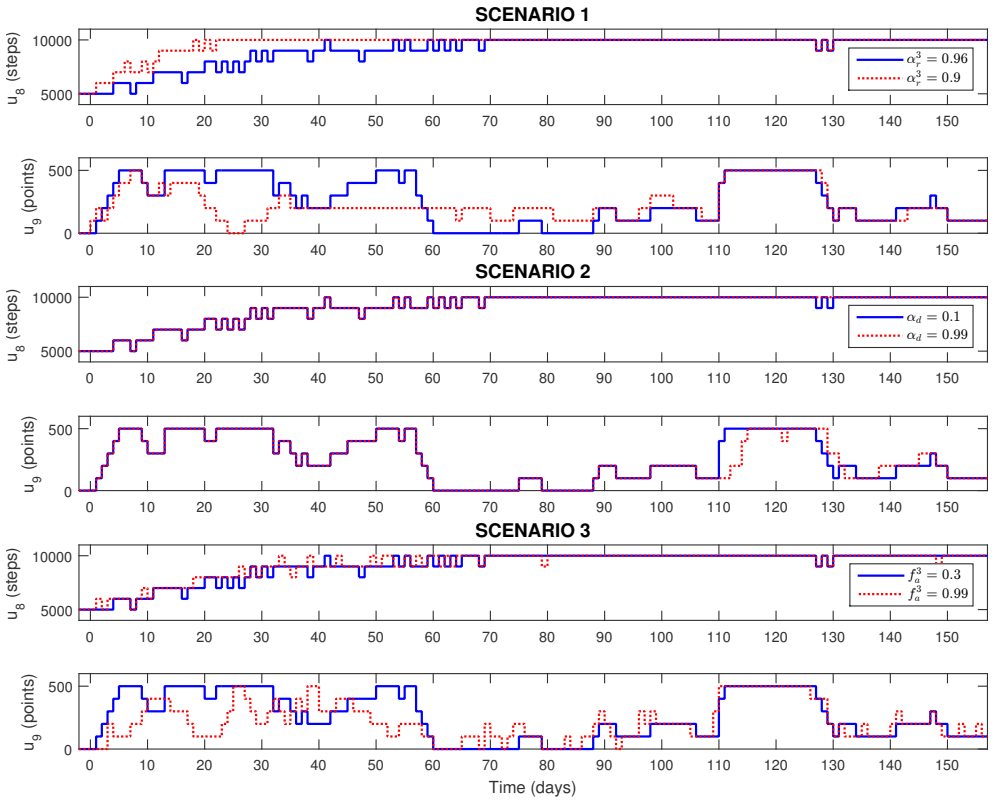

Figure 5.10: Evaluation of the Three Degree-of-Freedom Tuning Procedure Over the Inputs u_8 and u_9, Considering Three Different Scenarios.

response for setpoint tracking now acts faster as can be observed in Fig. 5.9. This is achieved through faster changes over the inputs u_8 (step goals) and u_9 (available points) as Fig. 5.10 illustrates.

2. **Scenario 2**: The measured disturbance rejection is now molded by increasing the filter parameter α_d from 0.1 to 0.99. As expected the speed of disturbance rejection is reduced as can be observed on the values of input u_9 at day 110 in Fig. 5.10. The system response, with and without changing α_d, remains the same until the change (downward step) in the measured disturbance appears. This suggests that parameter α_d acts over measured disturbance rejection independently of setpoint tracking and unmeasured disturbance rejection.

3. **Scenario 3**: Now the unmeasured disturbance rejection effect is tested by increasing f_a^3 from 0.3 to 0.99. The result is an increment on the effect of the prediction error (PE) over the model in the computation of the predicted output utilizing the observer/filter $X(k)$ as was described in (5.24). This effect can be observed in Fig. 5.10 via more aggressive changes in the inputs u_8 and u_9 to deal with the same level of unmeasured disturbance.

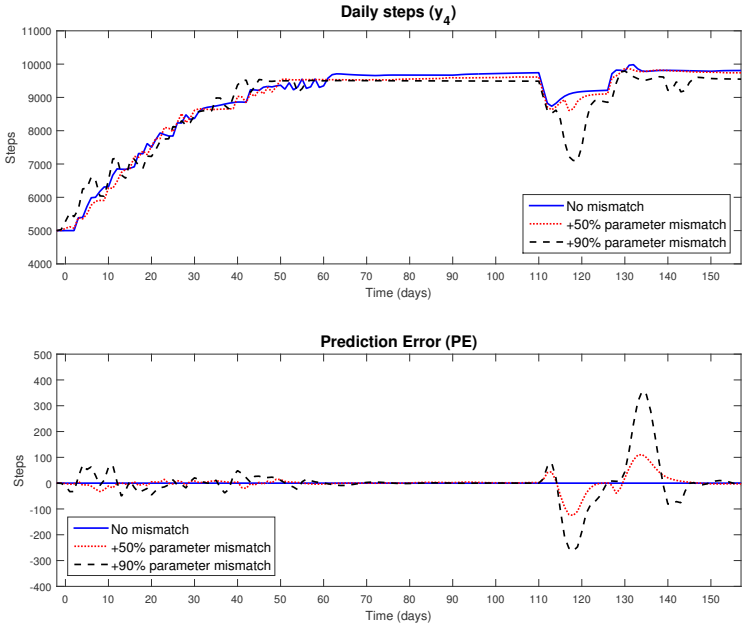

Figure 5.11: Performance of the HMPC Based Intervention for Different Scenarios of Positive Plant-Model Mismatch, With no Unmeasured Disturbance Considered.

Finally the performance of the system under different conditions of plant-model mismatch is tested. Plant-model mismatch is considered in the form of parameter uncertainty within a fixed structure. Unmodeled/unstructured uncertainty is not considered. Results are shown in Figures 5.11 – 5.13. The unmeasured disturbance is assumed to be zero ($d'(k) = 0, \forall k$). In the ensuing formulation the considered model parameters "MP" ($MP = \tau_i, \beta_i, \gamma_i, K_{sr}, or \lambda$) are labeled as MP_p for the real

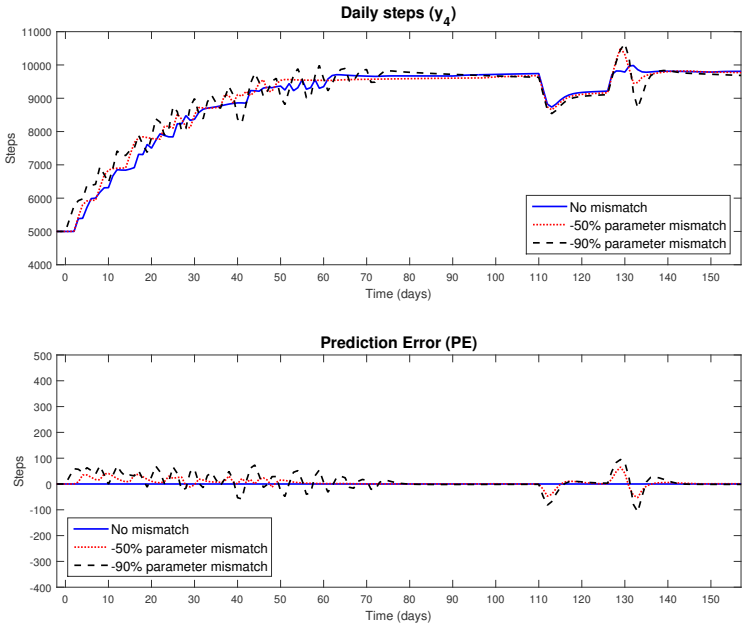

Figure 5.12: Performance of the HMPC Based Intervention for Different Scenarios of Negative Plant-Model Mismatch, With no Unmeasured Disturbance Considered.

process (plant), and MP_m for those utilized in the controller formulation (model). The following parameter modifications are considered:

- $MP_m = MP_p$: no plant-model mismatch,
- $MP_m = (1 \pm 0.5)MP_p$: changes of 50% in the value of each model parameter,
- $MP_m = (1 \pm 0.9)MP_p$: changes of 90% in the value of each model parameter.

Fig. 5.11 illustrates these cases for positive mismatch only, Fig. 5.12 for negative only, and Fig. 5.13 for simultaneous positive and negative mismatch. In general, results on the controlled output y_4 show that, for the 50% mismatch case, the performance of the controller has not changed considerably compared to the no-mismatch case. If the mismatch increases up to the 100% level, then more noticeable variations and setpoint deviations in the controlled output y_4 can be observed.

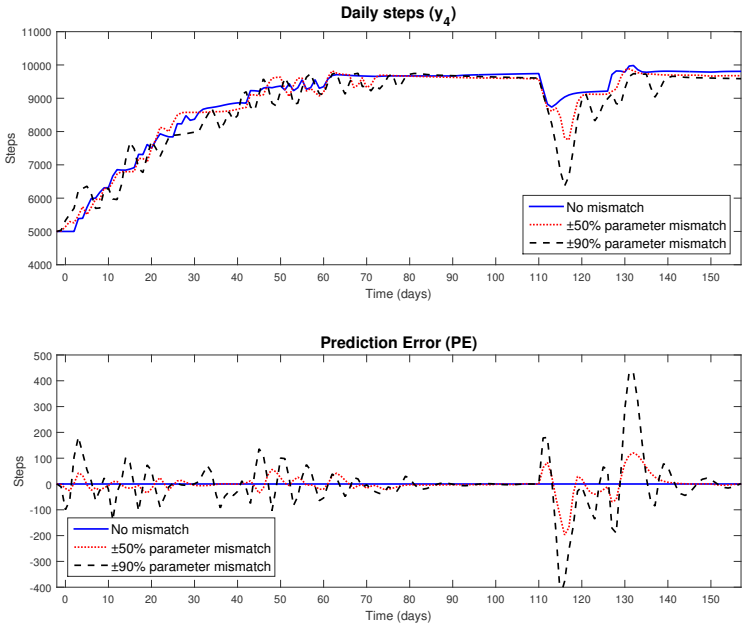

Figure 5.13: Performance of the HMPC Based Intervention for Different Scenarios of Positive/negative Plant-Model Mismatch, With no Unmeasured Disturbance Considered.

As was specified in (5.25) the prediction error term (PE) computes the differences between the predicted and the actual controlled outputs. These differences can be caused either by modeling errors or unmeasured disturbances. Here plant-model mismatch is the only source of such type of differences. The HMPC formulation is robust enough to admit some level of modeling errors, by using the prediction error in the computation of the future states, and hence in the definition of the new set of inputs. It is observed that for the positive 50% mismatch case the level of PE is small enough to sustain the controller action; however for the 100% mismatch case the increment on PE makes the setpoint tracking to be less effective, and hence a re-identification of the plant model might be required.

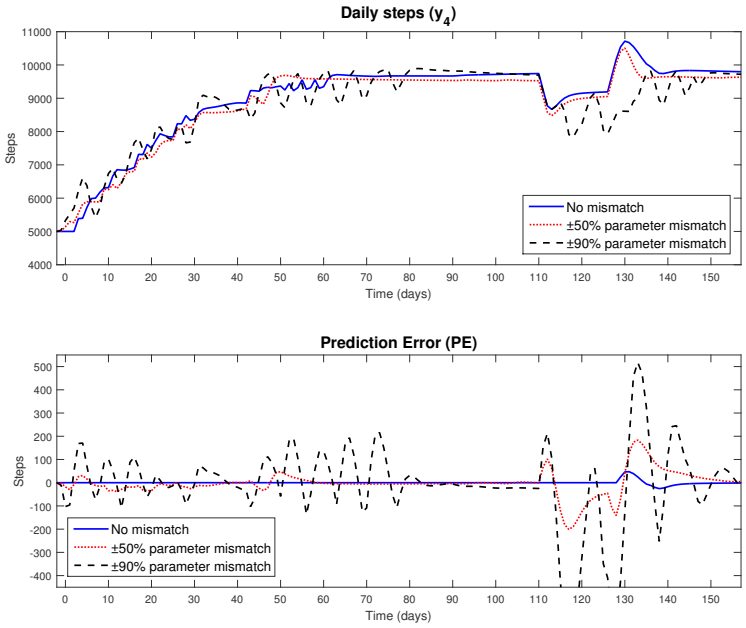

Figure 5.14: Performance of the HMPC Based Intervention for Different Scenarios of Positive/negative Plant-Model Mismatch, With $\alpha_d = 0.9$ and $f_a^3 = 0.01$.

Values of HMPC tuning parameters also affect how the system reacts to plant-model mismatch. Measured and unmeasured disturbance rejection effects are modified by manipulating the tuning parameters α_d from 0.1 to 0.9 and f_a^3 from 0.3 to 0.01. Simulations are performed for simultaneous positive and negative mismatch of 50% and 90%, and results are shown in Fig. 5.14. Set point tracking is considerable reduced for both cases. The speeds of measured and unmeasured disturbance rejection were reduced by manipulating the tuning parameters; hence the system, which structure has not changed, is responding slowly to mismatch causing increased errors. These results yield to the idea that the tuning procedure plays an important role in the overall performance of the HMPC formulation.

5.5 Chapter summary

In this chapter an HPMC formulation is proposed to design a behavioral physical activity intervention, including the discrete and logical characteristics of the problem that are incorporated by taking advantage of the MLD framework. Many features of HMPC are used to represent particular aspects of the problem, such as the use of a predefined categorical set of values for the inputs, the three degree-of-freedom tuning property to enable adjusting the set point tracking and disturbance rejection modes independently, and the use of penalty weights to influence the effect of intervention components in controller performance.

As the intervention progresses, the individual will gain confidence, and hence reward points are reduced and eventually removed. This feature was effectively represented through controller reconfiguration achieved via the use of penalty weights on points to discourage their use. During this maintenance stage the targeted behavior is accomplished by increases in *self-efficacy* of the participant, which allows the use of fewer points.

Simulation results demonstrate a good performance of the HMPC algorithm, with tight setpoint tracking and acceptable disturbance rejection. When the goal is achieved, the system is able to sustain behavior even with the point reduction imposed in by the maintenance stage. In the presence of significant disturbances and/or relapses the behavioral initiation training phase is reactivated. Results from simulation also provide a way to test some of the most important aspects of the HMPC such as the independent tuning effect imposed by the three degree-of-freedom formulation, and the robustness of the controller against different levels of plant-model mismatch in the form of parameter variations.

Chapter 6

SUMMARY AND FUTURE WORK

6.1 Summary of the Dissertation

This dissertation has demonstrated how control engineering principles can be applied to the design of intensively adaptive behavioral interventions, with emphasis on interventions to address low physical activity. Health behaviors are increasingly being acknowledged as the primary risk factors for disease worldwide. To date, there are many behavioral interventions that largely function as static interventions for promoting behavior change. While there is evidence that these interventions can promote positive changes during their active period, they often do not result in sustained behavior change. Smartphones and wearable sensors, such as physical activity monitors, have the potential to help individuals improve their lives through behavior change by monitoring individual's physical activity and then using that information to provide the most appropriate customized interventions when it would be most beneficial for that person. Control system engineering principles offer a systematic approach that considers the dynamic nature involving human behavior. Previous work has been developed to incorporate these concepts to the design of behavioral interventions (Rivera, 2012; Deshpande *et al.*, 2014a; Timms *et al.*, 2014b). This dissertation extends these ideas to low physical activity behavioral problems.

The first proposed step is the construction of a dynamical mathematical model of human behavior that provides the insights for making decisions about how an intensively adaptive mHealth physical activity intervention (IAI) should take place. Creating this dynamical behavioral model is a challenging problem that requires in-

sights from different disciplines, behavioral science and control systems engineering in particular. Behavioral science provides insights regarding what to measure, and behavioral intervention strategies that could be used dynamically. Social Cognitive Theory (SCT; Bandura (1986)) is a well-recognized framework that has been used as a basis of many behavioral interventions (Lopez *et al.*, 2011). Control systems engineering provides a methodology for creating dynamical models and decision-making, relying on the application of fluid analogies that are able to represent the interconnections between the different constructs as these are described by SCT. The postulated model is evaluated via reconciliation with data from an actual low physical activity study, and through the construction of some simulation scenarios that illustrate the most common features of SCT. By considering low physical activity problems, the model is enhanced through the incorporation of additional features, such as a nonlinear feature called habituation, and the ideal step-goal range effect. Both features are tested through the development of different simulation scenarios.

Another research goal is the formulation of effectively designed system identification experiments, with the goal of obtaining values for SCT model parameters, and keeping the intervention within "patient-friendly" (Deshpande *et al.*, 2012) conditions. This is achieved through the development of open-loop Intensively Adaptive Interventions (IAI) with the purpose of having individuals walking/running 10,000 steps per day as a weekly average. Two intervention components are defined: a goal-setting strategy, and a reinforcement scheme using points that later are exchanged for tangible rewards (e.g, gift cards). Points are given to participants when they achieve the set goal each day. This effect is incorporated to the model via the definition of an "If/Then" Block; this block is constructed as a nonlinear element, and it deserves special considerations in the remaining formulations. Two different open-loop system identification experiments are formulated: first an informative experiment with the

purpose of obtaining basic insights about the model parameters, and then an optimized experiment designed to refine and search the best model parameters using a formal optimization problem.

Since very little is known *a priori* about the dynamical properties of the system, the initial approach uses fixed-time random input signals, generated under operational constraints over the magnitude of the signals. Given the natural properties of behavioral health interventions, the duration of experiments plays an important role, affecting operational and economic aspects; hence a second approach is proposed using identification test monitoring, an idea presented by Rivera *et al.* (2003), that attempts to find the shortest possible experiment with sufficient information for system identification purposes. To represent how informative is an experiment, the formulation relies on the computation of transfer functions and uncertainties in frequency domain. The procedure utilizes multisinusoidal input signals that are constructed including user-defined properties at the frequencies of interest. To allow the independent estimation of transfer functions, the signals are designed using an orthogonal-in-frequency "zippered" formulation (Rivera *et al.*, 2009). Two different strategies are developed to compute uncertainties and to define a stopping criterion for the monitoring procedure.

The first strategy uses the Empirical Transfer Function Estimates (ETFE) method with an averaging procedure applied to sampled data for a given number of periods M according to the multisine formulation. These results are used at each frequency to compute additive uncertainties that are statistically valid for a predefined level of accuracy. These results can be extended to parallel connected systems, and to error-in-variables descriptions as is detailed in Section 3.2.2. The computed statistical uncertainties are then utilized to define a specific stopping criterion relying on percentage variations of uncertainties during consecutive iterations, and for input-

output elements of interest. At each iteration a stopping criterion is evaluated to decide if the experiment is halted, or if another period of similar input-output data is considered.

The purpose of the second approach to identification test monitoring is to incorporate the possibility of additional modifications to the input signals at every periodic evaluation. The allowed modifications are in the amplitude and harmonic frequency content of input signals. The Local Polynomial Method (LPM) is now applied for the computation of transfer functions in the frequency domain. This method accounts for transient responses that occur in dynamical systems; hence there is no necessity of considering data after steady state. This enables the presence of changes in the input signal content between iterations. Two different LPM variations are tested: the fast and transient methods; these are described in Section 3.3.2. Depending on which LPM variation is utilized, different configurations of spectral content are considered for the multisine design. The use of LPM yields to a different method for computation of asymptotically valid statistical additive uncertainties. Estimates of general MIMO additive uncertainties for each frequency are developed relying on singular value ideas. When one or more of the specified input signal modifications are applied, total uncertainties are obtained by aggregating the different signals, before and after changes, via a weighted approximation in terms of the estimated variance of each segment. In this case the presence of the nonlinear "If/Then" block imposes some obstacles for the computation of valid transfer functions; however uncertainties are proved to remain the same under specific conditions. The monitoring procedure is based on a new stopping criterion that is defined relying in robust performance ideas, and assuming an unstructured additive uncertainty representation in the closed-loop. Simulation scenarios are developed for each case, assuming a hypothetical physical activity behavioral intervention relying on previous similar interventions.

The optimized experiment relies on model parameters obtained from the informative experiment, and using semiphysical identification routines. A formal optimization problem is developed with the objective to follow a specified behavioral profile under operational constraints. These constraints are over the magnitude, move size, and switching time of input signals, and output magnitudes. The output of the system (i.e., actual steps) is predicted using the informative model. A big-M reformulation is utilized to represent the effect of the "If/Then" block. The experiment is performed under "patient-friendly" conditions that are enforced by the optimization routine. A new set of model parameters is obtained via input-output sampled data from the optimized experiment and relying again on semiphysical identification procedures. Simulations are developed with the same referential plant model, and some metrics are computed to test the "patien-friendliness" of results.

Finally, a closed-loop IAI is developed relying in model parameters obtained via system identification experiments. The purpose of this intervention is to dynamically adjust values of intervention components (i.e., manipulated inputs) to achieve the required amount of daily steps, using an ambitious but doable goal strategy, and supporting a sustained change in behavior. The intervention is designed using Hybrid Model Predictive Control (HMPC) ideas; the categorical nature of the intervention components is incorporated via the Mixed Logical Dynamical (MLD) framework of HMPC. The effect of the "If/Then" block is also included in the MLD formulation. The HMPC framework considers a three degree-of-freedom tuning strategy, which allows the independent regulation of set point tracking, measured and unmeasured disturbance rejections. The formulation includes the definition of a maintenance phase were participants achieve their goals by using their improved abilities, reinforced by the initial part of the intervention; during this phase, rewards are progressively reduced or eliminated. The transition to the maintenance phase is incorporated via

a reconfiguration of some HMPC parameters; here, input weight matrices in the objective function are manipulated to discourage the use of reward points. The transition to the maintenance phase occurs when the required level of daily steps has been achieved continuously during a predetermined number of days.

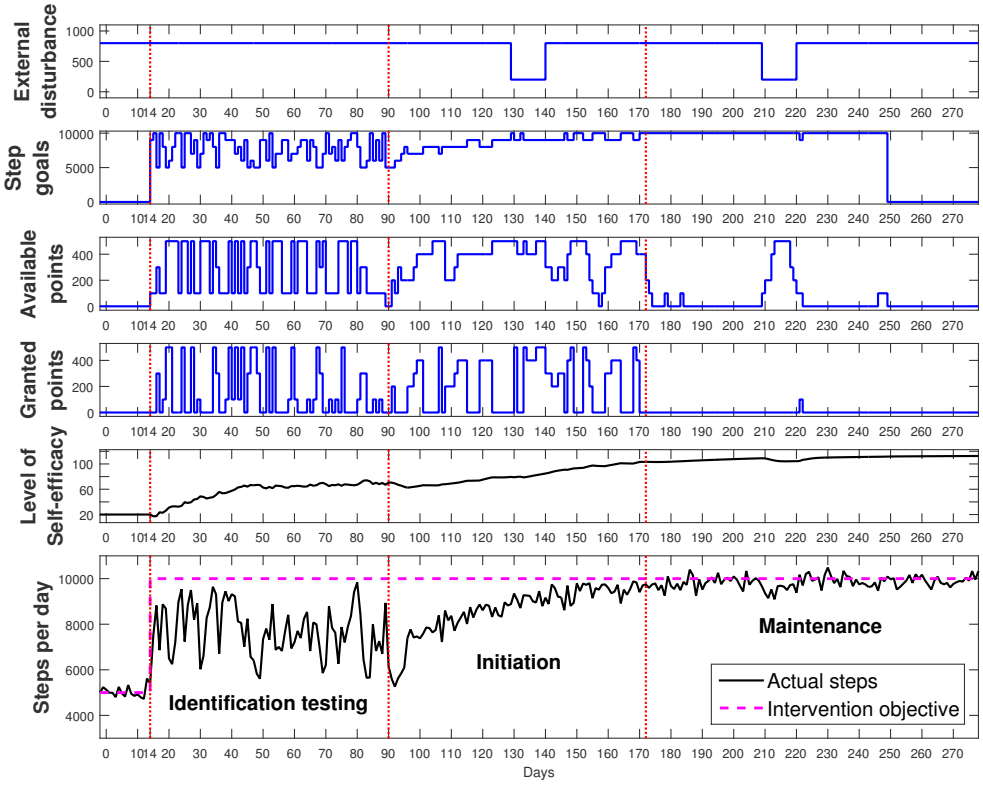

Figure 6.1: Comprehensive Illustration of a Representative Time Series Resulting From the "Just Walk" Intervention That Features Three Phases: Identification Testing, Initiation and Maintenance.

This work forms part of a series of innovative applications of system identification and control engineering concepts that have been performed as part of the "Just Walk" intervention at Arizona State University (Hekler, 2015). Fig. 6.1 illustrates the comprehensive nature of the proposed study: the first stage is an identification procedure where multisine signals and semi-physical parameter estimation using the

SCT model are applied to generate personalized system models. The second stage is an initiation phase where HMPC is used to make daily predictions and decisions from the system model, and then test the quality of those based on ground truth data gathered each day. Finally during the maintenance phase, based on an increase in the participant's *self-efficacy*, the HMPC algorithm decisions are directed for reducing the use of goals, points, and, if needed, reactivating them when a relapse occurs. These conditions eventually will lead to a complete suppression of points to conclude the intervention.

6.2 Directions for Future Work

This dissertation has presented some formative results and initial directions on the development of intensively adaptive behavioral interventions for physical activity using control engineering principles. There are many research opportunities that will lead to improvements and extensions of the proposed approach.

6.2.1 "Just in Time" Adaptive Interventions

"Just in time" adaptive interventions, offers transcendental possibilities for facilitating behavior change (Nahum-Shani *et al.*, 2015). These interventions provide support only when needed, that is, during a Just In Time (JIT) state when a person has both the opportunity to engage in a behavior and is receptive to support. This support adapts to the changing needs of each individual to enable specific bouts (e.g., helping to not smoke one cigarette) to accumulate into meaningful health targets (e.g., remaining smoke free). Specifically, context-relevant computational models of behavior could improve safety by translating what appear to be noise (e.g., fluctuating activity) into more predictable signals (e.g., predictions on if, when, and where a person will engage in a health behavior). The JIT states are defined during differ-

ent moments of the day; hence the design procedure turns into a multiple timescales problem to accommodate the within day JIT states and daily behavior change according to the SCT model. State estimation techniques as Model on Demand (Stenman, 1999), can be used to infer the values of states (i.e., latent constructs) on the basis of available measurements and models.

The closed-loop intervention presented in this dissertation uses a daily timescale. In the proposed approach, this intervention is influenced by the JIT block that works at a momentary timescale (e.g., minutes or hours). The proposed conceptual block is presented in Fig. 6.2. Based on exogenous measurements, JIT states can be estimated using Model on Demand predictors such that periods of opportunity and receptivity for an action can be obtained. A JIT decision algorithm can be designed to deliver or not intervention components depending on the estimated states. At the daily level the accumulation of these components can be translated as contextual external cues to the SCT model. This research activity involves the design of new system identification experiments that requires the development of informative databases using different approaches (e.g., micro-randomization; Klasnja *et al.* (2015)).

6.2.2 Enhancements to System Identification Experiments

Some of the ideas presented in this dissertation yielded to the implementation of a study called "Just Walk" (Hekler, 2015) covering the design of an open-loop IAI for system identification purposes. The following ideas are derived from analysis of preliminary results, to improve future experimental designs:

- Some of the metrics used for measuring SCT model variables must be reconfigured or redefined. For instance, *self-efficacy* and *outcome expectancy* inventories need the definition of more sensitive metrics that approximate continuous measurements, allowing the existence of more variability in the sampled data

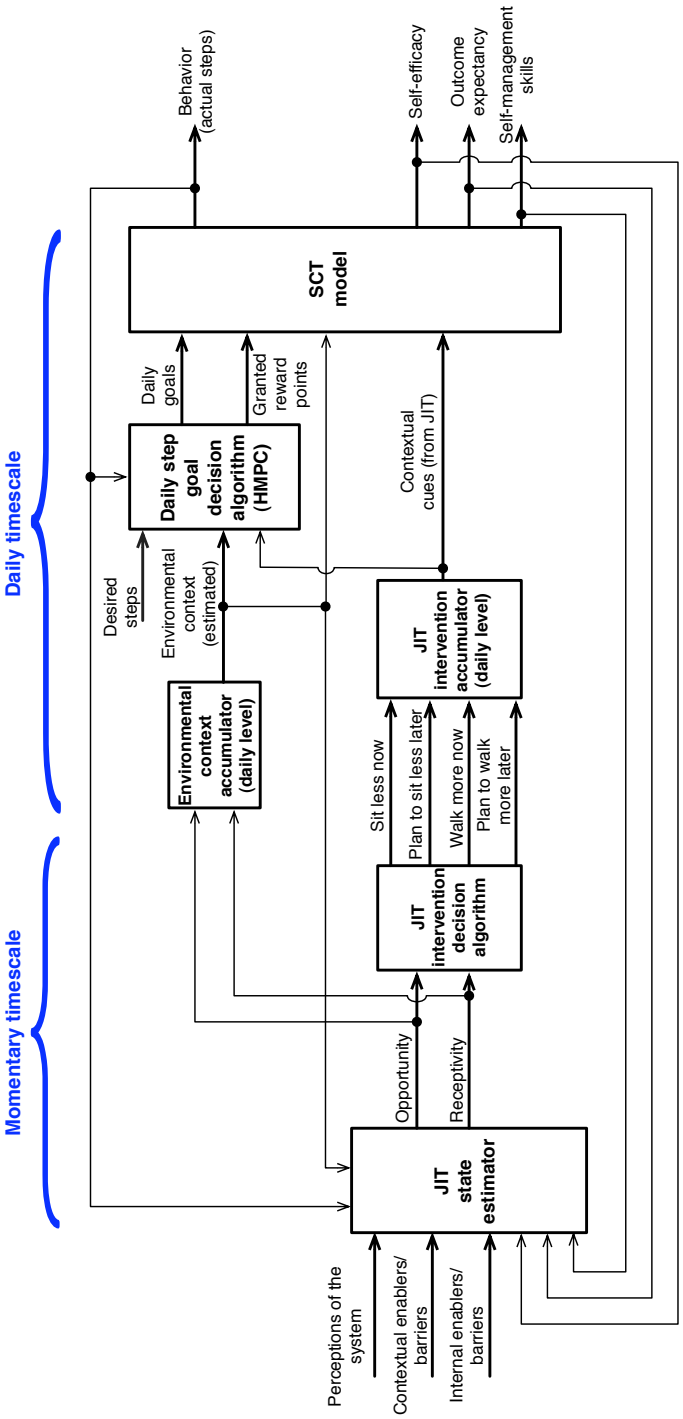

Figure 6.2: Conceptual Block Diagram Representation of a Multi-Timescales JIT Adaptive Intervention.

destined for system identification.

- The signal *environmental context* is composed of numerous exogenous signals that needs to be more deeply analyzed and specified. Different available external signals can be considered in this category (e.g., weather, busyness, and weekend); however proper metrics and scaling factors must be considered to combine them as a single *environmental context* signal. It is necessary to explore also the possibility to define additional dynamical elements (e.g., additional tanks in the fluid analogy) to represent the effect of each of the additional sub-signals.

- Preliminary step responses have been obtained using intervention data and AutoRegresive with eXternal input (ARX) models (Ljung, 1999). From results, it can be observed that input signals need to be designed with more low frequency content. This can be achieved by incrementing the number of samples per cycle N_s, and the number of excited frequencies n_s. An analysis must be performed to determine what are the required minimum low frequency elements of interest (i.e., for how long changes on one construct affect the outputs), versus how short the decision time between each iteration in the monitoring process, is required to be. These considerations will also help make the multisines appear more pseudo-random, which is a practical aspect of the intervention.

- To improve estimation fits to a subsection of the SCT mode, *goal setting* can be used as a single intervention component. From an analytical point of view this will alleviate some of the constraints in the formulation, since the "If/Then" block will no longer be active and transfer function estimates will be unbiased for any method. The robust performance based stopping criterion presented in Section 4.3.2.2 can also be used with no further approximations. These results can serve as initial steps to facilitate the formulation of a complete intervention

reincorporating the reward mechanism if needed.

6.2.3 Improvements to the Identification Test Monitoring Procedure

In Section 3.3.4.2, a stopping criterion for identification test monitoring was derived relying on robust performance ideas. This criterion cannot be applied directly for the open-loop behavioral intervention, because of the nonlinear effect inherently present in the "If/Then" block. When an input signal is modified, the resultant transfer function is different from the previous one; hence there is no physical sense on estimating the aggregated version of the transfer function that is required for the computation of the robust performance index in (3.184).

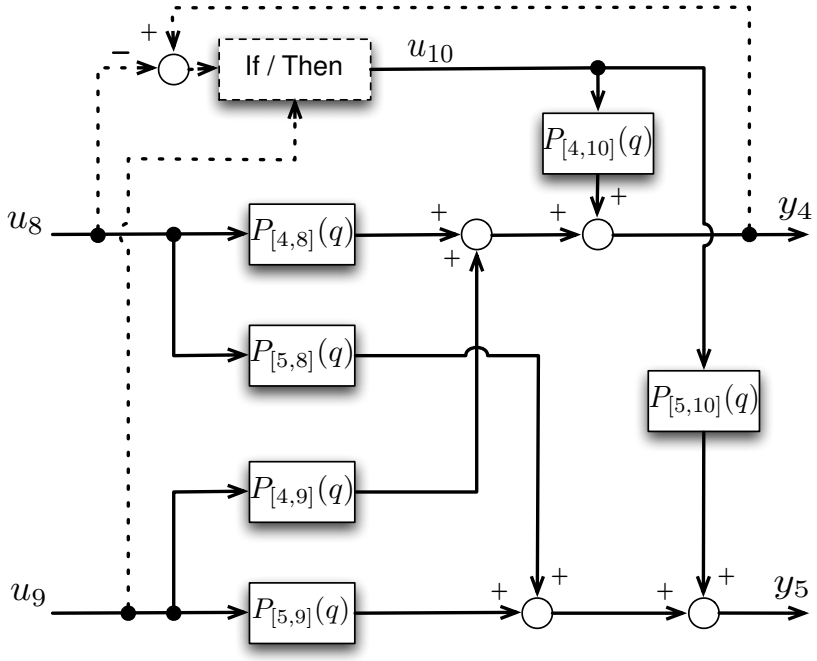

Figure 6.3: Block Diagram for the Physical Activity Behavioral Considering Independent Transfer Functions for Each Input/output Element.

Fig. 6.3 is a block diagram that illustrates the different transfer functions and elements involved in the intervention. When input signals are designed with a "zip-

pered" spectra, u_8 and u_9 are the only inputs that can be considered for transfer function estimates. These signals are designed orthogonally-in-frequency allowing the computation of independent transfer functions from any of them to each output. In this case the "If/then" block is always affecting each transfer function estimate. One solution is the use of the fast LPM that does not require the use of "zippered" signals. This will allow the incorporation of input signal u_{10} in the computation of transfer functions, and hence avoiding the effect of the nonlinear "If/then" block. As is mentioned in Chapter 3 the fast LPM is a more conservative method that usually produces biased results. There is a need for more research to contrast and compare the benefits of each approach according to the goals of the behavioral intervention.

6.2.4 Reconfiguration of the Semiphysical Identification Procedure

In Section 4.2.3 a grey-box parameter estimation procedure was proposed as the semiphysical identification strategy to find values for the SCT model parameters. Routines are executed in MATLAB using the system identification toolbox as well as the *idgrey* and *greyest* commands. After judiciously selection of scales and trend removal strategies, routines worked very well for most of the simulation scenarios. One particular case occurs when only maximum values are incremented for some input signals in the sequence during the identification test monitoring procedure; for example changing (min, max) from $(0, 500)$ to $(0, 700)$. In this case reductions in the percentage of fit are observed even in the presence of longer data sets. One reason for this estimation bias is the different average value of each signal with different amplitudes for inputs and outputs. Depending on the type of intervention, these types of amplitude increments may be required; hence a more robust solution in this sense is required. If the configuration options for MATLAB routines do not allow improvement in this sense, some other alternatives must be explored, as: definition

of an aggregated semiphysical estimation procedure, or construction of a redefined algorithm properly designed to account for this problem.

6.2.5 General Ideas

Looking to the future, the work from this dissertation can be modularized for use in health settings that require behavioral improvements in physical activity (e.g., the artificial pancreas, cardiovascular health, breast cancer prevention). These control system interventions can form part of novel cyberphysical systems for medical applications (Huyett *et al.*, 2015; Lee *et al.*, 2012; Costanzo *et al.*, 2016).

REFERENCES

Adams, M. A., J. F. Sallis, G. J. Norman, M. F. Hovell, E. B. Hekler and E. Perata, "An adaptive physical activity intervention for overweight adults: A randomized controlled trial", PloS one **8**, 12, e82901 (2013).

Ajzen, I. and T. J. Madden, "Prediction of goal-directed behavior: Attitudes, intentions, and perceived behavioral control", Journal of Experimental Social Psychology **22**, 5, 453–474 (1986).

Anderson-Bill, E. S., R. A. Winett and J. R. Wojcik, "Social cognitive determinants of nutrition and physical activity among web-health users enrolling in an online intervention: The influence of social support, self-efficacy, outcome expectations, and self-regulation", Journal of Medical Internet Research **13**, 1, e28 (2011).

Bandura, A., "Self-efficacy: toward a unifying theory of behavior change", Psychological Review **84**, 191–215 (1977).

Bandura, A., *Social Foundations of Thought and Action: A Social Cognitive Theory* (Prentice-Hall series in social learning theory, 1986).

Bandura, A., "Human agency in social cognitive theory", The American psychologist **44**, 9, 1175–1184 (1989).

Bandura, A., "Health promotion from the perspective of social cognitive theory", Psychology & Health **13**, 4, 623–649 (1998).

Bandura, A., "Health promotion by social cognitive means", Health Education & Behavior **31**, 2, 143–164 (2004).

Bandura, A. and R. H. Walters, *Social Learning and Personality Development* (New York : Holt, Rinehart and Winston, 1963).

Baum, W. M., "What is radical behaviorism? a review of jay moore's conceptual foundations of radical behaviorism", Journal of the experimental analysis of behavior **95**, 1, 119–126 (2011).

Bayard, D., "Statistical plant set estimation using Schroeder-phased multisinusoidal input design", Applied Mathematics and Computation **58**, 2-3, 169–198 (1993).

Bayard, D. S. and F. Y. Hadaegh, "Multivariable plant set estimation using multisinusoidal input designs", in "Proceedings of the 10th IFAC Symposium on System Identification", pp. 509 – 513 (1994).

Bemporad, A. and M. Morari, "Control of systems integrating logic, dynamics, and constraints", Automatica **35**, 3, 407–427 (1999).

Bohlin, T., "A case study of grey box identification", Automatica **30**, 2, 307–318 (1994).

Bohlin, T., *Practical Grey-box Process Identification: Theory and Applications*, Advances in Industrial Control (Springer, 2006).

Bollen, K. A., *Structural Equations with Latent Variables* (New York : Wiley, 1989), 1st edn.

Camacho, E. F. and C. Bordons, *Model Predictive Control* (Springer-Verlag London Limited, 2004), 2nd edn.

Carver, C. S. and M. F. Scheier, *On the Self Regulation of Behavior* (Cambridge University Press, 1998).

Clague, J. and L. Bernstein, "Physical activity and cancer", Current Oncology Reports **14**, 6, 550–558 (2012).

Collins, L. M., "Unpacking the black box: engineering more potent behavioral interventions to improve public health", in "Evan G. and Helen G. Pattishall Outstanding Research Achievement Award", (Penn State University, State College, PA, 2012).

Conn, V. S., A. R. Hafdahl and D. R. Mehr, "Interventions to increase physical activity among healthy adults: meta-analysis of outcomes", American Journal of Public Health **101**, 4, 751–758 (2011).

Costanzo, A., A. Faro, D. Giordano and C. Pino, "Mobile cyber physical systems for health care: Functions, ambient ontology and e-diagnostics", in "Proceedings of 13th IEEE Annual Consumer Communications & Networking Conference", pp. 972–975 (2016).

De Vries, D. K. and P. M. Van den Hof, "Quantification of uncertainty in transfer function estimation: a mixed probabilistic-worst-case approach", Automatica **31**, 4, 543–557 (1995).

Deshpande, S., *Optimal input signal design for data-centric identification and control with applications to behavioral health and medicine*, Ph.D. thesis, Electrical Engineering, Arizona State University (2014).

Deshpande, S., N. N. Nandola, D. E. Rivera and J. W. Younger, "Optimized treatment of fibromyalgia using system identification and hybrid model predictive control", Control Engineering Practice **33**, 1, 161–173 (2014a).

Deshpande, S., D. E. Rivera and J. Younger, "Towards patient-friendly input signal design for optimized pain treatment interventions", Proceedings of the 16th IFAC Symposium on System Identification pp. 1311–1316 (2012).

Deshpande, S., D. E. Rivera, J. W. Younger and N. N. Nandola, "A control systems engineering approach for adaptive behavioral interventions: illustration with a fibromyalgia intervention", Translational behavioral medicine **4**, 3, 275–289 (2014b).

Dong, Y., *A novel control engineering approach to designing and optimizing adaptive sequential behavioral interventions*, Ph.D. thesis, Chemical Engineering, Arizona State University (2014).

Dong, Y., S. Deshpande, D. E. Rivera, D. S. Downs and J. S. Savage, "Hybrid model predictive control for sequential decision policies in adaptive behavioral interventions", in "Proceedings of the American Control Conference", pp. 4198–4203 (2014).

Dong, Y., D. E. Rivera, D. S. Downs, J. S. Savage, D. M. Thomas and L. M. Collins, "Hybrid model predictive control for optimizing gestational weight gain behavioral interventions", in "Proceedings of the American Control Conference", pp. 1973 – 1978 (2013).

Dong, Y., D. E. Rivera, D. M. Thomas, J. E. Navarro-Barrientos, D. S. Downs, J. S. Savage and L. M. Collins, "A dynamical systems model for improving gestational weight gain behavioral interventions", in "Proceedings of the American Control Conference", pp. 4059–4064 (2012).

Eysenbach, G., "What is e-health?", Journal of medical Internet research **3**, 2, E20 (2001).

Ferster, C. B., "Schedules of reinforcement with Skinner", in "Festschrift for B. F. Skinner", edited by P. B. Dews, Century psychology series, pp. 37–46 (New York, Appleton-Century-Crofts, 1970).

Godin, G., P. Valois and L. Lepage, "The pattern of influence of perceived behavioral control upon exercising behavior: An application of ajzen's theory of planned behavior", Journal of Behavioral Medicine **16**, 1, 81–102 (1993).

Grant, A. M. and B. Schwartz, "Too much of a good thing: The challenge and opportunity of the inverted U", Perspectives on Psychological Science **6**, 1, 61–76 (2011).

Guillaume, P., J. Schoukens, R. Pintelon and I. Kollar, "Crest-factor minimization using nonlinear Chebyshev approximation methods", IEEE Transactions on Instrumentation and Measurement **40**, 6, 982–989 (1991).

Hanneman, R., *Computer-assisted Theory Building: Modeling Dynamic Social Systems* (Sage Publications, 1988).

Hekler, E. B., "Just walk study", `http://justwalkstudy.weebly.com/`, [Online; accessed September-23-2015] (2015).

Hekler, E. B., M. P. Buman, N. Poothakandiyil, D. E. Rivera, J. M. Dzierzewski, A. A. Morgan, C. S. McCrae, B. L. Roberts, M. Marsiske and P. R. Giacobbi, "Exploring behavioral markers of long-term physical activity maintenance: A case study of system identification modeling within a behavioral intervention", Health Education & Behavior **40**, 1, 51S–62S (2013a).

Hekler, E. B., C. M. Castro, M. P. Buman and A. C. King, "The CHOICE study: A "taste-test" of utilitarian vs. leisure walking among older adults", Health Psychology **31**, 1, 126–129 (2012).

Hekler, E. B., P. Klasnja, W. T. Riley, M. P. Buman, J. Huberty, D. E. Rivera and C. A. Martín, "Agile science: creating useful products for behavior change in the real world", Translational Behavioral Medicine **6**, 2, 317–328 (2016).

Hekler, E. B., P. Klasnja, V. Traver and M. Hendriks, "Realizing effective behavioral management of health: the metamorphosis of behavioral science methods", IEEE Pulse **4**, 5, 29–34 (2013b).

Hogg, R. V. and A. T. Craig, *Introduction to Mathematical Statistics* (Macmillan, New York, 1978), 4th edn.

Holt, B. R. and M. Morari, "Design of resilient processing plants – V: The effect of deadtime on dynamic resilience", Chemical Engineering Science **40**, 7, 1229–1237 (1985).

Huyett, L. M., E. Dassau, H. C. Zisser and F. J. Doyle, "The impact of glucose sensing dynamics on the closed-loop artificial pancreas", in "Proceedings of the American Control Conference", pp. 5116–5121 (2015).

ILOG CPLEX Optimization Studio, *version 12.6.0.0* (IBM Corporation, Armonk, New York, 2013).

J. Löfberg, "YALMIP : a toolbox for modeling and optimization in MATLAB", Proceedings of the IEEE International Symposium on Computer Aided Control Systems Design pp. 284–289 (2004).

King, A. C., E. B. Hekler, L. A. Grieco, S. J. Winter, J. L. Sheats, M. P. Buman, B. Banerjee, T. N. Robinson and J. Cirimele, "Harnessing different motivational frames via mobile phones to promote daily physical activity and reduce sedentary behavior in aging adults", PLoS ONE **8**, 4, e62613 (2013).

Klasnja, P., E. Hekler, S. Shiffman, A. Boruvka, D. Almirall, A. Tewari and S. Murphy, "Microrandomized trials: An experimental design for developing just-in-time adaptive interventions", HEALTH PSYCHOLOGY **34**, Suppl, 1220–1228 (2015).

Lee, I., O. Sokolsky, S. Chen, J. Hatcliff, E. Jee, B. Kim, A. King, M. Mullen-Fortino, S. Park, A. Roederer and K. K. Venkatasubramanian, "Challenges and research directions in medical cyber-physical systems", Proceedings of the IEEE **100**, 1, 75–90 (2012).

Lee, J. H., M. Morari and C. E. Garcia, "State-space interpretation of model predictive control", Automatica **30**, 4, 707–717 (1994).

Lee, J. H. and Z. H. Yu, "Tuning of model predictive controllers for robust performance", Computers and Chemical Engineering **18**, 1, 15–37 (1994).

Lindskog, P. and L. Ljung, "Tools for semiphysical modelling", International Journal of Adaptive Control and Signal Processing **9**, 6, 509–523 (1995).

Ljung, L., *System Identification : Theory for the User* (Upper Saddle River, NJ : Prentice Hall PTR, 1999), 2nd edn.

Lopez, L. M., E. E. Tolley, D. A. Grimes and M. Chen-Mok, "Theory-based interventions for contraception", The Cochrane database of systematic reviews **3**, CD007249 (2011).

Marcus, B., D. Williams, P. Dubbert, J. Sallis, A. King, A. Yancey, B. Franklin, D. Buchner, S. Daniels and R. Claytor, "Physical activity intervention studies - what we know and what we need to know - a scientific statement from the american heart association council on nutrition, physical activity, and metabolism (subcommittee on physical activity); council on cardiovascular disease in the young; and the interdisciplinary working group on quality of care and outcomes research", CIRCULATION **114**, 24, 2739–2752 (2006).

Marsland, S., "Using habituation in machine learning", Neurobiology of Learning and Memory **92**, 2, 260–266 (2009).

Martín, C. A., S. Deshpande, E. B. Hekler and D. E. Rivera, "A system identification approach for improving behavioral interventions based on Social Cognitive Theory", in "Proceedings of the American Control Conference", pp. 5878–5883 (2015a).

Martín, C. A., D. E. Rivera and E. B. Hekler, "Design of informative identification experiments for behavioral interventions", in "Proceedings of the 17th IFAC Symposium on System Identification", pp. 1325–1330 (2015b).

Martín, C. A., D. E. Rivera and E. B. Hekler, "An identification test monitoring procedure for MIMO systems based on statistical uncertainty estimation", in "Proceedings of the 54th IEEE Conference on Decision and Control", pp. 2719–2724 (2015c).

Martín, C. A., D. E. Rivera and E. B. Hekler, "A decision framework for an adaptive behavioral intervention for physical activity using hybrid model predictive control", in "Proceedings of the American Control Conference", pp. 3576–3581 (2016a).

Martín, C. A., D. E. Rivera and E. B. Hekler, "An enhanced identification test monitoring procedure for MIMO systems relying on uncertainty estimates", in "Submitted to the 55th IEEE Conference on Decision and Control", (2016b).

Martín, C. A., D. E. Rivera, W. T. Riley, E. B. Hekler, M. P. Buman, M. A. Adams and A. C. King, "A dynamical systems model of Social Cognitive Theory", in "Proceedings of the American Control Conference", pp. 2407–2412 (2014).

McGinnis, J. M., P. Williams-Russo and J. R. Knickman, "The case for more active policy attention to health promotion", Health Affairs **21**, 2, 78–93 (2002).

McMahon, S., M. Vankipuram, E. B. Hekler and J. Fleury, "Design and evaluation of theory-informed technology to augment a wellness motivation intervention", Translational Behavioral Medicine **4**, 1, 95–107 (2014).

Mokdad, A. H., J. S. Marks, D. F. Stroup and J. L. Gerberding, "Actual causes of death in the United States, 2000", The Journal of the American Medical Association (JAMA) **291**, 10, 1238–1245 (2004).

Monteyne, G., D. Ugryumova and G. Vandersteen, "Extension of local polynomial method for periodic excitations", in "Proceedings of the 16th IFAC Symposium on System Identification", pp. 61–65 (2012).

Morari, M. and E. Zafiriou, *Robust Process Control* (Prentice-Hall International, 1989).

Nahum-Shani, I., E. B. Hekler and D. Spruijt-Metz, "Building health behavior models to guide the development of just-in-time adaptive interventions: A pragmatic framework", Health Psychology **34**, suppl, 1209–1219 (2015).

Nandola, N. N. and D. E. Rivera, "An improved formulation of hybrid model predictive control with application to production-inventory systems", IEEE Transactions on Control Systems Technology **21**, 1, 121–135 (2013).

Navarro-Barrientos, J. E., D. E. Rivera and L. M. Collins, "A dynamical model for describing behavioural interventions for weight loss and body composition change", Mathematical and Computer Modelling of Dynamical Systems **17**, 2, 183–203 (2011).

Nilsen, W. J. and M. Pavel, "Moving behavioral theories into the 21st century: Technological advancements for improving quality of life", IEEE Pulse **4**, 5, 25–28 (2013).

Norman, G. J., M. F. Zabinski, M. A. Adams, D. E. Rosenberg, A. L. Yaroch and A. A. Atienza, "A review of eHealth interventions for physical activity and dietary behavior change", American Journal of Preventive Medicine **33**, 4, 336–345.e16 (2007).

Norman, P., M. Conner and R. Bell, "The theory of planned behaviour and exercise: Evidence for the moderating role of past behaviour", Journal of Behavioral Medicine **5**, 3, 249–261 (2000).

Payne, H. E., C. Lister, J. H. West and J. M. Bernhardt, "Behavioral functionality of mobile apps in health interventions: A systematic review of the literature", JMIR mHealth and uHealth **3**, 1, e20 (2015).

Pintelon, R. and J. Schoukens, *System Identification: A Frequency Domain Approach* (Wiley ; IEEE Press, 2012), 2nd edn.

Pintelon, R., J. Schoukens, G. Vandersteen and K. Barbé, "Estimation of nonparametric noise and FRF models for multivariable systems – Part I: Theory", Mechanical Systems and Signal Processing **24**, 3, 573–595 (2010).

Pintelon, R., G. Vandersteen, J. Schoukens and Y. Rolain, "Improved (non-)parametric identification of dynamic systems excited by periodic signals – the multivariate case", Mechanical Systems and Signal Processing **25**, 8, 2892–2922 (2011).

Powers, W. T., "Feedback: Beyond behaviorism", Science **179**, 4071, 351–356 (1973).

Prett, D. M. and C. E. Garcia, *Fundamental Process Control* (Butterworth, 1988), 1st edn.

Prochaska, J. O. and C. C. DiClemente, "Stages and processes of self-change of smoking: Toward an integrative model of change", Journal of Consulting and Clinical Psychology **51**, 3, 390–395 (1983).

Rankin, C. H., T. Abrams, R. J. Barry, S. Bhatnagar, D. F. Clayton, J. Colombo, G. Coppola, M. A. Geyer, D. L. Glanzman, S. Marsland, F. K. McSweeney, D. A. Wilson, C.-F. Wu and R. F. Thompson, "Habituation revisited: an updated and revised description of the behavioral characteristics of habituation", Neurobiology of learning and memory **92**, 2, 135–138 (2009).

Rauner, A., D. Jekauc, F. Mess, S. Schmidt and A. Woll, "Tracking physical activity in different settings from late childhood to early adulthood in Germany: the MoMo longitudinal study", BMC Public Health **15**, 1, 391 (2015).

Riley, W. T., C. A. Martín and D. E. Rivera, "The importance of behavior theory in control system modeling of physical activity sensor data", in "Proceedings of the 36th Annual International Conference of the IEEE Engineering in Medicine and Biology Society", pp. 6880 – 6883 (2014).

Riley, W. T., C. A. Martín, D. E. Rivera, E. B. Hekler, M. A. Adams, M. P. Buman, M. Pavel and A. C. King, "Development of a dynamical systems model of social cognitive theory", Translational Behavioral Medicine: Practice, Policy and Research pp. 1 – 13, URL `http://link.springer.com/article/10.1007/s13142-015-0356-6`, published online: 09 November 2015 (2015a).

Riley, W. T., D. E. Rivera, A. A. Autienza, W. Nilsen, S. Allison and R. Mermelstein, "Health behavior models in the age of mobile interventions: are our theories up to the task?", Translational Behavioral Medicine: Practice, Policy, Research **1**, 1, 53–71 (2011).

Riley, W. T., K. J. Serrano, W. Nilsen and A. A. Atienza, "Mobile and wireless technologies in health behavior and the potential for intensively adaptive interventions", Current Opinion in Psychology **5**, 67–71 (2015b).

Rivera, D. E., "Optimized behavioral interventions: What does system identification and control engineering have to offer?", in "Proceedings of the 16th IFAC Symposium on System Identification", pp. 882 – 893 (2012).

Rivera, D. E., H. Lee, M. W. Braun and H. D. Mittelmann, "Plant-friendly system identification: a challenge for the process industries", Proceedings of the 13th IFAC Symposium on system identification SYSID pp. 917–922 (2003).

Rivera, D. E., H. Lee, H. D. Mittelmann and M. W. Braun, "Constrained multisine input signals for plant-friendly identification of chemical process systems", Journal of Process Control **19**, 4, 623–635 (2009).

Rivera, D. E., M. D. Pew and L. M. Collins, "Using engineering control principles to inform the design of adaptive interventions: a conceptual introduction", Drug and alcohol dependence **88**, 2, S31–S40 (2007).

Schroeder, M. R., "Synthesis of low-peak-factor signals and binary sequences with low autocorrelation", IEEE Transactions on Information Theory **16**, 1, 85–89 (1970).

Schroeder, S. A., "We can do better - improving the health of the American people", The New England Journal of Medicine **357**, 12, 1221–1228 (2007).

Schwartz, J. D., W. Wang and D. E. Rivera, "Simulation-based optimization of process control policies for inventory management in supply chains", Automatica **42**, 8, 1311–1320 (2006).

Shiffman, S., A. A. Stone and M. R. Hufford, "Ecological momentary assessment", Clinical Psychology **4**, 1, 1–32 (2008).

Skogestad, S. and I. Postlethwaite, *Multivariable feedback control: analysis and design* (Wiley, Chichester, New York, 2005), 2nd edn.

Söderström, T., Reglerteknik, U. universitet, M. datavetenskapliga sektionen, I. för informationsteknologi, A. fr systemteknik and T. naturvetenskapliga vetenskapsområdet, "Errors-in-variables methods in system identification", Automatica **43**, 6, 939–958 (2007).

Spruijt-Metz, D., E. Hekler, N. Saranummi, S. Intille, I. Korhonen, W. Nilsen, D. E. Rivera, B. Spring, S. Michie, D. A. Asch, A. Sanna, V. T. Salcedo, R. Kukakfa and M. Pavel, "Building new computational models to support health behavior change and maintenance: new opportunities in behavioral research", Translational Behavioral Medicine **5**, 3, 335–346 (2015).

Steenis, R., *Plant-friendly input signal design for system identification and robust control performance*, Ph.D. thesis, Electical Engineering, Arizona State University (2009).

Steenis, R. and D. E. Rivera, "Probabilistic uncertainty description for an ETFE estimated plant using a sequence of multi-sinusoidal signals", in "Proceedings of the American Control Conference", pp. 3722 – 3728 (2010).

Stenman, A., "Model on demand: Algorithms, analysis and applications", Tech. rep., ISBN 91-7219-450-2. N. Bergman (1999).

Thompson, R. F. and W. A. Spencer, "Habituation: A model phenomenon for the study of neuronal substrates of behavior", Psychological Review **73**, 1, 16–43 (1966).

Timms, K. P., C. A. Martín, D. E. Rivera, E. B. Hekler and W. T. Riley, "Leveraging intensive longitudinal data to better understand health behaviors", in "Proceedings of the 36th Annual International Conference of the IEEE Engineering in Medicine and Biology Society", pp. 6888 – 6891 (2014a).

Timms, K. P., D. E. Rivera, L. M. Collins and M. E. Piper, "Continuous-time system identification of a smoking cessation intervention,", International Journal of Control **87**, 7, 1423–1437 (2014b).

Timms, K. P., D. E. Rivera, L. M. Collins and M. E. Piper, "A dynamical systems approach to understanding self-regulation in smoking cessation behavior change", Nicotine and Tobacco Research, Special Issue on New Methods for Advancing Research on Tobacco Dependence Using Ecological Momentary Assessments **16**, Suppl 2, S159–S168 (2014c).

Timms, K. P., D. E. Rivera, M. E. Piper and L. M. Collins, "A hybrid model predictive control strategy for optimizing a smoking cessation intervention", in "Proceedings of the American Control Conference", pp. 2389 – 2394 (2014d).

Torrisi, F. D. and A. Bemporad, "HYSDEL–a tool for generating computational hybrid models for analysis and synthesis problems", IEEE Transactions on Control Systems Technology **12**, 2, 235–249 (2004).

Villanti, A. C., H. S. McKay, D. B. Abrams, D. R. Holtgrave and J. V. Bowie, "Smoking-cessation interventions for U.S. young adults: A systematic review", American Journal of Preventive Medicine **39**, 6, 564–574 (2010).

Williams, H. P., *Model Building in Mathematical Programming* (John Wiley & Sons, 2013), 5th edn.